Thermodynamic and kinetic study on hydrolysis of concentrated sodium borohydride solution

PLEASE CITE THE PUBLISHED VERSION

PUBLISHER

© Yinghong Shang

PUBLISHER STATEMENT

LICENCE

REPOSITORY RECORD

Shang, Yinghong. 2015. "Thermodynamic and Kinetic Study on Hydrolysis of Concentrated Sodium Borohydride Solution". figshare. https://hdl.handle.net/2134/16598.

Thermodynamic and Kinetic Study on Hydrolysis of Concentrated Sodium Borohydride Solution

By

Yinghong Shang, BSc, MSc

Submitted to Loughborough University for partial fulfilment of the Degree of Doctor of Philosophy

Table of Contents

v

Nomenclature

A	Pre-exponential factor
C	Concentration
c	Heat capacity
D	Diffusivity
E	Energy
G	Gibbs free energy
H	Enthalpy
K	Chemical reaction equilibrium constant
L	Dimension
k	Reaction rate constant
M	Molecular weight
m	Molality
n	Mole number
P	Hydration analysis parameter
p	Pressure
q	Heat
R	Gas constant
r	Reaction rate
S	Entropy, or Heat transfer area
T	Temperature
t	Time
u	fluid flow rate
V	Volume
W	Mass
w	Concentration in weight percent
α	Convective heat transfer coefficient
η	efficiency factor
κ	Thermal diffusivity
γ	Activity coefficient
μ	Chemical potential

Acknowledgements

The list of acknowledgements for such an undertaking is seemingly endless, yet, there are a few that stands out above the rest. First of all, I would like to express my gratitude to my PhD supervisor, Dr Rui Chen, for his patient and intelligent guidance for this research. His clear thinking style and scientific attitude would be a benefit for my career. Secondly, my thanks would like to go to the technicians for their great help in setting up the experimental rig. Thirdly, I would like to thank Loughborough University for giving me the opportunity and financial support to fulfil the study. At last, I would like to thank my parents, my husband, Guozhan Jiang and my daughter, Nancy. It is their endless support to make this dream a reality.

Abstract

The hydrolysis of sodium borohydride ($NaBH_4$) over efficient metal catalysts is a promising approach to hydrogen storage. An alkali such as NaOH is often added to stabilise the system in practical applications. The concentration of the $NaBH_4$ solution should be as high as possible to improve energy density of the system. However, the by-product sodium metaborate ($NaBO_2$) would become saturated and precipitate from the solution when the concentration of sodium borohydride is over a limit, resulting in piping blockage and the decrease of the catalyst efficiency. The theme of this thesis was to investigate the maximum $NaBH_4$ concentration. Below the maximum concentration, the precipitation of the by-product will not occur, and above the maximum concentration, the by-product tends to precipitate from the solution. Hydrogen generation rate was then investigated up to high concentration.

The maximum concentration was studied using a thermodynamic approach. The relationship between the solubility and the temperature was derived based on the equality of the chemical potential of the solute in solution and in its solid state. The solubility data of $NaBH_4$ and $NaBO_2$ were obtained by analysing the phase diagrams of $NaBH_4$-NaOH-H_2O and $NaBO_2$-NaOH-H_2O respectively. The model parameters were then determined by regression of the solubility data and the temperature. Activity coefficients of $NaBH_4$ and $NaBO_2$ were needed during the regression and these were achieved by hydration analysis of the phase diagrams. The maximum concentration of $NaBH_4$ was obtained by taking the maximum between the water in saturated $NaBH_4$ solution and the sum of the water in saturated $NaBO_2$ solution and the water consumed for hydrolysis. The maximum concentration of $NaBH_4$ is mainly determined by the solubility of $NaBO_2$. The modelling of the maximum concentration was then validated experimentally.

The rate of hydrogen generation from $NaBH_4$ hydrolysis was then investigated over carbon supported ruthenium catalyst over a wide range of concentrations. The intrinsic hydrolysis rate is zero-order to $NaBH_4$ concentration, and has a linear relationship with the basicity of the solution (-ln[OH]). The overall kinetics was modelled by building diffusion and heat effect into the intrinsic rate expression. Experimental results agree well with model prediction.

ϕ Thiele modulus

Subscript

B $NaBO_2$ or $NaBH_4$

p   Pressure

eff   Effective

i   Initial

f   Final

H_2 hydrogen

HA   General acid

H_2O Water

m   Molar

$NaBH_4$ Sodium borohydride

$NaBO_2$ Sodium metaborate

NaOH   Sodium hydroxide

o   Initial value

rev   Reversible

tot   Total

±   Average

Superscript

0   Initial value

'   Another value

*   Standard

Publications from the thesis:

1. Y. Shang and R. Chen, Hydrogen Storage via the Hydrolysis of $NaBH_4$ Basic Solution: Optimization of $NaBH_4$ Concentration, Energy & Fuels, 2006, **20**, 2142-2148

2. Y. Shang and R. Chen, Semi Empirical Hydrogen Generation Model Using Concentrated Sodium Borohydride Solution, Energy & Fuels, 2006, **20**, 2149-2154

3. Y. Shang, R. Chen and R. Thring, The Concentration of Sodium Borohydride Hydrolysis System Used for Compact Hydrogen Storage, World Journal of Engineering, 2005, **2**, 1-9

4. Y. Shang, R. Chen and R. Thring, Hydrolysis of Sodium Borohydride – A Potential Compact Hydrogen Storage Method, World Journal of Engineering, 2006, **3**, 14-26

5. Y. Shang, R. Chen, G Jiang, Intrinsic kinetics of $NaBH_4$ hydrolysis over carbon supported ruthenium catalyst, Energy and Fuels (submitted).

6. Y. Shang, R. Chen, G Jiang, Modelling of the hydrolysis of $NaBH_4$ over carbon supported ruthenium catalyst, Energy and Fuels (submitted).

Chapter 1

Introduction

1.1 Motivation and Objectives

With the progress of human society and the population growth, the use of energy and the exploitation of energy resources has expanded rapidly. A good supply of energy has become an indispensable factor for economic development. The history of humanity is in fact the history of the availability and utilisation of energy. Each revolution in new energy utilisation brings about significant progress in human society.

In ancient times, people were able to use the power of water to drive watermills for grinding grain and the power of wind energy for pumping water and driving ships. The beginning of the industrial revolution in the 19th century in Great Britain saw the use of fossil fuels on a large scale. The extensive use of coal and oil has made a great contribution to the development of modern industries. Various energy conversion devices were then invented to enable the use of fossil fuels to drive automobiles, aeroplanes and other means of transport, to generate electricity, to heat and to cook. Nowadays, nuclear energy, wind energy, hydro-energy and solar energy are in use. However, fossil fuels still play a dominant role in the world, and it will still account for the main part of energy sources in the foreseeable future.

Unfortunately, fossil fuels are not a renewable resource. They will eventually become depleted. Moreover, the emission of carbon dioxide and NO_x gases has been linked to the problem of global warming. These present challenges to the world and have become key factors that must be considered for a sustainable development in the 21st century. A sustainable energy supply has thus become increasingly necessary. Prof. George A Olah, the winner of the Nobel Prize in chemistry in 1994, pointed out in 1991 that "Oil and gas resources under the most optimistic scenarios won't last much longer than through the next century. Coal reserves are more abundant, but are also limited. ... I suggest we should worry much more about our limited and diminishing fossil resources" [1]. In order to tackle the challenge of diminishing fossil fuel reserves and the ever-increasing environmental problems, great attempts have been made to improve energy efficiency and

1

to explore clean and renewable energy sources.

Renewable energy refers to the energy obtained from sources that are essentially inexhaustible [2], which includes bio-energy, hydro-energy, geothermal energy, solar energy and hydrogen energy. Bio-energy is the energy released from the reaction of biomass with oxygen [3]. Biomass is a flexible feedstock capable of conversion into solids, liquid and gas (such as methane, carbon monoxide, ethanol and charcoal) by gasification method [4]. The bio-fuels obtained can be used to substitute fossil fuels. The biomass feedstock can be agriculture and forestry waste, energy crops, landfill and sewage gas and municipal solid waste. Solar energy is the sun's radiant energy. Geothermal energy is the energy contained as heat in the interior of earth, such as natural steam and hot water. The origin of geothermal energy is linked with the internal structure of the earth and the physical processes occurring there [5]. Wind energy refers to the power produced by the flow of air harnessed by humans.

Strictly speaking, bio-fuels are not clean since the combustion products contain carbon dioxide. Geothermal energy, hydropower and wind energy are region-restricted. They are not available everywhere. For example, wind energy is distributed mainly in the US, Spain, Germany, India and Denmark [6], while hydro-energy is concentrated in the US, Brazil and China [7]. The most promising renewable energy sources should be solar energy and hydrogen fuel since they are clean.

Hydrogen is the only universal fuel that can run everything from spaceships to automobiles as summarized in Figure 1.1. It can be used in liquid or gaseous form in jet engines, internal combustion engines and fuel cells.
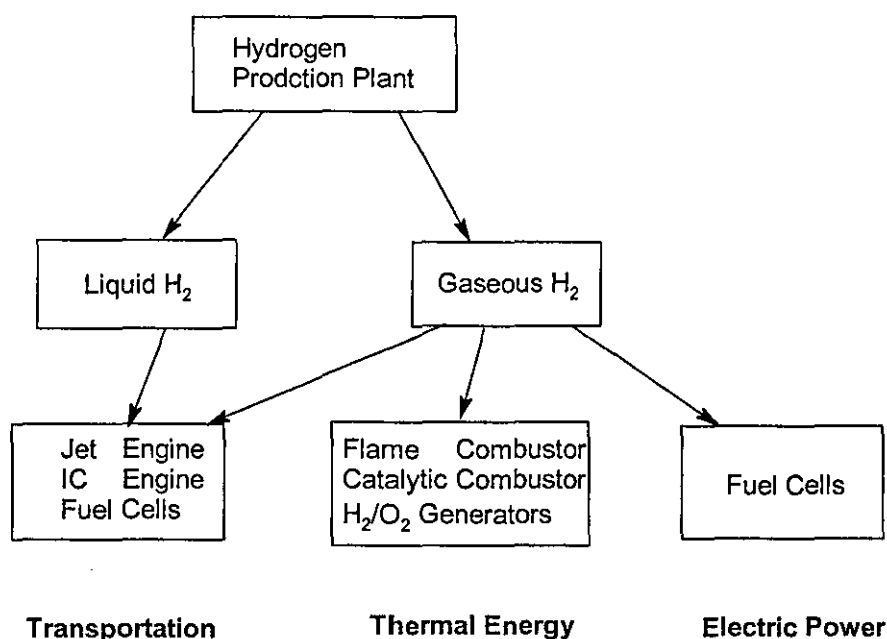
Figure 1.1 The uses of hydrogen in a liquid or gas form.

The main problems are how to generate hydrogen from renewable resources and how to store it in a manageable form since hydrogen has the minimum density among all the gases and hence takes up a lot of storage space for a comparable amount of energy. The two aspects of the problem are equally important. At the present time, the lack of practical storage methods has hindered the more widespread use of the renewable and environmentally friendly hydrogen fuels. Various methods have been investigated for hydrogen storage such as high-pressure gas cylinders, liquid hydrogen, adsorption using carbon nanotubes and metal hydride compounds. Research so far has proven that the use of the hydrolysis of sodium borohydride ($NaBH_4$) is one of the most promising methods of producing hydrogen. This is because $NaBH_4$ is a stable compound and the hydrolysis reaction can be carried out in very mild conditions[8, 9].

The main advantages of using sodium borohydride are as follows:

High temperature is needed for producing H_2 by some methods, but via the hydrolysis of $NaBH_4$, H_2 can be produced in a more controllable way at a wide and moderate temperature range (from $-5°C$ to $100°C$). $NaBH_4$ is a non-flammable liquid at normal pressure. During the hydrolysis, there are no side reactions or other volatile products. The generated hydrogen has a high purity (no carbon monoxide and sulphur) with just some water vapour. However, there are two main barriers for its commercialisation. One is

how to improve its energy density. The other is how to recycle the by-product sodium metaborate (NaBO$_2$).

The theme of this thesis is to gain insight into the utilization of the hydrolysis of sodium borohydride centred on the concentrated NaBH$_4$ solution. Using concentrated NaBH$_4$ solution for H$_2$ production is desirable because it can assure the H$_2$ storage density. However, if the concentration is too high it leads to precipitation of the by-product, NaBO$_2$, which leads to pipe blockage and a decrease in catalyst activity. In this thesis, the maximum concentration of NaBH$_4$ that can be used in the system is studied thermodynamically and kinetically.

The solution of NaBH$_4$ is not stable at room temperature because hydrolysis occurs and hydrogen is released gradually. A base, typically NaOH, is used as the stabilizer. The effect of NaOH on optimal concentration of NaBH$_4$ and the hydrogen generation rate is also extensively studied in this thesis.

Experiments are carried out to test the effects of various factors on the rate of hydrogen generation, including temperature and the concentration of NaBH$_4$, NaOH and NaBO$_2$. Based on the experimental results, an empirical model is obtained to simulate the reaction and predict the hydrogen storage density.

In the rest of this chapter, the basics of energy systems and the background of the research are reviewed. The related theories of chemical thermodynamics are introduced in the chapters where they are used.

1.2 Basics of Energy Systems

1.2.1 Energy and Power

Energy has various definitions. In physical sciences, energy refers to the capacity of doing work: that is to move an object against a resisting force [10]. In everyday language, the word 'power' is often used as a synonym for energy. But when speaking scientifically, power is defined as the rate of doing work, that is, the rate at which energy is converted from one form to another, or transmitted from one place to another [11]. The unit of measurement of energy in the SI system is 'joule' (J), and the unit of power in the SI system is 'watt' (W).

1.2.2 The Forms of Energy [7, 11]

Energy can take many different forms. At its most basic level, it can be classified into four types: kinetic energy, gravitational energy, electrical energy and nuclear energy.

Kinetic energy is the energy possessed by any moving object. Thermal energy, or heat, is the name given to the kinetic energy associated with the random motion of molecules of any matter.

Gravitational energy, also termed gravitational potential energy or potential energy, is (simplistically) the energy due to position difference with the earth. Gravity is an insignificant force at the molecular level. However, a major application of gravitational energy is hydro-electricity, in which the potential energy of water is changed into electrical energy.

Electrical energy is the energy associated with the electrical force between atoms that constitute matter. Chemical energy can be considered as a form of electrical energy. Another form of electrical energy is that carried by electrical currents: organized flows of electrons in a material. The third form of electrical energy is that carried by electromagnetic radiation (energy).

Nuclear energy is the energy bound up in the nuclei of atoms. It is released by the fission or fusion reactions of nuclei, notably uranium-235 and plutonium-239. The complete fission of a kilogram of uranium-235 should produce, in principle, as much energy as the combustion of over 3000 tonnes of coal. In practice, the fission is incomplete and there are other losses. The heat generated by nuclear fission in a nuclear power plant is used to generate high-pressure steam, which then drives steam turbines coupled to electrical generators, as in a conventional power station.

1.2.3 Fuel

A fuel is a substance which interacts with oxygen and in doing so releases energy and changes into different chemical compounds–the combustion products [11]. According to this definition, wood is a fuel but sand not. The energy released in this process is termed the energy content of the fuel.

1.2.4 Energy Services

Mankind does not actually need energy carriers such as coal, oil, wood or electricity. We need energy services. Unlike energy, energy services are independent of technology and can not be easily quantified. For example, when we drive a car, we have used an amount of fuel: energy. The energy service in this case might be described as the distance we travel. We live in a warm and cosy house; we burn gas, energy, to heat the radiators. For heating purposes, the energy service is often described as the room temperature desired [12].

1.2.5 Primary Energy

Primary energy is the total energy 'content' of the original resource. Present main resources are fossil fuels (coal, oil and natural gas), biofuels (wood, straw, etc.), nuclear power stations, hydroelectric and geothermal plants and other 'renewables' such as solar or wind power.

The measurement of the consumption of primary energy in the world has two units: units based on oil and units based on coal. One tonne of oil equivalent (toe) is the heat energy released in the complete combustion of 1000 kg of oil, which is 41.88 GJ (world average value). The commonly used unit is millions of tonnes of oil equivalent (Mtoe), which is approximately 4.2×10^{16} J.

1.2.6 Energy Efficiency

In the use of energy for various purposes, not all of the energy can be converted to the desired work according to the second law of thermodynamics. The concept of energy efficiency is thus raised. The conversion efficiency of any energy conversion system (often simply called the efficiency) is defined as the useful energy output divided by the total energy input, as shown in equation (1.1).

$$Efficiency = \frac{E_o}{E_i} \times 100\% \qquad (1.1)$$

where E_o is the energy output and E_i is the energy input. In another definition as given by the World Energy Council, energy efficiency has the sense of what is usually understood with an implicit reference to technological efficiency only: it encompasses all changes that result in decreasing the amount of energy used to produce one unit of economic activity (e.g. the energy used per unit of GDP or value added) or to meet the energy

requirements for a given level of comfort. Energy efficiency is associated with economic efficiency and includes technological, behavioural and economic changes. Energy efficiency improvements refer to a reduction in the energy used for a given energy service (such as heating and lighting) or level of activity.

1.2.7 Prime Mover

The prime mover is a device that converts the energy of any natural source into motive power: the driving power of machines. Any system designed to obtain continuous motive power from heat is called a heat engine. The heat energy comes from the combustion of fossil fuel or nuclear reaction. Heat engines can be classified into external combustion engines, such as steam turbines and jet turbines for aircraft, and internal combustion engines.

According to the second law of thermodynamics, it is impossible to have a perfect heat engine. The efficiency of any heat engine abides by Carnot's law: any other heat engine operating with the same input and exhaust temperatures must have a lower efficiency than the Carnot engine. The efficiency of the Carnot engine is expressed using equation (1.2).

$$Efficiency = \frac{T_1 - T_2}{T_1} \tag{1.2}$$

where T_1 is the temperature of 'boiler', T_2 is the temperature of the 'condenser' into which that exhaust is rejected.

1.2.8 The Grade of Energy

It is known that heat is the kinetic energy of randomly-moving molecules, a chaotic or 'low grade' form of energy. We know this process of changing energy into work should comply with the second law of thermodynamics: no process is possible in which the sole result is the absorption of heat from a reservoir and complete conversion of that heat into work. On the other hand, mechanical energy and electric energy have a higher grade, because they are due to the ordered movement of particles.

Therefore, energy sources can be graded in quality. High-grade sources provide the most organized forms of energy and low-grade sources are the least organized, or have low and negative entropy energy [13]. The higher grades include the kinetic energy of moving

7

matter, gravitational potential energy and electrical energy. These can be converted with small losses. Larger losses occur when the lower forms are converted. Regarding heat energy, high grade means high-temperature heat, and low grade means low-temperature heat.

1.3 Problems Caused by the Utilisation of Fossil Fuels

1.3.1 Present Energy Sources

In order to better understand the problems caused by current energy utilisation, an overview is given of the primary energy used by humanity. The evolution of energy consumption from 1971 to 2001 in the world is shown in Figure 1.2.
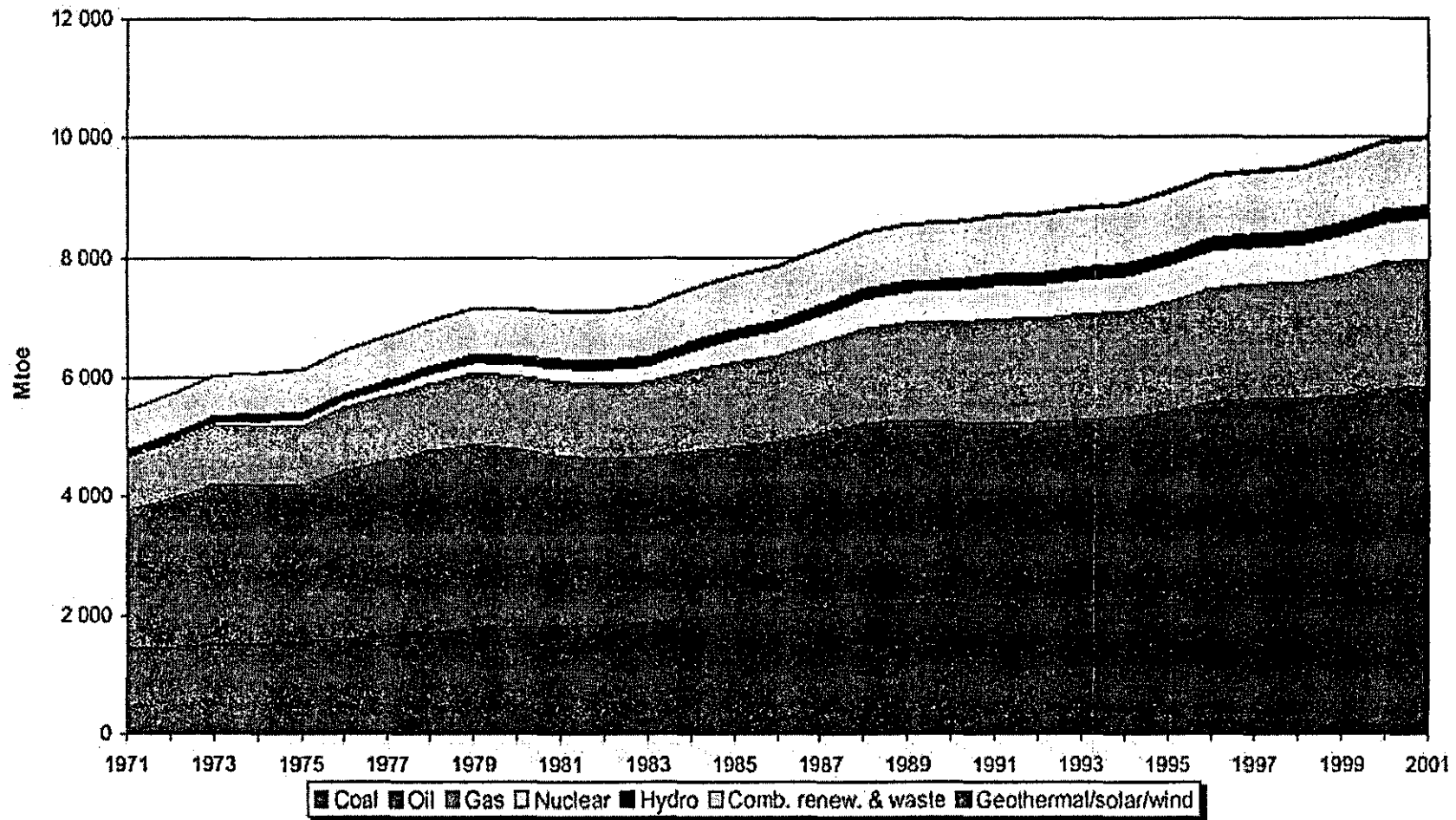
Figure 1.2 Evolution of total primary energy supply from 1971 to 2001 of the world (source: International Energy Agency (IEA)[14]).

From Figure 1.2, it can be seen that present energy sources include fossil fuels (coal, oil and natural gas), nuclear energy, bio-energy and other renewable energies. The rate of increase in total primary energy supply is very rapid. The total primary energy supply in the world was 6,043 Mtoe in 1973, 9,491 Mtoe in 1998, and 10,165 Mtoe in 2001, an increase of 68% in 28 years.

Fossil fuels include coal, oil and natural gas. They are extremely attractive due to their high energy concentration and easy distribution. Fossil fuels are formed after a long period of geological processes and originate in the growth and decay of plants and marine organisms that existed long ago. The fossil fuels now supply nearly 80% of the world's current energy consumption. The fossil fuels have various applications but mainly as fuels for means of transport and for electricity generation.

Nuclear energy accounts for about 7% of primary energy consumption at the present time. However, the growth rate in recent years has largely stopped, and may be in decline due to the difficulty of disposing of nuclear waste and the public concern over radiation disasters [14].

The item "combustible renewables and waste" mainly refers to bio-energy, which accounts for about 11% and has been stable for the last three decades.

Hydro-energy from flowing water has been used for centuries for purposes such as milling grain and driving machinery. Currently its main use has been in the generation of hydro-electricity. It provides about 2.2% of primary energy.

According to the present pattern of energy consumption, it can be noticed that fossil energy (oil, coal and gas) is the most widely used. Although its share decreased slowly from 86.1% to 79%, fossil fuel still accounts for the major part of present energy uses.

1.3.2 Problems by the Use of Fossil Fuels

1.3.2.1 Air Pollution

From the above analysis, the share of fossil energy accounts for about 80% of total primary energy consumption. The use of coal, oil and gas is mainly through combustion to produce heat, followed by conversion of that heat into secondary fuels and motive power in various engines. In this process, many emissions are produced, as shown in

Table 1.1. These emissions cause an ever-increasing environmental problem.

Table 1.1 Main emissions from combustion of fossil fuels [15].

Emissions	Greenhouse Effect	Ozone layer Depletion	Acid Precipitations	Smog
Carbon dioxide (CO_2)	+	±		
Methane (CH_4)	+	±		
Nitric oxides (NO_x)		±	+	+
Ozone (O_3)	+			+
Sulfur dioxide (SO_2)	–	+		
Nitrous oxide (N_2O)	+	±		

Note: + stands for positive factor; – stands for negative factor, and ± stands for uncertainty.

As can be seen from Table 1.1, there are two types of emissions that cause air pollution from burning fossil fuels. One is the noxious gases released: sulfur dioxide (SO_2), carbon monoxide (CO), nitrogen oxides (NO_x, N_2O), ozone (O_3) and volatile chemical vapours (VOCs). The other is particulate matter (PM) pollution, which has a size of about 2.5 μm.

1.3.2.2 Noxious Gas Pollution

Fossil fuels are composed mainly of carbon and hydrogen. An ultimate analysis reveals that they also contain other elements such as oxygen, nitrogen and sulphur. During combustion, nitrogen can combine with oxygen to produce oxides of nitrogen. These compounds (N_2O, NO, NO_2, etc.) are known as NO_x gases. The nitrogen in NO_x mainly comes from fossil fuels. However, nitrogen from the air also contributes. Any sulphur present in the fuels will readily form sulphur dioxide (SO_2). The incomplete combustion of the fuels will produce carbon monoxide (CO).

The formation of air-polluting ozone at ground level is the result of a chain reaction system initiated by the photolysis of nitrogen dioxide that effectively absorbs ultraviolet (UV) radiation reaching the earth's surface as shown in Scheme 1.1, where NO_2 adsorbs radiation to decompose into NO and atomic oxygen. The atomic oxygen then reacts with oxygen to form ozone directly, or on mediums such as particles or inert gases (as shown Scheme 1.2).

$$NO_2 \xrightarrow{h\nu} NO + O$$

Scheme 1.1 The reaction for the formation of atomic oxygen.

$$O_2 + O \longleftrightarrow O_3$$

$$O_2 + O + M \longleftrightarrow O_3 + M$$

Scheme 1.2 The formation of ozone.

where M represents a non-reactive gas or particle.

The pollution by particulate matter (PM) in the air is mainly due to the various means of transport as described by Heywood [16]. The particles to be emitted as PM are born as soot nuclei in the highly oxygen-deficient core of fuel sprays. Particulate matter is a danger to human health. Fundamentally the danger arises from the size spectrum, many of the particles being small enough to bypass the respiratory system's defences e.g. mucous filtering. PM may also slow capillary function and cause bronchitis. Particles smaller than $5\mu m$ can enter the trachea and primary bronchi; those smaller than $1\mu m$ can reach the alveolae.

1.3.2.3 Ozone Layer Depletion

Ozone (O_3) forms a layer in the stratosphere, which is 15-35 km above the earth's surface. This ozone layer acts like a giant sunshade, protecting plants and animals from much of the sun's harmful ultraviolet (UV) radiation. A depletion of the ozone layer will increase the UV radiation at ground level, which may cause skin cancer, eye cataracts, damage to the immune system in animals as well as human beings and have an adverse effect on plant growth.

In recent decades, it has been found that the layer of ozone in the stratosphere is thinning. This thinning is particularly extensive over the poles and a hole has formed above the Antarctic. Research indicates that this depletion is caused by the emissions of halon (chlorinated and brominated organic compounds) and NO_x.

1.3.2.4 Global Climate Change

Besides noxious gases, the combustion of fossil fuels emits a large amount of CO_2,

which is known as a greenhouse gas. The accumulation of CO_2 has reached such an extent that global warming has become a most serious problem which has caused climate change. The rate of global warming has increased rapidly in recent decades. It is expected that global surface temperature could increase by 0.6-2.5°C in the next fifty years. Although other gases such as CH_4, CFCs (chloroflurocarbons) and N_2O also contribute to the global warming, CO_2 accounts for most.

1.3.3 Immediate Remedies for Control of the Environmental Impact

1.3.3.1 Policy Approach

To prevent significant changes to the environment, important policies have been made to put in place an effective international mechanism for the reduction of emissions of the six greenhouse effect gases. This includes the introduction of the Kyoto Protocol in 1997, and the six gases are CO_2, CO, CH_4, hydrofluorocarbons (HFCs), perfluorocarbons (PFCs) and sulfur hexafluoride (SF_6). Meanwhile, more and more strict regulations have been introduced to enforce emission standards. For example, the EU Emission Standards for passenger cars and light vehicles decrease the allowable emissions to a much lower level than before.

1.3.3.2 Technological Approach

Two aspects of work have been undertaken to reduce the environmental impact of fossil fuels from a technological way: combustion of fossil fuels in an environmentally benign manner and post-treatment of exhaust gases to minimize their emission to the environment.

The combustion efficiency of coal has been improved mainly by the introduction of pulverized fuel boilers, where coal is ground into power of about 100 μm in size. In the 1970s and 1980s, fluidised bed boilers were developed and represent a great advance. The most commonly used process is circulating fluidised bed combustion. Recently, pressurized fluidised bed combustion has been developed to improve combustion efficiency, where the operating pressure is about 10 bar.

In the fluidised bed, most of the sulphur compounds are removed at source by introducing limestone particles into the bed. The SO_2 reacts with the limestone to produce calcium sulphate. NO_x is reduced by maintaining the bed temperature under 1000°C. The

particulate matter produced is removed by post treatment of the flue gas [7].

The combustion efficiency of oil has been mainly improved by reforming techniques. Fuel reforming is the process of turning the liquid fuel into a gaseous one. This concept was brought forward because fuel reforming produces hydrogen-rich gaseous fuel, which can not only lower pollutant emissions but also extend the lean limit of conventional fuels to achieve higher efficiency. Collier et al [17] have shown that feeding hydrogen containing gaseous fuel mixture to an internal combustion engine is quite successful in minimizing emission of NO_x to below 200 ppm.

Through improving combustion efficiency, the production of noxious gases and particulate matter is reduced significantly. To further lower hazardous emissions, post treatments of the exhaust are often carried out through catalytic decomposition of NO_x to N_2 and O_2 and oxidation of CO to CO_2. In a stationary source of noxious gas emissions, a demonstrated technology for NO removal in the flue gas is commercially available. It is known as selective catalytic reduction and uses V_2O_5-TiO_2 supported on ceramic or metallic monolith as catalyst(s)[18]. Other technologies under development for flue gas clean up include the thermal $DeNO_x$, urea injection, NO_xSO, the copper catalyst method and lean combustion [19]. With regard to mobile emission sources, the three-way catalyst in the automobile exhaust line controls NO_x, hydrocarbons and CO emissions well. The three-way catalysts are able to oxidise carbon monoxide and hydrocarbons and, at the same time, reduce oxides of nitrogen [20]. Most strategies for controlling ambient ozone concentrations are based on the control of hydrocarbons, CO and NO_x via catalytic converters. All of these methods have some problems such as catalyst poison, high cost and difficulty in control (usually needing a microprocessor). Moreover, the emission of CO_2 is inevitable when fossil fuels are used.

1.4 Development of Sustainable and Clean Energies

A once and for all solution to the use of fossil fuels is to develop clean and renewable energies to replace fossil fuels. The various renewable energy sources developed so far are listed in Table 1.2. It can be seen that there is a long way to go to get the renewable energy sources to play a leading role. Even intervention at government level to encourage new technologies may have comparatively little impact. This is because good operating practice generally develops gradually and it is also necessary to establish a strong

14

manufacturing base.

Table 1.2 Renewable energy sources and the means of utilization.

Energy source	Energy utilization	Availability
Agriculture and forestry waste	Combustion process	Now
Energy crops	Combustion process	Now
Landfill and sewage gas	Combustion process	Now
Municipal solid waste	Combustion process	Now
Direct solar (active and passive)	Heating	Now
Geothermal	Heating/electricity	Now/limited scope
Hydro power	Electricity	Now
Wind power	Electricity	Now and developing
Hydrogen/Fuel cells	Electricity	Now and developing
Solar photovoltaic	Electricity	Now and developing
Tidal power	Electricity	Now/limited scope
Wave power	Electricity	Medium-/long-term
Solar-thermal	Electricity	Medium-/long-term

Bio-fuels are not clean (their combustion products contain carbon dioxide). Geothermal energy, hydropower and wind energy are region-restricted. The most promising renewable energies should be solar energy and hydrogen fuel since there are no harmful by-products. In this section, solar energy exploitation is briefly introduced.

Solar energy is free and renewable for the sun should continue to supply power for another 5 billion years [11]. The use of solar energy is demonstrated in three options: solar thermal, solar photovoltaic and solar power plant [13]. Solar thermal refers to the use of solar energy in a collectors such as solar hot water heaters, solar cookers, solar dryers, and in solar desalination, which are commonly used in Jordan [21] and in Pakistan [22]. Solar power plant is the use of solar energy on a large scale such as the 350 kW power plant in Saudi Arab [23].

The conversion of solar energy into electricity is mainly by photovoltaic (PV) cells, which are devices that convert sunlight directly to electricity, bypassing thermodynamic cycles and mechanical generators. PV stands for photo (light) and voltaic (electricity), whereby sunlight photons free electrons from silicon to generate electricity. This phenomenon was first discovered by the French physicist Edmond Becquerel in the 18th century. The photovoltaic cells were developed at Bell Labs in 1950, primarily for space applications.

Photovoltaic cells are made of semi-conducting materials (usually silicon). The use of silicon crystals in the photovoltaic cells is expensive. First of all, silicon crystals are currently assembled manually. Secondly, silicon purification is difficult and a lot of silicon is wasted. In addition, the operation of silicon cells requires a cooling system because performance degrades at high temperatures. Therefore, the share of world consumption is extremely small. However, it has convinced analysts that solar cells will become a significant source of energy by the end of the century.

Hydrogen energy is universal and clean since its combustion product is only water. It has attracted extensive research regarding its production, storage and application. In the following sections, a detailed review will be presented on hydrogen, its production and its storage.

1.5 Hydrogen

1.5.1 Occurrence of Hydrogen

Hydrogen is the lightest element and accounts for about 73% of the observed mass of the universe [24]. It is believed that hydrogen atoms were the first atoms to form in the early universe and that the atoms of the other elements formed later from the hydrogen atoms.

Hydrogen is the tenth most common element on earth, where it is found primarily in water and organic compounds. However, since it is so light, hydrogen accounts for less than 1% earth's total mass. Pure hydrogen gas rarely occurs in nature, although volcanoes and some oil wells release small amounts of hydrogen gas. Many minerals and all living organisms contain hydrogen compounds.

1.5.2 Atomic and Physical Properties of Hydrogen

A hydrogen atom contains one proton and one electron. Pure hydrogen exists as hydrogen

gas (hydrogen molecules), in which pairs of hydrogen atoms are bonded together. Data on the atomic structure of hydrogen is provided in Table 1.3 and its physical properties are given in Table 1.4.

In the ionic compounds of hydrogen with metals, hydrogen can exist either in the form of an anion H^- or in the form of cation H^+. In hydrocarbon molecules, hydrogen atoms form covalent bonds with other atoms. Hydrogen can also behave like a metal and form alloys with metals or intermetallic compounds at ambient temperatures [25].

Table 1.3 Atomic structure of hydrogen.
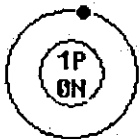
Atomic Radium	0.79Å
Atomic Volume	14.4cm^3/mol
Covalent Radius	0.32 Å
Cross Section	$0.33*10^{-24}$cm^2
Crystal Structure	Hexagonal
Electron Configuration	1s^1
Electrons per Energy Level	1
Shell Model	
Ionic Radius	0.012 Å
Filling Orbital	1s^1
Number of Electrons	1
Number of Neutrons (Stable nuclide)	0
Number of Protons	1
Oxidation States	1
Valance Electrons	1s^1
Electro negativity (Pauling)	2.2
Ionisation Potential (eV)	13.598
Valance Electron Potential (-eV)	1200

18

Table 1.4 Physical properties of hydrogen.

Description	Tasteless, colourless, odourless and extremely flammable gas
Atomic Mass Average	1.00794(7)
Boiling Point	- 252.732 °C
Density	0.0899 g L^{-1} at 0°C and 1bar
Enthalpy of Atomisation	217.6 kJ mol^{-1} at 298K
Enthalpy of Fusion	0.059 kJ mol^{-1}
Enthalpy of Vaporization	0.449 kJ mol^{-1}
Auto Ignition Temperature	500°C
Explosive Limits	Lower (LEL): 17%, Upper (UEL): 56%
Flammable Limits	Lower (LFL): 4%, Upper (UFL): 75%
Flash point	- 253 °C
Melting Point	- 258.975 °C
Molar Volume	14.1 cm^3 mol^{-1}
Optical Refractive Index	1.000132 (gas), 1.12 (liquid)
Relative Gas Density (Air = 1)	0.0694
Specific Heat	14.304 J g^{-1} K^{-1}
Vapour Pressure	1570 mmHg at –250 °C
Critical point	- 240.15°C

The phase diagram of hydrogen is shown in Figure 1.3. At a temperature of $-262^{\circ}C$, hydrogen becomes a solid with a density of 70.6 kg m^{-3}. At 0°C and 1 bar, the density of the gas is 0.089886 kg m^{-3}. Hydrogen is a liquid in a small zone between the triple and critical points with a density of 70.8 kg m^{-3} [26]. At ambient temperature, hydrogen gas can be described using the Van der Waals equation (1.3).

$$\left(p + \frac{0.02476n^2}{V^2}\right)(V - 0.00002661n) = nRT \tag{1.3}$$

where p is the gas pressure (Pa), V the volume (m^3), T the temperature (K), n the number of moles, and R the gas constant (8.314 J mol^{-1} K^{-1}).
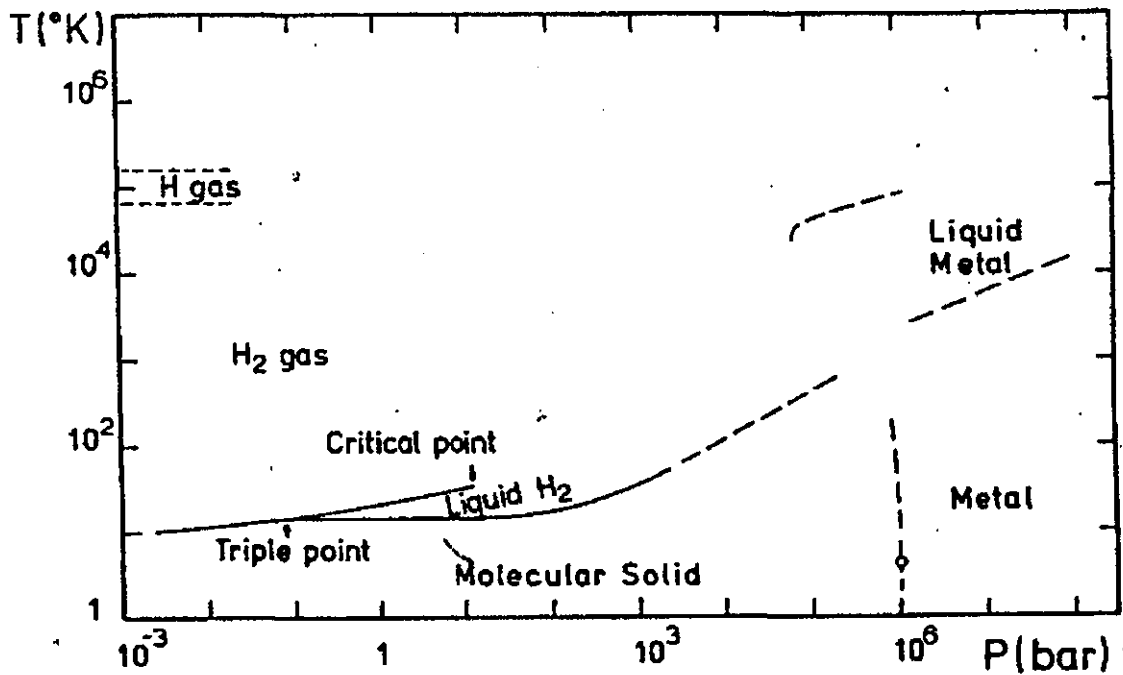

Figure 1.3 Phase diagram for hydrogen [25].

20

1.5.3 Hydrogen Production

As reviewed in the previous sections, hydrogen is the most abundant element in the universe. However, it mostly occurs in the form of water and hydrocarbons on earth. Hence it needs to be produced or, strictly speaking, extracted from other sources in order to facilitate its widespread use as a fuel. In the following, the main methods of extracting hydrogen are reviewed.

1.5.3.1 Hydrocarbon Reforming

The reason for the use of hydrogen as a fuel is to reduce the environmental impact of fossil fuels and the concerns over their depletion. Thus it seems ridiculous to produce hydrogen from hydrocarbons. However, currently hydrogen is produced by this method. On the other hand, a lot of research has shown that the extraction of hydrogen from hydrocarbons and the use of this hydrogen to fuel cells to produce energy can reduce emissions [27]. Hydrocarbon reforming uses heat and chemical reactions to convert hydrocarbon feedstocks into hydrogen. The feedstocks include natural gas, petrol, alcohols and biomass. So far three processes are used for the reforming. They are steam reforming, auto-thermal decomposition and partial oxidation.

Steam reforming

Steam reforming is the oldest method for reforming hydrocarbon feedstock to produce hydrogen. In this process, a hydrocarbon is converted to synthesis gas (H_2, CO and CO_2) by addition of steam in the presence of a nickel-based catalyst. The synthesis gas then undergoes a water shift reaction to increase the concentration of hydrogen in the product gas. Steam reforming is mainly used for light hydrocarbons because of the problems of soot formation with heavier hydrocarbons [28]. The reactions involved during hydrocarbon steam reforming are shown in Scheme 1.3.

$$CH_4 \ + \ H_2O \ \longrightarrow \ CO \ + \ 3\,H_2$$

$$C_mH_n \ + \ m\,H_2O \ \longrightarrow \ m\,CO \ + \ (m+1/2n)H_2$$

$$CO \ + \ H_2O \ \longrightarrow \ CO_2 \ + \ H_2$$
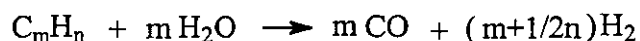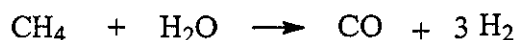
Scheme 1.3 Steam reforming of hydrocarbons.

The objective of a catalytic steam reforming process is to liberate the maximum quantity of hydrogen held in water and the feedstock fuel. Carbon in the fuel is converted into CO by oxidation with oxygen supplied in the steam. Hydrogen in the fuel, together with hydrogen in the steam, is released as free hydrogen. In other words, the resulting hydrogen comes from fuel as well as from the steam. The reaction is endothermic, i.e. it requires external heat input through a heat exchanger surface. In practice, a steam to carbon ratio in the range of 3.5 to 4.0 must be used to suppress soot formation. This has the effect of lowering the molar hydrogen output to 50% [29-31].

Partial Oxidation (POX)

Partial oxidation is based on extremely fuel-rich combustion (low air/fuel ratio). This technique involves the exothermic reaction of feed hydrocarbons in the presence of a small amount of air, such that incomplete combustion should occur. The extent of oxidation depends on the amount of oxygen used. The reformation reaction is followed by a shift reaction, where steam is used to convert carbon monoxide into hydrogen. POX is considered to be the most promising method after extensive reviews and case studies of the various reformer technologies [28]. The main reaction involved is shown in scheme 1.4.

$$CH_4 + 1/2O_2 \rightarrow CO + 2H_2$$

$$C_mH_n + (1/2)mO_2 \rightarrow mCO + (1/2)nH_2$$

$$CO + H_2O \rightarrow CO_2 + H_2$$
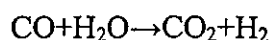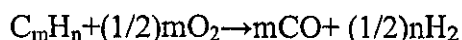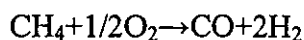
Scheme 1.4 Partial oxidation of hydrocarbon to convert it to hydrogen.

This process can be a non-catalytic flame reaction at high temperature (in the range 1000°C-1500°C) without catalysts. However, in the presence of a catalyst, the reaction temperature can be reduced, and the efficiency of hydrogen production depends on the catalyst.

The main challenge in partial oxidation is the development of efficient catalysts. There are mainly two components in the catalysts for POX. The first is one or more transition metal(s), especially the precious metals; the second is an oxide of a Group III or Group IV element[18].

Auto-Thermal Reforming (ATR)

Auto-thermal reforming is similar to partial oxidation in that the hydrocarbon feedstock is burned *in-situ*. However, ATR also resembles steam reforming in that steam is injected, and a catalyst is used to hasten the reactions and lower the reaction temperature. The steam reforming reaction utilises the heat produced by the partial oxidation reaction. Both a platinum based catalyst and a nickel based catalyst are used in this process. The reactions involved in ATR process are shown in scheme 1.5.

$$CH_4 + 1/2O_2 \rightarrow CO + 2H_2$$

$$C_mH_n + mH_2O \rightarrow mCO + (m + (1/2)n)H_2$$

$$CO + H_2O \rightarrow CO_2 + H_2$$
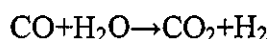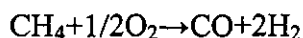
Scheme 1.5 Reactions involved in ATR process.

1.5.3.2 Water Electrolysis

Electrolysis is the process whereby electricity is passed through an electrolyte via electrodes in order to cause a non-spontaneous reaction to occur. Hydrogen reacting with oxygen to form water is a spontaneous reaction, while the reverse process is non-spontaneous. In order to produce hydrogen from water, an electrolytic cell is needed. Today, water electrolysis is one of the most utilized industrial processes for hydrogen production and all the on-site hydrogen generation and pure hydrogen requirements are

achieved by the electrolysis of water into hydrogen and oxygen.

1.5.3.3 Photo-Production

The photo-production method is to use sunlight for the splitting of water to produce hydrogen. This is one of the most promising ways and thus has promoted considerable research. The photo-production of hydrogen has been a goal of scientists and engineers since the early 1970s when Fujishima and Honda [32] reported the generation of hydrogen and oxygen in a photoelectrochemical cell using a titanium dioxide electrode illuminated with near ultraviolet light.

$$H_2O \xrightarrow{h\nu} H_2 + 1/2\,O_2$$
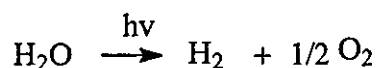
Scheme 1.6 The Photo-production of Hydrogen.

Pure water does not absorb solar radiation. Thus a sensitizer must be involved to induce the water-splitting reaction (Scheme 1.6): a molecule or semiconductor that can absorb sunlight to reach its excited state. According to the sensitizer, the system for carrying out this reaction can be classified into four categories: photochemical systems, semiconductor systems, photobiological systems and hybrid systems (a combination of the above systems).

There are three systems to produce hydrogen using this method, based on different sensitizers. Photochemical systems use a compound as sensitizer, semiconductor systems use a semiconductor as sensitizer and photobiological systems use a bacterium as the sensitizer (such as blue-green algae).

1.5.4 Hydrogen Storage

Interest in hydrogen as a fuel has grown dramatically and many advances in hydrogen production and utilisation technologies have been made. However, hydrogen storage technologies must be significantly advanced if a hydrogen based energy system is to be established, particularly if the intended use is in the transportation sector. The main obstacle in the way of a transition to a hydrogen economy at the present time is the absence of a practical means of hydrogen storage. For years the goal of researchers has

been to develop high-density hydrogen storage systems that can release hydrogen at temperatures lower than 100°C. A hydrogen economy will flourish when adequate storage technology exists, allowing people to tap and trade regional, renewable power sources. This cache of stored energy will offer viability to the full range of local and global renewable energy sources.

For practical use, the energy density for any storage methods must reach a high level. For example, the US Department of Energy (US DOE) recommended that an energy density of 6.5% and 62 kg m^{-3} must be achieved in order for a hydrogen storage system of appropriate weight and size to facilitate a fuel cell vehicle driving a distance of 560 km. Storing hydrogen is somewhat difficult due to its low density and low critical temperature. Currently, there are a number of technologies available for hydrogen storage and they are still rapidly evolving.

- High pressure gas cylinders (up to 800 bar)
- Liquid hydrogen in cryogenic tanks
- Adsorbed hydrogen on materials with a large specific surface area (at T < 100 K)
- Metal hydrides

1.5.4.1 Compressed Hydrogen at Higher Pressure

Storage as a compressed gas is inexpensive and provides for ease of operation but its weight and bulk are the main problem apart from fire/explosion risk. Generally, the common gas cylinder has a maximum pressure of 200 bar. New lightweight composite cylinders have been developed which support pressures of up to 800 bar, allowing hydrogen to reach a volumetric density of 36 kg m^{-3} [26]. To store a practical quantity for vehicles in high pressure vessels would result in a very large and heavy storage system. In addition, the storage of any high-pressure gas presents a safety hazard in the event of vehicle collision and the safety of pressurized cylinders is an issue of concern especially in highly populated regions. Additionally, compression of hydrogen gas, up to say 35 MPa, consumes nearly 20% of its total energy content.

1.5.4.2 Liquefied Hydrogen Storage

Hydrogen can be stored as a liquid at –253°C in a super insulated tank. The volumetric

density of liquid hydrogen is 70.8 kg m^{-3}. This method is the most frequently used fuel in space travel. For use as a fuel in automobiles, it presents too many problems to be practical, such as refuelling and a complex insulating system that is required to keep the temperature as low as $-253°C$. Moreover, loss rates of 1-2% per day have to be countered, and there is a 10-25% fuel boiling off during refuelling [33]. The cost and energy associated with the liquefaction process must also be considered, which consumes nearly 30% of the total energy contained in the hydrogen.

1.5.4.3 Slush Hydrogen

A mixture of about 50% solid and 50% liquid hydrogen at the triple point temperature (-259°C) and the correspondent vapour pressure (0.07 bar) is called 'slush hydrogen'. Its higher density (15% more than liquid hydrogen) and higher refrigeration capacity (18% more) as well as its flow behaviour similar to the liquid phase have been considered an advantage and this was investigated for space flight in the 1960s and for the planned supersonic space shuttle carrier in the 1980s [34]. The idea was abandoned due to, among others reasons, the high production costs and the difficult handling caused by the fact that the vapour pressure is lower than the atmospheric pressure.

1.5.4.4 Adsorption

Adsorption of hydrogen on activated carbon materials or other nano-materials has attracted great attention in recent years. The adsorption techniques rely on the affinity of hydrogen and substrate atoms. Hydrogen is pumped into a container with a substrate of fine particles where it is held by the interactions.

One of the most exciting advances recently has been the announcement of carbon nanotube technology [35, 36]. It has been proposed that hydrogen can be adsorbed by nanotubes in two ways: physical adsorption and chemical adsorption. Physical adsorption occurs in carbon nanotubes by trapping hydrogen molecules inside the cylindrical structure of the nanotube or by trapping hydrogen in the interstitial sites between nanotubes [26]. The maximum energy density can reach 12.5 kg m^{-3} at 10 MPa and 300 K from a simulation study [37]. The amount of hydrogen adsorption depends on the characteristics of the nanotubes such as their size and surface activity, temperature and pressure. Chemisorption of hydrogen on carbon nanotubes occurs by hydrogen dissociation and reaction with carbon [38]. The storage capacity of carbon naontube can

be improved by doping with some nano-particles [39, 40].

It would be appropriate here to mention that there is a great deal of disagreement surrounding the capacity of carbons [41], and there is a big gap between the energy density and its requirement for vehicle use. Up to now, there are no indications that carbon nanostructures can adsorb unusually high amounts of hydrogen and that these novel materials can be utilized for hydrogen storage in technical applications.

Zeolite adsorbents are another class of materials for hydrogen storage [42, 43]. Zeolite has the structure of a molecular sieve. Hydrogen can be held within its microporous media. The best result at the present time is 9.2 ml H_2 per gram by using a sodalite zeolite [42].

Graphite is a new material for hydrogen storage [44]. This type of carbonaceous material was ignored previously. However, hydrogen could be stored between two basic planes of graphite. By a computer simulation, graphite may store hydrogen with a capacity that can satisfy the requirements of US DOE standard.

1.5.4.5 Metal Hydrides

Many metals and alloys are able to absorb large amounts of hydrogen to form metal hydrides according to reaction (Scheme 1.7):

$$Me+x/2H_2 \leftrightarrow MeH_x$$
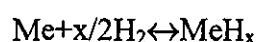
Scheme 1.7 Formation of metal hydrides.

where Me is a metal, a solid solution, or an intermetallic compound, MeH_x is the hydride and x the ratio of hydrogen to metal.

Metals can be charged with hydrogen using molecular hydrogen gas or hydrogen atoms from an electrolyte. The first step is the physisorbed state by Van der Waals force. The second step is the chemisorption, in which the hydrogen overcomes an activation barrier for dissociation and for the formation of the hydrogen metal bond. The third step is the diffusion of the dissociated hydrogen atoms rapidly through the bulk metal to form an M-H solid solution commonly referred to as α phase, where hydrogen occupies interstitial sites in many cases. The negative hydrogen is bonded ionically or covalently to a metal,

or is present as a solid solution in the metal lattice.

Besides binary metal hydrides, group 1, 2, 3 light metals, e.g. Li, Mg, B and Al can form a large variety of metal-hydrogen complexes, such as BH_4^-, AlH_4^-, and derivatives of these [26]. These complex metal hydrides are especially interesting for transport applications.

Thermal decomposition or pyrolysis of the metal hydrides is a reversible reaction. The metals can adsorb hydrogen and the hydrogen can be released when heat is applied. The decomposition of some metal hydrides is shown in Figure 1.4[45]. Work is being done on finding cheaper metal alloys which have the ability to absorb large amounts of hydrogen and at the same time release the hydrogen at a relatively low temperature. In this respect, $LiBH_4$ has been studied extensively [46].
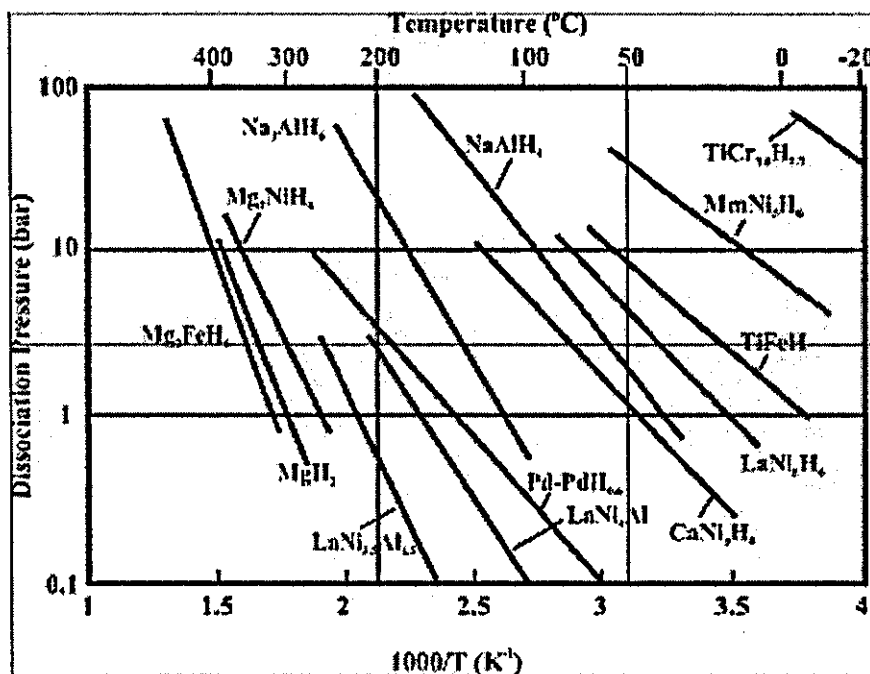
Figure 1.4 Van't Hoff plots of some technically important reversible metal hydrides.

The hydrolysis reaction is another method to release hydrogen from metal hydrides. Ever since World War II, lithium hydride (LiH), calcium hydride (CaH_2) and sodium borohydride ($NaBH_4$) have been used as fuel sources in case of emergency [47]. Since this reaction can extract hydrogen from water, the energy density is higher than thermal decomposition.

Most of the reactions between metal hydride and water are vigorous with a large amount of heat being released, which may cause an explosion. Therefore this reaction is difficult to control except in the case of sodium borohydride. Table 1.4 gives the heat released when one gram of hydrogen is produced by the reaction between water and different hydrides. It can be seen that the heat generated by the hydrolysis of sodium borohydride is only about 50% of that produced by the hydrolysis of other hydrides. It is therefore considerably safer compared with other hydrides such as LiH, LiAlH$_4$, NaAlH$_4$ and CaH$_2$.

Table 1.4 Heat released for 1 gram hydrogen with different hydrides [48].

Hydrides	NaBH$_4$	LiH	LiAlH$_4$	NaAlH$_4$	CaH$_2$
$\Delta H°$ (kJ g^{-1} H2)	-37.1	-54.3	-62.5	-56.2	-58.0

Another advantage of NaBH$_4$ as a hydrogen carrier is its high energy density. Assuming 100% stoichiometric conversion of NaBH$_4$, 37.8 g of NaBH$_4$ (1 mol) produces 8 g of hydrogen (4 mol), while more reagents by weight are needed for other reductants to produce the same amount of hydrogen. Table 1.5 lists the weight of reactants necessary to produce one gram of hydrogen. It is shown that the weight of NaBH$_4$ required to producing one gram of hydrogen is the least among the reactants except for LiH, while the reaction between LiH and water is vigorous and explosion inducing.

Table 1.5 Weight of hydrides necessary for generating one gram of hydrogen.

Metal hydrides	NaBH$_4$	LiH	LiAlH$_4$	NaAlH$_4$	CaH$_2$
Weight (g)	4.73	4.00	12.2	14.3	10.5

Therefore, the hydrolysis of sodium borohydride is the most effective, safe and controllable among the various hydrides, which renders it most suitable for generating hydrogen on-board.

1.5.4.6 Comparison of the Energy Density of Different Hydrogen Storage Methods

Five different hydrogen storage methods have been reviewed in this section. Although each method possesses desirable characteristics, no approach satisfies all of the efficiency, size, weight, cost and safety requirements for transport and utility use. The comparison

between the above methods is listed in Table 1.6, and the volumetric versus gravimetric hydrogen density for the various methods is shown in Figure 1.5.

High-pressure gas cylinders and liquid hydrogen technologies are well established. The energy density is low due to the weight of the cylinders. The liquid hydrogen method is very complex and not suitable for on-board applications. Although adsorption of hydrogen on carbonaceous materials has greatly advanced, there is still a gap between its capacity and requirements. It can be seen that only metal hydrides offer a safe and efficient way to store hydrogen. Direct thermal decomposition of metal hydrides is a reversible reaction. Research is being undertaken to lower the decomposition temperature. The hydrolysis reaction is not reversible. However, it can provide higher energy density since this reaction extracts one mole of hydrogen from water. Sodium borohydride is the most suitable material for hydrolysis due to the lower heats evolved and its higher hydrogen content. Extensive research is being performed for its commercilisation. This thesis mainly addresses the obstacles of using sodium borohydride as a hydrogen source.

Table 1.6 Comparison of the current hydrogen storage methods.

Storage method		Gravimetric density (mass%)	Volumetric density (kg H_2 m^{-3})	Temperature (°C)	Pressure (bar)	Comments
High pressure gas cylinders		13	<40	Room temperature	800	Loss of 1-2% per day
Liquid hydrogen in cryogenic tanks		Size dependent	70.8	-252	1	
Hydrogen adsorption		2	20	-80	100	Usually carbonaceous materials
Metal hydrides	pyrolysis	<18	150	>100	1	Usually at elevated temperature
	hydrolysis	<40	>150	Room temperature	1	Not reversible

Figure 1.5 Comparison of different hydrogen storage methods[49].
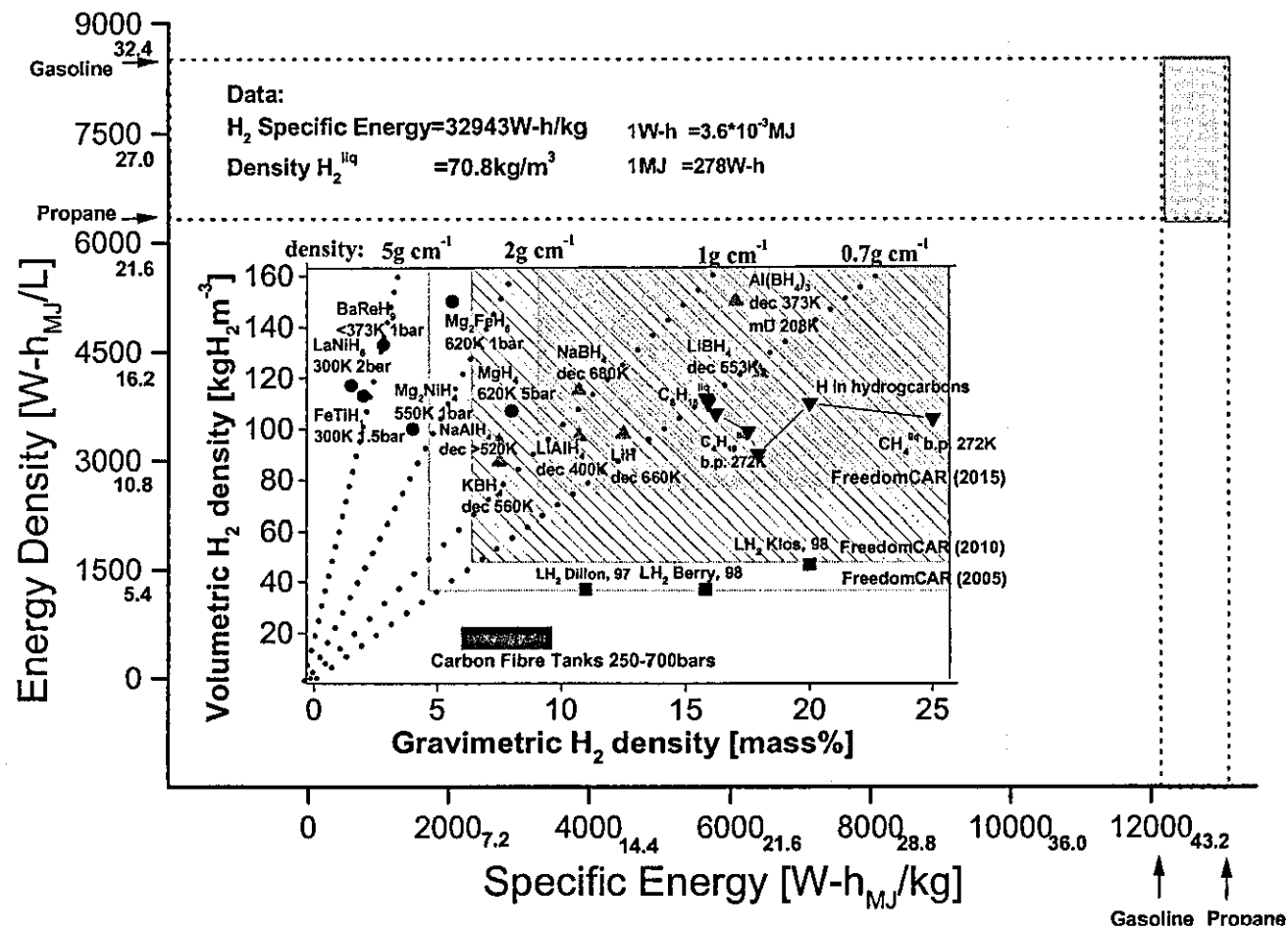
1.6 Summary

In this chapter, the current situation of world energy supply has been reviewed. Most of the problems are associated with the utilisation of fossil fuels, the use of which has caused extensive problems from air pollution to global warming. The main approach to this challenge is to develop clean and renewable energy.

Hydrogen is a universal energy. The use of hydrogen energy has therefore been studied extensively, from its production to usage. The main barrier hindering its wide application is the lack of efficient, low cost, and safe storage technologies for hydrogen. There are currently five main storage methods available: high-pressure cylinder, liquid hydrogen, slush hydrogen, hydrogen adsorption and metal hydrides. It is believed that the hydrolysis of an aqueous solution of sodium borohydride is a safe and efficient way to store hydrogen.

1.7 Thesis Organization

The later chapters of this thesis are organized as follows. Chapter 2 reviews $NaBH_4$ and its current status as a hydrogen storage method. Chapter 3 and 4 investigate the maximum concentration of $NaBH_4$ from a point of view of thermodynamics. Chapters 5-9 study the kinetics of hydrogen generation from $NaBH_4$ hydrolysis over metal catalyst. Chapter 10 concludes the thesis and recommends the future work.

1.8 References

1.   Olah, G.A., *Nonrenewable fossil fuels.* Chemical Engineering News, 1991. 11: p. 50-51.

2.   Andersson, L.A., *Hydrogen.* Microsoft Encarta Online Encyclopedia 2004, 2004: p. http://encarta.msn.com.

3.   Ramachandra, T.V., N.V. Joshi, and D.K. Subramanian, *Present and prospective role of bioenergy in regional energy system.* Renewable and Sustainable Energy Reviews, 2000. 4: p. 375-430.

4.   van Swaaj, W.P.M. and N.H. Afgan, *Heat and Mass transfer in fixed and fluidised bed.* 1985, Washington: Hemisphere Publishing Corporation.

5.   Barbier, E., *Geothermal energy technology and current status: an overview.* Renewable and Sustainable Energy Reviews, 2002. **6**: p. 3-65.

6.   Ackermann, T. and L. Soder, *Wind energy technology and current status: a review.* Renewable and Sustainable Energy Reviews, 2000. **4**: p. 315-374.

7.   Boyle, G., *Renewable Energy: Power for a sustainable future.* 2004, Oxford: Oxford University Press.

8.   Kim, J.-H., et al., *Production of hydrogen from sodium borohydride in alkaline solution: development of catalyst with high performance.* International Journal of Hydrogen Energy, 2004. **29**: p. 263-267.

9.   Richardson, B.S., J.F. Birdwell, and F.G. Pin, *Sodium borohydride based hybrid power system.* Journal of Power Sources, 2005. **145**: p. 21-29.

10.   Atkins, P.W. and J. de Paula, *Physical Chemistry.* 7th ed. 2002, Oxford: Oxford University Press. Chapter 9.

11.   Boyle, G., B. Everett, and J. Ramage, *Energy Systems and Sustainability.* 2003, Oxford: Oxford University Press. 23-28.

12.   Voorspools, K., *Sustainability of the future; rethinking the fundamentals of energy research.* Renewable and Sustainable Energy Reviews, 2004. **8**: p. 599-608.

13.   Afgan, N.H., *Sustainable energy development.* Renewable and Sustainable Energy Reviews, 1998. **2**: p. 235-286.

14.   *Key World Energy Statistics from the IEA.* 2004, International Energy Agency, Paris, France.

15.   Speight, J.G., *Environmental Technology Handbook.* 1996, Washington: Taylor and Francis.

16.   Heywood, J.B., *Internal Combustion Engine Fundamentals.* 1988, New York: McGraw-Hill.

17.   Collier, R.K.J., *Hydrogen enriched natural gas as a clean motor fuel.* 1997,

University of Central Florida (Orlando, FL): US 5660602.

18. Matsuda, S. and A. Kato, *Titanium oxide based catalysts - a review.* Applied Catalysis, 1983. **8**(2): p. 149-165.

19. Yeh, J.T., C.J. Drummond, and J.I. Fouber, *Process Simulation of the Fluidized-bed Copper Oxide Process Sulfation Reaction.* Environmental Progress, 1987. **6**(1): p. 44-50.

20. Taylor, K.C., *Catalysis and Automotive Pollutions Control*, ed. A. Crueg and A. Frennet. 1986, Amsterdam: Elsevier. 97.

21. Hrayshat, E.S. and M.S. Al-Soud, *Solar energy in Jordan: current state and prospects.* Renewable and Sustainable Energy Reviews, 2004. **8**: p. 193-200.

22. Mirza, U.K., M.M. Maroto-Valer, and N. Ahmad, *Status and outlook of solar energy use in Pakistan.* Renewable and Sustainable Energy Reviews, 2003. **7**: p. 501-514.

23. Alawaji, S.H., *Evaluation of solar energy research and its applications in Saudi Arabia-20 years of experience.* Renewable and Sustainable Energy Reviews, 2001. **5**: p. 59-77.

24. Knee, L.B.G. and C.M. Brunt, *A massive cloud of cold atomic hydrogen in the outer galaxy.* Nature, 2001. **412**(6844): p. 308-310.

25. Leung, W.B., N.H. March, and H. Motz, *Primitive phase diagram for hydrogen.* Physics Letters, 1976. **56**: p. 425-426.

26. Zuttel, A., *Materials for hydrogen storage.* Materials Today, 2003(9): p. 24-33.

27. Picazo, C.P.L., *Comparison of energy efficiency, emissions, and costs of internal combustion and fuel cell vehicles operating on various fuels*, in *Department of Civil Engineering.* 1999, MIT: Cambridge, MA.

28. Little, A.D., *Multi-fuel reformers for fuel cells used in transportation: Phase I. Final report.* 1994, US Department of Energy: Washington DC.

29. Minet, R.G., *Technical and Economic Advances in Steam Reforming of*

Hydrocarbons. 1980, Washington DC: American Chemical Society.

30. Houseman, C. *On board hydrogen generation for automobile*. in *The 11th Intersciety Energy Converson Engineering Conference*. 1976.

31. Houseman, J. and G.E. Voecks. *Hydrogen energies based on liquid fuels, A review: hydrogen energy progress*. in *Proceedings of 3rd World Hydrogen Energy Conference*. 1981. Tokyo: Pergamon Press.

32. Fujishima, A.K. and K. Honda, *Electrochemical photolysis of water at a semiconductor electrode*. Nature, 1972. **238**: p. 37-38.

33. Amann, C.A., *The passenger car and the greenhouse effect*. International Journal of Vehicle Design, 1992. **13**(4): p. 305-334.

34. DeWitt, R.L., et al., *Slush hydrogen (SLH$_2$) technology development for application to the National Aerospace Plane (NASP)*. Advances in Cryogenic Engineering, 1990. **35**: p. 1741-1754.

35. Dillon, A.C., et al., *Storage of hydrogen in single-walled carbon nanotubes*. Nature, 1997. **386**: p. 377-379.

36. Ye, Y., et al., *Hydrogen adsorption and cohesive energy of single-walled carbon nanotubes*. Applied Physics Letters, 1999. **74**: p. 2307-2309.

37. Rzepka, M., P. Lamp, and M.A. de la Casa-Lillo, *Pysisorption of hydrogen on microporous carbon and carbon nanotubes*. Journal of Chemical Physics, 1998. **102**: p. 10894.

38. Liu, C., et al., *Hydrogen storage in single-walled carbon nanotubes at room temperature*. Scicence, 1999. **285**: p. 1127.

39. Bogdanovic, B., et al., *Improved hydrogen storage properties of Ti-doped sodium alanate using titanium nanoparticles as doping agents*. Advanced Materials, 2003. **15**(12): p. 1012-1015.

40. Zidan, R. and A.M. Rao. *Doped carbon nanotubes for hydrogen storage*. in *Proceedings of the 2002 U.S. DOE hydrogen program review*. 2002.

41. Hirscher, M., et al., *Hydrogen storage in sonicated carbon materials.* Applied Physics A: Materials Science & Processing, 2001. **72**(2): p. 129-132.

42. Weitkamp, J., *Zeolites as media for hydrogen storage.* International Journal of Hydrogen Energy, 1995. **20**: p. 967-970.

43. Fraenkel, D. and J. Shabtai, *Encapsulation of hydrogen in molecular sieve zeolites.* Journal of American Chemical Society, 1977. **99**(21): p. 7074-7076.

44. Tse, J., *New look for hydrogen storage.* Proceedings of National Academy of Science, 2005. **to be published.**

45. Bogdanovic, B., et al., *Metal-doped sodium aluminium hydrides as potential new hydrogen storage materials.* Journal of Alloys and Compounds, 2000. **302**: p. 36-58.

46. Zuttel, A., et al., *LiBH₄ a new hydrogen storage material.* Journal of Power Sources, 2003. **118**(1-2): p. 1-7.

47. Mellor, J.W., *Supplement to Mellor's comprehensive treatise on inorganic and theoretical chemistry.* Vol. 5 Boron-Hydrogen compounds. 1981, London: London: Longman. 223.

48. Dean, J.A. and N.A. Lange, *Lange's Handbook of Chemistry.* 15th ed. 1999: New York: McGraw-Hill.

49. Zuttel, A. and L. Sclapbach, *Hydrogen-storage materials for mobile applications.* Nature, 2001. **414**: p. 353-358.

Chapter 2

Overview of Sodium Borohydride Hydrolysis for Hydrogen Generation

2.1 Introduction

The discovery of sodium borohydride by H. J. Schlesinger, H.C. Brown, H. R. Hoeckstra, and L. R. Rapp can be traced back to 1942 [1]. It was first synthesized as a consequence of the atomic bomb related efforts at the University of Chicago, together with many novel compounds containing boron and hydrogen. Soon after its discovery, it was found that this compound could be used as a hydrogen generation agent. After that, its chemical and physical properties were studied in detail. Extensive research of its synthesis and application was mainly conducted in 1950s. In the 1990s, the hydrolysis of $NaBH_4$ has been actively investigated due to the strong desire to look for alternative clean energies. In this chapter, a detailed review is given of the production, hydrolysis and applications of sodium borohydride, as well as the routes for transformation of sodium metaborate back to sodium borohydride.

2.2 Production of $NaBH_4$

Over 100 methods for the preparation of sodium borohydride have been described, but few of these have achieved any practical significance. There are two main technologies to produce it: one is the organic process (the Schlesiger method) and the other is the inorganic process (Bayer method).

2.2.1 Organic Process (Schlesiger Method)

The Schlesiger method to manufacture $NaBH_4$ uses sodium hydride and trimethyl borate in a mineral oil medium at about 275°C [2]. The flow diagram of the process is shown schematically in Figure 2.1, and the main reaction is given in Scheme 2.1.
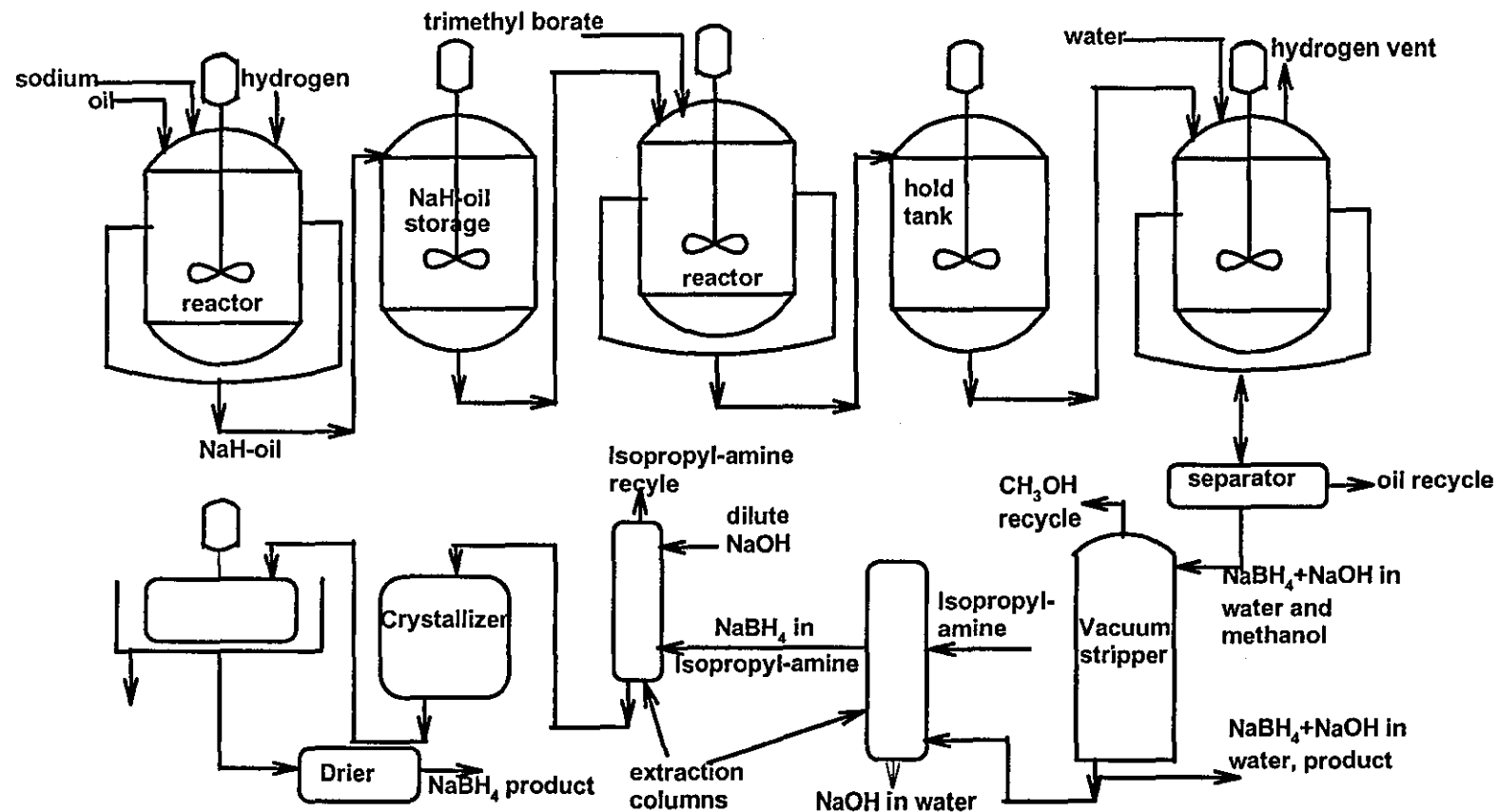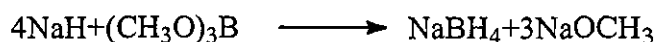
37

Figure 2.1 The Schlesiger process for production of NaBH₄.

$$4NaH + (CH_3O)_3B \longrightarrow NaBH_4 + 3NaOCH_3$$

Scheme 2.1 Organic process for preparation of sodium borohydride.

In this process, sodium hydride is prepared in mineral oil in a reactor and then transferred to another reactor, where trimethyl borate is added to react with the sodium hydride forming sodium borohydride. After that, a complex separation procedure is performed to recover pure sodium borohydride. The yield is over 90%.

2.2.2 Inorganic Process

This process was first developed by the Bayer Company [3], and is referred to as the Bayer process. The flow diagram of the Bayer method is shown schematically in Figure 2.2, and the main reaction is given in Scheme 2.2.

$$Na_2B_4O_7 \cdot 7SiO_2 + 16Na + 8H_2 \longrightarrow 4NaBH_4 + 7Na_2SiO_3$$
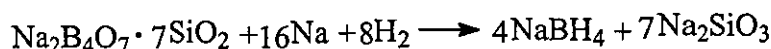
Scheme 2.2 The main reaction in the Bayer process.

In this process, the borosilicate ($Na_2B_4O_7.7SiO_2$) is produced by the fusion of borax ($Na_2B_4O_7$) and quartz sand (SiO_2). The borosilicate is cooled, ground, and then reacted with sodium in an atmosphere of hydrogen at 300 kPa and 400-500°C in a partly heterogeneous reaction. The sodium borohydride is extracted from the borosilicate-silicate mixture with liquid ammonia under pressure. The yield is over 90%.
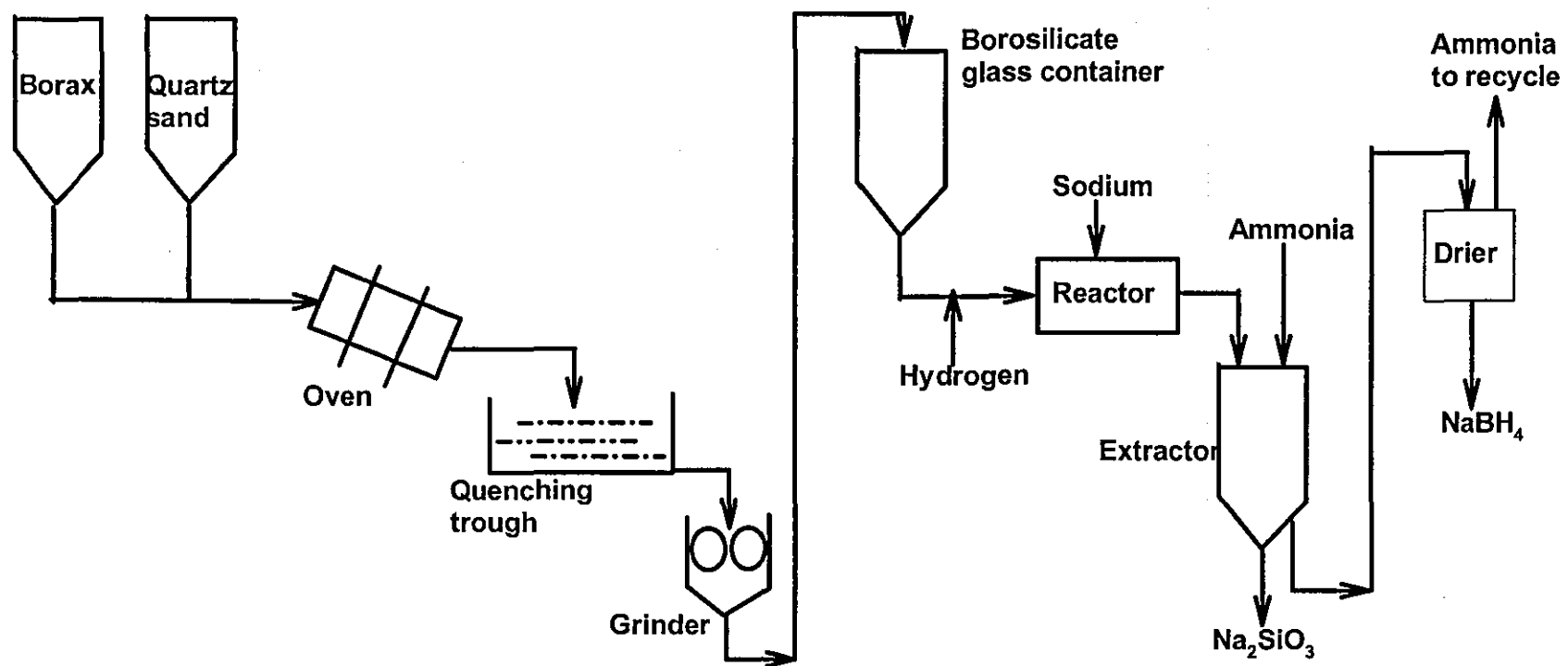
Figure 2.2 The Bayer process for production of NaBH₄.

2.3 Properties of NaBH₄

In order to better understand the hydrolysis reaction to produce hydrogen from NaBH₄, its main properties are introduced in this section. The physical and thermodynamic properties are listed in Table 2.1 and 2.2 respectively, which were mainly obtained from spectroscopic studies [4].

Table 2.1 Physical properties of sodium borohydride

Molecular weight	37.84
Colour	White
Crystalline form (anhydrous)	Face centred cubic a = 6.15Å
Melting point	505°C (10 bar H₂) Decomposes above 400° C in vacuum
Thermal stability	Will not ignite above 400°C on a hot plate. Ignites from free flame in air, Burning quietly
Density (g/cm³)	1.074

Table 2.2 Thermodynamic properties of sodium borohydride [4-7]

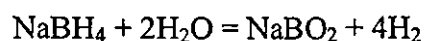| Sodium borohydride	
Free energy of formation	- 125.82 kJ mol^{-1}
Heat of formation	- 190.32 kJ mol^{-1}
Entropy	101.41 J mol^{-1} K^{-1}
Heat capacity	86.40 J mol^{-1} K^{-1}
Free energy of ionisation $NaBH_4(s)=Na^++BH_4^-$	- 23.66 kJ mol^{-1}
Borohydride ion BH$_4^-$	
Free energy of formation	- 119.55 kJ mol^{-1}
Heat of Formation	51.83 kJ mol^{-1}
Entropy	106.59 J mol^{-1} K^{-1}
Heat of hydrolysis $BH_4^-+H^++3H_2O(liq)=H_3BO_3+4H_2(g)$	- 371.18 kJ mol^{-1}
Half electric reaction $BH_4^-+8OH^-=B(OH)_4^-+4H_2O+8e^-$	1.24 V

An important physical property is its solubility in water, which is related to hydrolysis reaction. Jensen [8] has accurately measured the solubility of sodium borohydride in water at the different temperatures, and the results are reproduced in Figure 2.3. The data presented in Figure 2.3 shows the equilibrium temperature of the two crystal forms $NaBH_4$ and $NaBH_4$ $2H_2O$. The curve below 36.4°C represents the solubility of the dihydrate, and above 36.4°C, the solubility of anhydrous $NaBH_4$.

Table 5.4 Sieve set and catalyst size

Sieve aperture (μm)	Average catalyst size (μm)
600	–
500	550.
106	–
90	98
53	–
45	49
32	–
25	29

5.4.3 Experimental set-up to monitor reaction rate

For kinetic research, the change in concentration of $NaBH_4$ with respect to time should be monitored. The measurement of the concentration of $NaBH_4$ is rather difficult due to its hydrolysis even at room temperature. In this study, a method for measuring the hydrogen volume with time was used, since hydrogen volume and $NaBH_4$ concentration can be related using the stoichiometric coefficients in the following reaction scheme.

$$NaBH_4 + 2H_2O = NaBO_2 + 4H_2$$

A schematic diagram for the experimental set-up is shown in Figure 5.6. The rig consisted of three parts: the reaction system, a sytem to monitor temperature and a system to measure the volume of hydrogen that is generated. The reaction system consists of a three-port reactor and a magnetic stirrer, a water bath that was used to adjust reaction temperature and a feeding system. One side-port of the reactor was equipped with a thermocouple and another side-port was connected to the water replacement system. The middle port of the reactor was used to site a feeding funnel. Since $NaBH_4$ can be hydrolysed even at room temperature when contacting water, a special feeding system was used as shown in Figure 5.6. $NaBH_4$ and catalyst were added to the reactor first and then water was added through the feeding system to the reactor. Once the chemicals come into contact, hydrogen is produced and the amount that was generated was recorded.

The volume of hydrogen that was produced was measured using a water replacement system. The water replacement system consisted of a graduated cylinder full of water and a water reservoir that was used to immerse the cylinder. A container was placed onto an electronic balance. Before starting the experiment, the water in the reservoir was filled to such a level that any extra water would overflow from the cylinder through a slope into the container on the balance. The electronic balance was connected to a computer using a standard RS232 connector. Software provided by the balance manufacturer was used to record the time and the weight of the water displaced from the cylinder. The time interval for recording the weight was one second. Both the software and the electronic balance were purchased from A & D Company Ltd. (UK).

In order to monitor the temperature of the reaction system, a thermocouple was put into a side port of the reactor. This K-type thermocouple was connected to a data logger, which transferred the information to a computer. The data logger and the thermocouple were purchased from Pico Company Ltd (UK).

Before conducting the experiment, the reactor was cleaned using distilled water and then dried in an oven for 24 hours. After the temperature was stable, the reactor was put into the water bath with a fixed amount of catalyst inside. A pre-determined amount of $NaBH_4$ powder was then put into the reactor. After all these were ready, the cork of the feeding funnel was opened to let the water flow into the reactor to start the hydrolysis. The water that was displaced by the hydrogen production and the overall reaction temperature were both monitored by using the computer. When calculating the reaction rate, the saturated vapour pressure at room temperature was considered.

The amount of catalyst that was used was based on the convenience of reaction control. Reaction rate for heterogeneous catalysis is proportional to the mass of catalyst. The rate data is based on unit mass of catalyst.
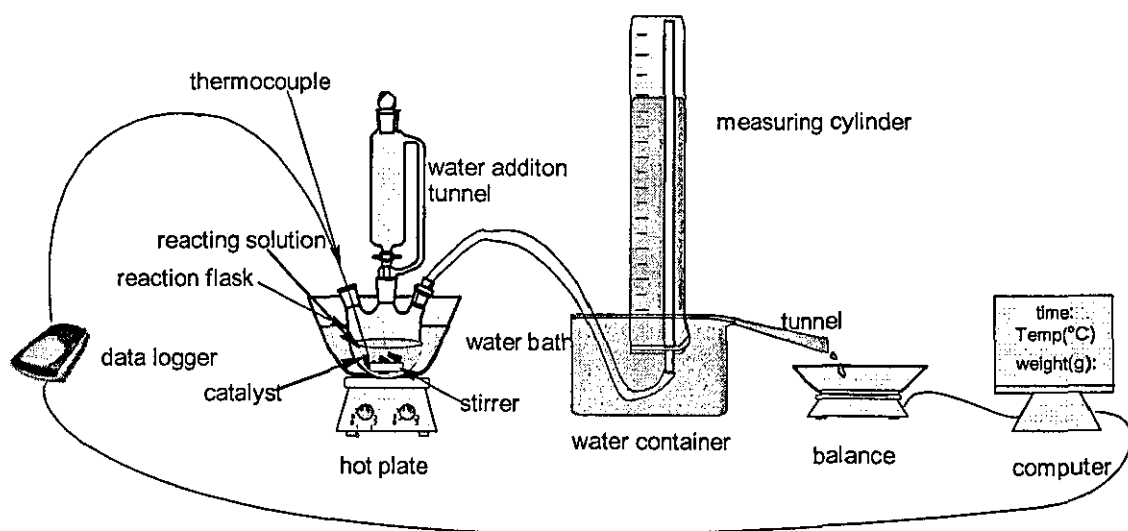
Figure 5.6 A schematic experimental set-up for the research of NaBH₄ hydrolysis kinetics.

5.4.4 Analysis of non-isothermal rate data in order to obtain isothermal rate data

The general analysis process is described briefly as follows and a detailed procedure will be described together with results and discussion in later chapters.

The rate for any reaction can be expressed using equation (5.11).

$$r = Ae^{-E/RT}C^{\alpha} \tag{5.11}$$

Where r is the reaction rate, E is the activation energy, R is the universal gas constant, T is the temperature, C is the concentration of reactant, α is the reaction order, and A is the pre-exponential factor.

To deriving isothermal rate data from non-isothermal rate data, take logarithms of both sides, yielding

$$\ln r = \ln A + \alpha \ln C - \frac{E}{RT} \tag{5.12}$$

Since A and α are constants for a specific reaction, ln$r$ against $1/T$ will have a linear relationship when C is fixed. In the following, the determination of the parameters (lnA + αlnC) and E/R is given using the illustration in Figure 5.6.

144

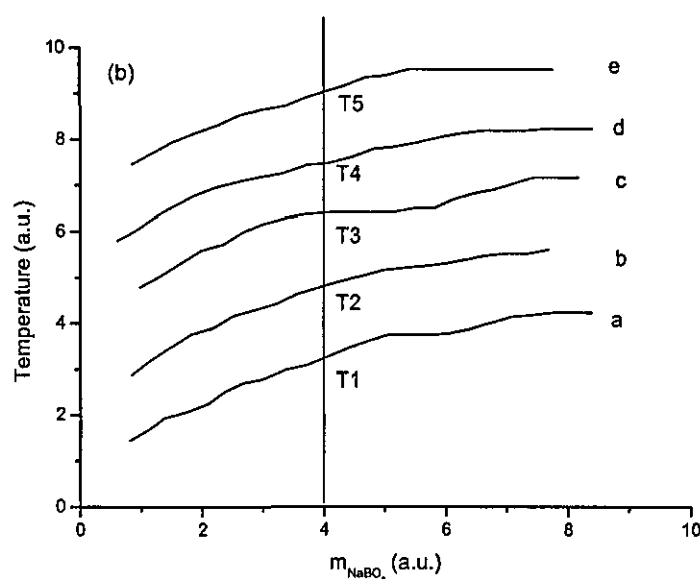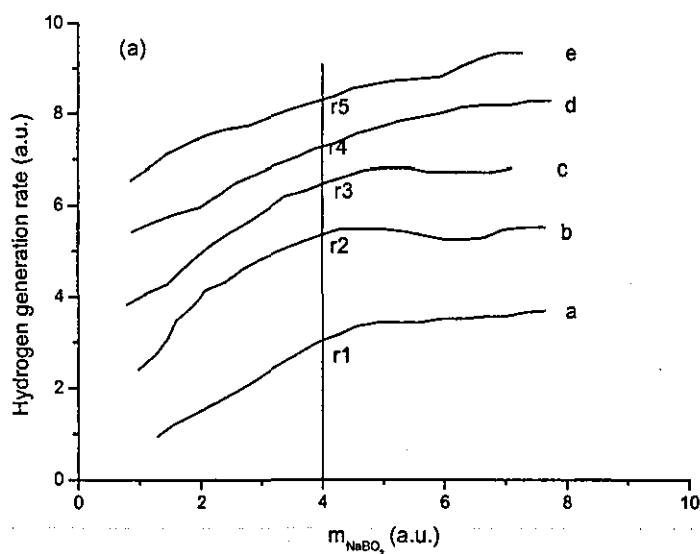**Figure 5.6** Schematic graphs showing analysis of non-isothermal rate data to obtain isothermal rate data, (a) reaction rate $\sim m_{NaBO2}$, (b) temperature $\sim m_{NaBO2}$.

As shown in Figure 5.6a and b, five runs (a, b, c, d and e) are performed with the same initial $NaBH_4$ concentration and the same amount of catalyst but with a different initial reaction temperature. The extent of the reaction is indicated using the concentration of $NaBO_2$. The initial temperature increases steadily from a to e. The reaction temperatures and rates are measured simultaneously with time as shown in Figures 5.6a and b

145

respectively.

At a given $NaBO_2$ concentration, such as in the position of the vertical line, five different rates (r_1, r_2, r_3, r_4 and r_5) can be obtained from Figure 5.6a, and the corresponding temperatures (T_1, T_2, T_3, T_4 and T_5) can be obtained from Figure 5.6b. When the reaction rates and the corresponding reciprocal temperatures ($1/T$) are plotted the result should be linear, with a slope corresponding to $-E/R$, and an intercept on the y axis of $\ln A + \alpha \ln C$. Hence equation (5.12) is determined, which can be then used to calculate the reaction rate at any temperature when the concentration of $NaBO_2$ is m_{NaBO2}. In the same way, equations for any other $NaBO_2$ concentrations can be determined. Reaction rates at these $NaBO_2$ concentrations can also be determined for any temperature. Through this method, isothermal reaction rates are obtained for different $NaBO_2$ concentrations.

If five groups of the above experiments are performed, each of which has a different initial $NaBH_4$ concentration, then equation (5.12) can be determined at the same $NaBO_2$ concentration in each group. Since initial $NaBH_4$ concentration in each group is different, the rate at different $NaBH_4$ concentrations is obtained with the same $NaBO_2$ concentration and temperature.

Therefore, the following procedures are used for each group of experiments.

- Hydrogen release experiments were conducted to obtain $V_{H2} \sim t$, and $T \sim t$.
- Transform $V_{H2} \sim t$ to $r_{H2} \sim t$ by differentiation.
- Transform $r_{H2} \sim t$ to $r_{H2} \sim m_{NaBO_2}$, and $T \sim t$ to $T \sim m_{NaBO_2}$ by using equations (5.13) or (5.14).
- Using the relationship $r_{H2} \sim m_{NaBO_2}$ and $T \sim m_{NaBO_2}$, plot $\ln r_{H2} \sim 1/T$.
- Derive the reaction rate for any temperature at specific $NaBH_4$ or $NaBO_2$ concentrations.

$$m_{NaBO_2} = \frac{(P_0 - P_{H_2O})V_{H_2}/(4RT)}{w_{H_2O}^0 - (P_0 - P_{H_2O})V_{H_2}M_{H_2O}/(2RT)}$$ (5.13)

146

$$m_{NaBH_4} = \frac{w^0_{NaBH_4} - [(P_0 - P_{H_2O})V_{H_2}M_{NaBH_4}]/(4RT)}{M_{NaBH_4}[w^0_{H_2O} - (P_0 - P_{H_2O})V_{H_2}M_{H_2O}/(2RT)]} \qquad (5.14)$$

Where V_{H2} is the volume of hydrogen released at time t, T is the reaction temperature, r_{H2} is the hydrogen generation rate, w is mass, P_0 is atmospheric pressure (assumed to be 101325 Pa), P_{H2O} represents saturated vapour pressure at ambient temperature for measuring hydrogen volume, M is the molecular mass, V is the volume, and R is the universal gas constant (8.314 J mol^{-1} K^{-1}). The superscript 0 represents initial value.

5.5 Summary

In this chapter, the fundamentals of heterogeneous catalysis are reviewed. When deriving intrinsic kinetic equations for the hydrolysis of NaBH$_4$, diffusion limitations must be removed including both heat and mass transfer. Due to the extensive heat effect, an isothermal heterogeneous reaction is difficult to perform.

A rig has been designed to monitor the kinetics thorough a water placement method. Instead of maintaining constant temperature, a new analysis method is established to obtain isothermal rate data from non-isothermal rate data.

5.6 References

1.   Davis, R.E., Bromels, E., and Kibby, C.L., *Boron hydrides. III. Hydrolysis of sodium borohydride in aqueous solution.* Journal of American Chemical society, 1962. **84**: 885-892.

2.   Davis, R.E. and Swain, C.G., *General acid catalysis of the hydrolysis of sodium borohydride.* Journal of American Chemical society, 1960. **82**: 5949-5950.

3.   Kaufman, C.M., *Catalytic generation of hydrogen from the hydrolysis of sodium borohydride: application in a hydrogen/oxygen fuel cell/.* 1981, lousiana State University and Agricultural and Mechanical College. 166.

4.   Satterfield, C.N., *Mass Transfer in Heterogeneous Catalysis.* 1970, Cambridge, MA: MIT Press. Chapter 3.

5.   Vannice, M.A., *Kinetics of Catalytic Reactions.* 2005, New York: Springer

Science+Business Media. 59.

6.   Levenspiel, O., *Chemical Reaction Engineering*. 1999, New York: John Wieley and Sons. 393.

7.   Weekman, V.W., *Laboratory reactors and their limitations*. AIChE Journal, 1974. **20**: 833-840.
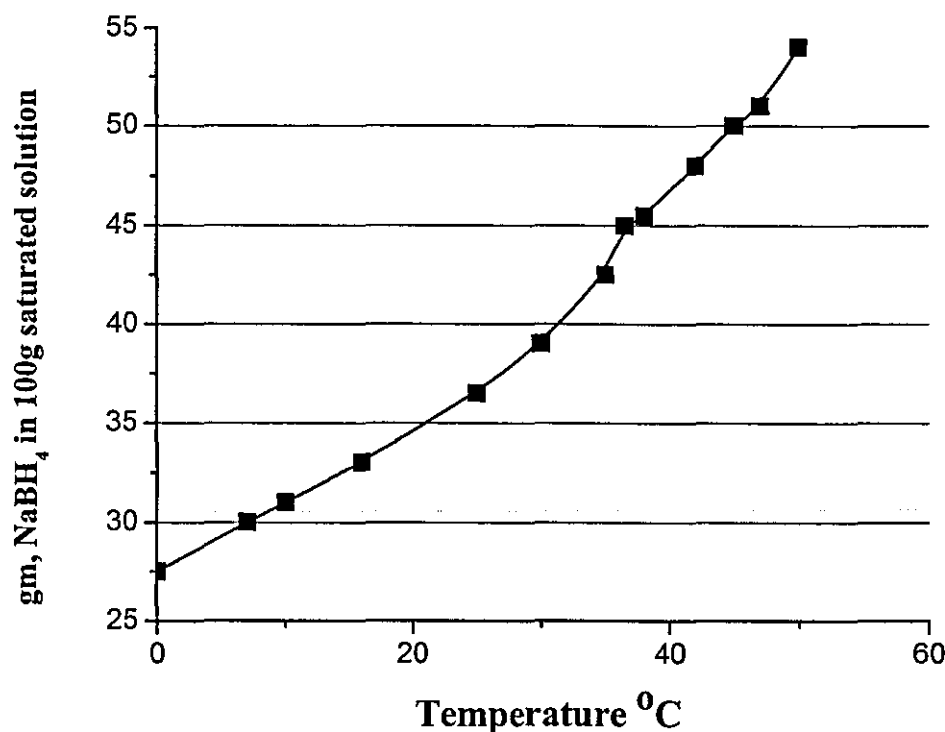
Figure 2.3 The solubility of sodium borohydride in water.

Sodium borohydride is used extensively for the reduction of organic compounds. Its broad synthetic utility is based on its ability to reduce aldehydes and ketones selectively and efficiently in the presence of other functional groups, and to reduce other functional groups, e.g., esters, di- and polysulfides, imines and quaternary iminiium compounds, under special conditions or with added catalysts or co-reagents.

2.4 Hydrolysis of $NaBH_4$

Sodium borohydride is a white solid, stable in dry air up to a temperature of 300 °C. It decomposes slowly in moist air or in vacuum at 400 °C [9]. The aqueous solution of sodium borohydride is also stable at normal environmental temperatures and pressures provided that the pH of the solution is high, which is usually achieved by adding NaOH to stabilize it [10, 11]. However, when an acid, a metal salt or a selective catalyst is added, $NaBH_4$ starts to hydrolyse to release hydrogen. In the following, the mechanisms for the three types of hydrolysis are reviewed respectively.

2.4.1 Acid Catalysis

Acid catalysis can be classified into two types: general acid catalysis and specific acid catalysis [12].

In a typical acid catalysed reaction A + B = product, a reactive protonated intermediate AH^+ is formed as shown in Scheme 2.3, where A and B are the reaction substrates.

$$A + H^+ \underset{k_{-1}}{\overset{k_1}{\rightleftharpoons}} AH^+$$

$$AH^+ + B \xrightarrow{k_2} product$$
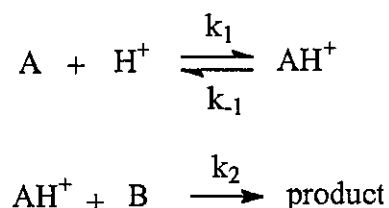
Scheme 2.3 The mains steps for acid catalysis reaction.

If step 2 is the rate-determining step and step 1 is the acid-base equilibrium, the mechanism is called specific acid catalysis. The rate depends only on the concentration of specific acid H^+, i.e. the pH value of the solution, as shown in equation (2.1).

$$rate = k_2[AH^+][B] = \frac{k_1 k_2}{k_{-1}}[A][B][H^+] \tag{2.1}$$

If step 1 is the rate-determining step, the mechanism is called general acid catalysis. The rate depends not only on pH but also on total acid concentration since any general acid can provide H^+ as shown in Scheme 2.4. The rate equation for this type of mechanism is shown in equation (2.2). A general case is shown in Table 2.3.
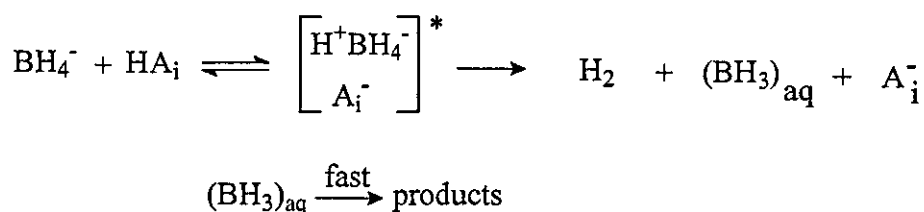
$$A + HX \xrightarrow{k_3} AH^+ + X^-$$
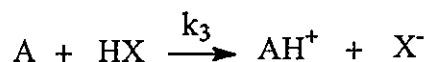
Scheme 2.4 General acid catalysis reaction.

$$rate = k_1[A][H^+] + k_3[A][HX] \tag{2.2}$$

44

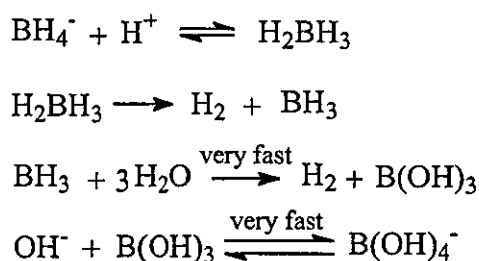**Table 2.3** Different rate laws for acid catalysed hydrolysis of sodium borohydride.

Specific acid catalysis	General acid catalyss
$rate = \dfrac{d[\text{Products}]}{dt}$ $= \dfrac{d[\text{Substrate}]}{dt}$ $= k_{obs}[\text{Substrate}]$ $k_{obs} = k_0 + k_{H^+}[\text{H}^+]$ k_0 = rate constant for uncatalyzed reaction (s^{-1}) k_{H^+} = hydroxide ion catalytic coefficient $(M^{-1}s^{-1})$	$rate = \dfrac{d[\text{Products}]}{dt}$ $= \dfrac{d[\text{Substrate}]}{dt}$ $= k_{obs}[\text{Substrate}]$ $k_{obs} = k_0 + k_{H^+}[\text{H}^+] + \sum k_{HA,J}[\text{HA}]_j$ k_0 = rate constant for uncatalyzed reaction (s^{-1}) k_{H^+} = hydroxide ion catalytic coefficient $(M^{-1}s^{-1})$ $k_{HA,J}$ = catalytic coefficient for general acid HA_j $(M^{-1}s^{-1})$

It has been confirmed that the hydrolysis reaction of sodium borohydride is a general acid catalysis not specific acid catalysis [13]. Davis and Swain [10] studied alkali metal borohydrides hydrolysis in dilute buffer solutions. They found that the rate expression was first order in hydrogen ion concentration in the pH range of 7.7 to 10.1, and the rate is less sensitive to hydrogen ion concentration at high pH (12 to 14). The apparent reaction order in hydrogen ion concentration decreases to about 0.4. Davis and Bromels [10, 14] found that the rate depended upon the ionic strength and upon the anion component of the buffer solution. They suggested a mechanism which involved a rate-determining proton transfer from a general acid onto the borohyride ion (as shown in Scheme 2.5), in which the hydrolysis of the borohydride solution was controlled by the formation of $[\text{H}^+\text{BH}_4^-\text{A}_i^-]^*$. The intermediate hydrolyzed immediately to an aquated borine radical $((\text{BH}_3)_{aq})$ which also hydrolyzed rapidly:

$$BH_4^- + HA_i \rightleftharpoons \begin{bmatrix} H^+BH_4^- \\ A_i^- \end{bmatrix}^* \longrightarrow H_2 + (BH_3)_{aq} + A_i^-$$

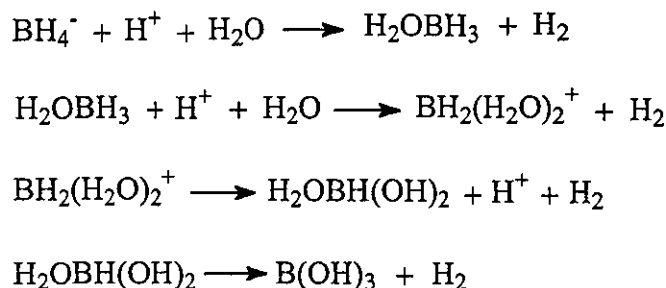$$(BH_3)_{aq} \xrightarrow{\text{fast}} \text{products}$$

Scheme 2.5 Proposed hydrolysis mechanism for borohydride catalysed by acid.

Kreevoy's work [11, 13, 15, 16] on the hydrolysis of BH_4^- by acid has shown that the loss of the first hydrogen determines the overall rate, and the reaction is first order to both the concentrations of BH_4^- and H^+. In acidic solution, the rate-determining step is the formation of H_2BH_3. He proposed the mechanism of this reaction as shown in Scheme 2.6.

$$BH_4^- + H^+ \rightleftharpoons H_2BH_3$$

$$H_2BH_3 \longrightarrow H_2 + BH_3$$

$$BH_3 + 3H_2O \xrightarrow{\text{very fast}} H_2 + B(OH)_3$$

$$OH^- + B(OH)_3 \rightleftharpoons[\text{very fast}] B(OH)_4^-$$

Scheme 2.6 Proposed reaction mechanism for the hydrolysis of borohydride

Wang and Jolly [17], however, suggested H_2OBH_3, $BH_2(H_2O)_2^+$, $H_2OBH(OH)_2$ as intermediates in low temperature reactions as shown in Scheme 2.7.

$$BH_4^- + H^+ + H_2O \longrightarrow H_2OBH_3 + H_2$$

$$H_2OBH_3 + H^+ + H_2O \longrightarrow BH_2(H_2O)_2^+ + H_2$$

$$BH_2(H_2O)_2^+ \longrightarrow H_2OBH(OH)_2 + H^+ + H_2$$

$$H_2OBH(OH)_2 \longrightarrow B(OH)_3 + H_2$$

Scheme 2.7 Proposed reaction mechanism for the hydrolysis of borohydride

No matter what the intermediate is, the hydrolysis of the borohydride is confirmed to be first order in both hydrogen ion and borohydride ion. The rate equation can be expressed

using equation (2.3).

$$\frac{dH_2}{dt} = k_H (BH_4^-)(H_3O^+) + k_{H_2O}(BH_4^-)(H_2O) + k_{HA}(BH_4^-)(HA) \qquad (2.3)$$

Equation (2.3) can be simplified to equation (2.4), where (BH_4^-), (H_3O^+), (H_2O) and (HA) represent the activities of the corresponding species in the system.

$$\frac{dH_2}{dt} = (BH_4^-)[\sum k_{HA}(HA_i)]$$

$$(2.4)$$

Schlesinger et al [18] have shown that the rate of hydrogen release slows down rapidly as the pH increases due to the increased presence of borate ion. Since the borate ions produced are alkaline, acids are therefore not an efficient catalyst.

2.4.2 Transition Metal Salt Catalysis

Acid catalysis comprised the majority of the research on the hydrolytic reaction of $NaBH_4$. In the 1950s and 1960s, the search for more practical catalysts led to investigations of some first row transition metal chlorides [18], which includes $MnCl_2$, $FeCl_2$, $CoCl_2$, $NiCl_2$ and $CuCl_2$. Kaufman [19, 20] conducted detailed research on the effect of these salts and concluded that the transition metal salts can accelerate the hydrolysis greater than acids.

The catalysis by metal salts can be described as an additive combination of acid catalysis and metal surface catalysis, the kinetics of which can be approximated by equation (2.5) [19].

$$rate = k_{H^+}(BH_4^-)(H^+) + k_M \qquad (2.5)$$

where k_{H^+} is the rate constant for the acid catalysis and k_M is the rate constant for the metal surface catalysis.

2.4.3 Metal Catalysis

Due to the low efficiency of acid catalysis, high efficiency catalysts have been investigated to hydrolyse sodium borohydride to hydrogen. The most efficient catalysts so far are the transition metals.

The advantages of transition metal catalysis over acid catalysis are as following [19]:

- The hydrolysis rate can be controlled by the amount of catalyst used and is usually unaffected by changes in solution alkalinity.
- Minimal foaming of solutions.
- Possible recovery and reuse of catalysts.

As early as the 1950s, Schlesinger et al [18] reported that alkaline borohydride solutions undergo hydrolysis, in the presence of various transition metal catalysts, to produce hydrogen. Based on this data, various metals such as Pt, Ru, Ni, Co and their supporting materials have been developed for hydrogen production from borohydride solutions and reported in recent years.

Brown [21] examined several metal catalysts for the hydrolysis of sodium borohydride solutions and found that Ru and Rh liberated hydrogen rapidly. Amendola [22] used supported high surface area Ru on ion exchange resin beads to catalyse the hydrolysis. Wu [23] used carbon supported platinum as the catalyst for the hydrolysis. Richardson [24] used Ru as the catalyst without any carrier. Krishnan [25] stated that CoO_2 can be used as an efficient carrier for Pt, Ru and Li for catalysis.

The mechanism of metal catalysis is not well understood. Some researchers proposed a zero-order reaction mechanism [19], while some others proposed a first-order reaction mechanism [24].

2.4.4 The Factors Affecting the Hydrolysis of NaBH₄

The pH of the solution has a great effect on the hydrolysis of sodium borohydride in the absence of catalyst. The solution temperature also has a significant effect on the hydrolysis. Kreevoy and Jacobson [11] proposed the following empirical equation to predict the rate of hydrolysis of NaBH₄.

$$\log(t_{1/2}) = pH - (0.034T - 1.92) \tag{2.6}$$

Where $t_{1/2}$ is the time it takes for one-half of a NaBH₄ solution to decompose (min), pH represents the pH value of the solution and T is the temperature (K).

In the following, the change of the half-life of NaBH₄ solution with NaOH concentration

is calculated according to equation (2.6). In all aqueous systems, water maintains an equilibrium with the H^+ and OH^- ions. The value of the equilibrium constant is $K_w = 1.0 \times 10^{-14}$ at 25°C.

$$K_w = [H^+][OH^-] = 1.0 \times 10^{-14} \qquad (2.7)$$

$$pH = -\log[H^+] = -\log\frac{K_w}{[OH^-]} = 14 + \log[OH^-] \qquad (2.8)$$

where $[H^+]$ and $[OH^-]$ are the concentration of hydrogen ion and hydroxide ion (mol/dm^3), which can be calculated from the concentration of NaOH, assuming that the density of the solution is approximately equal to that of water.

$$[OH^-] = [NaOH] \approx \frac{10 \times w_{NaOH}}{M_{NaOH}} = \frac{w_{NaOH}}{4} \qquad (2.9)$$

where w_{NaOH} is the concentration of NaOH in the solution (wt%).

Combining equations (2.7) and (2.8), yields

$$pH = 13.4 + \log(w_{NaOH}) \qquad (2.10)$$

Substitute equation (2.10) into equation (2.6), the relationship between the half-life of NaBH$_4$ hydrolysis and the concentrations of NaOH is obtained.

$$\begin{aligned} \log t_{1/2} &= 13.4 + \log(w_{NaOH}) - (0.034T - 1.92) \\ &= 15.3 + \log(w_{NaOH}) - 0.034T \end{aligned} \qquad (2.11)$$

The effect of NaOH on the stabilisation of NaBH$_4$ solution can be seen clearly by plotting $\log t_{1/2}$ against w_{NaOH} at different temperatures according to equation (2.11), as shown in Figure 2.4.
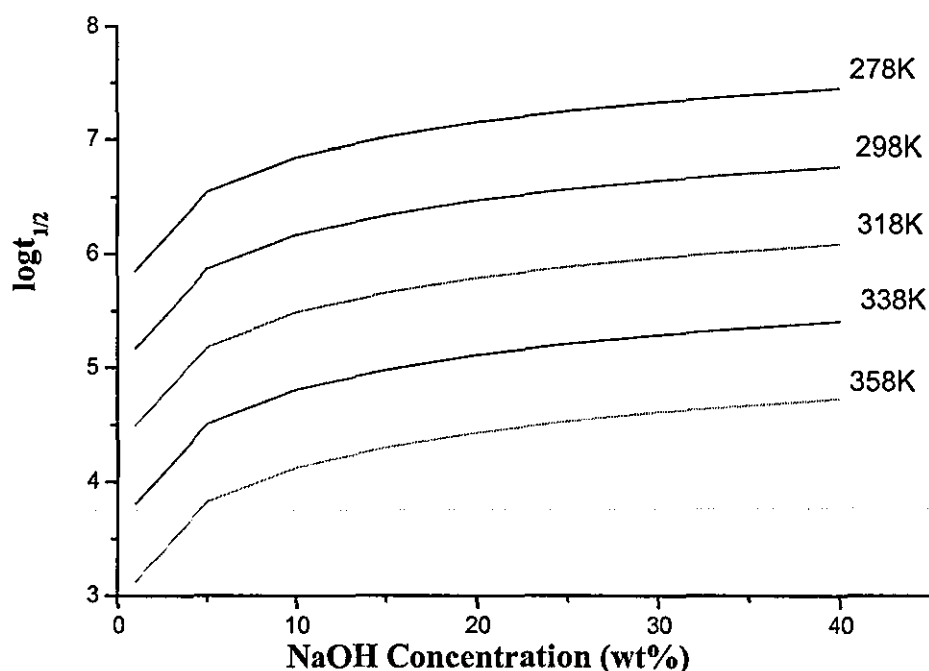
Figure 2.4 NaOH effect on the stability of NaBH$_4$ at different temperature.

From Figure 2.4, it can be seen that the stability of NaBH$_4$ increases with an increase in NaOH concentration, while it decreases with an increase in temperature. Table 2.4 lists values of the half-life of NaBH$_4$ solutions with different NaOH concentration at room temperature (25°C).

Table 2.4 Stability of NaBH$_4$ in NaOH solution at room temperature.

w_{NaOH}	$t_{1/2}$(days)	$t_{1/2}$(years)
1	110	0.3
5	550	1.5
10	1100	3
20	2200	6

2.5 Current Status of NaBH$_4$ as a Hydrogen Source

Sodium borohydride has been known as a viable hydrogen generator since 1943 [26]. At first, it was used as a convenient hydrogen source when a small amount of hydrogen was needed. It was overlooked after World War II due to its high cost. However, in recent

years, it has attracted great attention as an alternative hydrogen storage method. Currently, several companies and groups such as Millennium Cell, Toyota Motor Company, and Hydrogenics are investing in this research.

Great efforts have been made to commercialise the sodium borohydride system as a hydrogen source. For example, Millennium Cell has established a portable hydrogen generator using aqueous sodium borohydride solution with Ru catalyst [22]. In Oak Ridge National Laboratory of USA, a 500 W power system based on sodium borohydride hydrolysis has been constructed [24].

2.6 Transformation of Sodium Metaborate to Sodium Borohydride

When sodium borohydride undergoes hydrolysis, sodium metaborate is formed (Scheme 2.8). In this section, the properties of sodium metaborate and possible routes to transform it back to $NaBH_4$ are reviewed.

$$NaBH_4 + 2H_2O \rightarrow NaBO_2 + 4H_2$$

Scheme 2.8 The hydrolysis of sodium borohydride.

2.6.1 Properties of Sodium Metaborate

$NaBO_2$ is relatively inert and non-toxic; it is a common detergent and soap additive but is toxic to ants and is an ingredient in ant poisons. An anhydrous form can be obtained when crystallizing from melts of 1:1 of $Na_2O.B_2O_3$. The octahydrate, $Na_2O.B_2O_3.8H_2O$, the tetrahydrate, $Na_2O.B_2O_3.4H_2O$, and the monohydrate, $Na_2O.B_2O_3.H_2O$, occur in the system $Na_2O-B_2O_3-H_2O$. However, there is no evidence for the existence of a dihydrate [27].

The simple ionic unit (BO_2^-) only exists in the sodium metaborate vapour in the form $M+(O^--B^+-O^-)$ [27]. The anhydrous solid sodium metaborate is composed of sodium ion and trimeric metaborate ion, $(B_3O_6)^{3-}$, as shown in Scheme 2.9. However, the solution of sodium metaborate is a binary electrolytes system, which has been proved by cryoscopic results and Raman spectrum of dissolved sodium metaborate [27]. The cyclic triborate ions present in the crystals of the solid salts evidently break up on dissolution. Therefore, what is referred to as a solution of sodium metaborate is in fact a solution of

the binary electrolyte $NaB(OH)_4$ that is usually simplified as $NaBO_2$.
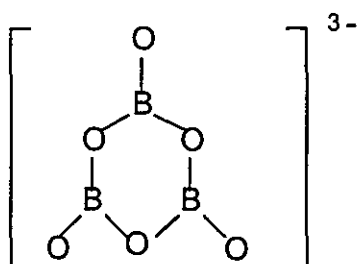
Scheme 2.9 The structure of the trimeric metaborate ion, $(B_3O_6)^{3-}$.

A solution of sodium metaborate is highly basic. It can be used as a component of photographic developers and replenishers due to its strong buffering ability which can control the pH within close limits. It is also a component for the preparation of starch and dextrin adhesives, due to the high degree of alkalinity. Sodium metaborate can also be used as a stabilizer for textile processing. It can also be incorporated into liquid laundry detergents for pH control and enzyme stabilization.

2.6.2 Routes for Transforming Sodium Metaborate back to Sodium Borohydride

In order to use $NaBH_4$ hydrolysis in a sustainable way, the by-product must be converted back into $NaBH_4$. Little attention has been paid so far to the conversion of $NaBO_2$ to $NaBH_4$ in the literature. This section gives possible routes for the conversion.

2.6.2.1 Coupling reaction

One possible way to convert $NaBO_2$ into $NaBH_4$ is to use the reaction expressed in Scheme 2.10. However, this reaction has a very high positive Gibbs energy ($\Delta_r G^\theta$ = 796.8 KJ.mol^{-1}), as shown in Table 2.5 for the relationship between reaction Gibbs energy, equilibrium constant for chemical reaction (K) and reaction directions. This indicates that direct reaction through this route is impossible.

$$NaBO_2 + 2H_2 \rightarrow NaBH_4 + O_2$$
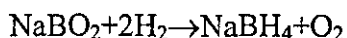
Scheme 2.10 A direct reaction to convert sodium metaborate into sodium borohydride.

Table 2.5 The relationship between ΔG° and K at 298 K [28].

ΔG° (kJ)	K	Significance
200	1×10^{-35}	Essentially no forward reaction; reverse
100	3×10^{-18}	reaction goes to completion
50	2×10^{-9}	
10	2×10^{-2}	
1	7×10^{-1}	
0	1	Forward and reverse reactions proceed to
-1	1.5	some extent
-10	50	
-50	5×10^{8}	
-100	3×10^{17}	Forward reaction goes to completion;
-200	1×10^{35}	essentially no reverse reaction

It is known that some reactions with negative ΔG can drive a reaction that is not spontaneous as coupling reactions (just as the combustion of petroleum supplies enough free energy to move a car [29]). Therefore, some reactions with very negative reaction Gibbs energy are proposed to couple with reaction (2.10) to make it possible to convert $NaBO_2$ back into $NaBH_4$. The potential chemical species for coupling with the $NaBO_2$ conversion reaction should not have any chemical reactions with $NaBH_4$ and the resulting $NaBH_4$ should be separated from the reaction mixture easily. Metal oxidation, such as that of sodium, silicon and aluminium, satisfy the above criteria and therefore can be used to couple with the conversion reaction. The nature of the industrial inorganic method for producing $NaBH_4$ can be classified as a coupling reaction. The calculation of the reaction Gibbs energy for the overall reaction is given in Table 2.6.

Table 2.6 Calculation of possible coupling reaction with reaction 2.10. The value of the fundamental thermodynamic function was taken from Literature [30]

Basic reaction	Coupling reaction	Overall reaction	$\Delta_r G^{\ominus}$ (kJ.mol^{-1})
$NaBO_2 + 2H_2 =$ $NaBH_4 + O_2$	$4Na + O_2 = 2Na_2O$ $SiO_2 + Na_2O = Na_2SiO_3$	$NaBO_2 + 2SiO_2 + 4Na$ $+2H_2 =$ $NaBH_4 + 2Na_2SiO_3$	-40.7
	$Na_2O + Si + O_2 =$ Na_2SiO_3	$NaBO_2 + Na_2O + Si$ $+2H_2 = NaBH_4$ $+Na_2SiO_3$	-290.5
	$2Mg + O_2 = 2MgO$	$NaBO_2 + Mg + 2H_2 =$ $NaBH_4 + 2MgO$	-341.8
	$4Al + Na_2O + 3O_2 =$ $4NaAlO_2$	$3NaBO_2 + 4Al +$ $2NaO + 6H_2 =$ $NaBH_4 + 4NaAlO_2$	-3720.8

As can be seen from Table 2.6, all of the above coupling reactions can be used to drive reaction 2.10 to completion. Coupling reactions are possible routes for coverting $NaBO_2$ back into $NaBH_4$.

2.6.2.2 Electrochemical methods

From the thermodynamic analysis, it is known that it is impossible to transfer $NaBO_2$ into $NaBH_4$ without the use of a coupling reaction. In order to make the reaction proceed quickly, tricky conditions such as high temperature and hydrogen pressure are needed to fulfil the requirements of the coupling reaction. Electrolysis may be an alternative to solve the problem. In contrast to the coupling reaction approach, this is a relatively simple technology.

There are two electrode reactions dealing with BH_4^- preparation in the Handbook of Physics and Chemistry [31] as shown in Scheme (2.11) and (2.12). Electrode reaction (2.12) may not be suitable for use in the production of borohydride because the borohydride ion is readily hydrolysed in an acidic environment.

$$H_2BO_3^- + 5H_2O + 8e \leftrightarrow BH_4^- + 8OH^- \qquad E° = -1.24 \text{ V}$$
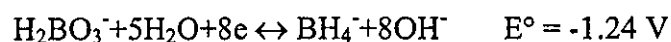
Scheme 2.11 Half-cell reaction of boric acid in basic conditions.

$$H_3BO_3 + 7H^+ + 8e \leftrightarrow BH_4^- + 3H_2O \qquad E° = -0.481 \text{ V}$$
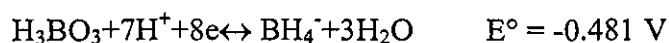
**Scheme 2.12** Half-cell reaction of boric acid in acidic conditions.

The solution of sodium metaborate is a binary electrolytes system. However, the ions in its aqueous solution are not Na^+ and BO_2^-. Actually, the anion in the solution is $B(OH)_4^-$ [32]. Hence, Scheme 2.11 should be written as Scheme 2.13, which can be designed as the cathode reaction of an electrolytic cell [33]. Oxygen evolution is the main anodic reaction, as shown in Scheme 2.14. The overall reaction is given in Scheme 2.15. A schematic diagram of the cell required to produce $NaBH_4$ from a $NaBO_2$ solution is shown in Figure 2.5. The cell contains one anode, one cathode, one semi-permeable membrane. Under an external electric power, $B(OH)_4^-$ is reduced to BH_4^- in the cathode and OH^- is oxidized to O_2 in the anode.

$$B(OH)_4^- + 4H_2O + 8e = BH_4^- + 8OH^-$$
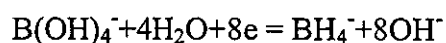
Scheme 2.13 The actual half cell reaction of metaborate ion in basic conditions.

$$4OH^- = O_2 + 2H_2O + 4e$$
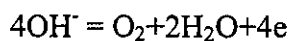
Scheme 2.14 Oxygen-evolution reaction on anode.

$$B(OH)_4^- = BH_4^- + 2O_2$$
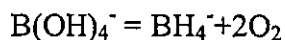
Scheme 2.15 Overall reaction of electrolysis of metaborate ions.
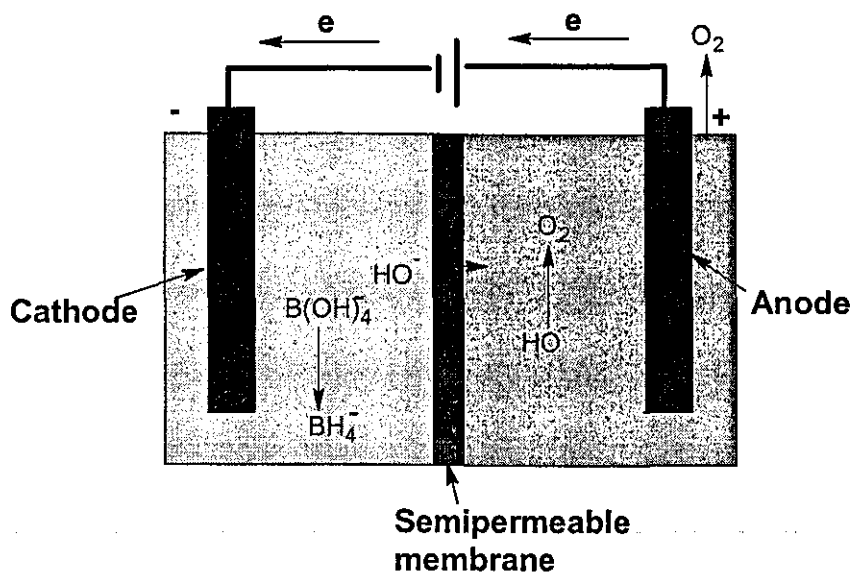
Figure 2.5 A schematic diagram of the proposed electrolytic cell for $NaBO_2$

In practice, there are competing reactions on the cathode. Because the cathode reaction with the higher reduction potential reacts at the cathode first, water may be reduced into hydrogen on the cathode instead of the metaborate ion, $B(OH)_4^-$, due to its low standard electrode potential, as shown in Schemes 2.16.

$$2H_2O + 2e = H_2 + 2OH^- \quad E^\circ = -0.8277 \text{ V}$$

Scheme 2.16 Hydrolysis of water on cathode.

By selecting suitable cathode materials and hydrogen pressure, the electrochemical method may be possible.

2.6.2.3 Raw materials for existing processes

Sodium metaborate may be changed into the raw materials for the existing processes. For an inorganic process, $NaBO_2$ can be transformed into borax through the following reactions. When contacted with boric acid, sodium metaborate can be changed into borax.

$$2NaBO_2 + 2B(OH)_3 \rightarrow Na_2B_4O_7 + 3H_2O$$
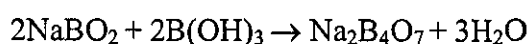
Scheme 2.17 Transformation of sodium metaborate into borax using boric acid

Sodium metaborate can absorb atmospheric carbon dioxide, forming borax and sodium

56

carbonate.

$$4NaBO_2 + CO_2 \rightarrow Na_2B_4O_7 + Na_2CO_3$$
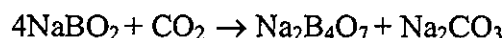
Scheme 2.18 Transformation of sodium metaborate into borax using CO_2

For the organic process, sodium metaborate reacts with strong mineral acids to form boric acid, which can react with methanol further to give trimethyl borate. This is the raw material for the production of sodium borohydride by the Schlesiger method. The process can be expressed as shown in Schemes 2.19 and 2.20.

$$NaBO_2 + H^+ + H_2O \rightarrow Na^+ + B(OH)_3$$
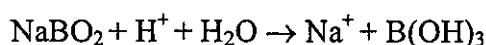
Scheme 2.19 Transformation of metaborate into boric acid

$$B(OH)_3 + 3MeOH \rightarrow B(OMe)_3 + 3H_2O$$
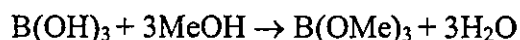
Scheme 2.20 Transformation of boric acid into trimethyl borate

2.7 Conclusions

- There are two commercially available methods for producing $NaBH_4$: an organic process and an inorganic process. Both processes are commercially available.

- Three mechanisms are used for the hydrolysis of $NaBH_4$: acid catalysis, metal salt catalysis and metal catalysis. Metal catalysis is believed to be the most efficient.

- Although there is a significant amount of research and development being focused on the use of $NaBH_4$ as a hydrogen source, some important issues remain with regard to its utilisation, such as its optimal concentration and conversion of the side product $NaBO_2$.

- Three routes to transform sodium metaborate into sodium borohydride have been proposed: coupling reaction, electrochemical methods and a raw materials approach.

- From a calculation of Gibbs free energy, direct hydrogen adsorption by $NaBO_2$ is

thermodynamically impossible due to the high positive Gibbs energy. Direct hydrogen adsorption by $NaBO_2$ can be conducted by coupling with other reactions with high negative Gibbs energy change such as the oxidation reaction of magnesium, sodium and silicon.

- A simple and practical transformation is the electrochemical approach. The key to this method is the choice of suitable cathode materials to prevent hydrogen evolution.

- Transformation of the by-product $NaBO_2$ into raw materials for the existing process of manufacturing $NaBH_4$ is a feasible method.

2.8 References

1. Brown, H.C., *Boranes in Organic Chemistry*. Cornell University, Press, Ithaka, 1972.

2. Schlesinger, H.I., Brown, H.C., and Finholt, A.E., *The preparation of sodium borohydride by the high temperature reaction of sodium hydride with borate esters*. Journal of American Chemical Society, 1953. **75**: 205 - 209.

3. Buchner, W. and Niederprum, H., *Sodium Borohydride and Amine-Boranes, Commercially Important Reducing Agents*. Pure and Applied Chemistry, 1977. **49**: 733-743.

4. Davis, W.D., Mason, L.S., and Stegeman, G., *The heats of formation of sodium borohydride, lithium borohydride and lithium aluminum hydride*. Journal of American Chemical Society, 1949. **71**(8): 2775 - 2781.

5. Stockmayer, W.H., Rice, D.W., and Stephenson, C.C., *Thermodynamic properties of sodium borohydride and aqueous borohydride ion*. Journal of American Chemical society, 1955. **77**: 1980-1983.

6. Johnston, H.L. and Hallett, N.C., *Low temperature heat capacities of inorganic solids. XIV. Heat capacity of sodium borohydride from 15-300K*. Journal of American Chemical society, 1953. **75**: 1467-1468.

7. Gunn, S.R. and Green, L.G., *The Heat of Solution of Sodium Borohydride and the Entropy of Borohydride Ion.* Journal of American Chemical society, 1955. **77**: 6197-6198.

8. Jensen, E.H., *A study on sodium borohydride.* NytNordisk Forlag Amold Busck, Copenhagen, 1954- (out of print).

9. Kroschwitz, J.I., *Encyclopedia of Chemical Technology.* Vol. 13. 1995, New York: Wiley. 616-624.

10. Davis, R.E. and Swain, C.G., *General acid catalysis of the hydrolysis of sodium borohydride.* Journal of American Chemical society, 1960. **82**: 5949-5950.

11. Kreevoy, M.M. and Jacobson, R.W., *The rate of decomposition of NaBH4 in basic aqueous solutions.* Ventron Alembic, 1979. **15**: 2-3.

12. Miller, B., *Advanced Organic Chemistry.* 2nd ed. 2004, Upper Saddle River, N.J., USA: Prentice Hall.

13. Abts, L.M., Langland, J.T., and Kreevoy, M.M., *Role of water in the hydrolysis of tetrahydroborate(1-) ion.* Journal of American Chemical Society, 1975. **97**(11): 3181 - 3185.

14. Davis, R.E., Bromels, E., and Kibby, C.L., *Boron hydrides. III. Hydrolysis of sodium borohydride in aqueous solution.* Journal of American Chemical society, 1962. **84**: 885-892.

15. Kreevoy, M.M. and Hutchins, J.E.C., *H₂BH₃ as an Intermediate in Tetrahydridoborate Hydrolysis.* Journal of American chemical society, 1972. **94**: 6371 - 6376.

16. Kreevoy, M.M. and Oh, S.-W., *Relation between rate and equilibrium constants for proton-transfer reactions.* Journal of American Chemical society, 1973. **95**(15): 4805 - 4810.

17. Wang, F.T. and Jolly, W.L., *Kinetic study of the intermediates in the hydrolysis of the hydroborate ion.* Journal of American Chemical society, 1972. **11**(8): 1933 -

1941.

18.   Schlesinger, H.I., et al., *Sodium borohydride, its hydrolysis and its use as a reducing agent and in the generation of hydrogen.* Journal of American Chemical society, 1953. **75**: 215-219.

19.   Kaufman, C.M., *Catalytic generation of hydrogen from the hydrolysis of sodium borohydride: application in a hydrogen/oxygen fuel cell/.* 1981, lousiana State University and Agricultural and Mechamical College. 166.

20.   Kaufman, C.M. and Sen, B., *Hydrogen generation by hydrolysis of sodium tetrahydroborate: effects of acids and transition metals and their salts.* Journal of the Chemical Society, Dalton Transaction, 1985: 307-313.

21.   Brown, H.C. and Brown, C.A., *New, highly active metal catalysts for the hydrolysis of borohydride.* Journal of American Chemical Society, 1962. **84**: 1493.

22.   Amendola, S.C., et al., *A safe, portable, hydrogen gas generator using aqueous borohydride solution and Ru catalyst.* International Journal of Hydrogen Energy, 2000. **25**: 969-975.

23.   Wu, C., Zhang, H., and Yi, B., *Hydrogen generation from catalytic hydrolysis of sodium borohydride for proton exchange membrane fuel cells.* Catalysis Today, 2004. **93-95**: 477-483.

24.   Richardson, B.S., Birdwell, J.F., and Pin, F.G., *Sodium borohydride based hybrid power system.* Journal of Power Sources, 2005. **145**: 21-29.

25.   Krishnan, P.K., et al., *PtRu-LiCoO$_2$-an efficient catalyst for hydrogen generation from sodium borohydride solutions.* Journal of Power Sources, 2005. **143**: 17-23.

26.   Schlesinger, H.I., Brown, H.C., and Schaeffer, G.W., *The borohydrides of galium.* Journal of American Chemical Society, 1943. **65**: 1786.

27.   Kemp, P.H., *The Chemistry of Borates, Part I.* 1956, London: Borax Consolidated Limited.

28.   Silberberg, M., *Chemistry: the Molecular Nature of Matter and Change.* 2001, St

Louis, Missouri: Mosby-Year Book Inc. 864.

29.   Silberberg, M., *Chemistry: the Molecular Nature of Matter and Change*. 2001, St Louis, Missouri: Mosby-Year Book Inc. 860.

30.   Alberty, S., *Physical Chemistry*. 3rd ed. 2001, New York: John Wiley & Sons.

31.   Dean, J.A. and Lange, N.A., *Lange's Handbook of Chemistry*. 15th ed. 1999: New York: McGraw-Hill.

32.   Mellor, J.W., *Supplement to Mellor's comprehensive treatise on inorganic and theoretical chemistry*. Vol. 5 Boron-Hydrogen compounds. 1981, London: London: Longman. 223.

33.   Paidar, M., Bouzek, K., and Bergmann, H., *Inflence of cell construction on the electrochemical reduction of nitrate*. Chemical Engineering Journal, 2002. **85**: 99-109.

Chapter 3

Maximum Concentration of NaBH₄ in the Absence of NaOH

3.1 Introduction

As discussed in the previous chapters, the hydrolysis of sodium borohydride is a promising method for delivering hydrogen to vehicles and other power systems. Previous studies have focused on the kinetics and mechanism of the hydrolysis in dilute solution. However, for use as a power source, a concentrated aqueous solution is desirable in order to improve the energy density.

As is known, the by-product $NaBO_2$ is produced from the hydrolysis of $NaBH_4$. The higher the concentration of $NaBH_4$, the more $NaBO_2$ is produced. When the $NaBO_2$ concentration is too high, it tends to precipitate from solution resulting in catalyst clogging and a reduction in system efficiency. Hence, knowledge of the maximum concentrations of $NaBH_4$ is needed. Below this concentration, the highest energy density is not achieved, while above this concentration, precipitation of $NaBO_2$ may occur. In this chapter, the maximum concentration of $NaBH_4$ is investigated in the hydrolysis system when NaOH is not present. This is a generalised case when $NaBH_4$ is used in its solid state.

The maximum concentration of $NaBH_4$ changes with temperature since the solubilities of $NaBO_2$ and $NaBH_4$ are temperature dependent. Available solubility data for $NaBH_4$ and $NaBO_2$ in the literature is limited, hence a modelling approach is used in this investigation.

In the work, a thermodynamic model is established in order to correlate the relationship between solubility and temperature by using the equality of chemical potential for a substance in its solution and its solid form. The parameters in the model are determined by using solubility data from the literature [1, 2]. The model is then used to predict the maximum concentration of $NaBH_4$ in the hydrolysis system, which is validated experimentally.

3.2 Construction of the Theoretical Solubility Model

3.2.1 Theoretical Background

In this work, the relationship between the solubility of a substance and the temperature was derived. During derivation, the fact is used that the chemical potential of the substance present in its solution must be equal to the chemical potential of the substance in its solid state when the dissolution process reaches equilibrium.

The chemical potential of a substance B (μ_B) in a mixture B, C... is related to the Gibbs energy (G) of the mixture by

$$\mu_B = \left(\frac{\partial G}{\partial n_B}\right)_{P,T,n_c \neq n_B} \tag{3.1}$$

where T is the thermodynamic temperature, p is the pressure, and n_B, n_C, ... are the moles of substance B, C, ... Hence the chemical potential s the partial derivative of G with respect to the mole number n_J when pressure, temperature and other components are kept constant. The Gibbs energy of a system depends on the composition, pressure, and temperature of the system.

For a pure substance B, The chemical potential $\mu_B{}^*$ is given by

$$\mu_B^* = \frac{G}{n_B} = G_m^* \tag{3.2}$$

where $G_m{}^*$ is the molar Gibbs energy, and where the superscript * attached to a symbol denotes the property of a pure substance. The superscript $^\circ$ attached to a symbol may be used to denote a standard thermodynamic quantity. It can be seen that the chemical potential is another name for the molar Gibbs energy for a pure substance. Conventionally the standard pressure (p°) is set to be 1 bar.

For a perfect gas mixture, chemical potential is related to its standard value as in equation (3.3) by integrating the thermodynamic fundamental equation (Maxwell equation) $\left(\partial \mu_i / \partial p\right)_T = V$

$$\mu_i = \mu_i^\circ + RT \ln \frac{p_i}{p^\circ} \tag{3.3}$$

where p_i is the partial pressure of component i.

In a liquid solution composed of a solvent A and solute B, the chemical potential of solvent A in the liquid is μ_A, and its vapour pressure is p_A. The chemical potential of solvent A in the liquid solution must be equal to the chemical potential of the solvent present in the vapour at equilibrium.

$$\mu_A = \mu_A^\circ + RT \ln \frac{p_A}{p^\circ} \tag{3.4}$$

For pure solvent A with a vapour pressure of p_A^*, its chemical potential can be expressed using equation (3.5).

$$\mu_A^* = \mu_A^\circ + RT \ln \frac{p_A^*}{p^\circ} \tag{3.5}$$

Combining equations (3.4) and (3.5), yields

$$\mu_A = \mu_A^* + RT \ln \frac{p_A}{p_A^*} \tag{3.6}$$

Raoult's law for an ideal solution is

$$p_A = x_A p_A^* \tag{3.7}$$

Substituting this into equation (3.6)

$$\mu_A = \mu_A^* + RT \ln x_A \tag{3.8}$$

The standard state of the solvent is the pure liquid (at 1 bar) and is obtained when $x_A = 1$. When the solution does not obey Raoult's law, i.e. if it is a real solution, the activity is introduced in order to preserve the form of equation (3.8).

$$\mu_A = \mu_A^* + RT \ln a_A \tag{3.9}$$

where a_A is the activity of A, the effective mole fraction.

Because all solvents obey Raoult's law (that $p_A/p_A^* = x_A$) increasingly closely as the concentration of solute approaches zero, the activity of the solvent a_A approaches as the mole fraction x_A approaches unity.

$$a_A \rightarrow 1 \text{ as } x_A \rightarrow 1 \tag{3.10}$$

A convenient way of expressing this convergence is to introduce the activity coefficient, γ, by the definition

$$a_A = \gamma_A x_A \qquad \gamma_A \rightarrow 1 \text{ as } x_A \rightarrow 1 \tag{3.11}$$

For the solute B, the vapour pressure is given by Henry's law

$$p_B = k_B x_B \tag{3.12}$$

where k_B is an empirical constant.

In this case, the chemical potential of B is

$$\mu_B = \mu_B^* + RT \ln \frac{p_B}{p_B^*} = \mu_B^* + RT \ln \frac{k_B}{p_B^*} + RT \ln x_B \tag{3.13}$$

By defining a new standard chemical potential:

$$\mu_B^\circ = \mu_B^* + RT \ln \frac{k_B}{p_B^*} \tag{3.14}$$

Then it follows

$$\mu_B = \mu_B^\circ + RT \ln x_B \tag{3.15}$$

The standard state of solute B is a hypothetical state of the pure solute when Henry's law still holds. For a real solute, some deviations may occur, and the activity is introduced again.

$$\mu_B = \mu_B^\circ + RT \ln a_B \tag{3.16}$$

65

The standard state of solute B remains unchanged in this last stage. As for the solvent A, it is sensible to introduce an activity coefficient

$$a_B = x_B \gamma_B \qquad (3.17)$$

Because the solute obeys Henry's law as its concentration goes to zero, it follows that

$$a_B \rightarrow x_B \qquad \gamma_B \rightarrow 1 \text{ as } x_B \rightarrow 0 \qquad (3.18)$$

When the solvent is water and the solute is an electrolyte, the solution becomes an electrolyte solution. Electrolytes dissociate in aqueous solution but the ions cannot be studied separately because the condition of electric neutrality applies. Since this is the case, the thermodynamics of electrolytes have to be treated in a different way from non-electrolytes. In work with electrolyte solutions it is customary to use the molal scale. The molality m_i is equal to the amount of electrolyte per kilogram of solvent. Thus, the molality has the units mol kg^{-1}.

For an electrolyte $A_{\nu+}B_{\nu-}$, where ν_+ is the number of cations and ν_- is the number of anions, electroneutrality requires that

$$m = \frac{m_+}{\nu_+} = \frac{m_-}{\nu_-} \qquad (3.19)$$

The chemical potential for an electrolyte is the sum of chemical potentials of the cations and the anions as expressed in equation (3.20)

$$\mu = \nu_+ \mu_+ + \nu_- \mu_- \qquad (3.20)$$

The chemical potentials of the cation and anion are given by

$$\mu_+ = \mu_+^\circ + RT \ln \gamma_+ m_+ \qquad (3.21)$$

$$\mu_- = \mu_-^\circ + RT \ln \gamma_- m_- \qquad (3.22)$$

where μ_+° and μ_-° are the standard state chemical potentials and γ_+ and γ_- are the activity coefficients of the cation and anion.

In equations (3.21) and (3.22), the standard values of the molality m° in the denominator are omitted to simplify the notation. Substituting equation (3.21) and (3.22) into equation (3.20), gives

$$\mu = (v_+ \mu_+^\circ + v_- \mu_-^\circ) + RT \ln \gamma_+^{v+} \gamma_-^{v-} m_+^{v+} m_-^{v-} \tag{3.23}$$

A mean ionic molality $m_\pm$ and a mean ionic activity coefficient $\gamma_\pm$ are defined as

$$m_\pm = (m_+^{v+} m_-^{v-})^{1/v\pm} = m(v_+^{v+} v_-^{v-})^{1/v\pm} \tag{3.24}$$

$$\gamma_\pm = (\gamma_+^{v+} \gamma_-^{v-})^{1/v\pm} \tag{3.25}$$

where

$$v_\pm = v_+ + v_- \tag{3.26}$$

Then equation (3.23) becomes

$$\mu = \mu^\circ + v_\pm RT \ln \gamma_\pm m_\pm \tag{3.27}$$

This is the chemical potential expression of an electrolyte in solution. The standard chemical potential μ° of the electrolyte is the chemical potential in a solution of unit activity on the molality scale.

3.2.2 Semi-Empirical Model for Electrolyte Solubility and Temperature

In this section, the relationship between the solubility of an electrolyte and temperature is derived. When a solid solute is left in contact with a solvent, it dissolves until the solution is saturated. Saturation is a state of equilibrium, with the undissolved solute in equilibrium with the dissolved solute. Therefore, in a saturated solution the chemical potential of the pure solid solute, $\mu_B^*(s)$, and the chemical potential of B in solution, μ_B, are equal [3]. According to the definition given by equation (3.27), equation (3.28) is obtained.

$$\mu_B^*(s) = \mu_B^\circ + v_\pm RT \ln \gamma_{\pm,B} m_{\pm,B} \tag{3.28}$$

Rearranging equation (3.28) gives

$$\ln m_\pm = \frac{\mu_B^*(s) - \mu_B^\circ}{v_\pm RT} - \ln \gamma_\pm \tag{3.29}$$

The difference between the chemical potentials in equation (3.29) is the mole Gibbs energy change of the solute from its solid state to unit activity in its solution on the molality scale. This difference is further related to other thermodynamic property changes during dissolution as shown in equation (3.30).

$$\Delta G_{m,B}^\circ = \mu_B^\circ - \mu_B^*(s) = \Delta H_{m,B}^\circ - T\Delta S_{m,B}^\circ \tag{3.30}$$

where $\Delta G_{m,B}^\circ$, $\Delta H_{m,B}^\circ$, and $\Delta S_{m,B}^\circ$ are the mole Gibbs energy change, mole enthalpy change and mole entropy change of B of the dissolution of one mol of solid state solute to unit activity in solution.

Substituting equation (3.30) into equation (3.29), gives

$$\ln m_\pm = -\frac{\Delta H_{m,B}^\circ}{v_\pm RT} + \frac{\Delta S_{m,B}^\circ}{v_\pm R} - \ln \gamma_\pm \tag{3.31}$$

$\Delta H_{m,B}^\circ$ and $\Delta S_{m,B}^\circ$ can be considered to be constants if the temperature change is not large. $\gamma_\pm$ is a function of temperature and concentration. At higher concentrations it levels off to a constant, which can be seen from the calculation of the activity coefficient of $NaBO_2$ in the following sections. Due to the lack of the parameters for $NaBH_4$, the activity of $NaBH_4$ has not been calculated. If the temperature effect on $\gamma_\pm$ is negligible, it can be assumed constant. In this work, the effect of temperature is shown to have no significant effect and this is justified by the good linearity of $\ln(m_\pm)$ against $1/T$ in the following section.

3.2.3 Calculation of the Activity Coefficient for $NaBO_2$

The Pitzer equations for mean ionic activity coefficient for single electrolyte solutions [4] can be written as follows.

$$\ln \gamma_m = -|z_M z_X| A^{\phi} \left[\frac{I^{1/2}}{1 + bI^{1/2}} + \frac{2}{b} \ln(1 + bI^{1/2}) \right]$$
$$+ 4m \left(\frac{v_M v_X}{v} \right) \left(B_{MX} + \frac{I}{2} B'_{MX} \right) + 6m^2 \left(\frac{v_M v_X}{v} \right) v_M z_M C_{MX}$$

(3.32)

where γ_m is the mean activity coefficient when the concentration is in terms of molality, (that is, $\gamma_m = a_m / m$), a_m is the activity of the solute and z_M and z_X are the charges on the cation and anion in the solution corresponding to stoichiometric coefficient v_M and v_X. The values of v_M, v_X, z_X, z_M and a_m are all equal to 1.0 for $NaBO_2$. Also $v = v_M + v_X = 2$.

$I = \frac{1}{2} \sum_i m_i z_i^2$ is the ionic strength.

In $NaBO_2$ solution, the amount of I is equal to its molality. A^{ϕ} is the Debye-Hückel coefficient for the osmotic coefficient and is given by

$$A^{\phi} = \frac{1}{3} \left(\frac{2\pi N_0 d_w}{1000} \right)^{1/2} \left(\frac{e^2}{DkT} \right)^{3/2}$$

(3.33)

where N_0 is Avogadro's number, d_w is the density of water and D is the static dielectic constant of water at temperature T. k is the Boltzmann's constant and e is the electronic charge.

The value of A^{ϕ} at 25°C is 0.392 and the term b in equation (4.33) is an empirical parameter equal to 1.2 at 25°C [5]. The parameters B_{MX} and B'_{MX} which describe the interaction of pairs of oppositely charged ions represent measurable combinations of the second virial coefficients. They are defined as explicit functions of ionic strength by using the following equations

$$B_{MX} = \beta_{MX}^{(0)} + \beta_{MX}^{(1)} f(\alpha_1 I^{1/2})$$

(3.34)

$$B'_{MX} = \beta_{MX}^{(1)} f'(\alpha_1 I^{1/2}) / I$$

(3.35)

where

$$f(x) = 2[1 - (1 + x)e^{-x}] / x^2 \qquad (3.36)$$

$$f'(x) = -2[1 - (1 + x + 0.5x^2)e^{-x}] / x^2 \qquad (3.37)$$

where $\alpha_1 = 2$ for ions in univalent type electrolytes. The single electrolyte third viral coefficients, C_{MX}, account for short-range interactions of ion triplets and are important at high concentrations. They are independent of ionic strength. The parameters C_{MX} and C^{ϕ}_{MX}, are related by

$$C_{MX} = C^{\phi}_{MX} / (2 |z_M z_X|^{1/2}) \qquad (3.38)$$

The ion interaction parameters for NaBO$_2$ at 25°C are given in the literature [5-7] and are listed in Table 3.1, which is valid for molalities below 4, the highest molality of NaBO$_2$ at 25°C in its saturated solution.

Table 3.1 The ion interaction parameters for NaBO$_2$ at 25°C.

$\beta^{(0)}$	$\beta^{(1)}$	C^{ϕ}
-0.05289	-0.10888	0.01497

The calculated results for the activity coefficient of NaBO$_2$ are shown in Figure 3.1. It can be seen that the activity coefficient levels off at higher concentrations. This is a justification for the assumption that activity coefficient is a constant in saturated solutions.
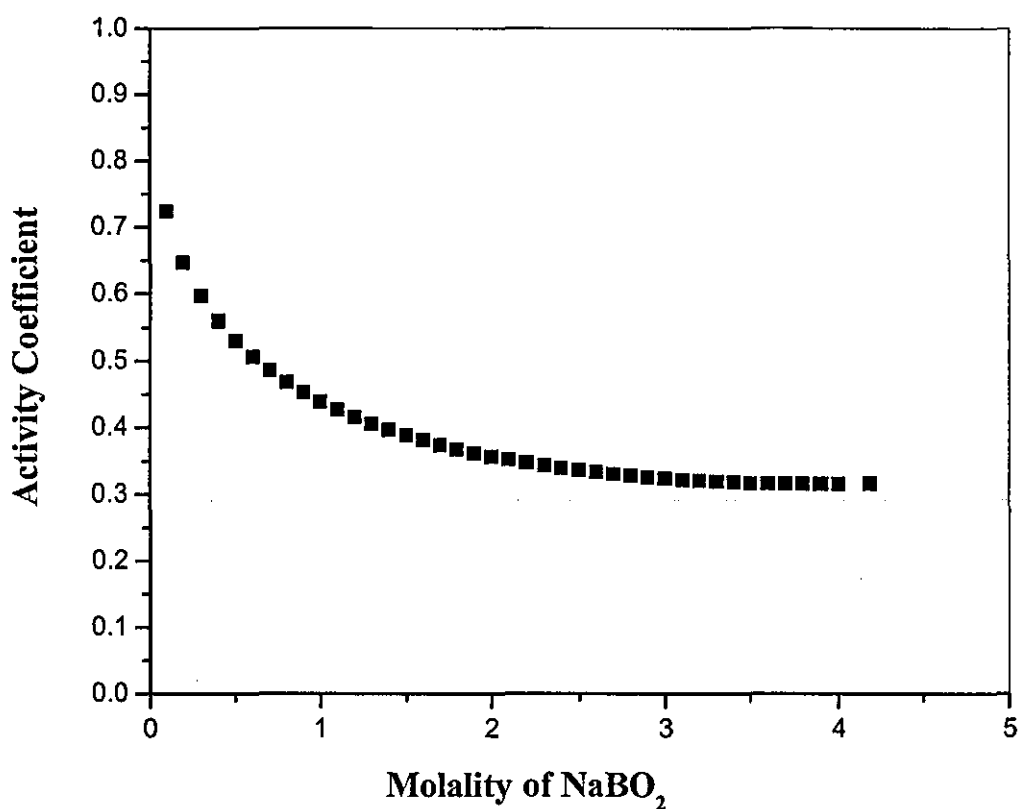
Figure 3.1 The activity coefficient of $NaBO_2$ in water at $25°C$.

3.2.4 Determination of Model Parameters for $NaBH_4$ and $NaBO_2$

In order to calculate the solubility of $NaBH_4$ and $NaBO_2$ at any temperature, the parameters $\Delta H^\circ_{m,B}$ and $\Delta S^\circ_{m,B}$ must be determined using solubility data obtained at different temperatures. Since the number of cations and the number of anions in $NaBH_4$ or $NaBO_2$ is 1, $\nu_+ = \nu_- = 1$ for both $NaBH_4$ and $NaBO_2$. $\nu_\pm = \nu_+ + \nu_- = 2$ and $m_\pm = m$. Hence, equation (3.31) becomes

$$\ln m_B = -\frac{\Delta H^\circ_{m,B}}{2RT} + \frac{\Delta S^\circ_{m,B}}{2R} - \ln \gamma_\pm \qquad (3.39)$$

In this work, the solubility data for $NaBH_4$ and $NaBO_2$ in water were taken from the literature [1, 2] and reproduced in Table 3.2 and 3.3. The solubility data in the literature was given as weight percent. For $NaBH_4$, equation (3.54) was used to convert the

solubility in weight percent into the solubility in the molality scale. The converted data is shown in the third column of Table 3.2.

$$m_{NaBH_4} = \frac{w_{NaBH_4}/M_{NaBH_4}}{100 - w_{NaBH_4}} \times 1000 \tag{3.40}$$

where w_{NaBH_4} is the solubility of $NaBH_4$, which is expressed as the weight of solute B in 100 g solution. M_{NaBH_4} is the molar mass of $NaBH_4$.

Table 3.2 The solubility of $NaBH_4$ at various temperatures.

Temperature (°C)	Weight percentage of $NaBH_4$ (5)	Solubility in molality (mol kg^{-1})
0	27.5	10.027
7	30	11.329
10	31	11.876
16	33	13.020
25	36.5	15.194
30	39	16.900
35	42.5	19.538
36.5	45	21.628
38	45.5	22.069
42	48	24.401
45	50	26.434
47	51	27.513
50	54	31.031

The calculation of solubility from the weight percentage for $NaBO_2$ is more complicated than that for $NaBH_4$ because the existing form of BO_2^- ion in aqueous solution is $B(OH)_4^-$. Therefore, the molality of $NaBO_2$ in its saturated solution is calculated using equation (3.41):

$$m_{NaBO_2} = \frac{w_{NaBO_2} / M_{NaBO_2}}{100 - w_{NaBO_2} - 2 \times M_{H_2O} \times (w_{NaBO_2} / M_{NaBO_2})} \times 1000 \qquad (3.41)$$

where w_{NaBO_2} is the solubility of $NaBO_2$ (which is expressed as the weight of solute $NaBO_2$ in 100 g solution) and M_{NaBO_2} and M_{H_2O} are the molecular weights of $NaBO_2$ and H_2O respectively. The converted solubility in the molality scale is shown in the third column of Table 3.3.

Table 3.3 The solubility of $NaBO_2$ at various temperatures.

Temperature (°C)	Weight percentage of $NaBO_2$ (%)	Solubility in molality (mol kg^{-1})
20	20	4.402
25	21.6	4.931
30	23.6	5.651
35	25.6	6.444
40	27.9	7.463
45	30.8	8.945
50	34.1	10.974
53.6	36.9	13.075
55	37.2	13.326
60	38.3	14.294
65	39.5	15.446
70	40.9	16.938
75	42.2	18.490
80	43.7	20.520
85	45.4	23.205
90	47.4	27.043
95	49.6	32.445
100	52.4	42.136

After converting the solubility data for NaBH$_4$ and NaBO$_2$ in water into molality, ln(m_B) was plotted against $\dfrac{1}{T}$ as shown in Figures 3.2 and 3.3, where the subscript B denotes NaBH$_4$ or NaBO$_2$, m is the solubility of B in molality and T is the absolute temperature (K).
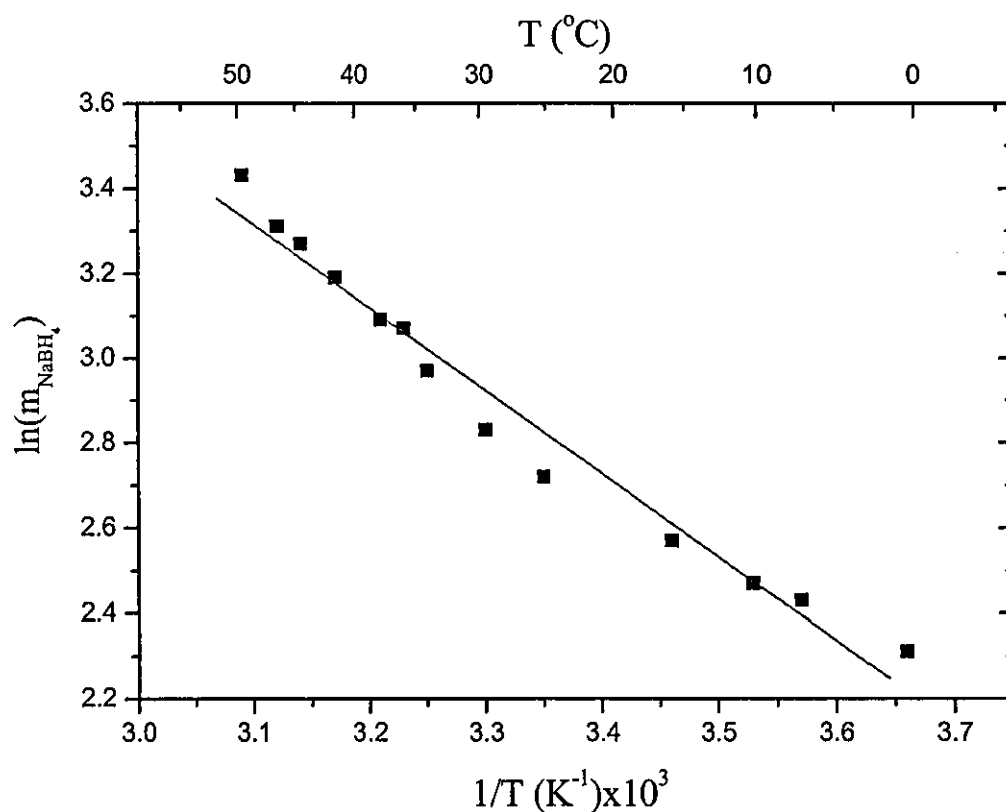
Figure 3.2 The effect of temperature on the solubility of NaBH$_4$.
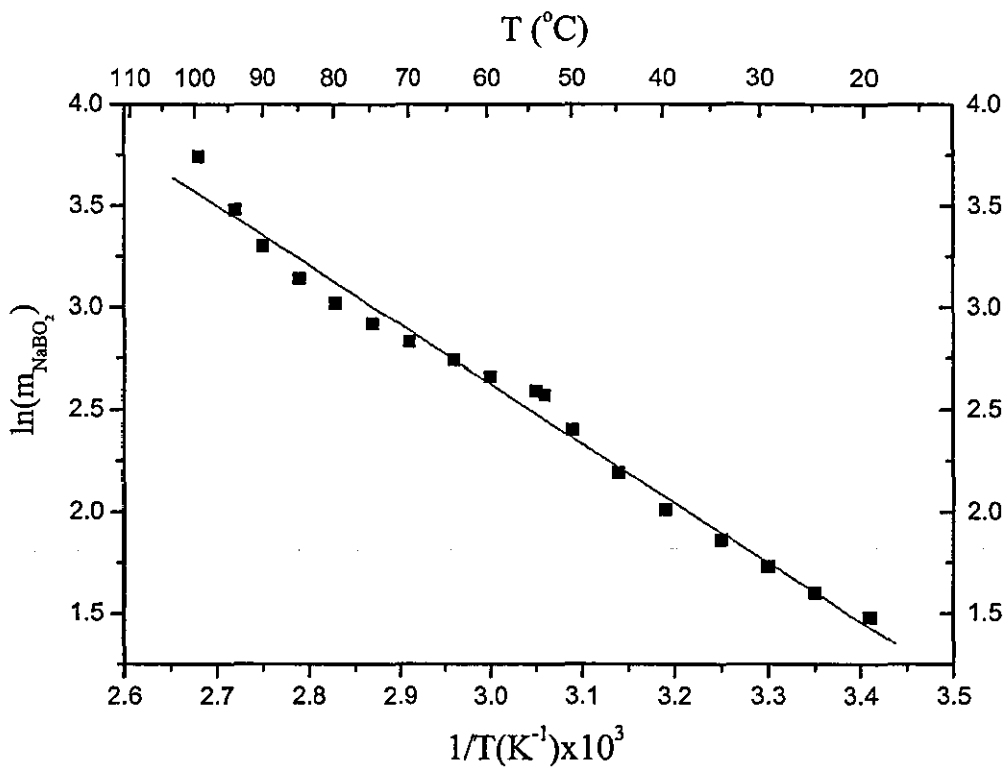
Figure 3.3 The effect of temperature on the solubility of $NaBO_2$.

It can be seen that $\ln m_B$ and $\dfrac{1}{T}$ does not exhibit a good linear relationship for both $NaBH_4$ and $NaBO_2$ solution, though the discrepancy may be attributed to experimental error. From equation (3.39), the slope of the line represents $-\dfrac{\Delta H^{\circ}_{m,B}}{R}$ and the intercept represents $\dfrac{\Delta S^{\circ}_{m,B}}{R} - \ln \gamma_{\pm}$. The enthalpy change $\Delta H^{\circ}_{m,B}$ can thus be calculated from the slope. The values of $\Delta H^{\circ}_{m,B}$ and $\dfrac{\Delta S^{\circ}_{m,B}}{R} - \ln \gamma_B$ for $NaBH_4$ and $NaBO_2$ are listed in Table 3.4.

Table 3.4 Parameters for equation (3.39) for $NaBH_4$ and $NaBO_2$ solution.

Species	$-\dfrac{\Delta H^{\circ}_{m,B}}{2R}$	$\Delta H^{\circ}_{m,B}$ (kJ mol^{-1})	$\dfrac{\Delta S^{\circ}_{m,B}}{R} - \ln \gamma_B$ (K)
$NaBH_4$	1982.3	32.96	9.47
$NaBO_2$	2912.9	48.43	11.37

3.3 Calculation of the Maximum NaBH₄ Concentration

Substituting the parameters for $NaBH_4$ and $NaBO_2$ into equation (3.45), the solubility dependencies of $NaBH_4$ or $NaBO_2$ on the solution temperature are expressed using equations (3.42) and (3.43) respectively.

$$\ln m_{NaBH_4} = -\frac{1982.3}{T} + 9.47 \tag{3.42}$$

$$\ln m_{NaBO_2} = -\frac{2912.9}{T} + 11.37 \tag{3.43}$$

For one mole of $NaBH_4$, the water contained in the saturated solution W_1 can be calculated using equation (3.44).

$$W_1 = \frac{1000}{m_{NaBH_4}} \tag{3.44}$$

For one mole of $NaBO_2$, the water contained in the saturated solution W_2 can be calculated using equation (3.45).

$$W_2 = \frac{1000}{m_{NaBO_2}} \tag{3.45}$$

The mass of water that is required to react with one mole of $NaBH_4$, W_3, can be calculated using equation (3.46) since four moles of water are needed to hydrolyse one mole of $NaBH_4$.

$$W_3 = 4 \times M_{H_2O} \tag{3.46}$$

where M_{H_2O} is the molar mass of water.

The results shown in Figure 3.4 compare the amount of water contained in a $NaBH_4$ solution with the amount of water needed to dissolve one mole of $NaBO_2$ and the water for the hydrolysis at various temperatures.
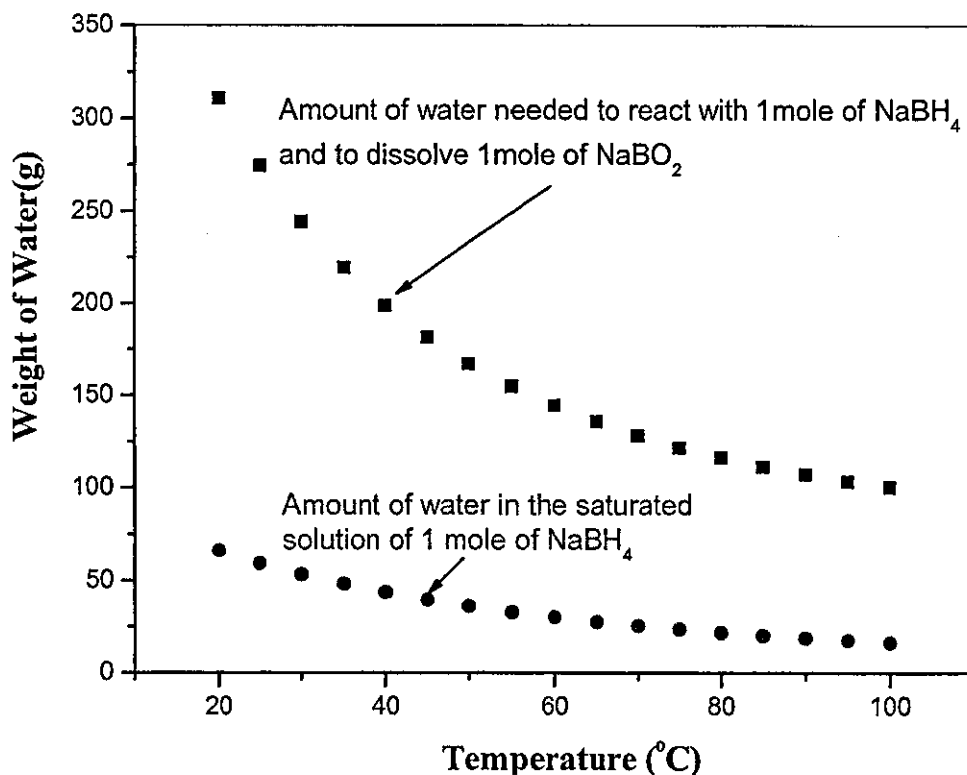
Figure 3.4 Comparison of the amount of water in $NaBH_4$ saturated solution with that required for the hydrolysis and to dissolve the by-product $NaBO_2$.

It can be seen that the amount of water required to hydrolyse one mole of $NaBH_4$ and to dissolve the $NaBO_2$ that is produced is significantly larger than the amount of water contained in the saturated $NaBH_4$ solution that contains one mole of $NaBH_4$. Hence, it is the water required to hydrolysis $NaBH_4$ and dissolve the by-product $NaBO_2$ that determines the minimum water required in the system.

The maximum concentration of the system w can thus be calculated using equation (3.47):

$$w = \frac{1 * M_{NaBH_4}}{1 * M_{NaBH_4} + W_2 + W_3} \tag{3.47}$$

where w is the maximum concentration of $NaBH_4$ (wt%), and M_{NaBH_4} is the molar mass of $NaBH_4$ (g mol^{-1}).

Figure 3.5 shows both the calculated maximum $NaBH_4$ concentration in the hydrolysis system and the concentration of saturated $NaBH_4$ solution at various temperatures. Two interesting phenomena need to be addressed here. First, the maximum concentration of $NaBH_4$ for the hydrolysis system is about half that of a saturated solution of $NaBH_4$. Secondly, the maximum concentration increases as the hydrolysis temperature increases, which clearly increases the energy density.
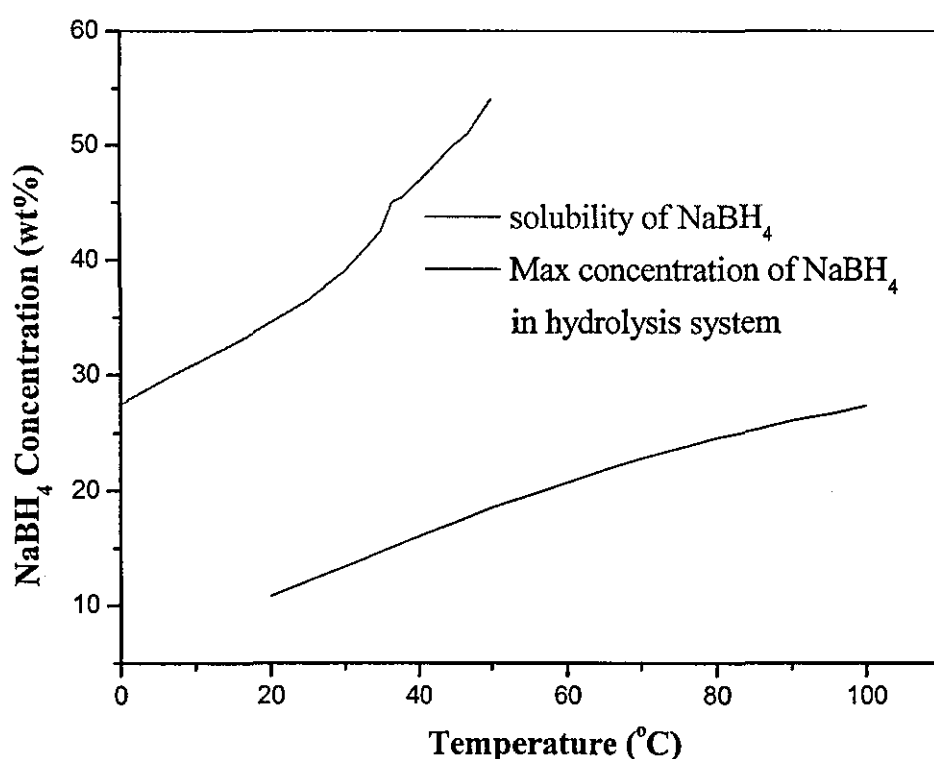
Figure 3.5 Comparison of the calculated $NaBH_4$ solubility and its maximum concentration in the hydrolysis system.

3.4 Experimental

3.4.1 Materials

Sodium borohydride ($NaBH_4$) was purchased from Sigma-Aldrich Company Ltd, being in a powder form with a purity of 98%. The ruthenium catalyst used to accelerate the hydrolysis of $NaBH_4$ was purchased from Johnson Matthey Ltd, 3% ruthenium supported on carbon. The catalyst was in a pellet form with a diameter of 2 mm.

3.4.2 Method

When the $NaBH_4$ concentration is at its maximum value, the by-product $NaBO_2$ will precipitate from the solution. Visual observation of the precipitation of $NaBO_2$ from solution was used to determine the maximum concentration of $NaBH_4$ that can be used.

A series of $NaBH_4$ solutions were prepared in 10 ml glass vials from low to high $NaBH_4$ concentration around the theoretical maximum concentration as shown in Figure 3.5. The weight of each vial containing reaction mixture was measured. Hydrolysis was conducted at the temperature at which the maximum concentration was to be determined. After the reaction was finished, the weight of the vial containing products was measured again. The water loss due to the evaporation was added to the vial. The water loss was calculated using equation (3.48).

$$m_4 = m_1 - m_2 - m_3 \tag{3.48}$$

Where m_1 is the weight of the vial before hydrolysis, m_2 is the weight of the vial after hydrolysis and m_3 is the water consumed during reaction, which can be calculated using chemical equation.

The glass vials were then sealed and transferred to an oven, which was set at the reaction temperature. After 24 hours, the glass vials was examined visually to determine if there was any $NaBO_2$ precipitate. The minimum solution concentration in which precipitation occurred was considered to be the maximum concentration of $NaBH_4$ solution at that temperature. The experimental set up is shown in Figure 3.6 and the experimental results are given in Table 3.5.

Since the interval of the weight percentage between the vials in which precipitation of $NaBO_2$ did and did not occur was 0.5%, the error for each experimental measurement was taken to be 0.5%.
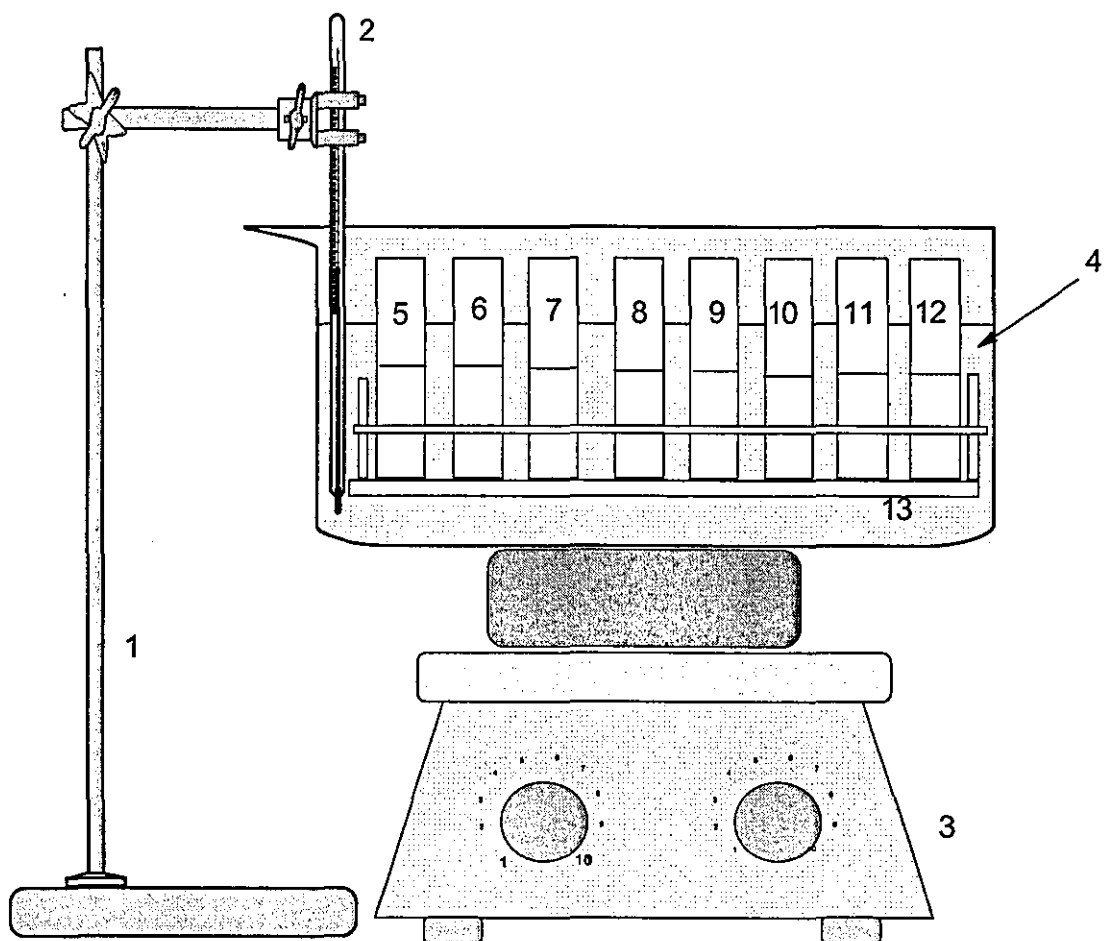
Figure 3.6 Schematic diagram for measuring maximum NaBH₄ concentration. 1: Support; 2: thermometer; 3: hot plate; 4: water; 5-12: reaction vials; 13: support for reaction vials.

Table 3.5 Experimental determination of maximum concentration of $NaBH_4$.

Reaction temperature (°C)	$NaBH_4$ concentration (%)	Did precipitation occur?
26	9.0	×
	10.0	×
	11.0	×
	11.5	√
	12.0	√
	12.5	√
	13.0	√
	13.5	√
35	12.0	×
	13.0	×
	14.0	×
	14.5	×
	15.0	×
	15.5	√
	16.0	√
	16.5	√
42	14.0	×
	15.0	×
	15.5	×
	16.0	×
	16.5	×
	17.0	×
	17.5	√
	18.0	√
56	18.0	×
	18.5	√
	19.5	√
	20.0	√
	20.5	√
	21.0	√
	21.5	√
	22.0	√
70	20.0	×
	21.0	×
	22.0	×
	22.5	×
	23.0	×
	23.5	×
	24.0	√
	24.5	√

3.5 Comparison of Modelling Results with Experimental Data

Experiments were conducted at five temperatures (26, 35, 42, 55, and 70 $^{\circ}$C) to observe the precipitation of $NaBO_2$ from the reaction system according to the above experimental procedure. The experimental data and the calculated line are shown in Figure 3.7.

It is shown clearly that the maximum concentration of $NaBH_4$ in the hydrolysis system increases steadily with an increase in temperature. The experimentally determined maximum concentration of $NaBH_4$ increased from 13.5% at 26°C to 24% at 70°C. The calculated values are in good agreement with experimental data.
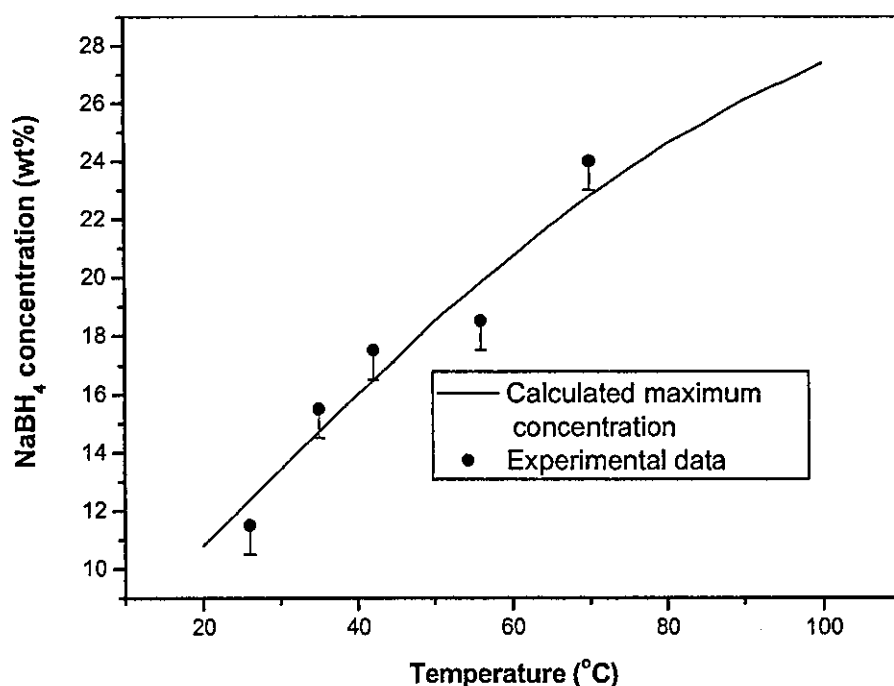
Figure 3.7 Comparison between the calculated and experimental concentration of $NaBH_4$.

3.6 Conclusions

In this chapter, a model was established based on the equality of the chemical potential in solution and in solid form in order to calculate the maximum concentration of $NaBH_4$ in its aqueous solution before $NaBO_2$ begins to precipitate. The maximum concentration was then determined experimentally. The experimental data agrees well with and theoretical

calculation and the following conclusions can be drawn.

- The relationship between the solubility of NaBH$_4$ and NaBO$_2$ with temperature was satisfied by the equation:

$$\ln m_\pm = -\frac{\Delta H^\circ_{m,B}}{\nu_\pm RT} + \frac{\Delta S^\circ_{m,B}}{\nu_\pm R} - \ln \gamma_\pm$$

- The activity coefficient of NaBO$_2$ levels off approximately to a constant with an increase in concentration.

- The water required to hydrolyse NaBH$_4$ and to dissolve the by-product NaBO$_2$ is much greater than is available in the saturated sodium borohydride solution. The latter controls the maximum concentration in the hydrolysis system.

- The maximum concentration of NaBH$_4$ increases significantly with an increase in reaction temperature.

3.7 References

1. Mellor, J.W., *Supplement to Mellor's comprehensive treatise on inorganic and theoretical chemistry.* Vol. 5 Boron-Hydrogen compounds. 1981, London: London: Longman. 223.

2. Mellor, J.W., *Supplement to Mellor's comprehensive treatise on inorganic and theoretical chemistry.* Vol. 5, Boron-Oxygen compounds. 1980, London: Longman. 257.

3. Atkins, P.W., *Solubility*, in *Physical Chemistry.* 1990, Oxford University Press: Oxford. 226.

4. Kim, H.-T. and Frederick, W., *Evaluation of Pitzer Ion Interaction Parameters of Aqueous Mixed Electrlyte solutions at 25C. 1. Single Salts Parameters.* Journal of chemical Engineering Data, 1988. **33**: 177-184.

5. Pitzer, K.S. and Mayorga, G., *Thermodynamics of Electrolytes. II Activity and Osmotic Coefficients for Strong Electrolytes with One or Both Ions Univalent.* the Journal of Physical Chemistry, 1973. **77**(19).

6. Pitzer, K.S. and Kim, J., *Thermodynamics of Electrolytes, IV.Activity and Osmotic Coefficient for Mixed Electrolytes.* Journal of American Chemical society, 1974. **96**.

7. Song, W. and Larson, M.A., *Activity Coefficient Model of Concentrated Electrolyte Solutions.* AIChE Journal, 1990. **36**(12): 1896-1900.

Chapter 4

Maximum Concentration of NaBH$_4$ in the Presence of NaOH

4.1 Introduction

In Chapter 3, the maximum concentration of NaBH$_4$ in the absence of NaOH was investigated. In some situations it is convenient to use NaBH$_4$ in solution rather than in its solid state since the solution is easier to handle. However, an aqueous solution of NaBH$_4$ is not stable. Hydrogen is generated when there is no stabilizer in the solution, even at room temperature. This would cause a decrease in the energy density and would also bring about safety problems. The hydrolysis of NaBH$_4$ can be slowed by increasing the pH of the solution [1-6]. Hence, NaOH is added to the solution in order to stabilise it. In practice, various NaOH concentrations have been suggested: 4 % (wt) [1], 10 %(wt) [4] and 5-10 % (wt) [7].

The addition of NaOH significantly affects the solubility of both NaBH$_4$ and NaBO$_2$. In this chapter, the maximum concentration of NaBH$_4$ is discussed when NaOH is present. Due to the lack of solubility data, thermodynamic modelling is used.

4.2 Construction of Models

When solute B dissolves in water in the presence of a third component, A, (that is, solute B dissolves in A's solution) the chemical potential of B in the solution is equal to the chemical potential of the solid state in equilibrium considering that solution A is the solvent. Hence, equation (4.1) can be derived in the same way as described in Chapter 3, where component A was not present.

$$\ln m_{\pm,\text{B}} = -\frac{\Delta H^0_{m,\text{B}}}{v_{\pm}RT} + \left(\frac{\Delta S^0_{m,\text{B}}}{v_{\pm}R} - \ln \gamma'_{\pm,B}\right) \tag{4.1}$$

where $m_{\pm,B}$ is the average solubility of B on the molality scale, $\Delta H^0_{m,B}$ and $\Delta S^0_{m,B}$ are the molar enthalpy change and entropy change respectively when species B dissolves from solid state to an activity of 1 mol kg^{-1} in solution of A. Since the initial and final states are the same as those for dissolution in pure water, the same symbols are used for enthalpy and entropy change as in Chapter 3. $\gamma'_{\pm,B}$ is the mean activity coefficient of B in a solution of A.

The molar enthalpy change and entropy change can be considered to be constant when the temperature range is not large. To determine the parameters $\Delta H^0_{m,B}$ and $\Delta S^0_{m,B}$, equation (4.1) is modified by adding $-\ln\gamma_{\pm,B}$ to both sides. $\gamma_{\pm,B}$ is the activity coefficient of B in the absence of component A.

$$\ln m_{\pm,B} - \ln\gamma_{\pm,B} = -\frac{\Delta H^0_{m,B}}{v_{\pm}RT} + \frac{\Delta S^0_{m,B}}{v_{\pm}RT} - \ln\gamma'_{\pm,B} - \ln\gamma_{\pm,B} \tag{4.2}$$

Rearranging equation (4.2), gives

$$\ln m_{\pm,B} + \ln\frac{\gamma'_{\pm,B}}{\gamma_{\pm,B}} = -\frac{\Delta H^0_{m,B}}{v_{\pm}RT} + \left(\frac{\Delta S^0_{m,B}}{v_{\pm}RT} - \ln\gamma_{\pm,B}\right) \tag{4.3}$$

For both NaBH$_4$ and NaBO$_2$, $v_{\pm} = 2$. Substituting the value into equation (4.3), gives

$$\ln m_{\pm,B} + \ln\frac{\gamma'_{\pm,B}}{\gamma_{\pm,B}} = -\frac{\Delta H^0_{m,B}}{2RT} + \left(\frac{\Delta S^0_{m,B}}{2RT} - \ln\gamma_{\pm,B}\right) \tag{4.4}$$

$\gamma_{\pm,B}$ is a constant for the saturated solutions of NaBH$_4$ and NaBO$_2$ as shown in Chapter 3. Therefore, a plot of $\ln m_{\pm,B} + \ln\frac{\gamma'_{\pm}}{\gamma_{\pm}}$ and $1/T$ should yield a straight line graph whereby the intercept on the y-axis is $\left(\frac{\Delta S^0_{m,B}}{v_{\pm}RT} - \ln\gamma_{\pm,B}\right)$ and the slope is $-\frac{\Delta H^0_{m,B}}{v_{\pm}RT}$. The ratio of the activity coefficients $\frac{\gamma'_{\pm,B}}{\gamma_{\pm,B}}$ can be calculated using the hydration analysis method [8-10].

4.3 Solubility Data of $NaBH_4$ and $NaBO_2$ in NaOH Solutions

4.3.1 Solubility Data for $NaBH_4$ in NaOH Aqueous Solutions

4.3.1.1 Description of the Phase Diagram

The solubility of $NaBH_4$ in NaOH aqueous solutions is not available directly in the literature. However, the phase diagram of the $NaBH_4$-NaOH-H_2O system is available [11]. The phase diagram shows the equilibrium composition of $NaBH_4$, NaOH and H_2O at specific temperatures. The solubility of $NaBH_4$ in NaOH solutions can thus be derived from the phase diagram.

The isothermal phase diagram of the $NaBH_4$-NaOH-H_2O system at 0°C, 18°C, 30°C, and 50°C was reproduced in Figure 4.1 [11]. As can be seen, the original phase diagram is in triangle form. The three vertexes of the triangle phase diagram represent $NaBH_4$, NaOH and H_2O respectively. The three sides of the triangle represent the composition of two components: $NaBH_4$-H_2O, $NaBH_4$-NaOH and NaOH-H_2O. Any point inside the triangle represents the composition of the three components. For the convenience of calculation in a model, the triangle phase diagram was transformed into a rectangular phase diagram as shown in Figure 4.2. The x-axis represents the weight percentage of NaOH in the solution and the y-axis represents the weight percentage of $NaBH_4$ in the solution.
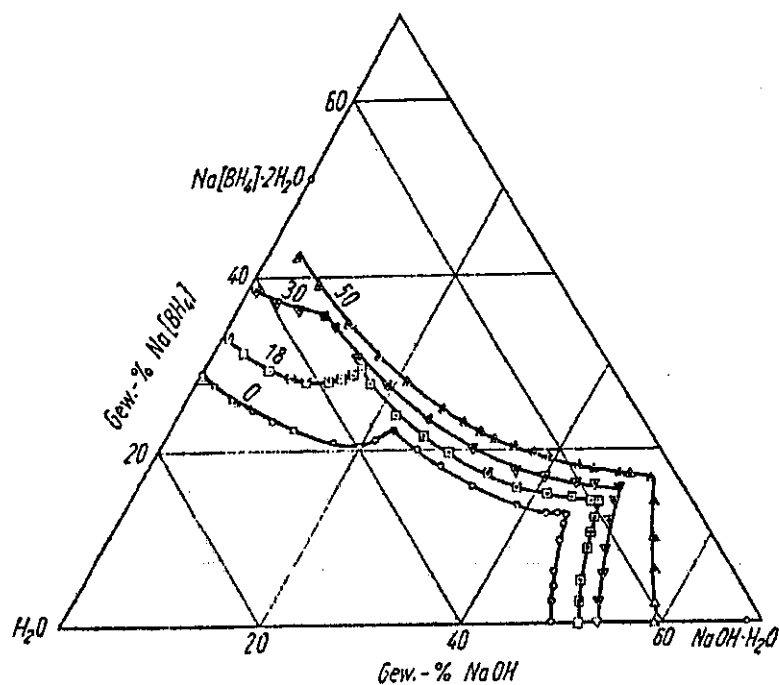
Figure 4.1 Phase diagram of the NaBH₄-NaOH-H₂O system at 0°C-50°C [11].
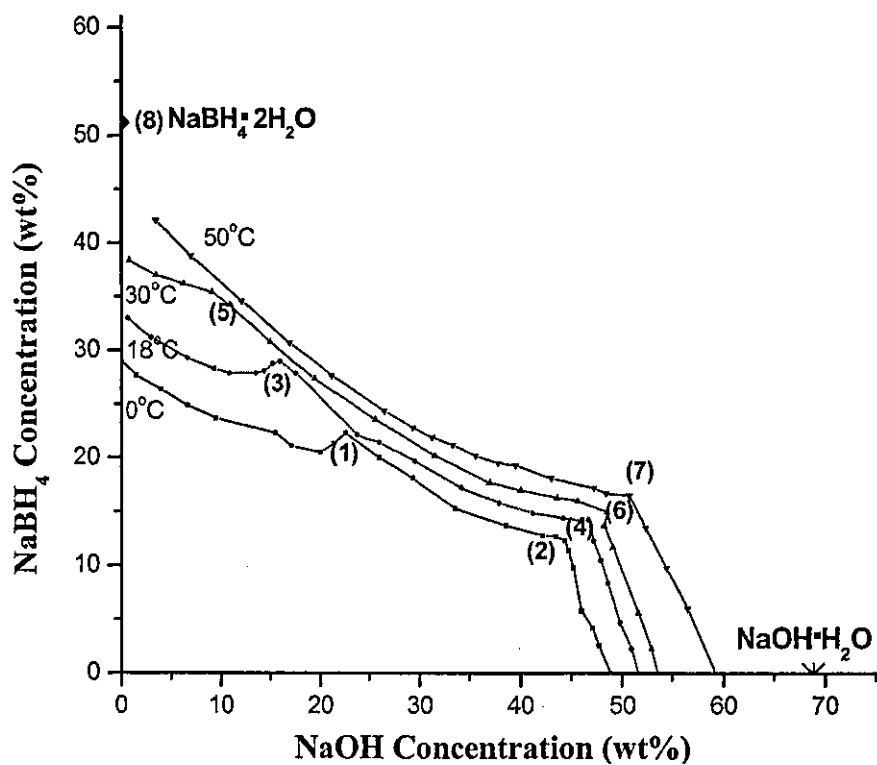
Figure 4.2 Phase diagram of the NaBH₄-NaOH-H₂O system at 0°C-50°C transformed from Figure 4.1.

The following information can be seen from Figure 4.2:

- At a given temperature, the solubility line consists of smooth parts and inflection points. In the smooth parts, only one crystalline form co-exists with the solution. A different smooth part corresponds to a different crystalline form. At the inflection point between two smooth parts, two different crystalline forms co-exist with the solution. The inflection point between two smooth parts is termed the invariant point since the composition and temperature are fixed at this point. For example, at invariant point (1) in Figure 4.2, the crystalline states of $NaBH_4 \bullet 2H_2O$ and $NaBH_4$ co-exist with the $NaBH_4$ in $NaOH$ solution. The temperature at this point is $0°C$, and the composition is 22.5% $NaOH$, 22.3% $NaBH_4$ and 55.2% water. Table 4.1 lists the invariant points and their composition in the phase diagram. There are seven invariant points in total in the phase diagram, which are labelled using points (1)-(7).

- The line for $0°C$ is divided into three parts by two invariant points (1) and (2). The solution phase consists of $NaBH_4$, $NaOH$ and H_2O. To the left of the invariant point (2), $NaBH_4$ is saturated and $NaOH$ is not saturated in the solution. To the left of the invariant point (1), the equilibrium solid phase is crystalline $NaBH_4 \bullet 2H_2O$. At the invariant point (1), the equilibrium solid phase consists of two crystals, $NaBH_4 \bullet 2H_2O$ and $NaBH_4$. Between points (1) and (2), the equilibrium solid state is $NaBH_4$. At the invariant point (2), $NaOH$ becomes saturated in the solution phase and the corresponding equilibrium crystalline state is $NaOH \bullet H_2O$. The solid state in the solution is the co-existence of $NaBH_4$ and $NaOH \bullet H_2O$. To the right of the invariant point (2), $NaBH_4$ is no longer saturated in the solution phase, and the equilibrium solid state consists only of $NaOH \bullet H_2O$. At $18°C$ and $30°C$, the situations are similar to that at $0°C$ except for the invariant point compositions.

- At $50°C$, there is only one invariant point (7). To the left of the invariant point (7), the equilibrium solid state is $NaBH_4$. At the invariant point (7), $NaOH$ also becomes saturated in the solution, and the equilibrium solid state consists of two crystals, $NaBH_4$ and $NaOH \bullet H_2O$. To the right of the invariant point (7), $NaBH_4$ is no longer saturated and the equilibrium solid state consist of only $NaOH \bullet H_2O$.

- At a specific NaOH concentration, the solubility of NaBH₄ increases with an increase in temperature.

- At a specific temperature, the solubility of NaBH₄ decreases with an increase in NaOH concentration.

Table 4.1 The invariant point compositions on the phase diagram for $NaBH_4$-$NaOH$-H_2O system.

Temperature (°C)	Invariant point	w_{NaBH_4} (%)	w_{NaOH} (%)	Crystalline states
0	(1)	22.3	22.5	$NaBH_4 \bullet 2H_2O + NaBH_4$
	(2)	12.3	44.4	$NaBH_4 + NaOH \bullet H_2O$
18	(3)	29	16	$NaBH_4 \bullet 2H_2O + NaBH_4$
	(4)	13.9	46.8	$NaBH_4 + NaOH \bullet H_2O$
30	(5)	35.4	9.1	$NaBH_4 \bullet 2H_2O + NaBH_4$
	(6)	15	48.5	$NaBH_4 + NaOH \bullet H_2O$
50	(7)	16.5	50.8	$NaBH_4 + NaOH \bullet H_2O$

4.3.1.2 Regression of the Phase Diagram for NaBH₄-NaOH-H₂O

For the convenience of calculation, the relationship between NaOH concentration w_{NaOH} and NaBH₄ concentration w_{NaBH_4} at each smooth part in Figure 4.2 were regressed using polynomial equations. The use of the polynomial equation was by observation of the line shape and it was justified by the error of the regression. The regressions are shown in Figure 4.3. The equations obtained and the errors incurred are listed in Table 4.2. Good fits were obtained when the polynomial equations were used for the regression.
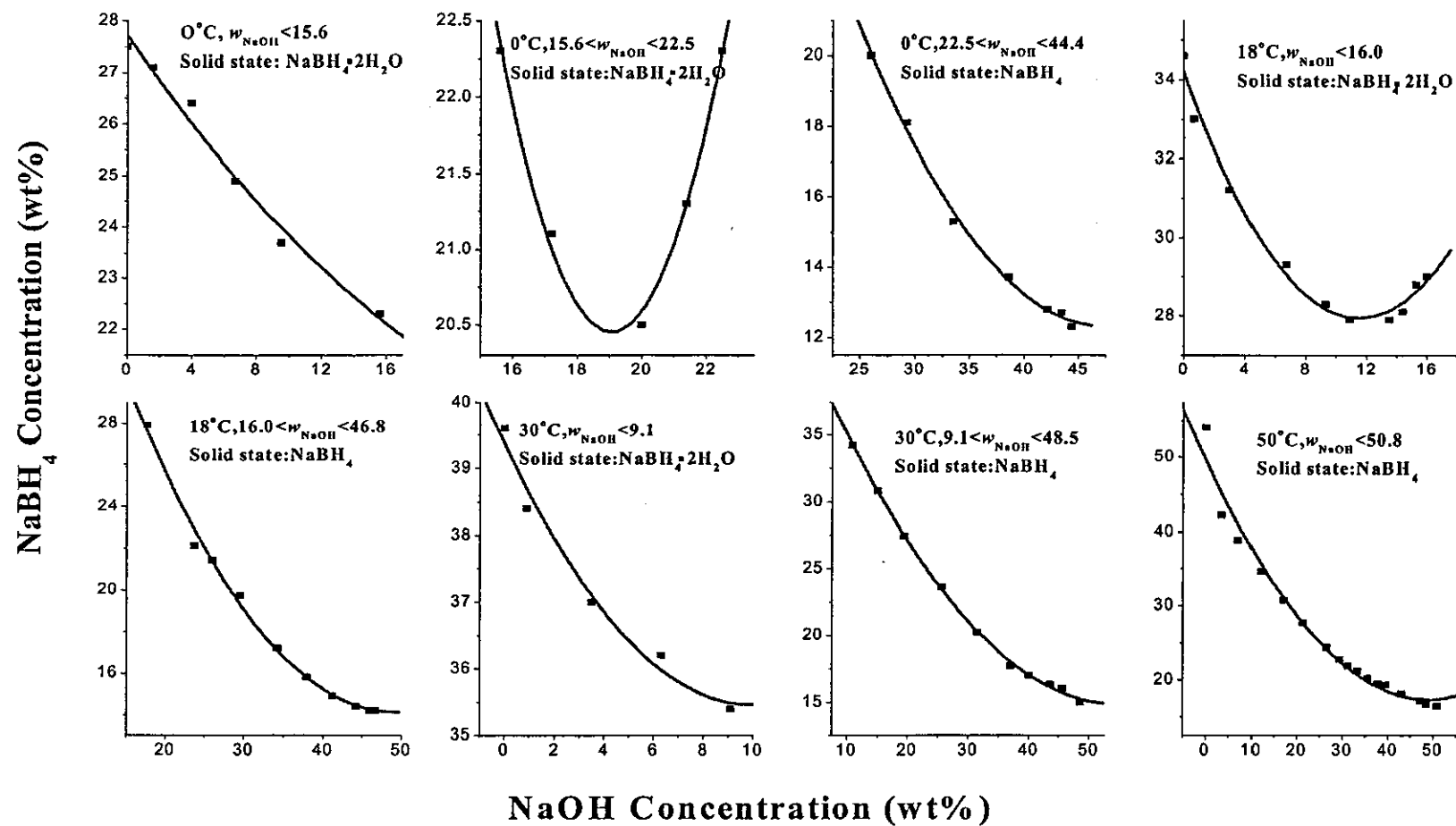
Figure 4.3 Regression of the phase diagram of NaBH₄-NaOH-H₂O using polynomial equations.

Table 4.2 The polynomial equations of phase diagram in Figure 4.2.

Temperature (°C)	w_{NaOH} (%)	Solid state	Equations, $y = w_{NaBH_4}$, $x = w_{NaOH}$	Error (R^2)
0°C	<15.6	$NaBH_4 \cdot 2H_2O$	$y = 0.0209x^2 - 0.7568x + 29.016$	0.99
0°C	15.6~22.5	$NaBH_4 \cdot 2H_2O$	$y = 0.1567x^2 - 5.9788x + 77.49$	0.99
0°C	22.5~44.4	$NaBH_4$	$y = 0.0171x^2 - 1.6197x + 50.613$	1.0
18°C	<16	$NaBH_4 \cdot 2H_2O$	$y = 0.0471x^2 - 1.085x + 34.186$	0.99
18°C	16~46.8	$NaBH_4$	$y = 0.0135x^2 - 1.3286x + 46.802$	1.0
30°C	<9.1	$NaBH_4 \cdot 2H_2O$	$y = 0.0397x^2 - 0.7859x + 39.357$	0.98
30°C	9.1~48.5	$NaBH_4$	$y = 0.0102x^2 - 1.1084x + 45.112$	1.0
50°C	<50.8	$NaBH_4$	$y = 0.0101x^2 - 1.0991x + 46.439$	0.98

At this stage, there are only four points to regress when the left-hand side of equation (4.4) is plotted against $1/T$ at each NaOH concentration. The more points that are regressed, the more accurate the parameters that are obtained can be. Another temperature point can be obtained by regression of the invariant points.

NaOH concentration above 25% was not considered, since higher concentrations have no practical significance. When NaOH concentration is lower than 25%, there are four known invariant points; (1), (3), (5) and (8) as shown in Figure 4.2. For a given NaOH concentration, for example the vertical line at a NaOH concentration of 5%, there are four intersections with the four temperature lines. The intersections with 0°C, 18°C and 30°C correspond to the solid state $NaBH_4 \cdot 2H_2O$, but the intersection with the 50°C line corresponds to the solid state $NaBH_4$. It can be inferred that there is an invariant point between 30°C and 50°C, at which these two crystals co-exist. This invariant point can be obtained by regressing the four known invariant points.

Invariant points have a fixed composition and temperature. The composition and temperature for the four known invariant points are shown in Figures 4.4 and 4.5 respectively. They were then regressed using a polynomial equation. The equations that are obtained are given in Table 4.3.
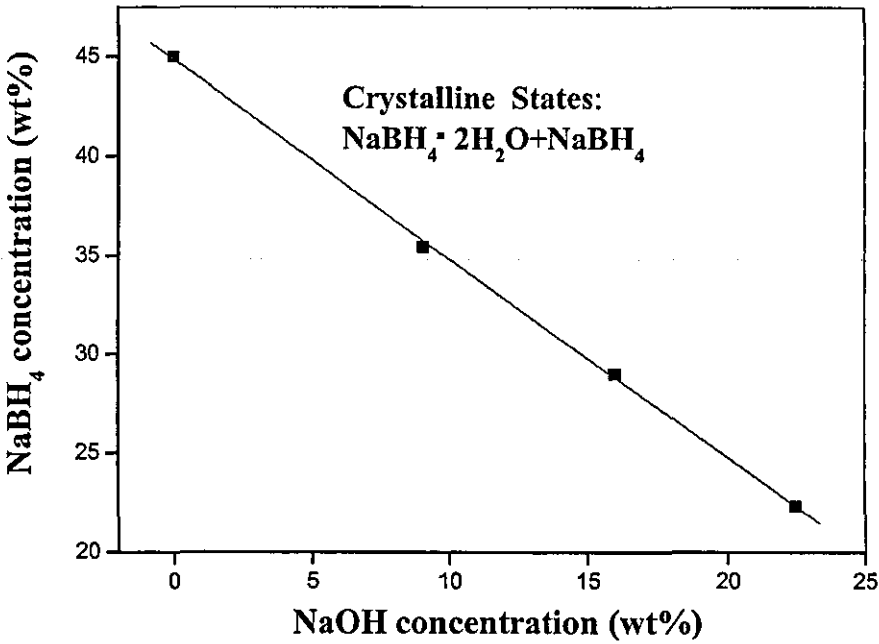
Figure 4.4 Regression of the composition of the invariant points for NaBH$_4$-NaOH-H$_2$O with NaOH concentration below 25 %.
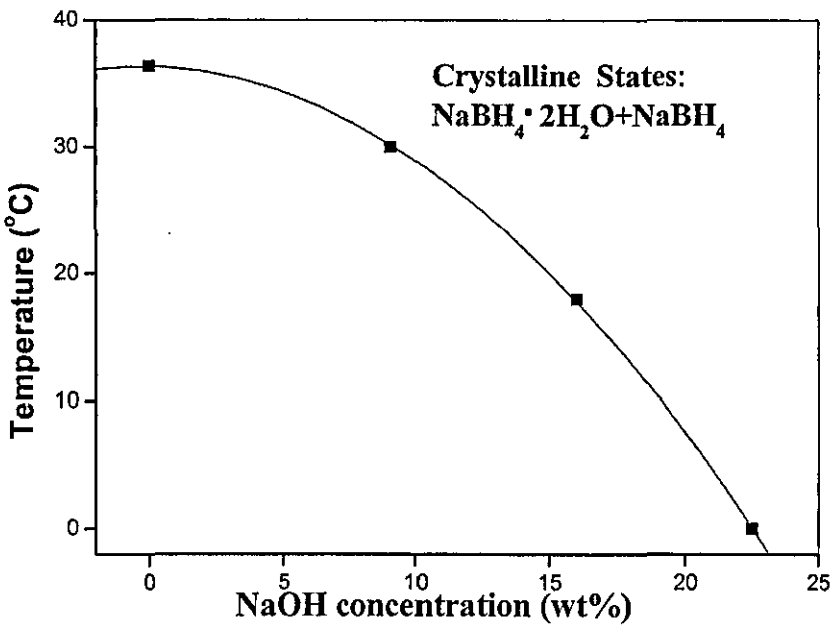
Figure 4.5 Regression of the temperature of the invariant points for NaBH$_4$-NaOH-H$_2$O with NaOH concentration below 25 %.

Table 4.3 The regression of the invariant points for $NaBH_4$-$NaOH$-H_2O with $NaOH$ concentration lower than 25%.

	Equation	Error (R^2)
Composition	$y = -1.0026x + 44.856$	0.99
Temperature	$T = -0.0696x^2 - 0.0458 + 36.356$	0.99

4.3.2 Solubility Data of $NaBO_2$ in $NaOH$ Aqueous Solutions

4.3.2.1 Description of the Phase Diagram

The solubility data of $NaBO_2$ in $NaOH$ solutions are not available directly from the literature. A phase diagram for Na_2O-B_2O_3-H_2O is available [12], as reproduced in Figure 4.6. The solubility data for $NaBO_2$ can be calculated from this phase diagram.

As shown in Figure 4.6, the horizontal axis represents the composition of Na_2O (wt%) in the solution. The vertical axis represents the composition of B_2O_3 (wt%) in the solution. The remaining part is water. The ratio data on the lines are the compositions of the solid phase equilibrated with the solution. The other data on the line are the temperatures of the solutions. For example, the data 1:1:8 represents Na_2O:B_2O_3:H_2O = 1:1:8, i.e. $NaBO_2 \bullet 4H_2O$.

When the ratio of Na_2O to B_2O_3 equals to 1:1, it represents the solubility of $NaBO_2$ in $NaOH$ solutions. This is the lower right part of the diagram. The phase diagram for $NaBO_2$-$NaOH$-H_2O is derived by using the following equations to calculate the composition for $NaBO_2$ and $NaOH$

$$w_{NaBO_2} = \frac{w_{B_2O_3}}{M_{B_2O_3}} \times 2M_{NaBO_2} \qquad (4.5)$$

$$w_{NaOH} = (\frac{w_{Na_2O}}{M_{Na_2O}} - \frac{w_{B_2O_3}}{M_{B_2O_3}}) \times 2M_{NaOH} \qquad (4.6)$$

94

where M_{NaBO_2} and M_{NaOH} are the molecular weight of $NaBO_2$ and NaOH respectively. The derived phase diagram is shown in Figure 4.7.
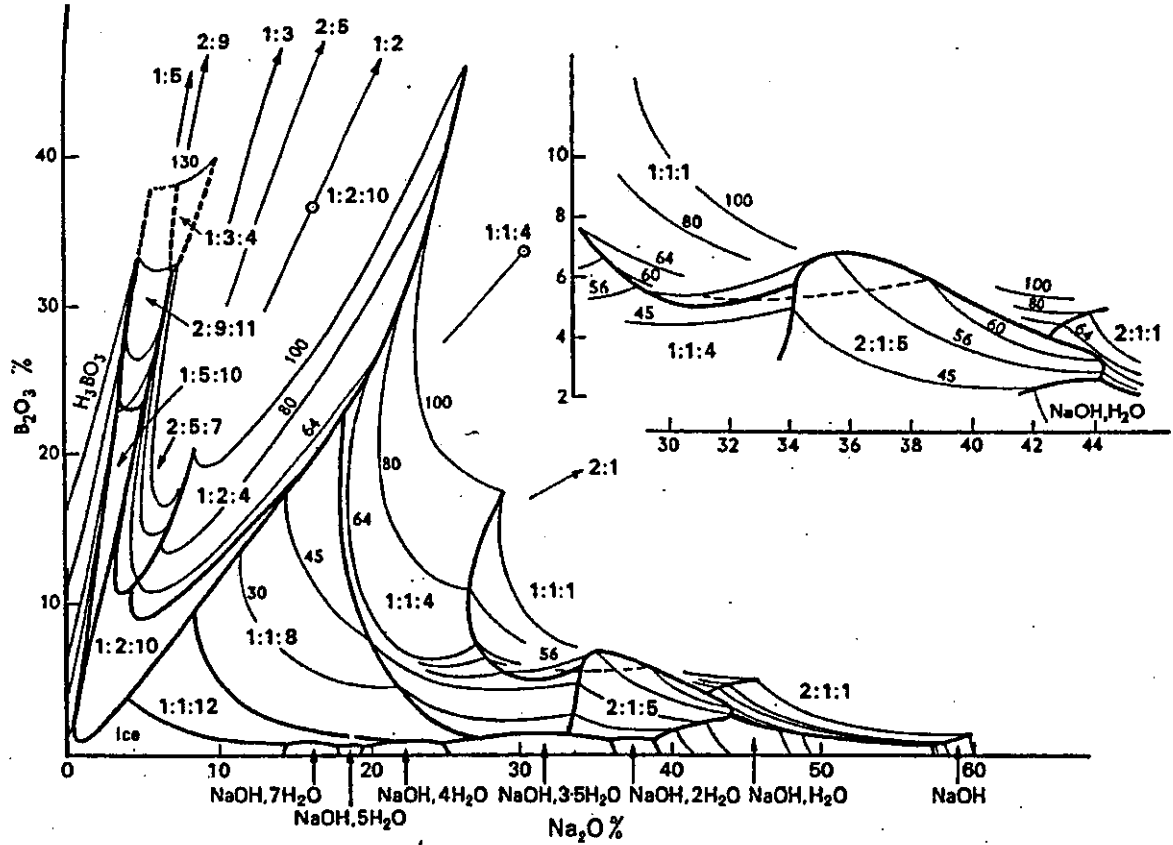
Figure 4.6 Phase diagram for the Na_2O-B_2O_3-H_2O system from 0 to 100 °C.
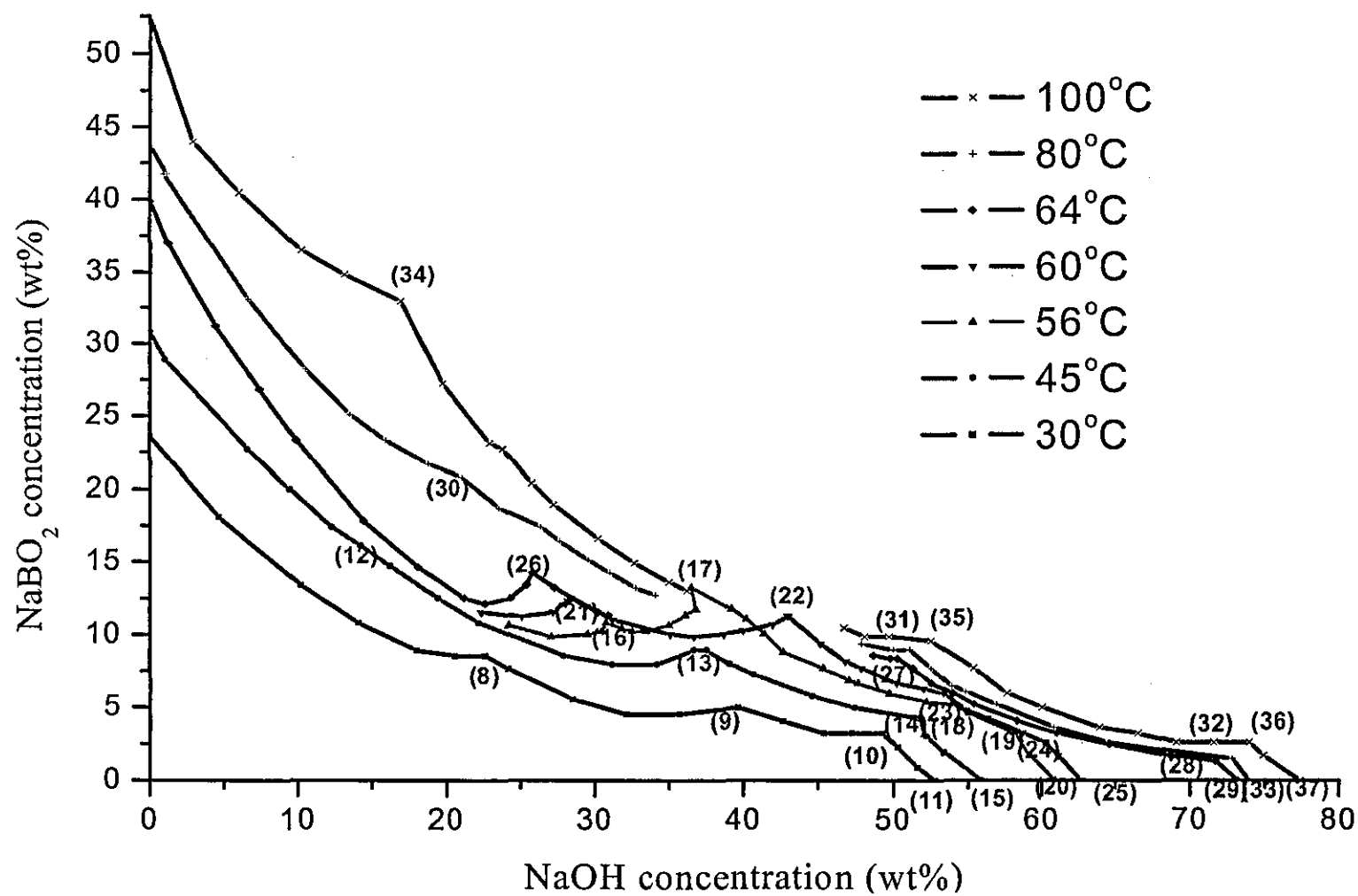
Figure 4.7 Phase diagram for the $NaBO_2$-$NaOH$-H_2O system transformed from Figure 4.6.

The phase diagram for $NaBO_2$-$NaOH$-H_2O in Figure 4.7 can be interpreted as follows:

- As in the phase diagram for $NaBH_4$-$NaOH$-H_2O, there are invariant points at which two different crystals exist. The invariant points, the compositions and the corresponding equilibrium compositions are listed in Table 4.4. In the smooth parts, the corresponding solid phases consist of only one crystal. On the invariant points, the solid phases consist of two types of crystal.

- With an increase in NaOH concentration, new compounds $Na_4B_2O_5 \bullet 5H_2O$ and $Na_4B_2O_5 \bullet H_2O$ are formed.

- At a specific NaOH concentration, the solubility of $NaBO_2$ increases with an increase in temperature.

- As a specific temperature, the solubility of $NaBO_2$ decreases rapidly with an increase in NaOH concentration.

Table 4.4 The invariant points for $NaBO_2$-$NaOH$-H_2O at 0-100 °C.

Temperature (°C)	w_{NaBO_2} (%)	w_{NaOH} (%)	Crystalline states	Related point in the phase diagram
30	8.5	22.6	$NaBO_2 \bullet 4H_2O + NaBO_2 \bullet 2H_2O$	(8)
	4.9	39.6	$NaBO_2 \bullet 2H_2O + Na_4B_2O_5 \bullet 5H_2O$	(9)
	3.2	49.2	$Na_4B_2O_5 \bullet 5H_2O + NaOH \bullet H_2O$	(10)
	0	52.8	$NaOH \bullet H_2O$	(11)
45	14.7	16.2	$NaBO_2 \bullet 4H_2O + NaBO_2 \bullet 2H_2O$	(12)
	8.9	37.5	$NaBO_2 \bullet 2H_2O + Na_4B_2O_5 \bullet 5H_2O$	(13)
	4.2	51.7	$Na_4B_2O_5 \bullet 5H_2O + NaOH \bullet H_2O$	(14)
	0	55.9	$NaOH \bullet H_2O$	(15)
56	10.8	30.8	$NaBO_2 \bullet 2H_2O + NaBO_2 \bullet 1/2H_2O$	(16)
	13.2	37.6	$NaBO_2 \bullet 1/2H_2O + Na_4B_2O_5 \bullet 5H_2O$	(17)
	5.1	53.9	$Na_4B_2O_5 \bullet 5H_2O + Na_4B_2O_5 \bullet H_2O$	(18)
	3.2	58.1	$Na_4B_2O_5 \bullet H_2O + NaOH \bullet H_2O$	(19)
	0.0	60.9	$NaOH \bullet H_2O$	(20)
60	12.5	28.4	$NaBO_2 \bullet 2H_2O + NaBO_2 \bullet 1/2H_2O$	(21)
	11.2	43.0	$NaBO_2 \bullet 1/2H_2O + Na_4B_2O_5 \bullet 5H_2O$	(22)
	5.9	53.4	$Na_4B_2O_5 \bullet 5H_2O + Na_4B_2O_5 \bullet H_2O$	(23)
	2.6	60.2	$Na_4B_2O_5 \bullet H_2O + NaOH \bullet H_2O$	(24)
	0.0	62.7	$NaOH \bullet H_2O$	(25)
64	14.2	25.8	$NaBO_2 \bullet 2H_2O + NaBO_2 \bullet 1/2H_2O$	(26)
	8.3	50.3	$NaBO_2 \bullet 1/2H_2O + Na_4B_2O_5 \bullet H_2O$	(27)
	1.3	71.7	$Na_4B_2O_5 \bullet H_2O + NaOH$	(28)
	0.0	73.2	$NaOH$	(29)
80	20.8	21.0	$NaBO_2 \bullet 2H_2O + NaBO_2 \bullet 1/2H_2O$	(30)
	8.9	51.1	$NaBO_2 \bullet 1/2H_2O + Na_4B_2O_5 \bullet H_2O$	(31)
	1.5	72.8	$Na_4B_2O_5 \bullet H_2O + NaOH$	(32)
	0.0	74.0	$NaOH$	(33)
100	32.9	16.9	$NaBO_2 \bullet 2H_2O + NaBO_2 \bullet 1/2H_2O$	(34)
	9.5	52.5	$NaBO_2 \bullet 1/2H_2O + Na_4B_2O_5 \bullet H_2O$	(35)
	2.6	74.0	$Na_4B_2O_5 \bullet H_2O + NaOH$	(36)
	0.0	77.4	$NaOH$	(37)

4.3.2.2 Data Regression of the System of $NaBO_2$-$NaOH$-H_2O

As with the $NaBH_4$ system, the smooth parts in Figure 4.7 at each temperature were regressed using polynomial equations. The equations are expressed using the relations between w_{NaOH} and w_{NaBO_2}. The regressions are shown in Figures 4.8 and 4.9. The equations that were obtained are listed in Table 4.5.

Table 4.5 The regressed equations for $NaBO_2$-$NaOH$-H_2O system.

Temperature (°C)	w_{NaOH} (%)	Solid state	Equations, $y = w_{NaBO_2}$, $x = w_{NaOH}$	Error (R^2)
30°C	<22.6	$NaBO_2 \bullet 4H_2O$	$y = 0.0322x^2 - 1.4366x + 24.461$	1.0
30°C	22.6~39.6	$NaBO_2 \bullet 2H_2O$	$y = 0.027x^2 - 1.8885x + 37.426$	1.0
45°C	<16.2	$NaBO_2 \bullet 4H_2O$	$y = 0.023x^2 - 1.3483x + 30.556$	1.0
45°C	16.2~37.5	$NaBO_2 \bullet 2H_2O$	$y = 0.0298x^2 - 1.8967x + 38.107$	0.98
56°C	<30.8	$NaBO_2 \bullet 2H_2O$	$y = 0.0352x^2 - 1.9305x + 36.505$	1.0
56°C	30.8~37.6	$NaBO_2 \bullet 1/2H_2O$	$y = 0.1595x^2 - 10.624x + 186.94$	0.98
60°C	<28.4	$NaBO_2 \bullet 2H_2O$	$y = 0.0474x^2 - 2.2507x + 38.005$	1.0
60°C	28.4~43.0	$NaBO_2 \bullet 1/2H_2O$	$y = 0.0347x^2 - 2.5687x + 57.395$	0.98
64°C	<25.8	$NaBO_2 \bullet 2H_2O$	$y = 0.045x^2 - 2.2123x + 40.093$	0.99
64°C	25.3~50.3	$NaBO_2 \bullet 1/2H_2O$	$y = 0.0152x^2 - 1.3814x + 39.537$	0.99
80°C	<21.0	$NaBO_2 \bullet 2H_2O$	$y = 0.0368x^2 - 1.8631x + 43.654$	1.0
80°C	21.0~51.1	$NaBO_2 \bullet 1/2H_2O$	$y = 0.0131x^2 - 1.3395x + 43.242$	1.0
100°C	<16.9	$NaBO_2 \bullet 2H_2O$	$y = 0.0677x^2 - 2.2083x + 51.419$	0.98
100°C	16.3~52.5	$NaBO_2 \bullet 1/2H_2O$	$y = 0.0202x^2 - 1.973x + 57.92$	1.0
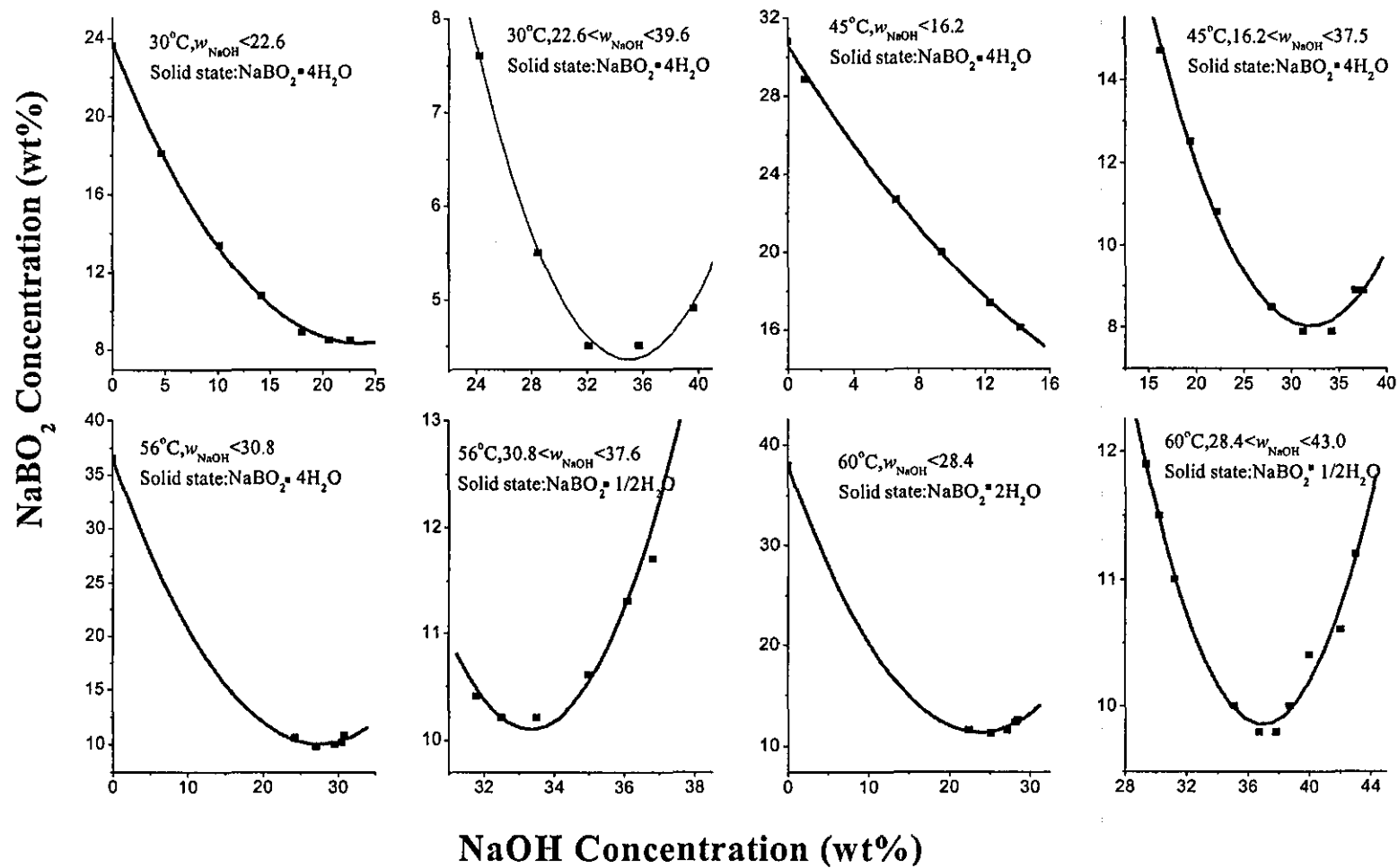
Figure 4.8 Regression of the phase diagram of the $NaBO_2$-$NaOH$-H_2O system.
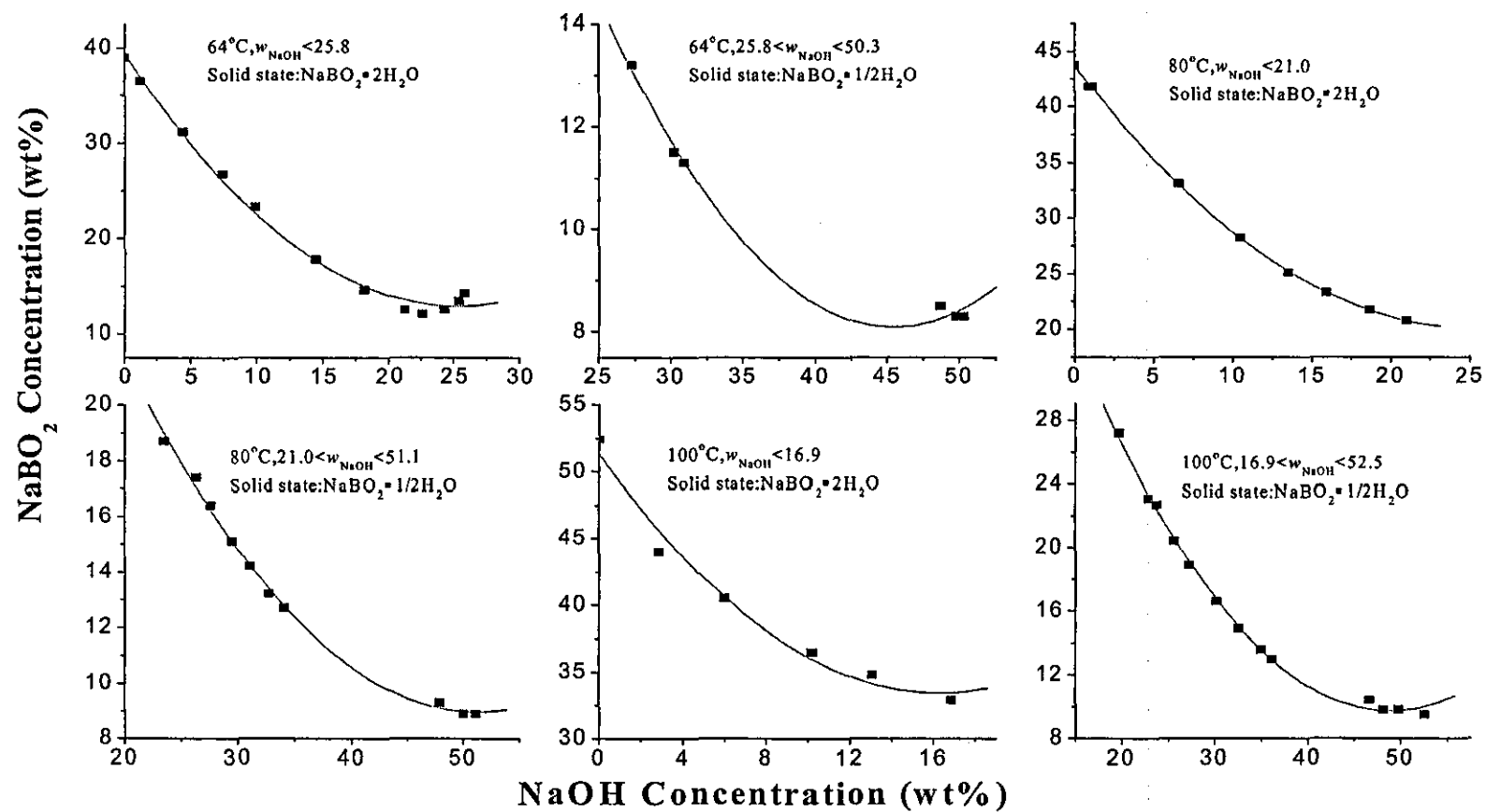
Figure 4.9 Regression of the phase diagram of the NaBO₂-NaOH-H₂O system.

As with $NaBH_4$-$NaOH$-H_2O, the invariant points were also regressed in order to increase the number of data points when plotting the left-hand side of equation (4.4) against $1/T$ at a specific NaOH concentration. For $NaBO_2$-$NaOH$-H_2O, there are two sets of invariant points when NaOH concentration is below 30%: $NaBO_2{\bullet}4H_2O$ and $NaBO_2{\bullet}2H_2O$ co-existence and $NaBO_2{\bullet}2H_2O$ and $NaBO_2{\bullet}1/2H_2O$ co-existence. The regressions for the former are shown in Figures 4.10 and 4.11 for composition and temperature respectively. The regressions for the latter are shown in Figures 4.12 and 4.13 for composition and temperature respectively. The equations that were obtained are listed in Table 4.6.
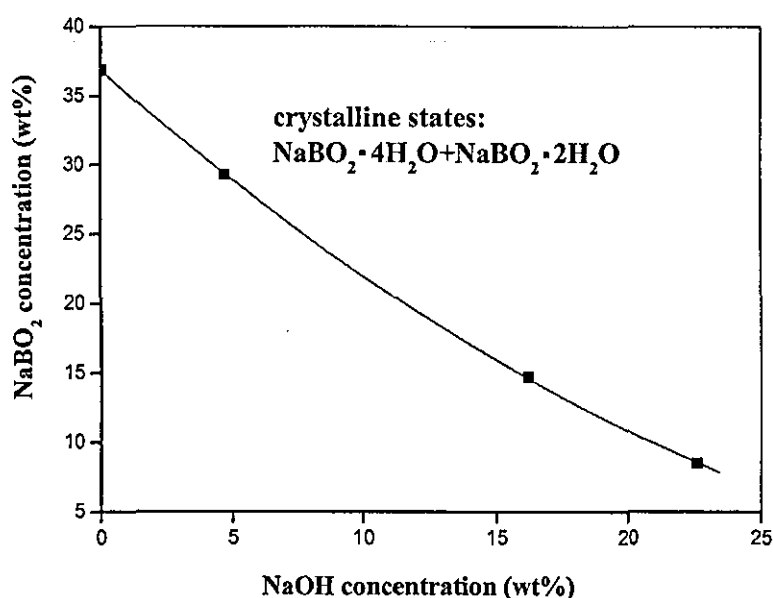
Figure 4.10 Regression of the composition of the invariant points for $NaBO_2$-$NaOH$-H_2O with NaOH concentration below 30% for the co-existence of $NaBO_2$ $4H_2O$+ $NaBO_2$ $2H_2O$.
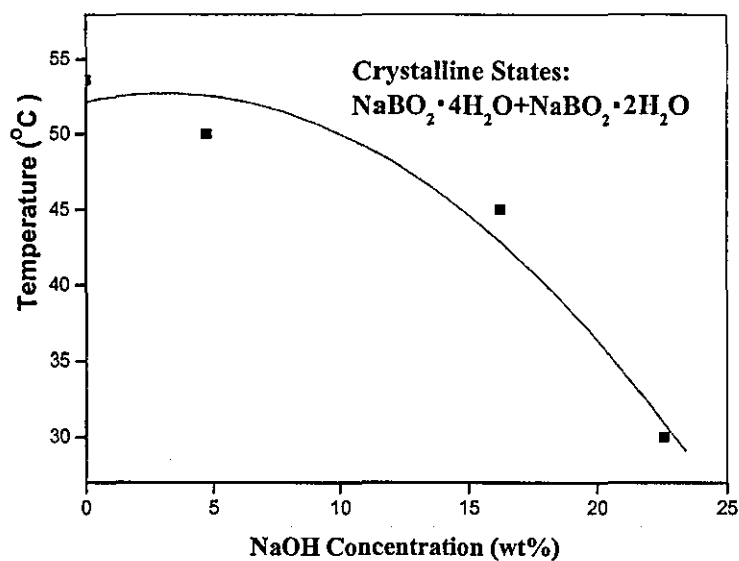
Figure 4.11 Regression of the temperature of the invariant points for $NaBO_2$-$NaOH$-H_2O with NaOH concentration below 30% for the co-existence of $NaBO_2$ $4H_2O$+ $NaBO_2$ $2H_2O$.
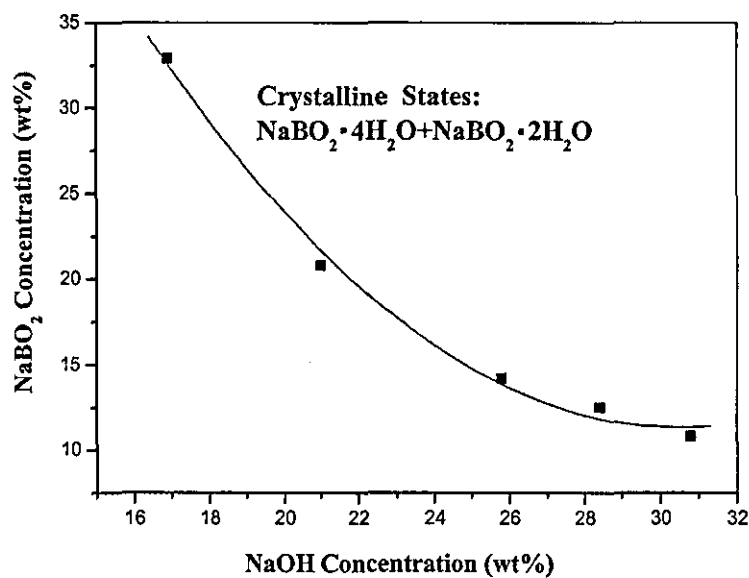
Figure 4.12 Regression of the composition of the invariant points for $NaBO_2$-$NaOH$-H_2O with NaOH concentration below 30% for the co-existence of $NaBO_2$ $2H_2O$+ $NaBO_2$ $1/2H_2O$.
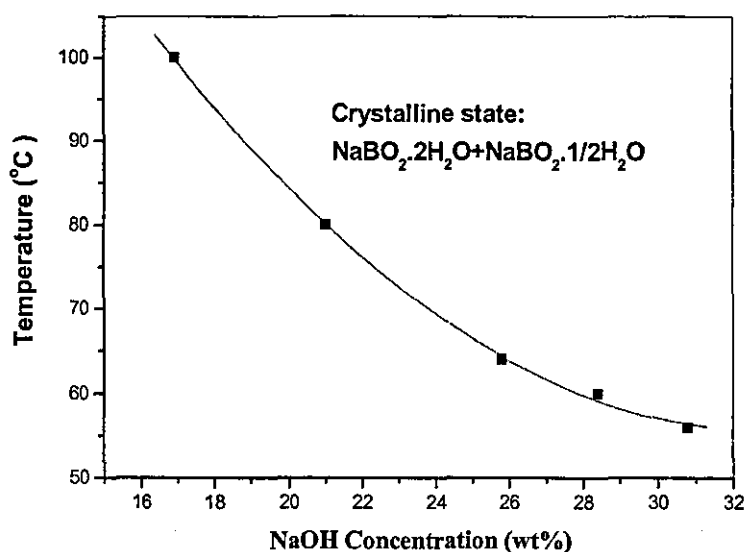
Figure 4.13 Regression of the temperature of the invariant points for $NaBO_2$-$NaOH$-H_2O with NaOH concentration below 30% for the co-existence of $NaBO_2\ 2H_2O$+ $NaBO_2\ 1/2H_2O$.

Table 4.6 Regression of invariant points for $NaBO_2$-$NaOH$-H_2O with NaOH concentration lower than 30%.

Solid state	$y = w_{NaBO_2}$ $x = w_{NaOH}$	$T = t(°C)$, $x = w_{NaOH}$
$NaBO_2•4H_2O$+ $NaBO_2•2H_2O$	$y = 0.0182x^2 - 1.6644x + 36.835$	$T = -0.0576x^2 + 0.3631x + 52.148$
$NaBO_2•2H_2O$ +$NaBO_2•1/2H_2O$	$y = 0.1146x^2 - 6.9968x + 118.14$	$T = 0.17x^2 - 11.248x + 241.58$

4.4 Hydration Analysis

4.4.1 Theoretical Background

The hydration analysis method is used to calculate the ratio of the activity coefficient of $NaBH_4$ or $NaBO_2$ in the presence of NaOH $\gamma'_{\pm,B}$ to the activity coefficient of $NaBH_4$ or $NaBO_2$ in the absence of NaOH $\gamma_{\pm,B}$. Hydration analysis is a method of analysing the solubility data to explain the ionic processes in ternary saturated solution [8-10].

104

Imagine a binary saturated solution, in which component B is dissolved in water. A third component A is added to the binary solution. A ternary solution is thus formed. The total amount of water in the ternary saturated solution is split into two parts: one part refers to the water that preserves the properties of the water in the binary saturated solution; the other part refers to the water that has changed its properties under the influence of component A.

A parameter P is defined as the mole fraction of water that has changed its properties, as shown by equation (4.7).

$$P = \frac{w_{H_2O} - w_{eff}}{M_{H_2O} \sum_{0}^{2} n_i} \tag{4.7}$$

where w_{H_2O} is the mass percentage of water in the ternary solution, w_{eff} is the mass percentage of 'property-unchanged' water in the ternary solution, M_{H_2O} is the relative molar mass of water (which is equal to 18.02), and $\sum_{0}^{2} n_i$ is the total mole number of the solution.

The dependence of parameter P on the amount of non-saturated component serves as a source of information on ionic properties in the solution. From the definition of P, the positive values of P indicate that water molecules have moved to the hydration sphere or envelope of the added ions. Values of $P \approx 0$ may be expected when the added ions are unable to compete with the component B for attracting water molecules. Negative values of P are expected in two situations:

a) The added component is a structure-breaking agent with respect to the saturated solution of component B.

b) The addition of component A may lead to ion-pairing, replacing some water molecules that had previously been in hydration envelopes.

In real systems, hydration and ionic interaction occur simultaneously. Both of these affect the value of P, i.e. the value of P is the result of two activities: a positive term related to

105

hydration and a negative term related to ion-pairing. For this reason the values of P cannot be used solely as an indication of hydration. In making such a 'hydration analysis', the analytical concentration of water is an important factor, and it must be taken into account.

For the ternary systems of $NaBH_4$-$NaOH$-H_2O or $NaBO_2$-$NaOH$-H_2O, an interaction parameter, I (analogous to solubility product on the molar scale) is defined as

$$I = m_{Na^+} m_{B^-} \qquad (4.8)$$

where m_{Na^+} is the molality of sodium ion, and m_{B^-} is the molality of the borohydride ion BH_4^- or metaborate ion BO_2^-.

For a binary solution, equation (4.8) changes into equations (4.9) since the molality of Na^+ and the molality of B^- are all equal to the molality of the salt.

$$I = \left(m_{NaB}^0 \right)^2 \qquad (4.9)$$

where m_{NaB}^0 is the molality of the $NaBH_4$ or $NaBO_2$ in the binary solution.

In the ternary system, the molality of the sodium ion comes from either $NaBH_4$ or $NaBO_2$ and $NaOH$. Equation (4.8) becomes

$$I' = (m_{NaOH} + m_{NaB}) m_{NaB} \qquad (4.10)$$

where m_{NaOH} is the molality of $NaOH$, and m_{NaB} is the molality of $NaBH_4$ or $NaBO_2$.

It can be seen that I and I' are not equal if the total water are taken into account. When the concept of effective water is introduced, $NaBH_4$ or $NaBO_2$ can be considered in an imaginary environment where $NaOH$ has no influence on the dissolution, since the effect of $NaOH$ has been included into the non-effective water. Therefore, when the 'property-unchanged' water (effective water) is taken into the calculation of the molalities in the ternary solution, I and I' are equal in the same temperature and pressure. Substituting the definition of molality, $m = \dfrac{\text{moles of solute}}{1000\text{g solvent}}$, into equation equations (9) and (10), gives

$$\left(\frac{1000 n_{NaB}^0}{w_{H_2O}^\circ}\right)^2 = \left(\frac{1000 n_{NaOH}}{w_{eff}} + \frac{1000 n_{NaB}}{w_{eff}}\right)\left(\frac{1000 n_{NaB}}{w_{eff}}\right) \tag{4.11}$$

Solving equation (4.9) for w_{eff}, yields

$$w_{eff} = \frac{w_{H_2O}^\circ \sqrt{n_{NaB}^2 + n_{NaB} n_{NaOH}}}{n_{NaB}^\circ} \tag{4.12}$$

where n_i is the moles of each component, $n_i = \dfrac{w_i}{M_i}$.

Combining equation (4.12) with (4.7), gives

$$P = \frac{n_{H_2O} n_{NaB}^\circ - n_{H_2O}^\circ \sqrt{n_{NaB}^2 + n_{NaB} n_{NaOH}}}{n_{NaB}^\circ (n_{H_2O} + n_{NaB} + n_{NaOH})} \tag{4.13}$$

In order to find the relationship between P and the activity coefficient, the usual description of the equilibrium with the aid of activity coefficients was discussed, forgetting the hydration analysis for a moment. In $NaBH_4$ or $NaBO_2$ saturated solution, dissolution equilibrium is shown in Scheme 4.1

$$NaB \Leftrightarrow Na^+ + B^-$$

Scheme 4.1 The ionic equilibrium of $NaBH_4$ or $NaBO_2$ in aqueous solutions.

The equilibrium constant can be expressed using equation (4.14).

$$K = \frac{a_{Na^+} a_{B^-}}{a_{NaB}} = \gamma_{\pm,B}^2 m_{Na^+} m_{B^-} \tag{4.14}$$

where a_{Na^+} and a_{B^-} are the activities of the sodium ion and BH_4^- or BO_2^- respectively, a_{NaB} is the activity of solid $NaBH_4$ or $NaBO_2$, the value of which is unity, m_{Na^+} is the molality of the sodium ion, and m_{B^-} is the molality of BH_4^- or BO_2^-. $\gamma_{\pm,B}$ is the mean activity coefficient. Since the value of the equilibrium constant does not depend on the existence of another component, equation (4.15) holds.

107

$$(\gamma_{\pm,B})^2 (m^0_{\text{NaB}})^2 = \gamma'^2_{\pm,B}(m_{\text{NaOH}} + m_{\text{NaB}})m_{\text{NaB}} \tag{4.15}$$

where $\gamma'_{\pm,B}$ is the mean activity coefficient of saturated $NaBH_4$ or $NaBO_2$ solution in the presence of NaOH, m^0_{NaB} is the molality of $NaBH_4$ or $NaBO_2$ in the absence of NaOH, m_{NaOH} is the molality of NaOH, and m_{NaB} is the molality of $NaBH_4$ or $NaBO_2$.

Rearranging equation (4.15), yields

$$\frac{\gamma'_{\pm}}{\gamma_{\pm}} = \left(\frac{(m^0_{\text{NaB}})^2}{(m_{\text{NaOH}} + m_{\text{NaB}})m_{\text{NaB}}} \right)^{1/2} \tag{4.16}$$

When using the hydration analysis method, the moles of water and NaB are needed. Substitute the molalities with the number of moles into equation (4.16), yields

$$\frac{\gamma'_{\pm}}{\gamma_{\pm}} = \left(\frac{\left(\dfrac{1000 n^{\circ}_{\text{NaB}}}{w^{\circ}_{H_2O}} \right)^2}{\left(\dfrac{1000 n_{\text{NaOH}}}{w_{H_2O}} + \dfrac{1000 n_{\text{NaB}}}{w_{H_2O}} \right) \dfrac{1000 n_{\text{NaB}}}{w_{H_2O}}} \right)^{1/2} \tag{4.17}$$

where n represents the number of moles, w represents the weight of water, the subscripts represents the corresponding substances, and the superscript 'o' represents the system when NaOH is not present.

Simplifying equation (4.17), yields

$$\frac{\gamma'_{\pm}}{\gamma_{\pm}} = \frac{w^{\circ}_{H_2O}\sqrt{n^2_{\text{NaB}} + n_{\text{NaB}}n_{\text{NaOH}}}}{n^{\circ}_{\text{NaB}}w_{H_2O}} \tag{4.18}$$

Substituting equation (4.12) into equation (4.18), yields

$$\frac{\gamma_{\pm}}{\gamma'_{\pm}} = \frac{w_{\text{eff}}}{w_{H_2O}} \tag{4.19}$$

Rearranging equation (4.19), gives

$$w_{\text{eff}} = w_{H_2O} \frac{\gamma_\pm}{\gamma'_\pm} \qquad (4.20)$$

Substituting equation (4.20) into equation (4.7), gives

$$P = x_{H_2O} (1 - \frac{\gamma_\pm}{\gamma'_\pm}) \qquad (4.21)$$

where $x_{H_2O} = \dfrac{w_{H_2O}}{M_{H_2O} \sum\limits_{0}^{2} n_i}$.

Rearranging equation (4.21), gives

$$\frac{\gamma'_\pm}{\gamma_\pm} = \frac{x_{H_2O}}{x_{H_2O} - P} \qquad (4.22)$$

It can be seen that the ratio of $\dfrac{\gamma'_\pm}{\gamma_\pm}$ can be calculated when the value of P is known. The

value of P can be calculated using equation (4.13).

4.4.2 Hydration Analysis of NaBH$_4$-NaOH-H$_2$O and NaBO$_2$-NaOH-H$_2$O

In the phase diagram of NaBH$_4$-NaOH-H$_2$O (Figure 4.2), each NaOH concentration corresponds to a NaBH$_4$ concentration for a specific temperature line. The weight percentage of water equals 100% minus the sum of NaBH$_4$ concentration and NaOH concentration. The same is the case for NaBO$_2$-NaOH-H$_2$O (Figure 4.4). The values of n_{H_2O}, n_{NaB} and n_{NaOH} in equation (4.13) were calculated from the phase diagrams. The values of $n^0_{H_2O}$ and n^0_{NaB} were obtained by setting $w_{NaOH} = 0$ in Figure 4.2 or Figure 4.4. The values of P's were then calculated using equation (4.13), which is shown in Figure 4.14 for NaBH$_4$-NaOH-H$_2$O and in Fig 4.17 for NaBO$_2$-NaOH-H$_2$O.

After obtaining the values of P for the two systems, they were divided by the molality of NaBH$_4$ or NaBO$_2$ at that point. The ratio is a measure of the effect of NaOH concentration on unit molality of NaBH$_4$ or NaBO$_2$. The quotient of P/m_{NaB} is given in Figures 4.15 and 4.18 for NaBH$_4$ and NaBO$_2$ respectively. The ratios of $\gamma'_{\pm,B}/\gamma_{\pm,B}$ were then calculated

109

using equation (4.20) and are shown in Figures 4.16 and 4.19 for $NaBH_4$ and $NaBO_2$ respectively.
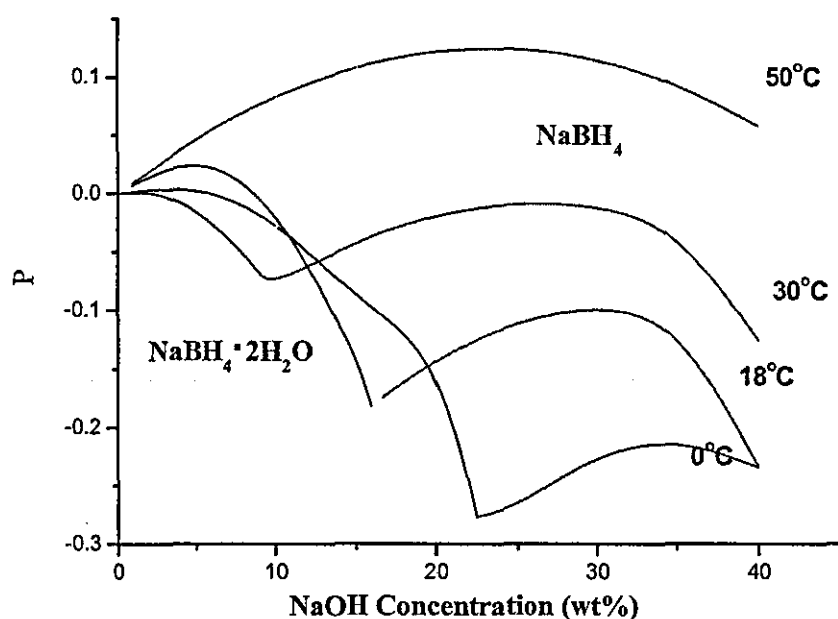
Figure 4.14 Calculated P value for the $NaBH_4$-$NaOH$-H_2O system.
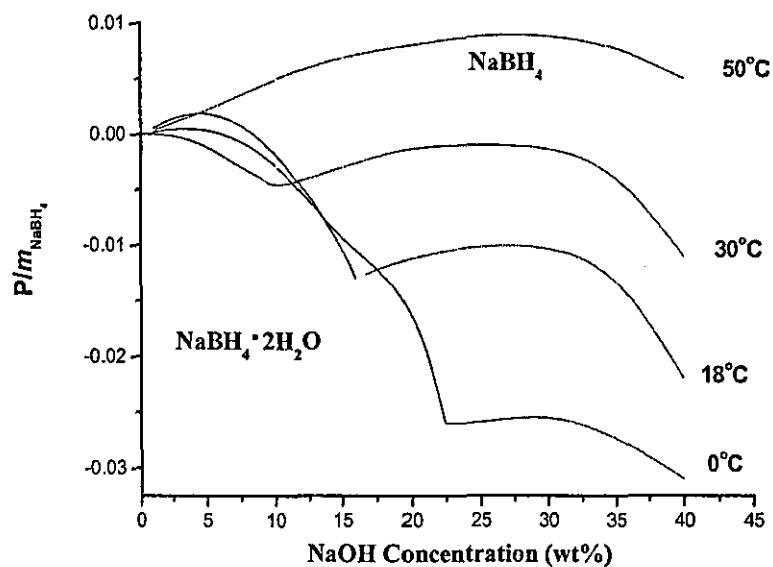
Figure 4.15 The effect of $NaOH$ on P value per unit molality of $NaBH_4$.

110
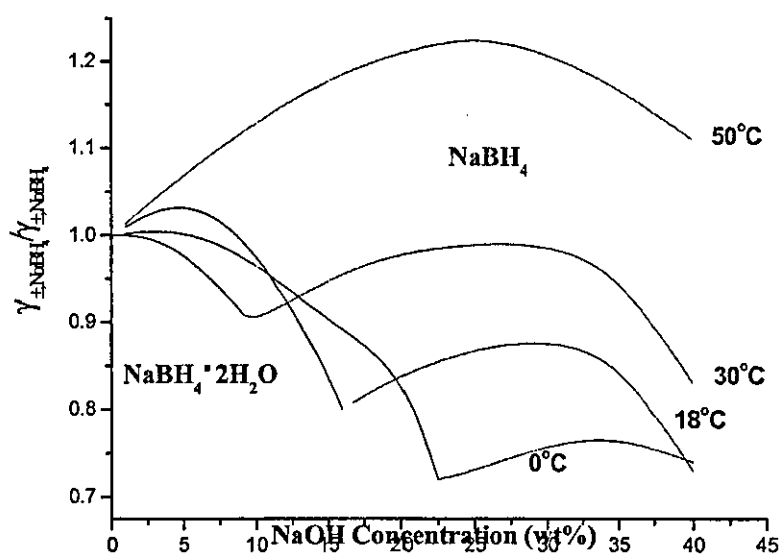
Figure 4.16 The values of $\gamma'_{\pm,B}/\gamma_{\pm,B}$ for the NaBH$_4$-NaOH-H$_2$O system.
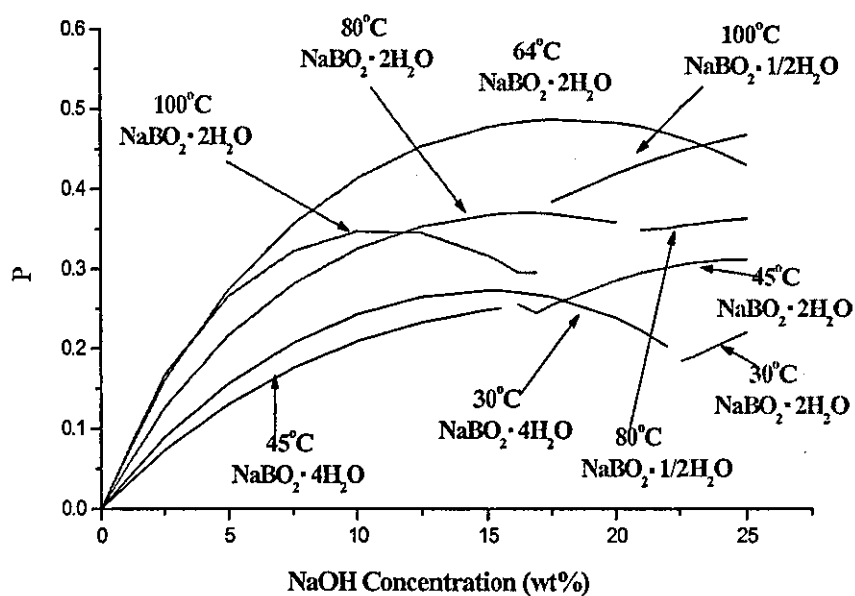
Figure 4.17 Calculated P value for the NaBO$_2$-NaOH-H$_2$O system.

111
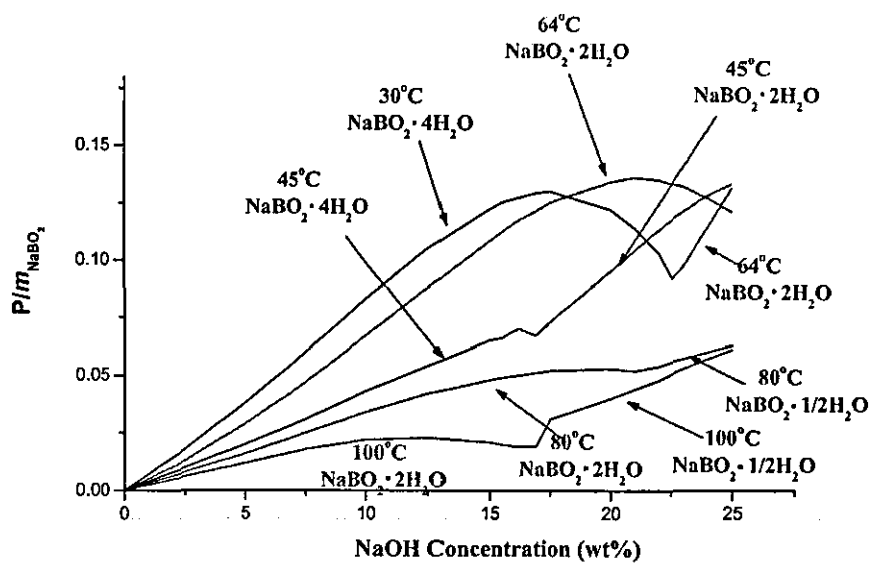
Figure 4.18 The effect of NaOH on P value per unit molality of $NaBO_2$.
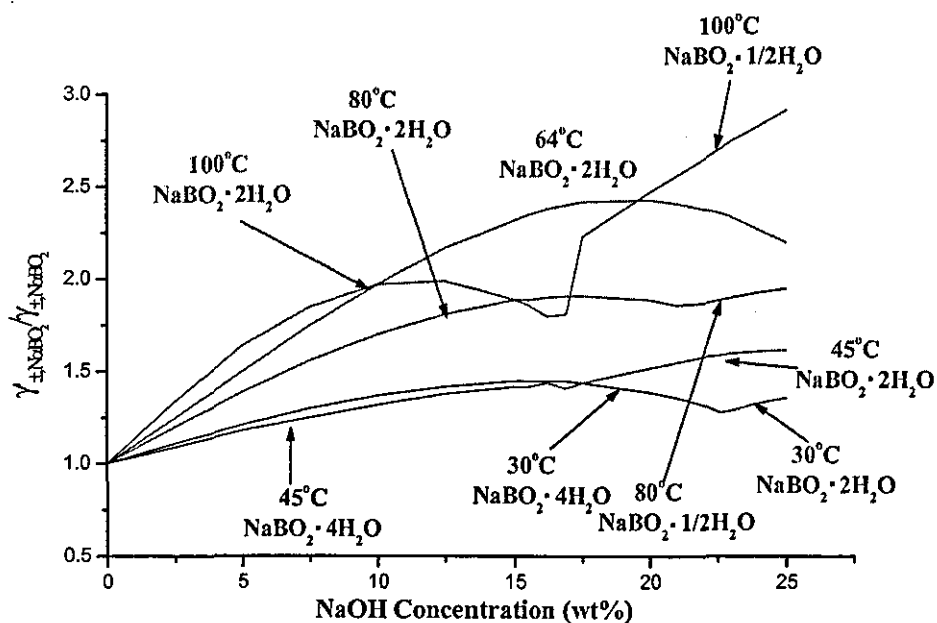
Figure 4.19 The values of $\gamma'_{\pm,B} / \gamma_{\pm,B}$ for the $NaBO_2$-NaOH-H_2O system.

As shown in Figure 4.15, the value of P/m_{NaBH4} for the $NaBH_4$-NaO-H_2O system is between -0.031 and 0.0090. At lower temperatures (0 – 30°C), P/m_{NaBH4} is negative. This may be due to the stronger hydrogen bonds between OH^- and water than that BH_4^- and water, which leads to structure-breaking of the hydration sphere around BH_4^- before NaOH is added. At higher temperatures (50°C), P/m_{NaBH4} is positive. The elevation of temperature decreases the role of hydrogen bonds. However, neither negative nor positive values are very small. This suggests that the addition of NaOH will not have significant effect on the dissolution of $NaBH_4$. As shown in Figure 4.16, the values of $\gamma'_{\pm,B}/\gamma_{\pm,B}$ range from 0.72 to 1.25.

However, for $NaBO_2$-NaOH-H_2O, all the P/m_{NaBO2} values are positive (from 0 to 0.17 as shown in Figure 4.18). The original interaction in the solution is between BO_2^- and water. When NaOH is added to the solution, OH^- may also have interactions with water. Since the basicity of OH^- is stronger than BO_2^-, water from the hydration sphere of BO_2^- will move to the surroundings of OH^-. This will result in a positive value of P. The calculated values of $\gamma'_{\pm,B}/\gamma_{\pm,B}$ are from 1 to 2.8 as shown in Figure 4.19. It can be seen that NaOH has a significant effect on $\gamma'_{\pm,B}/\gamma_{\pm,B}$ for $NaBO_2$.

4.5 Determination of Model Parameters

After $\gamma'_{\pm,B}/\gamma_{\pm,B}$ was calculated using the hydration analysis method, the parameters in equation (4.4) can be determined by plotting $\ln m_{\pm,B} + \ln\dfrac{\gamma'_{\pm,B}}{\gamma_{\pm,B}}$ against $1/T$ at the known temperatures. In this work, the calculation was coded in Excel®. The parameters for any NaOH concentrations can be calculated by implementing the model.

In order to make a comparison, $\ln m_{\pm,B}$ was first plotted against $\dfrac{1}{T}$ for $NaBH_4$ or $NaBO_2$ in NaOH solution, as shown in Figure 4.20 and Fig. 4.21. The deviation from linearity is obvious, although a good linearity has been achieved when NaOH is not present as shown in Chapter 3. This indicates that $\gamma'_{\pm,B}/\gamma_{\pm,B}$ is not a constant when NaOH is present. The linearity was much improved, however, when plotting $\ln m_{\pm,B} + \ln\dfrac{\gamma'_{\pm,B}}{\gamma_{\pm,B}}$ against $\dfrac{1}{T}$ as

shown in Figure 4.22 and Fig 4.23.
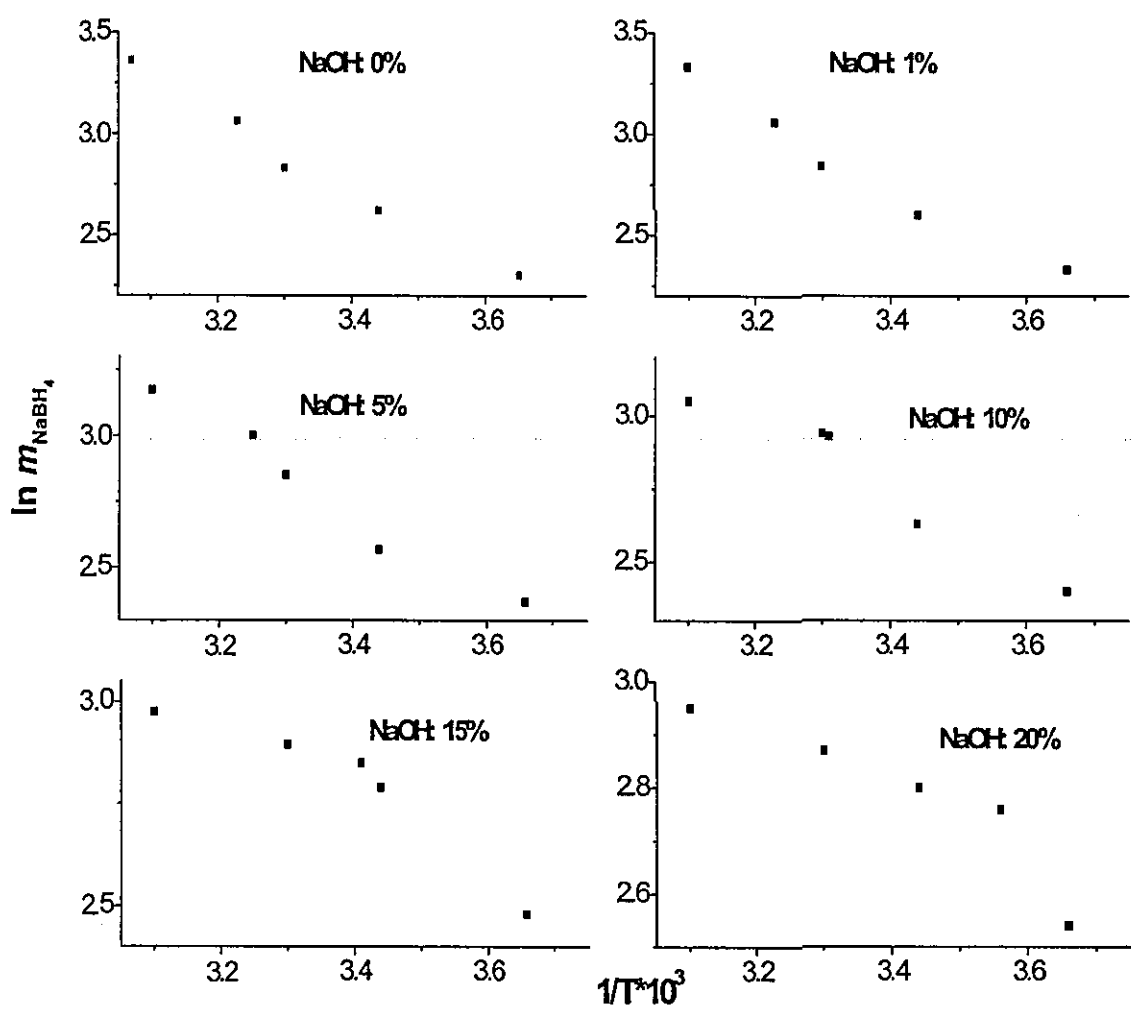
Figure 4.20 The relationship between $\ln m_{\text{B}}$ and $\dfrac{1}{T}$ for a $NaBH_4$ solution containing varying amounts
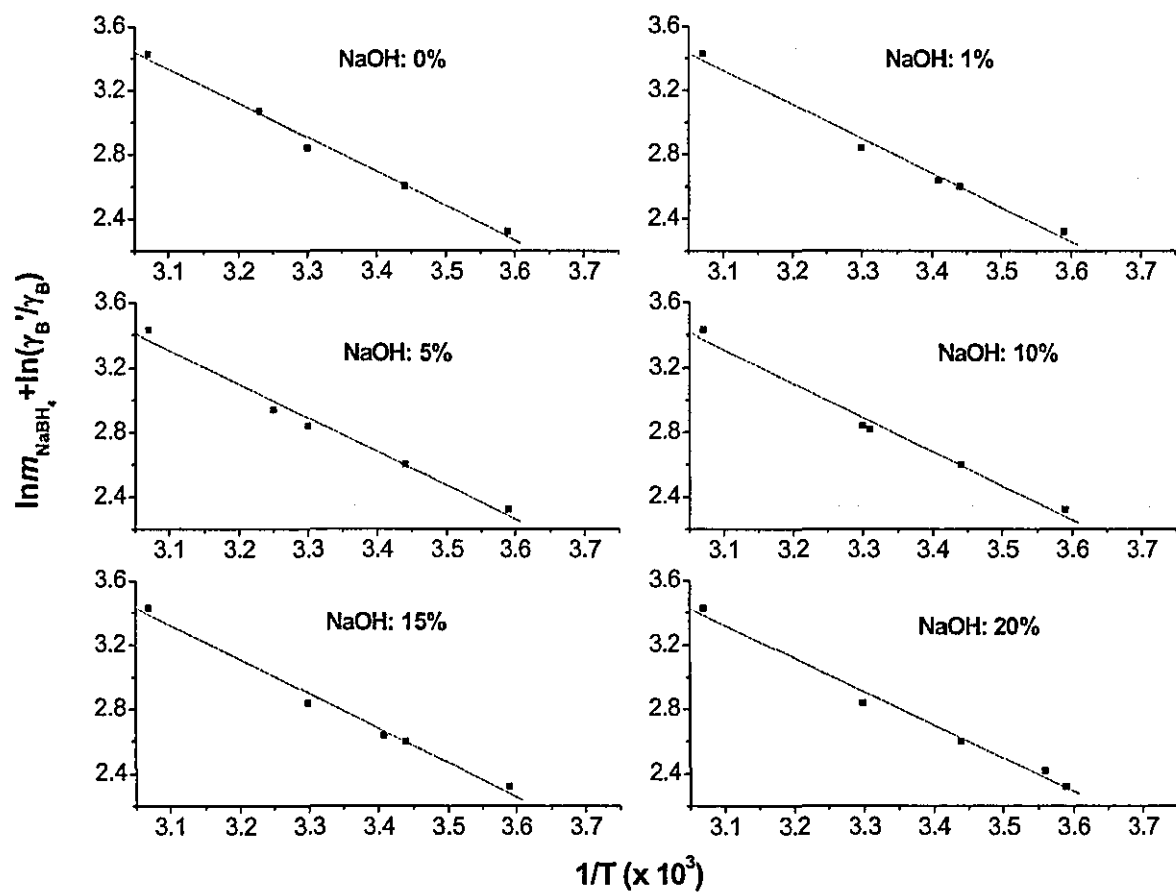
Figure 4.21 The relationship between $\ln m_B$ and $\dfrac{1}{T}$ for NaBH$_4$ in a NaOH solution.
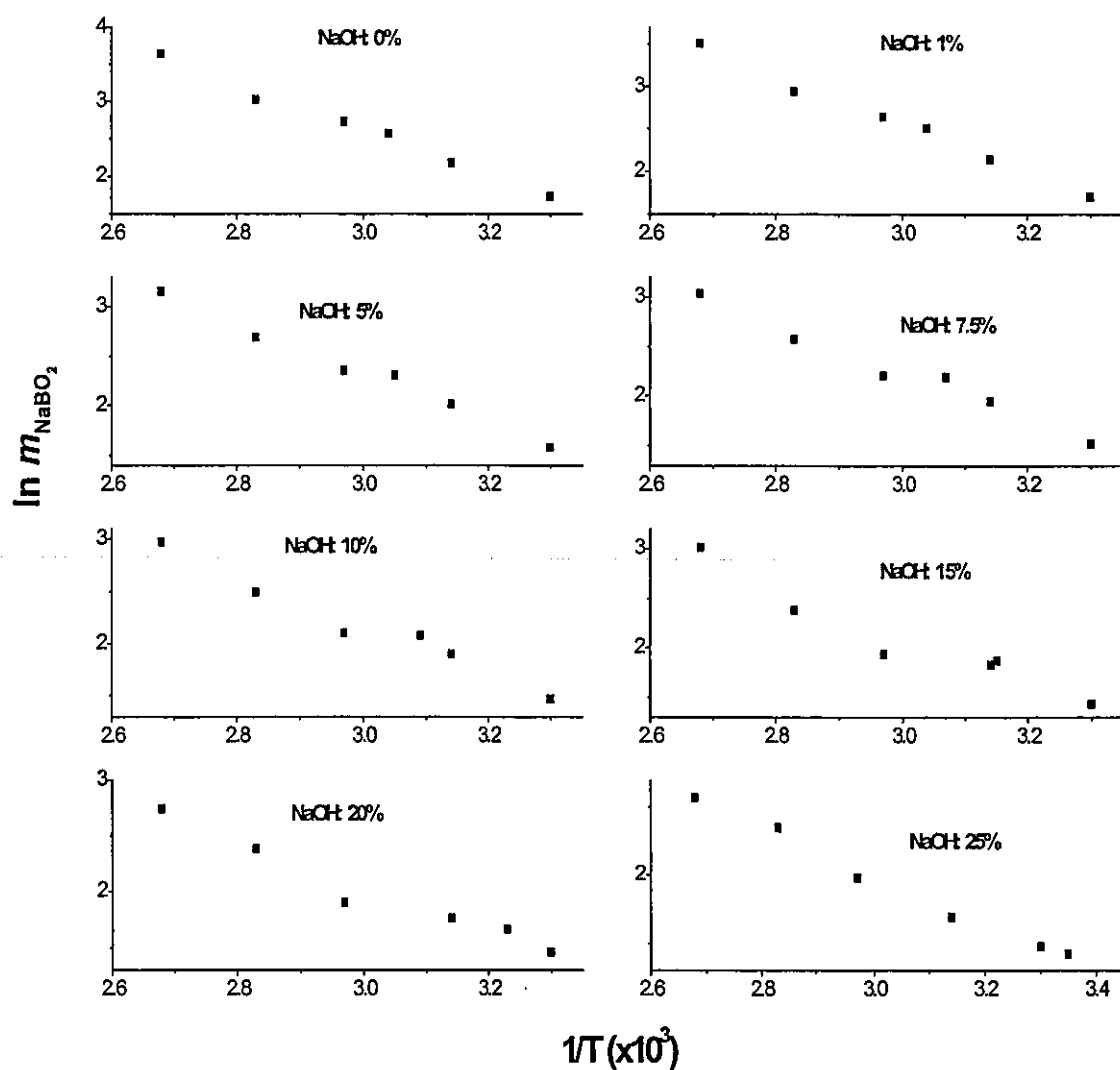
Figure 4.22 The relationship between $\ln m_B$ and $\dfrac{1}{T}$ for a $NaBH_4$ solution in the presence of various NaOH concentrations.
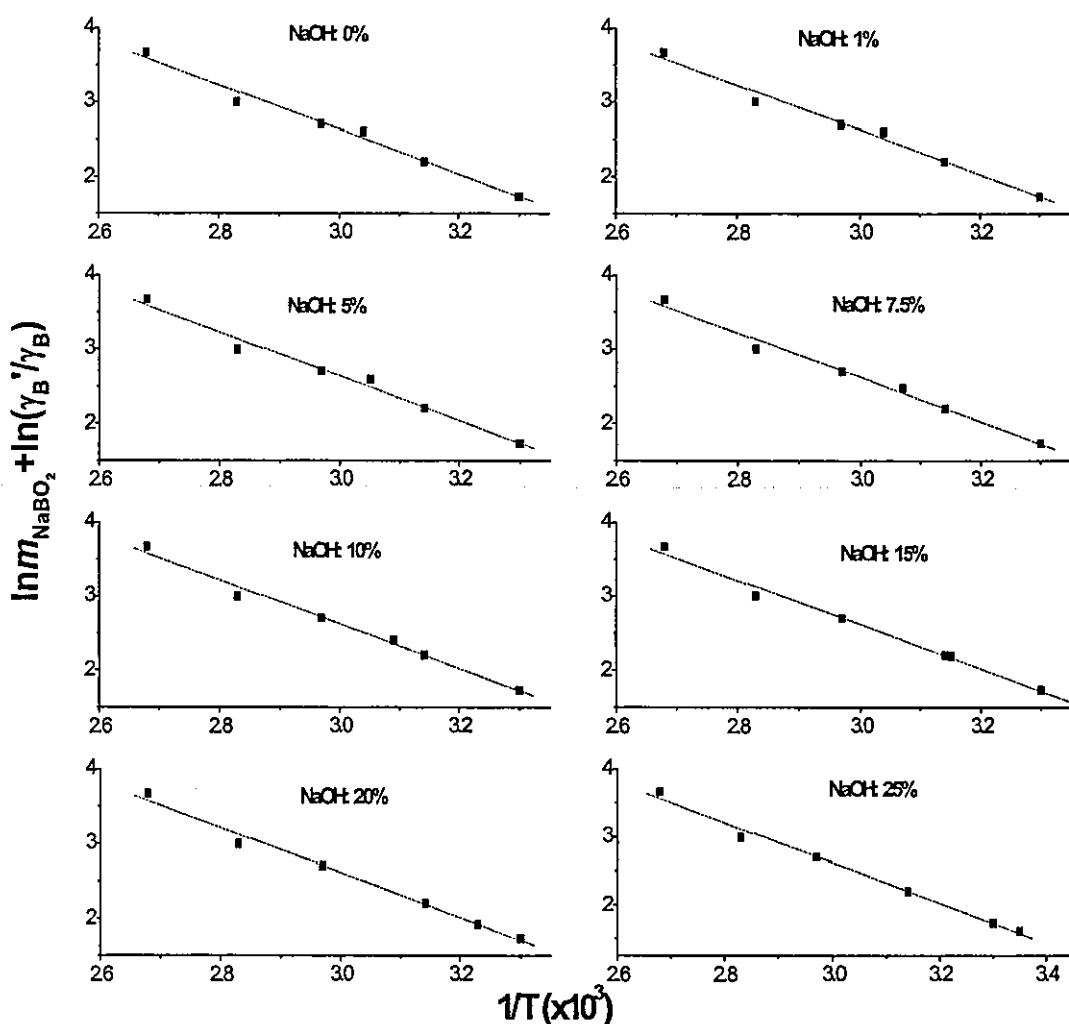
Figure 4.23 The relationship between $\ln m_B$ and $\dfrac{1}{T}$ for $NaBO_2$ in a NaOH solution.

In Figures 4.22 and 4.23, the slope of the line represents $-\dfrac{\Delta H^0_{m,B}}{2RT}$ and the intercept

represents $\dfrac{\Delta S^0_{m,B}}{2R} - \ln \gamma_{\pm,B}$. The values of $\Delta H^0_{m,B}$ and $\dfrac{\Delta S^0_{m,B}}{2R} - \ln \gamma_{\pm,B}$ at various NaOH

concentrations were calculated for both $NaBH_4$ and $NaBO_2$. The results are shown in Table 4.6 and 4.7 respectively. The values are very close regardless of the change of NaOH concentration. This is because that the standard changes of enthalpy and entropy are from a solid state of the salts to 1 mol kg^{-1} in solution. They have no relationship with NaOH.

117

Table 4.7 The values of the parameters for $NaBH_4$ at various NaOH concentrations.

w_{NaOH}	$\Delta H^\circ_{m,NaBH_4} / 2R$ (K^{-1})	$\Delta H^\circ_{m,NaBH_4}$ $(kJ\,mol^{-1})$	$\Delta S^\circ_{m,NaBH_4} / 2R - \ln\gamma'_\pm$ (K^{-1})
0	1935.6	32.2	9.3275
1	1886.9	31.4	9.1485
5	1890.2	31.4	9.1581
10	1910.4	31.8	9.2237
15	1954.6	32.6	9.3755
20	1943.3	32.2	9.3534
Average	1920.2	32.0	9.2645

Table 4.8 The values of the parameters for $NaBO_2$ at various NaOH concentrations.

w_{NaOH}	$\Delta H^\circ_{m,NaBO_2} / 2R$ (K^{-1})	$\Delta H^\circ_{m,NaBO_2}$	$\Delta S^\circ_{m,NaBO_2} / 2R - \ln\gamma_\pm$ (K^{-1})
0	3007.2	50.0	11.660
1	3006.8	50.0	11.659
5	2997.9	49.8	11.635
7.5	3009.9	50.0	11.661
10	3012.0	50.1	11.664
15	3021.9	50.2	11.687
20	3026.6	50.3	11.700
25	2985.5	49.6	11.582
Average	3008.5	50.0	11.656

Substituting the average values of the parameters into equation (4.4) gives the relationship between solubility and temperature for $NaBH_4$ and $NaBO_2$ respectively.

$$\ln m_{\pm,NaBH_4} + \ln\frac{\gamma'_{\pm,NaBH_4}}{\gamma_{\pm,NaBH_4}} = -\frac{1920.2}{T} + 9.3 \tag{4.23}$$

118

$$\ln m_{\pm,NaBO_2} + \ln \frac{\gamma'_{\pm,NaBHO_2}}{\gamma_{\pm,NaBO_2}} = -\frac{3008.5}{T} + 11.7 \tag{4.24}$$

In order to get the relationship between m_B and T at a specific NaOH concentration, the value of $\gamma'_{\pm,B}/\gamma_{\pm,B}$ must be determined at the NaOH concentration. As shown in Figure 4.16 and 4.19, the value varies with the change of temperature. The average value over temperature was taken and then plotted against NaOH concentration. The graph was then regressed into polynomial equations as shown in Figures 4.24 and 4.25 for NaBH$_4$ and NaBO$_2$ respectively. The regressed equations are given as equations (4.25) and (4.26).
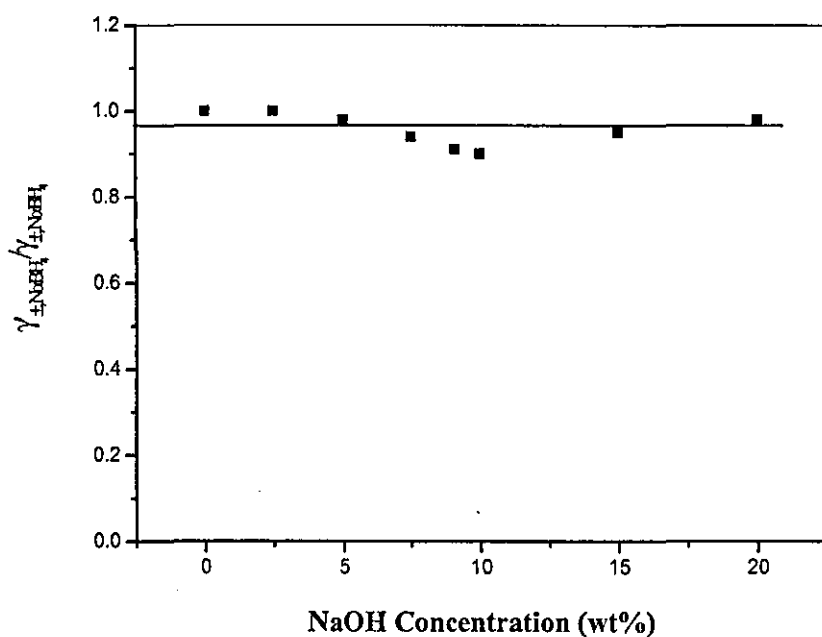
Figure 4.24 The change of $\gamma'_{\pm,B}/\gamma_{\pm,B}$ with NaOH concentration for NaBH$_4$.

119
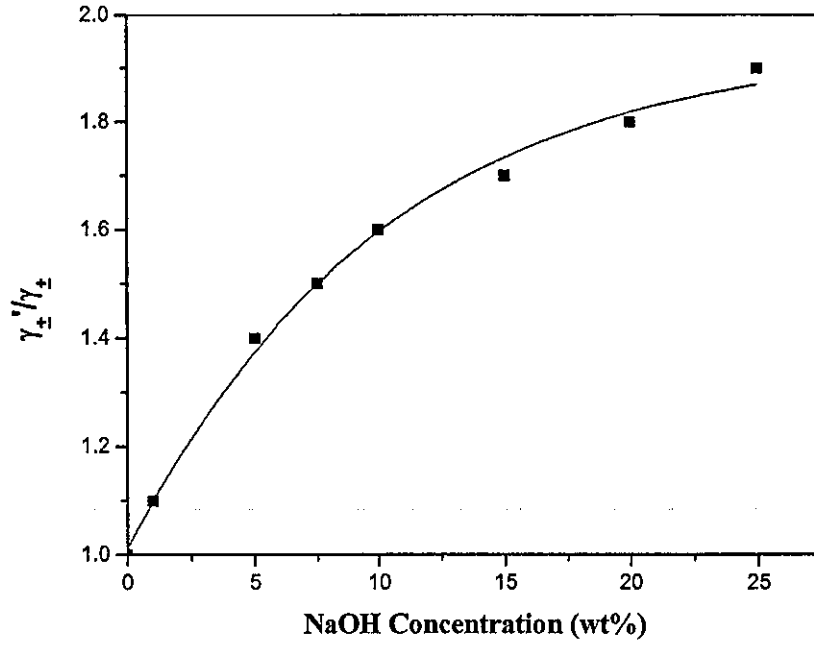
Figure 4.25 The effect of NaOH on the average $\gamma'_{\pm,B}/\gamma_{\pm,B}$ of NaBO$_2$ in its saturated solution.

$$\gamma'_\pm / \gamma_\pm = 0.97 \tag{4.25}$$

$$\gamma'_\pm / \gamma_\pm = -0.0015 w_{NaOH}^2 + 0.07 w_{NaOH} + 1.0 \tag{4.26}$$

In the following, the errors introduced by using the average value of $\gamma'_{\pm,B}/\gamma_{\pm,B}$ over temperature are analysed. It can be seen from Figures 4.16 and 4.19 that the error is small at lower NaOH concentrations but becomes larger with an increase in NaOH concentration. The error was estimated using equation (4.27). The results are given in Tables 4.9 and 4.10.

$$error = \frac{\left| \Delta \ln \dfrac{\gamma'_{\pm,B}}{\gamma_{\pm,B}} \right|}{\ln m_{\pm,B} + \ln \dfrac{\gamma'_{\pm,B}}{\gamma_{\pm,B}}} \tag{4.27}$$

And

$$\left| \Delta \ln \frac{\gamma'_{\pm,B}}{\gamma_{\pm,B}} \right| = \ln\left(\gamma'_{\pm,B}/\gamma_{\pm,B}\right)_{max} - \ln\left(\gamma'_{\pm,B}/\gamma_{\pm,B}\right)_{av} \tag{4.28}$$

Table 4.9 The errors introduced by using the average activity ratios over temperature for $NaBH_4$-$NaOH$-H_2O.

NaOH concentration (wt%)	Maximum $\gamma'_{\pm,B}/\gamma_{\pm,B}$	Average $\gamma'_{\pm,B}/\gamma_{\pm,B}$	$\left\| \Delta \ln \frac{\gamma'_{\pm,B}}{\gamma_{\pm,B}} \right\|$	Errors at 20°C ($\ln m_{\pm,B} + \ln \frac{\gamma'_{\pm,B}}{\gamma_{\pm,B}} = 2.75$) (%)	Errors at 90°C ($\ln m_{\pm,B} + \ln \frac{\gamma'_{\pm,B}}{\gamma_{\pm,B}} = 4.01$) (%)
1	1.03	0.97	0.060	2.2	1.5
5	1.07	0.97	0.098	3.6	2.4
10	1.13	0.97	0.153	5.6	3.8
15	1.16	0.97	0.179	6.5	4.5
20	1.21	0.97	0.221	8.0	5.5

Table 4.10 The errors introduced by using the average activity ratios over temperature for $NaBO_2$-$NaOH$-H_2O.

NaOH concentration (wt%)	Maximum $\gamma'_{\pm,B}/\gamma_{\pm,B}$	Average $\gamma'_{\pm,B}/\gamma_{\pm,B}$	$\left\| \Delta \ln \frac{\gamma'_{\pm,B}}{\gamma_{\pm,B}} \right\|$	Errors at 20°C ($\ln m_{\pm,B} + \ln \frac{\gamma'_{\pm,B}}{\gamma_{\pm,B}} = 1.44$) (%)	Errors at 90°C ($\ln m_{\pm,B} + \ln \frac{\gamma'_{\pm,B}}{\gamma_{\pm,B}} = 3.42$) (%)
1	1.15	1.10	0.044	3.1	1.3
5	1.60	1.39	0.141	9.8	4.1
10	1.95	1.59	0.204	14.2	6.0
15	2.20	1.71	0.252	17.5	7.4
20	2.30	1.78	0.256	17.8	7.5

The errors increase with both the increase of NaOH concentration and reaction temperature. The practical range for NaOH should be less than 5% and the reaction temperature should be as high as possible to increase the reaction rate. Bearing this in mind, the relative error for using the average value of $\gamma'_{\pm,B} / \gamma_{\pm,B}$ over temperature will be less than 5%. This is acceptable for practical application of the model.

In order to get the relationship between solubility m_B and T from equations (4.23) or (4.24), the presence of common ions must be considered when calculating the mean molality of mixed electrolytes [13]. In both $NaBH_4$-$NaOH$-H_2O and $NaBO_2$-$NaOH$-H_2O systems, the common ion is Na^+. The mean molality $m_\pm$ is calculated using equation (4.29).

$$m_\pm = (m_{Na^+} m_{B^-})^{1/2} = [(m_{NaB} + m_{NaOH}) m_{NaB}]^{1/2} \tag{4.29}$$

where m_{NaB} represents the molality of $NaBH_4$ or $NaBO_2$, m_{Na^+} is the molality of sodium ion, m_{B^-} is the molality of BH_4^- or BO_2^-, and m_{NaOH} is the molality of NaOH.

Rearranging equation (4.23), yields

$$m_{NaB}^2 + m_{NaOH} m_{NaB} - m_\pm^2 = 0 \tag{4.30}$$

In practice, the concentration of NaOH is often expressed in weight percentage. The relationship weight percentage and molality can be expressed using equation (4.31).

$$\frac{m_{NaOH} M_{NaOH}}{w_{NaOH}} = \frac{1000 + m_{NaB} M_{NaB}}{100 - w_{NaOH}} \tag{4.31}$$

where w_{NaOH} is the weight percentage of NaOH in the solution.

Solving w_{NaOH} from equation (4.31), gives

$$
\begin{aligned}
m_{NaOH} &= \frac{w_{NaOH}(1000 + m_{NaB} M_{NaB})}{(100 - w_{NaOH}) M_{NaOH}} \\
&= \frac{w_{NaOH} \times 1000}{(100 - w_{NaOH}) M_{NaOH}} + \frac{w_{NaOH} M_{NaB}}{(100 - w_{NaOH}) M_{NaOH}} m_{NaB} = A_1 + A_2 m_{NaB}
\end{aligned}
\tag{4.32}
$$

where

$$A_1 = \frac{w_{NaOH} \times 1000}{(1 - w_{NaOH})M_{NaOH}}$$

$$A_2 = \frac{w_{NaOH}M_{NaB}}{(1 - w_{NaOH})M_{NaOH}}$$

Substituting equation (4.32) into equation (4.30), gives

$$(1 + A_2)m_{NaB}^2 + A_1 m_{NaB} - m_{\pm}^2 = 0 \tag{4.33}$$

Solving m_{NaB} from equation (4.27), gives the relationship between mean molality and solubility.

$$m_{NaB} = \frac{-A_1 + \sqrt{A_1^2 + 4(1 + A_2)m_{\pm}^2}}{2(1 + A_2)} \tag{4.34}$$

4.6 Calculation of Maximum NaBH₄ Concentration

The solubility of $NaBH_4$ in NaOH solution at any temperatures and NaOH concentrations can be obtained by simultaneously solving equations (4.23), (4.25) and (4.34); the solubility of $NaBO_2$ in NaOH solution at any temperatures and NaOH concentrations can be obtained by simultaneously solving equations (4.24), (4.26) and (4.34). The amount of water (g) contained in the saturated solution containing one mole of $NaBH_4$ can be calculated using equation (4.35):

$$W_1 = \frac{1000}{m_{NaBH_4}} \tag{4.35}$$

The amount of water (g) contained in the saturated solution containing one mole of $NaBO_2$ is calculated using equation (4.36).

$$W_2 = \frac{1000}{m_{NaBO_2}} \tag{4.36}$$

The amount of water (g) needed to react with one mole of $NaBH_4$ is calculated using

equation (4.37).

$$W_3 = 4 \times M_{H_2O} \tag{4.37}$$

The maximum concentration of NaBH₄ in the hydrolysis system is determined by the maximum value between W_1 and (W_2 + W_3). The comparison between W_1 and (W_2 + W_3) is shown in Figure 4.26. It can be seen that the value of W_1 is much smaller than (W_2 + W_3). Therefore, the maximum concentration of NaBH₄ is determined by (W_2 + W_3).

The calculated maximum concentration of NaBH₄ is shown in Figure 4.27 for various NaOH concentrations. It increases with the increase of temperature but decreases with the increase of NaOH concentration.
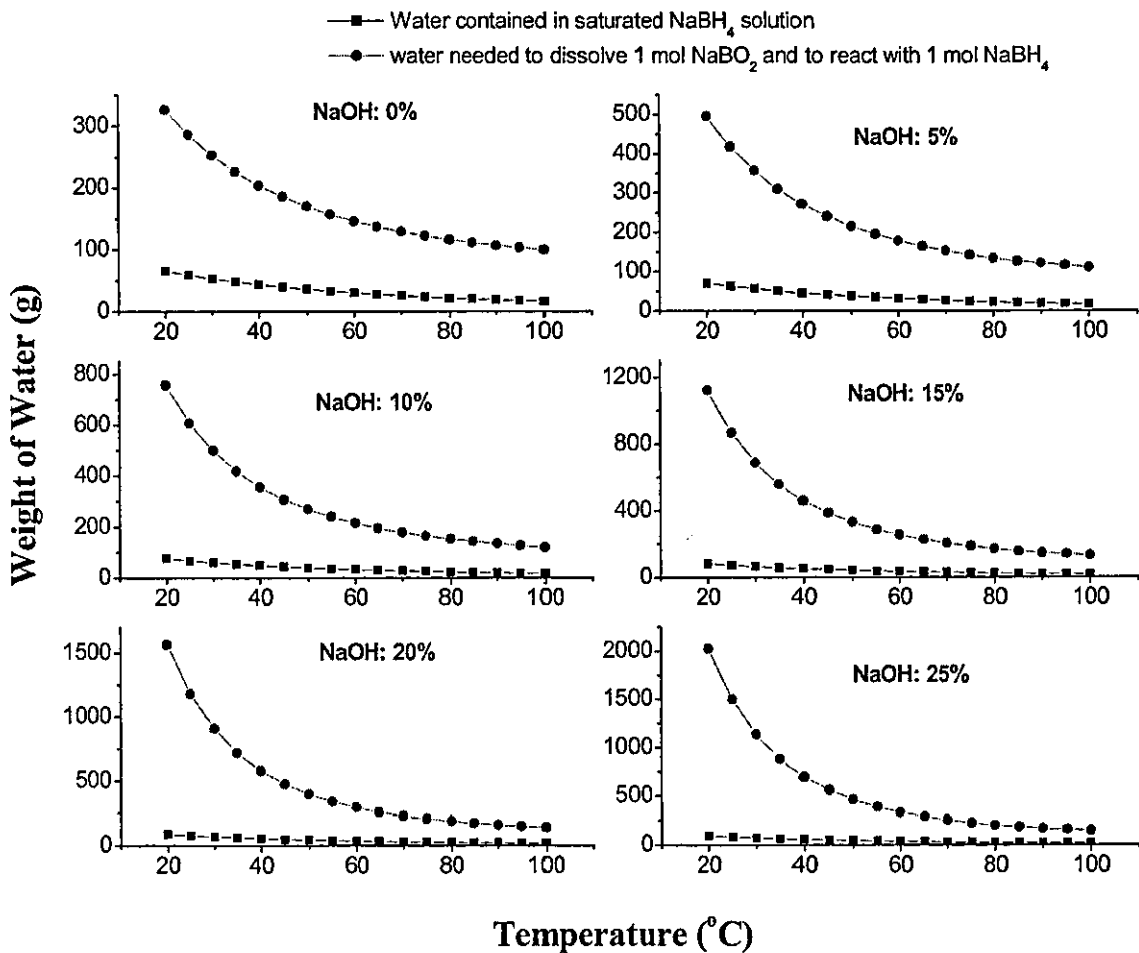
Figure 4.26 Comparison of the quantity of water needed to dissolve 1 mol NaBO₂ and to react with 1 mol NaBH₄ with that contained in saturated NaBH₄ solution.
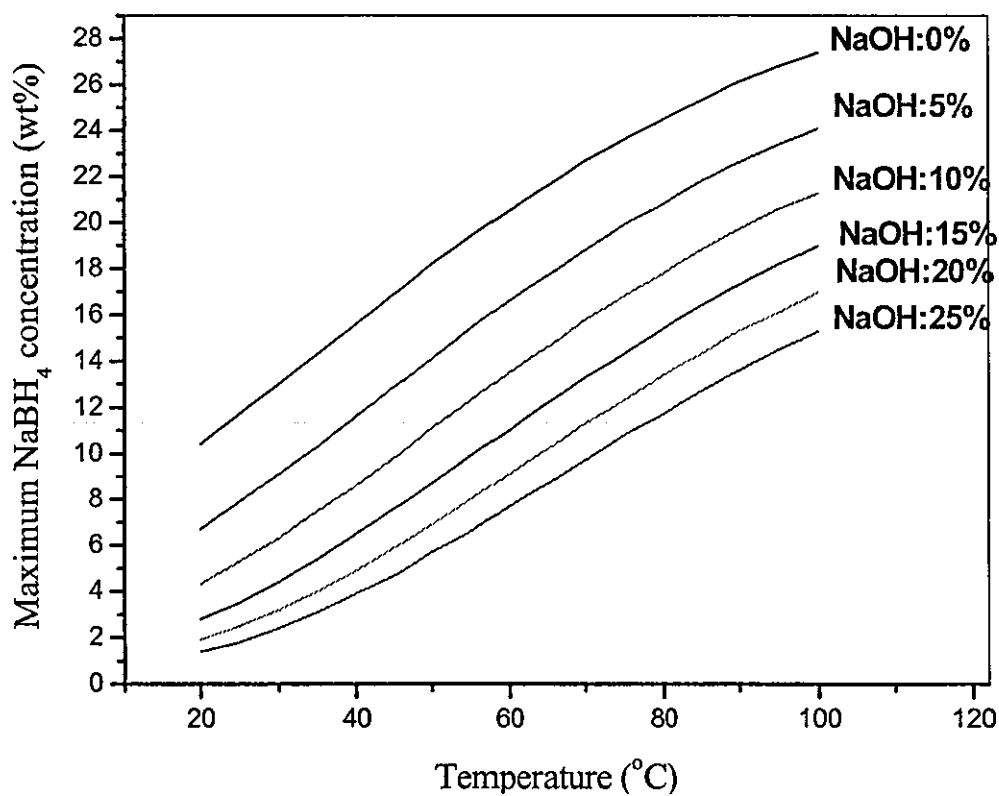
Figure 4.27 The calculated maximum concentration of NaBH₄ in the hydrolysis system.

4.7 Experimental

As in Chapter 3, experiments were conducted to validate the modelling results. The same experimental procedure and materials were used except that the solution used in the reactions containing 1% or 5% NaOH. The experimental results are listed in Table 4.8 and Table 4.9 for 1% and 5% NaOH respectively.

Since the interval of weight percentage between the occurrence and non-occurrence of precipitation of $NaBO_2$ was 0.5% or 1%, the errors in these measurements were 0.5% or 1%.

Table 4.11 Experimental determination of maximum concentration of $NaBH_4$ in 1% NaOH solutions.

Reaction temperature (°C)	$NaBH_4$ concentration (%)	Did precipitation occur?
26	9.0	×
	10.0	×
	11.0	×
	11.5	×
	12.0	×
	12.5	√
	13.0	√
	13.5	√
35	11.0	×
	12.0	×
	13.0	×
	13.5	×
	14.0	×
	14.5	√
	15.0	√
	15.5	√
42	13.0	×
	14.0	×
	15.0	√
	16.0	√
	17.0	√
	18.0	√
	19.0	√
	20.0	√
56	18.0	×
	19.0	×
	19.5	×
	20.0	√
	20.5	√
	21.0	√
	21.5	√
	22.0	√
70	20.0	×
	21.0	×
	22.0	×
	22.5	√
	23.0	√
	23.5	√
	24.0	√
	24.5	√

Table 4.12 Experimental determination of maximum concentration of NaBH$_4$ in 5% NaOH solutions.

Reaction temperature ($^\circ$C)	NaBH$_4$ concentration (%)	Did precipitation occur?
26	6.0	$\times$
	7.0	$\times$
	7.5	$\times$
	8.0	$\times$
	8.5	$\times$
	9.0	$\sqrt{}$
	9.5	$\sqrt{}$
	10.0	$\sqrt{}$
35	7.0	$\times$
	8.0	$\times$
	9.0	$\times$
	9.5	$\sqrt{}$
	10.0	$\sqrt{}$
	10.5	$\sqrt{}$
	11.0	$\sqrt{}$
	11.5	$\sqrt{}$
42	10.0	$\times$
	11.0	$\times$
	12.0	$\times$
	12.5	$\times$
	13.0	$\sqrt{}$
	13.5	$\sqrt{}$
	14.0	$\sqrt{}$
	14.5	$\sqrt{}$
56	13.0	$\times$
	14.0	$\times$
	14.5	$\sqrt{}$
	15.0	$\sqrt{}$
	15.5	$\sqrt{}$
	16.0	$\sqrt{}$
	16.5	$\sqrt{}$
	17.0	$\sqrt{}$
70	16.0	$\times$
	17.0	$\times$
	18.0	$\times$
	19.0	$\times$
	20.0	$\sqrt{}$
	21.0	$\sqrt{}$
	22.0	$\sqrt{}$
	23.0	$\sqrt{}$

4.8 Comparison of Modelling Results with Experimental Data

In order to validate the model, experiments were conducted at five different temperatures for 1% and 5% NaOH concentration respectively. A series of $NaBH_4$ solutions were prepared from low to high concentration to hydrolyse with a concentration interval of 1% or 0.5%. The experimental results are given in Table 4.7 and Table 4.8 respectively. The experimentally measured maximum concentrations, together with modelling results, were plotted in Figure 4.28.

The experimentally measured maximum $NaBH_4$ concentration increased with the increase of the hydrolysis temperature for both 1% and 5% NaOH aqueous solutions. Within the experimental error, the calculated maximum concentration of $NaBH_4$ agrees well with the experimental data. The agreement indicates that the modelling method is reasonable.
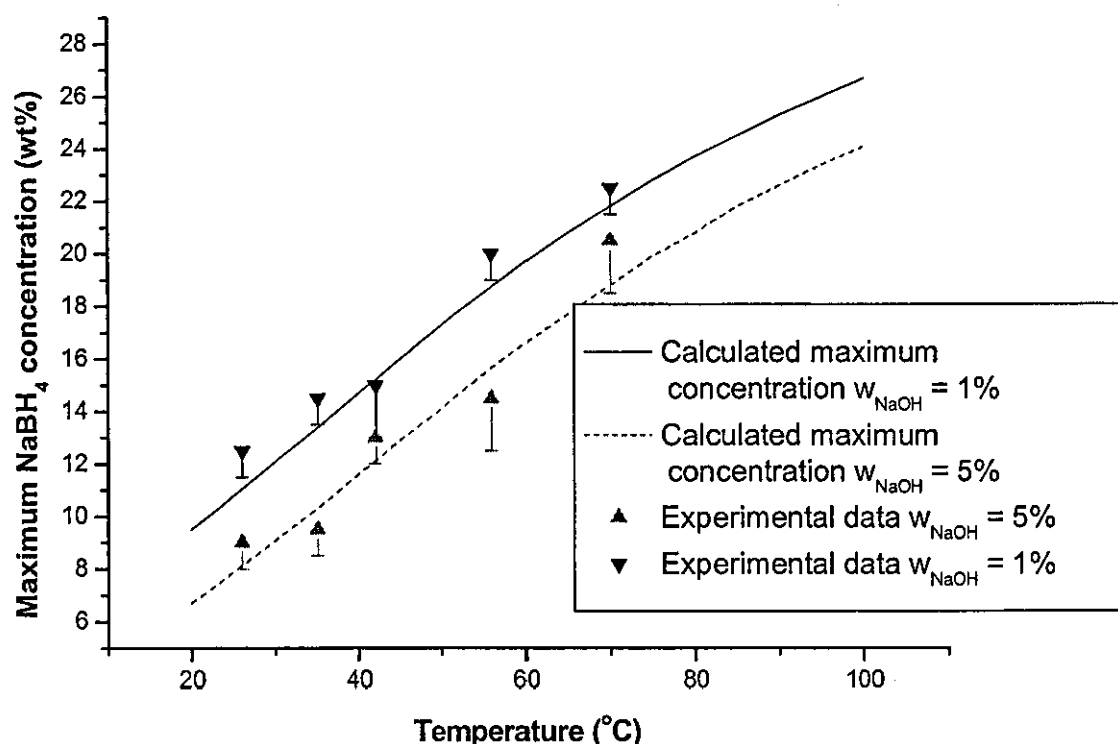
Figure 4.28 Comparison between the calculated and experiment concentration of $NaBH_4$ when sodium metaborate is precipitated from the system.

4.9 Conclusions

Thermodynamic modelling was conducted in this chapter to calculate the maximum concentration of $NaBH_4$ hydrolysis in the presence of NaOH. The modelling results were then validated experimentally at two NaOH concentrations.

- In the presence of a third component, the solubility and temperature meets the following relationship.

$$\ln m_{\pm,B} + \ln \frac{\gamma'_{\pm,B}}{\gamma_{\pm,B}} = -\frac{\Delta H^0_{m,B}}{2RT} + \left(\frac{\Delta S^0_{m,B}}{2RT} - \ln \gamma_{\pm,B} \right)$$

For $NaBH_4$ the equation is: $\ln m_{\pm,NaBH_4} + \ln \frac{\gamma'_{\pm,NaBH_4}}{\gamma_{\pm,NaBH_4}} = -\frac{1920.2}{T} + 9.3$

For $NaBO_2$ the equation is: $\ln m_{\pm,NaBO_2} + \ln \frac{\gamma'_{\pm,NaBHO_2}}{\gamma_{\pm,NaBO_2}} = -\frac{3008.5}{T} + 11.7$

- The value of $\gamma'_{\pm,B} / \gamma_{\pm,B}$ was calculated using the hydration analysis method. It is shown in this study that this is a suitable method for calculation of the effect of NaOH on $NaBH_4$ and $NaBO_2$.

- The solubility data for $NaBH_4$ can be obtained by analysing the phase diagram of $NaBH_4$-NaOH-H_2O, and the solubility data for $NaBO_2$ can be obtained by analysing the phase diagram of Na_2O-B_2O_3-H_2O.

- The amount of water in saturated $NaBH_4$ solution was compared with the amount of water required to dissolve the by-product $NaBO_2$ and to react with $NaBH_4$. The former is much less than the latter.

- The maximum concentration of $NaBH_4$ in the hydrolysis system is determined by the amount of water needed to dissolve the by-product $NaBO_2$ and to react with $NaBH_4$.

- The maximum concentration increases with the increase of reaction temperature

129

and decreases with the increase of NaOH concentration.

4.10 References

1.   Kojima, Y., et al., *Development of 10 kW-scale hydrogen generator using chemical hydride.* Journal of Power Sources, 2004. **125**(1): p. 22-26.

2.   Amendola, S.C., et al., *A safe, portable, hydrogen gas generator using aqueous borohydride solution and Ru catalyst.* International Journal of Hydrogen Energy, 2000. **25**: p. 969-975.

3.   Davis, R.E. and C.G. Swain, *General acid catalysis of the hydrolysis of sodium borohydride.* Journal of American Chemical society, 1960. **82**: p. 5949-5950.

4.   Suda, S., Y.-M. Sun, and B.-H. Liu, *Catalytic generation of hydrogen by applying fluorinated-metal hydrides as catalysts.* Applied Physics A: Materials Science & Processing, 2001. **72**: p. 209-212.

5.   Abts, L.M., J.T. Langland, and M.M. Kreevoy, *Role of water in the hydrolysis of tetrahydroborate(1-) ion.* Journal of American Chemical Society, 1975. **97**(11): p. 3181 - 3185.

6.   Kreevoy, M.M. and R.W. Jacobson, *The rate of decomposition of NaBH4 in basic aqueous solutions.* Ventron Alembic, 1979. **15**: p. 2-3.

7.   Hua, D., et al., *Hydrogen production from catalytic hydrolysis of sodium borohydride solution using nickle boride catalyst.* International Journal of Hydrogen Energy, 2003. **28**: p. 1095-1100.

8.   Eysseltova, J., *Hydration analysis based calculation of solute activity coefficients in ternary saturated solutions.* Collection of Czechoslovak Chemical Communications, 1994. **59**: p. 2351-2356.

9.   Eysseltova, J., *A study of the use of solubility isotherms to obtain information about ion hydration and ion pairing in concentrated solutions of electrolysts.* Collection of Czechoslovak Chemical Communications, 1994. **59**: p. 126-137.

10. Nyvlt, J. and J. Eysseltova, *Physical interpretation of solubility interaction constants from the series expansion of the relative activity coefficients.* Collection of Czechoslovak Chemical Communications, 1994. **59**: p. 1911-1921.

11. Gmelins, L., *Natrium und Bor.* Handbuch der anorganischen Chemie, 1974: p. 21.

12. Mellor, J.W., *Supplement to Mellor's comprehensive treatise on inorganic and theoretical chemistry.* Vol. 5, Boron-Oxygen compounds. 1980, London: Longman. 257.

13. Klotz, I.M. and R.M. Rosenberg, *Chemical Thermodynamics: Basic Theory and Methods.* 1994, New York: John Wiley & Sons.

Chapter 5

Kinetic Study of NaBH₄ Hydrolysis over Metal Catalyst: Theory and Experimental Method

5.1 Introduction

In Chapters 3 and 4, the maximum concentration of $NaBH_4$ in its hydrolysis solution was studied from the point of view of thermodynamics. In this and subsequent chapters, the kinetic aspect of the hydrolysis will be considered. Kinetics are concerned with the rate of a reaction, in this case with the quantitative description of how fast hydrogen is generated during hydrolysis and the factors affecting this rate. Understanding these factors is essential to the rational design and analysis of the performance of a reactor and the application of $NaBH_4$ hydrolysis to a practical hydrogen generation system.

Most of the previous works in kinetic studies of $NaBH_4$ hydrolysis were performed using protonic acid catalysis [1-3]. Acid catalysis, as reviewed in Chapter 2, are not efficient for hydrogen generation. The most efficient catalysts for $NaBH_4$ hydrolysis are transition metals, which are usually supported on an inert carrier. Unlike acid catalysis, metal catalysed $NaBH_4$ hydrolysis is a heterogeneous catalysis.

In this chapter, the theory of heterogeneous catalysis is introduced first, after which an experimental method is established for the kinetic study. In the next four chapters, kinetic expression is determined experimentally and an overall kinetic model is derived and validated.

5.2 Literature review on heterogeneous catalysis

As shown in Figure 5.1, heterogeneous catalysis reactions usually include five steps:
- Mass transfer (diffusion) of the reactants from the bulk fluid to the external surface of the catalyst pellet.
- Diffusion of the reactant from the pore mouth through the catalyst pores to the immediate vicinity of the internal catalytic surface.

132

- Reaction on the surface of the catalyst.

- Diffusion of the products from the interior of the pellet to the pore mouth at the external surface.

- Mass transfer of the products from the external pellet surface to the bulk fluid.
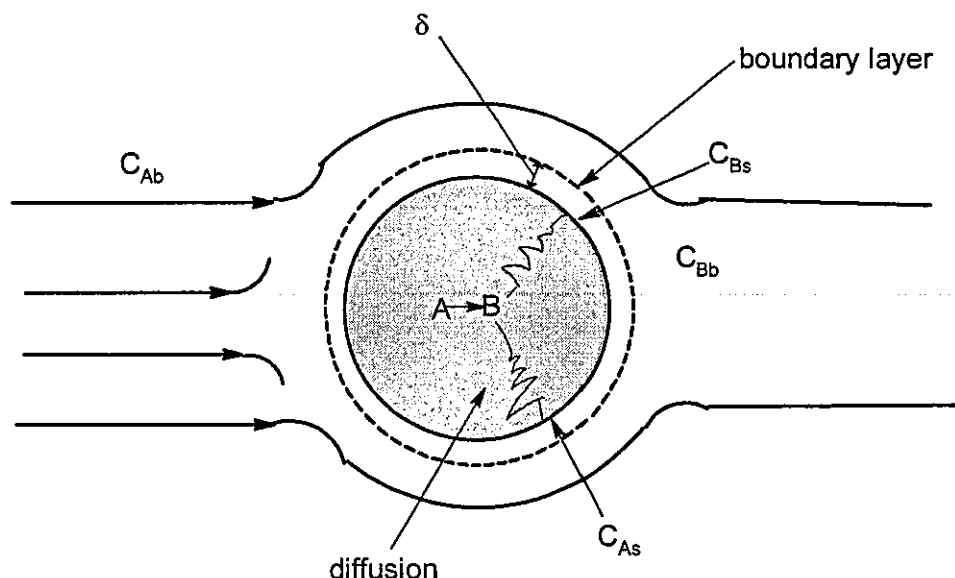
Figure 5.1 General steps of heterogeneous catalysis for reaction A → B. Where C_{Ab} is the bulk concentration of reactant A, C_{Bb} is the bulk concentration of product B, C_{As} is the surface concentration of A, C_{Bs} is the surface concentration of B and δ is the thickness of boundary layer.

An important factor in heterogeneous catalysis is that the observed rate of reaction may include effects due to the rates of transport processes in addition to intrinsic reaction rates. The intrinsic kinetics of a heterogeneous catalytic reaction involves three elementary steps successively: adsorption of reactant molecules onto the surface and attachment to an active site on the catalyst surface, surface reaction, and desorption of product molecules from the surface. The active site is used to describe a location on the surface which bonds with reaction intermediates, which is usually a defect or crystal edge on the surface of the catalyst. The surface reaction may involve a single site mechanism or a dual-site mechanism. All species of molecules, free reactants and free products as well as site-attached reactants, intermediates, and products taking part in these three processes are assumed to be in equilibrium.

133

There are various postulated mechanisms for the intrinsic kinetics such as Langmuir-Hinshelwood kinetics, which involve several arbitrary parameters. In order to prove that a mechanism is true, it has to be shown that the family of curves representing the rate equation type of the favoured mechanism fit the data much more closely than the other possible families of curves, so that all the others can be rejected. It is often rather difficult to find a good mechanism. Also, the rate expression from a mechanism is difficult to apply when macrokinetics are involved due to the large number of arbitrary parameters. However, it is sufficient to use the simplest available correlating rate expression; hence first-order or n^{th} order kinetics to represent the intrinsic reaction.

Solid catalyst particles are usually porous, with the interior surface accessible to the reacting species usually being much greater than the gross exterior surface. The porous nature of the catalyst particles gives rise to the possible development of significant gradients of both concentration and temperature across the particle, because of the diffusion rate of material and heat transfer, respectively.

To obtain a rate law for the particle as a whole, the variation of concentration (c_A) and temperature (T) must be taken into account. Since c_A and T may vary from point to point within a catalyst particle, the rate of reaction also varies. To account for this variation, particle effectiveness factor η is introduced. η is the ratio of the observed rate of reaction for the particle as a whole to the intrinsic rate at the surface conditions (c_{AS} and T_S), as given in equation (5.1):

$$\eta = r_A(observed) / r_A(c_{AS}, T_S) \tag{5.1}$$

The effects of concentration and temperature will be considered separately. For isothermal conditions, η depends on reaction and particle characteristics.

To obtain an expression for η at isothermal conditions, mathematical equations of simultaneous diffusion and reaction inside porous catalytic particles at constant temperature are typically formulated. The general solution involves the derivation of the ordinary differential equations that describe the material balance within the particle geometry. This treatment also requires the use of Fick's law for diffusion, which is usually assumed to involve only the diffusion of the reactant with an effective diffusivity for the

catalyst particle.

Diffusion in a porous structure may consist of three modes: molecular diffusion (big pores), Knudsen diffusion (pore size comparable with molecule free path) and surface diffusion (along surface). Since the pore structure is usually not well known, Fick's law is used to obtain a phenomenological description of the rate of diffusion along the x direction.

$$N_A = -D_e dc_A / dx \qquad (5.2)$$

where D_e is the effective diffusivity for species A and N_A is the molar flux (mol m^{-2} s^{-1}).

Taking a spherical shape as an example (as shown in Figure 5.2), the equation that correlates diffusion and reaction can be obtained in accordance with the material balance, as given in equation (5.3).
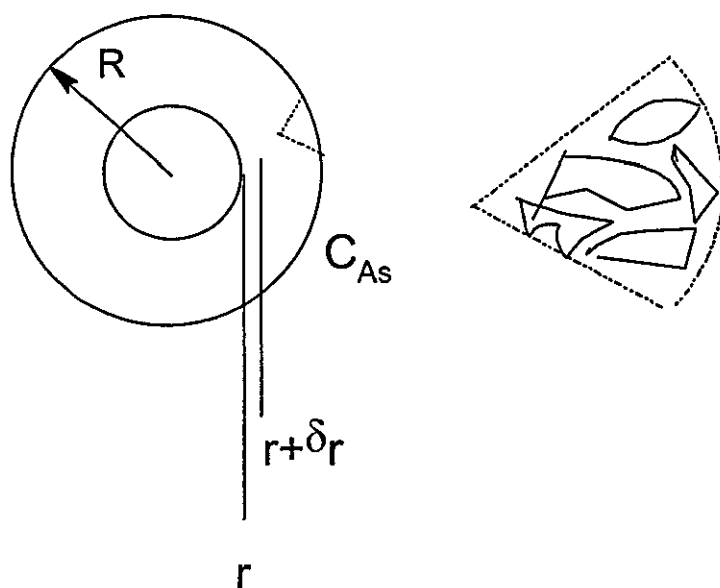
Figure 5.2 Material balance on a spherical catalyst pellet.

$$\frac{d^2 C_A}{dr^2} + \frac{2}{r}\left(\frac{dC_A}{dr}\right) - \frac{k_n}{D_e} C_A^n = 0 \qquad (5.3)$$

The boundary conditions are as follows

135

$dC_A / dt = 0$ at r = 0.

$C_A = C_{As}$, at r = R.

Where C_A is the reactant A concentration at position r, C_{As} is the surface concentration of reactant A, k_n is the reaction rate constant, n is the reaction order, and D_e is the effective diffusion coefficient.

By defining dimensionless variables

$$\psi = \frac{C_A}{C_{As}}$$

$$\lambda = \frac{r}{R}$$

Equation (5.3) becomes

$$\frac{d^2\psi}{d\lambda^2} + \frac{\lambda}{2}\left(\frac{d\psi}{d\lambda}\right) - \frac{k_n R^2 C_{As}^{n-1}}{D_e}\psi^n = 0 \tag{5.4}$$

By defining Thiele modulus ϕ_n,

$$\phi_n^2 = \frac{k_n R^2 C_{As}^{n-1}}{D_e}$$

Equation (5.4) becomes

$$\frac{d^2\psi}{d\lambda^2} + \frac{2}{\lambda}\left(\frac{d\psi}{d\lambda}\right) - \phi_n^2\psi^n = 0 \tag{5.5}$$

The Thiele modulus is an important parameter in chemical reaction engineering. It is a measure of the ratio of the surface reaction rate to the rate of diffusion through the catalyst pellet. For arbitrary reaction kinetics and geometric shape, the Thiele modulus can be generalised using equation (5.6).

$$\phi_n = L_e\left(\frac{(n+1)k_n C_{As}^{n-1}}{2D_e}\right)^{1/2} \tag{5.6}$$

where L_e is the characteristic length of a geometric shape. The values for some common shapes are given in Table 5.1.

Table 5.1 Characteristic lengths of various geometric shapes

Geometric shape	Characteristic length
Flat plates	Thickness/2
Cylinders	R/2, R = radius
Spheres	R/3, R = radius
Any other shape	Volume of particle/exterior surface available for reactant penetration

In the following, a first-order reaction is taken as an example for the solution of equation (5.5). For a first-order reaction, equation (5.5) becomes

$$\frac{d^2\psi}{d\lambda^2} + \frac{2}{\lambda}\frac{d\psi}{d\lambda} - \phi_1^2\psi = 0 \tag{5.7}$$

where $\phi_1 = R\sqrt{\dfrac{k_1}{D_e}}$ and k_1 in the above equation is the first-order catalytic reaction rate constant based on per unit volume of catalyst, which is equal to $k_1'\rho_c$. ρ_c is the density of the catalyst, and k_1' is the first-order catalytic reaction rate constant based on per unit weight of catalyst.

Through some mathematical manipulation (details can be seen in reference [4]), equation (5.7) is readily solved by combining the boundary conditions.

$$\psi = \frac{C_A}{C_{As}} = \frac{1}{\lambda}\left(\frac{\sinh\phi_1\lambda}{\sinh\phi_1}\right) \tag{5.8}$$

After solving out $\psi = C_A/C_{As}$, it is now possible to obtain the total reaction rate throughout the single catalyst pellet, corresponding to the concentration profile of ψ. This may be obtained by integrating the reaction rate in the spherical annulus over the entire sphere. For a first-order reaction in a spherical catalyst pellet, the effectiveness factor η is solved as given by equation (5.9). Other shapes and reaction order can be solved in a

similar fashion. Typical curves for effectiveness for various reaction orders and catalyst geometrical shapes are shown in Figure 5.3.

$$\eta = \frac{3}{\phi_1^2}(\phi_1 \coth \phi_1 - 1)$$ (5.9)
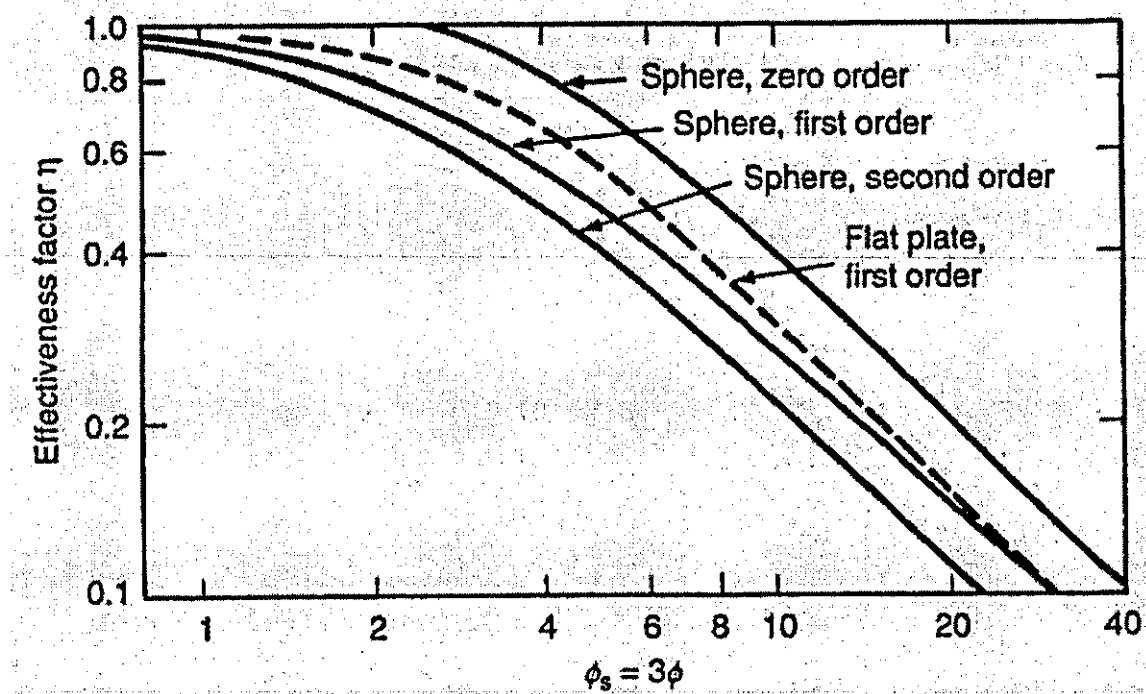
Figure 5.3 Effectiveness factors for power-law kinetics. For spheres, the abscissa is ϕ_s, while for a flat plate the abscissa is 3ϕ [5].

From Figure 5.3, it can be seen that equation (5.10) is true regardless of order n. It is often called strong pore-diffusion resistance when ϕ is large.

$$\eta \to \frac{1}{\phi} \quad \text{as } \phi \to l \arg e$$ (5.10)

So far, it has been assumed that the particle is isothermal. If a temperature gradient arises due to a strong exothermal or endothermic reaction, effectiveness η will change with temperature. The change of η with temperature can be obtained by simultaneously solving differential equations of diffusion and heat transfer. Figure 5.4 shows typical solution curves. The effectiveness may be greater than 1 when the heat produced can not be released immediately from the reaction sites within the catalyst particles, as shown in

138
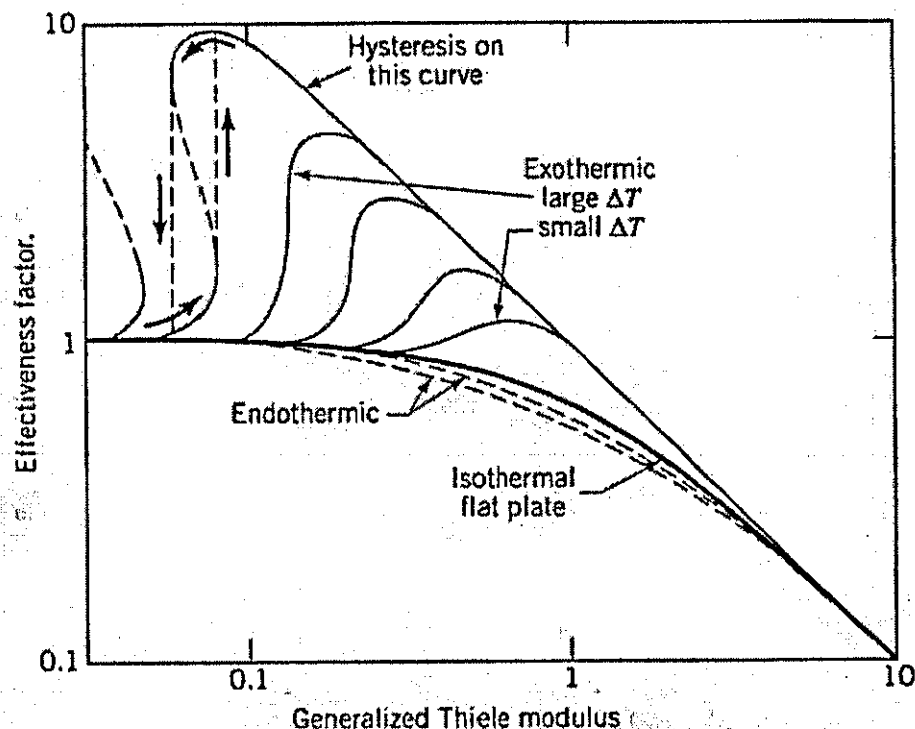
Figure 5.4.

Figure 5.4 Non-isothermal effectiveness factor curve for temperature variation within a particle [6].

5.3 General consideration for experimental design

As reviewed above, heat and mass transfer effects frequently impact upon the overall performance of the reaction. Accurate kinetic rate equations can seldom be extracted from data obtained under the influence of significant heat and/or mass transport limitations. Thus it is important that the rate data obtained from kinetic runs be acquired in the regime of kinetic control so that the intrinsic kinetics of $NaBH_4$ can be obtained. Effectiveness factor can be then built into the kinetic rate expression in order to model hydrogen generation in practice when large catalyst particles are used.

A carbon-supported ruthenium catalyst is one of the most efficient catalysts for $NaBH_4$ hydrolysis. It has the characteristics of a heterogeneous catalyst. The methodology and results can be applied to other catalysts for $NaBH_4$ hydrolysis. In a heterogeneous catalytic reaction, heat removal is a difficult factor to overcome in order to obtain isothermal rate data. A number of different batch reactors have been designed and three of them are shown in Figure 5.5 [7]. The first one is the now famous Carberry reactor,

wherein the catalyst is mounted in the paddle or agitator. The next shown is a turbine reactor, where a small fixed bed of catalyst is mounted at the throat of the Venturi and the reacting mixture is pumped through the impeller. The third is a circulating reactor with a fixed bed of catalyst.
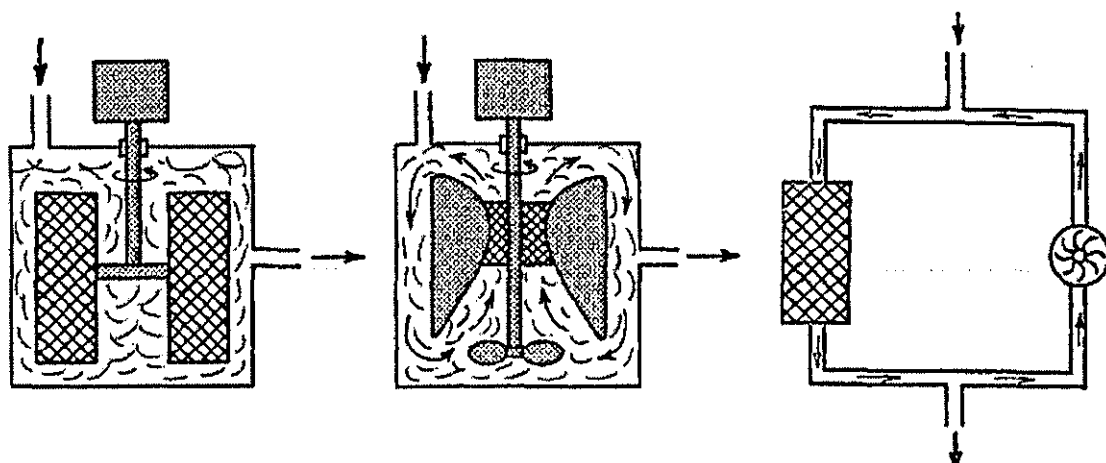
Figure 5.5 Stirred batch reactors for studying heterogeneous chemical reactions [7].

The main consideration for the above type of heterogeneous reactors is to remove heat generated efficiently. Since the contact time for reaction mixture and catalyst is short enough for the heat to be removed very rapidly, the reaction system can thus be maintained at a constant temperature. However, these reactors will not work for studying the hydrolysis of $NaBH_4$, since $NaBH_4$ hydrolysis has a significant rate at higher temperatures even without a catalyst.

Another difficulty in the study of the hydrolysis of $NaBH_4$ is the effect of the by-product, $NaBO_2$. Even for an isothermal reaction, it is difficult to separate the effects of the concentration of $NaBH_4$ and $NaBO_2$.

In this work, instead of making an effort to control reaction temperature precisely and to separate the effects of $NaBH_4$ and $NaBO_2$, an alternative method was developed. This new approach does not involve a new reactor design, but instead uses a new method of analysing the non-isothermal rate data in order to obtain isothermal rate data. In the following, the rig for monitoring the reaction rate is described and then the method is introduced.

5.4 Experimental Method

5.4.1 Materials

The specifications of the materials used are listed in Table 5.2, and the specifications of the catalyst are given in Table 5.3.

Table 5.2 Materials used in the experiment.

Materials	Appearance	Purity (wt%)	Supplier
$NaBH_4$	Powder	98.0	Aldrich
$NaBO_2$	Powder	98.0	Aldrich
Ruthenium catalyst on carbon	Pellet	3% Ru	Johnson Matthey
NaOH	Pellet	99.9	Aldrich

Table 5.3 The specifications of the catalyst

Item	Specifications
Description	steam activated 2mm carbon extrudates (ϕ2x5mm)
BET surface:	$1000 \, m^2 \, g^{-1}$
Bulk density	$0.5 \, g \, cm^{-3}$
Average pro diameter:	15 A

5.4.2 Catalyst Grinding

The ruthenium on carbon catalyst was received in the form of particles with a diameter of 2 mm and 3 mm in length. To investigate the intrinsic kinetics, the particles must be fine enough so that internal diffusion can be neglected. In this study, the catalyst was ground using a pestle and mortar and then sieved using a set of sieves with different mesh apertures. Eight different sieves were stacked on top of each other, and the average diameters of the catalyst particles trapped in each sieve were assumed to match the average aperture sizes of the two adjacent sieves. The sieves set used and the catalyst sizes obtained are listed in Table 5.4. The sieve set was purchased from Fisher Scientific Ltd (UK).

Table 5.4 Sieve set and catalyst size

Sieve aperture (μm)	Average catalyst size (μm)
600	–
500	550.
106	–
90	98
53	–
45	49
32	–
25	29

5.4.3 Experimental set-up to monitor reaction rate

For kinetic research, the change in concentration of $NaBH_4$ with respect to time should be monitored. The measurement of the concentration of $NaBH_4$ is rather difficult due to its hydrolysis even at room temperature. In this study, a method for measuring the hydrogen volume with time was used, since hydrogen volume and $NaBH_4$ concentration can be related using the stoichiometric coefficients in the following reaction scheme.

$NaBH_4 + 2H_2O = NaBO_2 + 4H_2$

A schematic diagram for the experimental set-up is shown in Figure 5.6. The rig consisted of three parts: the reaction system, a sytem to monitor temperature and a system to measure the volume of hydrogen that is generated. The reaction system consists of a three-port reactor and a magnetic stirrer, a water bath that was used to adjust reaction temperature and a feeding system. One side-port of the reactor was equipped with a thermocouple and another side-port was connected to the water replacement system. The middle port of the reactor was used to site a feeding funnel. Since $NaBH_4$ can be hydrolysed even at room temperature when contacting water, a special feeding system was used as shown in Figure 5.6. $NaBH_4$ and catalyst were added to the reactor first and then water was added through the feeding system to the reactor. Once the chemicals come into contact, hydrogen is produced and the amount that was generated was recorded.

The volume of hydrogen that was produced was measured using a water replacement system. The water replacement system consisted of a graduated cylinder full of water and a water reservoir that was used to immerse the cylinder. A container was placed onto an electronic balance. Before starting the experiment, the water in the reservoir was filled to such a level that any extra water would overflow from the cylinder through a slope into the container on the balance. The electronic balance was connected to a computer using a standard RS232 connector. Software provided by the balance manufacturer was used to record the time and the weight of the water displaced from the cylinder. The time interval for recording the weight was one second. Both the software and the electronic balance were purchased from A & D Company Ltd. (UK).

In order to monitor the temperature of the reaction system, a thermocouple was put into a side port of the reactor. This K-type thermocouple was connected to a data logger, which transferred the information to a computer. The data logger and the thermocouple were purchased from Pico Company Ltd (UK).

Before conducting the experiment, the reactor was cleaned using distilled water and then dried in an oven for 24 hours. After the temperature was stable, the reactor was put into the water bath with a fixed amount of catalyst inside. A pre-determined amount of $NaBH_4$ powder was then put into the reactor. After all these were ready, the cork of the feeding funnel was opened to let the water flow into the reactor to start the hydrolysis. The water that was displaced by the hydrogen production and the overall reaction temperature were both monitored by using the computer. When calculating the reaction rate, the saturated vapour pressure at room temperature was considered.

The amount of catalyst that was used was based on the convenience of reaction control. Reaction rate for heterogeneous catalysis is proportional to the mass of catalyst. The rate data is based on unit mass of catalyst.

Figure 5.6 A schematic experimental set-up for the research of NaBH₄ hydrolysis kinetics.

5.4.4 Analysis of non-isothermal rate data in order to obtain isothermal rate data

The general analysis process is described briefly as follows and a detailed procedure will be described together with results and discussion in later chapters.

The rate for any reaction can be expressed using equation (5.11).

$$r = Ae^{-E/RT}C^{\alpha} \tag{5.11}$$

Where r is the reaction rate, E is the activation energy, R is the universal gas constant, T is the temperature, C is the concentration of reactant, α is the reaction order, and A is the pre-exponential factor.

To deriving isothermal rate data from non-isothermal rate data, take logarithms of both sides, yielding

$$\ln r = \ln A + \alpha \ln C - \frac{E}{RT} \tag{5.12}$$

Since A and α are constants for a specific reaction, ln$r$ against $1/T$ will have a linear relationship when C is fixed. In the following, the determination of the parameters (lnA + αlnC) and E/R is given using the illustration in Figure 5.6.

144

Figure 5.6 Schematic graphs showing analysis of non-isothermal rate data to obtain isothermal rate data, (a) reaction rate ~ m_{NaBO2}, (b) temperature ~ m_{NaBO2}.

As shown in Figure 5.6a and b, five runs (*a*, *b*, *c*, *d* and *e*) are performed with the same initial $NaBH_4$ concentration and the same amount of catalyst but with a different initial reaction temperature. The extent of the reaction is indicated using the concentration of $NaBO_2$. The initial temperature increases steadily from *a* to *e*. The reaction temperatures and rates are measured simultaneously with time as shown in Figures 5.6a and b

145

respectively.

At a given $NaBO_2$ concentration, such as in the position of the vertical line, five different rates (r_1, r_2, r_3, r_4 and r_5) can be obtained from Figure 5.6a, and the corresponding temperatures (T_1, T_2, T_3, T_4 and T_5) can be obtained from Figure 5.6b. When the reaction rates and the corresponding reciprocal temperatures ($1/T$) are plotted the result should be linear, with a slope corresponding to $-E/R$, and an intercept on the y axis of $\ln A + \alpha \ln C$. Hence equation (5.12) is determined, which can be then used to calculate the reaction rate at any temperature when the concentration of $NaBO_2$ is m_{NaBO2}. In the same way, equations for any other $NaBO_2$ concentrations can be determined. Reaction rates at these $NaBO_2$ concentrations can also be determined for any temperature. Through this method, isothermal reaction rates are obtained for different $NaBO_2$ concentrations.

If five groups of the above experiments are performed, each of which has a different initial $NaBH_4$ concentration, then equation (5.12) can be determined at the same $NaBO_2$ concentration in each group. Since initial $NaBH_4$ concentration in each group is different, the rate at different $NaBH_4$ concentrations is obtained with the same $NaBO_2$ concentration and temperature.

Therefore, the following procedures are used for each group of experiments.

- Hydrogen release experiments were conducted to obtain $V_{H2} \sim t$, and $T \sim t$.
- Transform $V_{H2} \sim t$ to $r_{H2} \sim t$ by differentiation.
- Transform $r_{H2} \sim t$ to $r_{H2} \sim m_{NaBO_2}$, and $T \sim t$ to $T \sim m_{NaBO_2}$ by using equations (5.13) or (5.14).
- Using the relationship $r_{H2} \sim m_{NaBO_2}$ and $T \sim m_{NaBO_2}$, plot $\ln r_{H2} \sim 1/T$.
- Derive the reaction rate for any temperature at specific $NaBH_4$ or $NaBO_2$ concentrations.

$$m_{NaBO_2} = \frac{(P_0 - P_{H_2O})V_{H_2}/(4RT)}{w^0_{H_2O} - (P_0 - P_{H_2O})V_{H_2}M_{H_2O}/(2RT)} \qquad (5.13)$$

146

$$m_{NaBH_4} = \frac{w^0_{NaBH_4} - [(P_0 - P_{H_2O})V_{H_2}M_{NaBH_4}]/(4RT)}{M_{NaBH_4}[w^0_{H_2O} - (P_0 - P_{H_2O})V_{H_2}M_{H_2O}/(2RT)]} \tag{5.14}$$

Where V_{H2} is the volume of hydrogen released at time t, T is the reaction temperature, r_{H2} is the hydrogen generation rate, w is mass, P_0 is atmospheric pressure (assumed to be 101325 Pa), P_{H2O} represents saturated vapour pressure at ambient temperature for measuring hydrogen volume, M is the molecular mass, V is the volume, and R is the universal gas constant (8.314 J mol^{-1} K^{-1}). The superscript 0 represents initial value.

5.5 Summary

In this chapter, the fundamentals of heterogeneous catalysis are reviewed. When deriving intrinsic kinetic equations for the hydrolysis of NaBH$_4$, diffusion limitations must be removed including both heat and mass transfer. Due to the extensive heat effect, an isothermal heterogeneous reaction is difficult to perform.

A rig has been designed to monitor the kinetics thorough a water placement method. Instead of maintaining constant temperature, a new analysis method is established to obtain isothermal rate data from non-isothermal rate data.

5.6 References

1.   Davis, R.E., Bromels, E., and Kibby, C.L., *Boron hydrides. III. Hydrolysis of sodium borohydride in aqueous solution.* Journal of American Chemical society, 1962. **84**: 885-892.

2.   Davis, R.E. and Swain, C.G., *General acid catalysis of the hydrolysis of sodium borohydride.* Journal of American Chemical society, 1960. **82**: 5949-5950.

3.   Kaufman, C.M., *Catalytic generation of hydrogen from the hydrolysis of sodium borohydride: application in a hydrogen/oxygen fuel cell/.* 1981, lousiana State University and Agricultural and Mechanical College. 166.

4.   Satterfield, C.N., *Mass Transfer in Heterogeneous Catalysis.* 1970, Cambridge, MA: MIT Press. Chapter 3.

5.   Vannice, M.A., *Kinetics of Catalytic Reactions.* 2005, New York: Springer

Science+Business Media. 59.

6. Levenspiel, O., *Chemical Reaction Engineering*. 1999, New York: John Wieley and Sons. 393.

7. Weekman, V.W., *Laboratory reactors and their limitations*. AIChE Journal, 1974. **20**: 833-840.

Chapter 6

Preparatory Work for the Kinetic Study

6.1 Introduction

As discussed in the last chapter, the $NaBH_4$ molecule must be transported from the well-mixed, homogenous bulk phase to the surface of a catalyst particle before it can react. This is external diffusion. Since the catalyst that is used is a porous material containing active sites distributed within its structure, $NaBH_4$ molecules must further diffuse into the pores. This is internal diffusion. Inter-phase gradients can exist between the bulk and solid phases. Diffusive-convective transport processes link the source of reactants to the sink of the reaction. Moreover, in order to obtain an intrinsic kinetic equation, heat that is generated must be removed quickly enough so that catalyst particles do not form 'hot spots'. Also there must be no temperature gradient within the porous catalyst particles.

The objective of this investigation is to obtain the conditions at which the effects of heat and mass diffusion can be neglected. This is the preparatory work for studying intrinsic kinetics.

6.2 External diffusion

In order to eliminate the limitation of external diffusion in the reaction rate, the stirring rate can be increased until the mass transport rate is greater than the reaction rate. Therefore, it is necessary to compare rate data at various stirring rates whilst the temperature and the $NaBH_4$ and $NaBO_2$ concentrations are fixed.

Figures 6.1a and 6.1b are the $V_{H2} \sim t$ and $T \sim t$ curves respectively for the hydrolysis of $NaBH_4$ at different initial reaction temperatures when there is no stirring. Hydrogen volume increases as the reaction proceeds and then levels off, indicating that all of the $NaBH_4$ is consumed. When the initial reaction temperature is lower, the temperature remains nearly constant. However, when the initial reaction temperature is higher, the temperature is difficult to control and the reaction proceeds in a non-isothermal way due

to a higher reaction rate, which leads to a rapid generation of heat.

Figure 6.2 shows the rate of hydrogen generation versus reaction time, which was transformed by differentiation of the corresponding $V_{H2} \sim t$ curves in Figure 6.1a. Figure 6.3 is the relationship between $r_{H2} \sim m_{NaBO_2}$ and $T \sim m_{NaBO_2}$, which was transformed by using equations (5.13) or (5.14). By measuring r_{H2} and T at the same concentration of $NaBO_2$ (which indicates the same reaction extent), $\ln r_{H2}$ against $1/T$ was plotted in Figure 6.4. It can be seen from Figure 6.4 that $\ln r_{H2}$ and $1/T$ have a good linear relationship, indicating that equation (5.12) is reasonable. After obtaining the linear relationship, reaction rates were plotted against $NaBO_2$ concentration at various temperatures, as shown in Figure 6.5.

In the same way, another two sets of experiments were conducted when the stirring rates were 390 rpm and 650 rpm respectively. The corresponding figures are shown in Figure 6.6 to Figure 6.10 for the stirring rate of 390 rpm, and Figure 6.11 to Figure 6.15 for the stirring rate of 650 rpm.
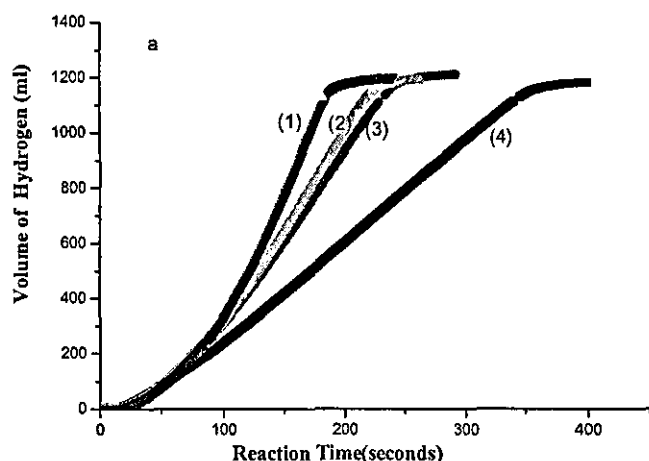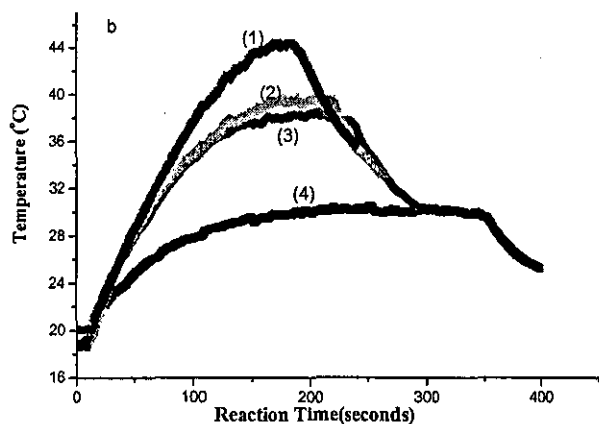
Figure 6.1 Hydrogen generation from the hydrolysis of NaBH₄ at various initial temperatures. The hydrolysis was conducted with an initial molality of NaBH4 of 1.32 mol kg⁻¹, in 10 ml of water with 0.3 g of ground catalyst with a mean particle diameter of 0.049 mm, without stirring. (a) Hydrogen production-time curves; (b) Temperature-time curves.
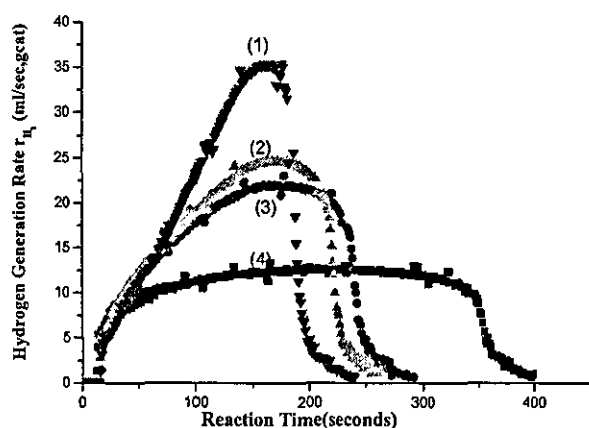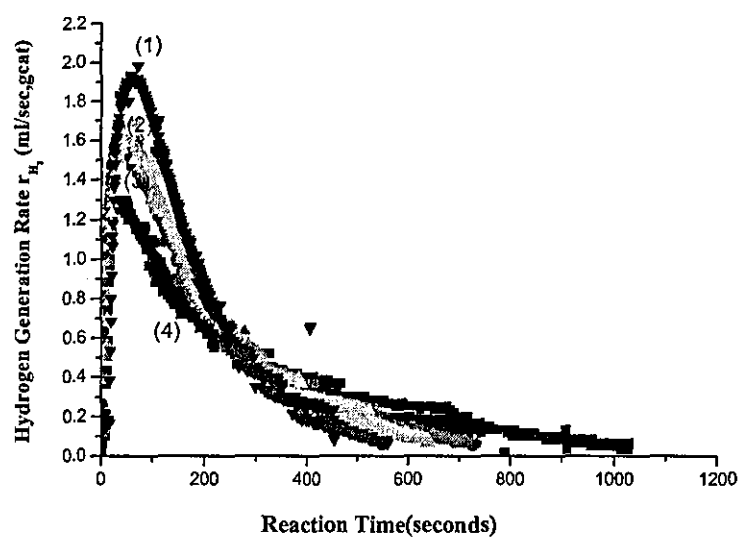

Figure 6.2 The rate of hydrogen generation versus time at various temperatures, obtained by differentiation of Figure 6.1a.

151
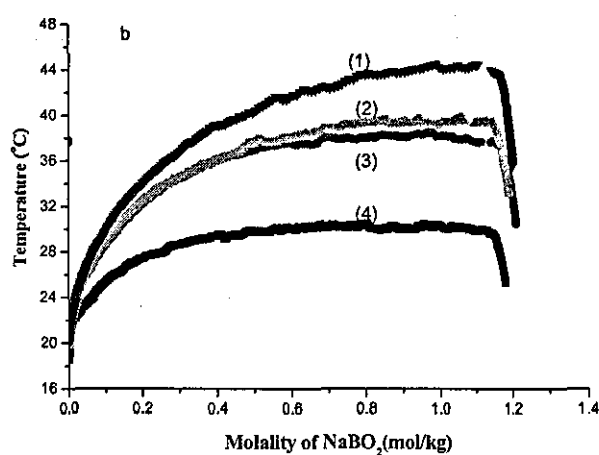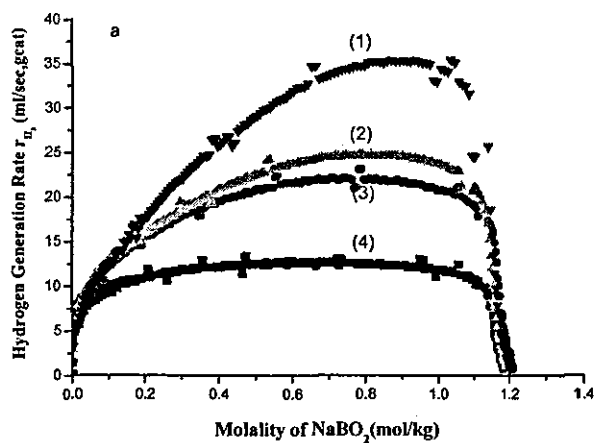
Figure 6.3 The rate of hydrogen generation versus $NaBO_2$ concentration (a) and temperature versus $NaBO_2$ concentration (b). They were transformed from Figure 6.2 and Figure 6.1b respectively.

152
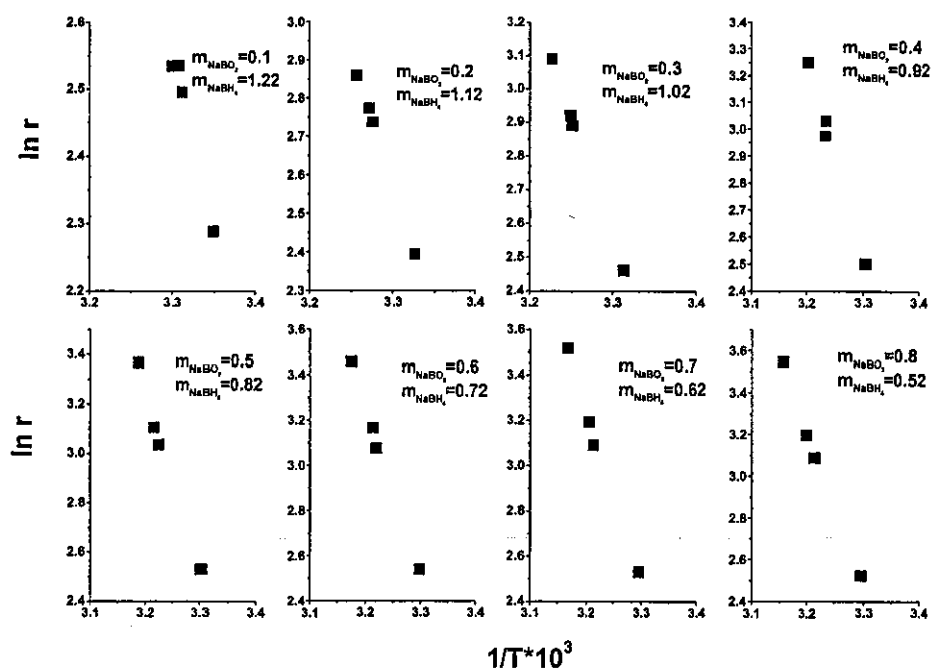
Figure 6.4 The relationship between lnr_{H2} and 1/T, derived from Figure 6.3.
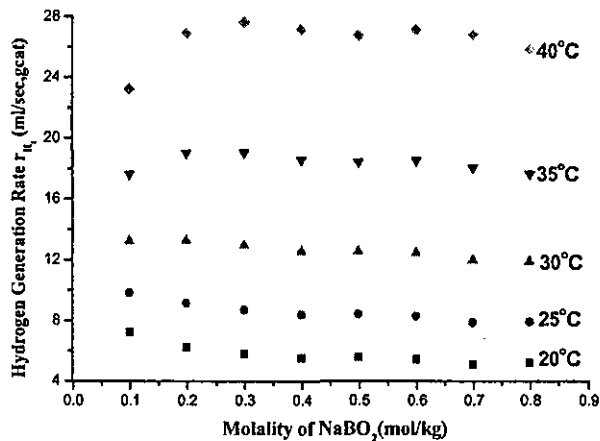
Figure 6.5 r_{H2} versus the extent of the reaction at various temperatures when there was no stirring.
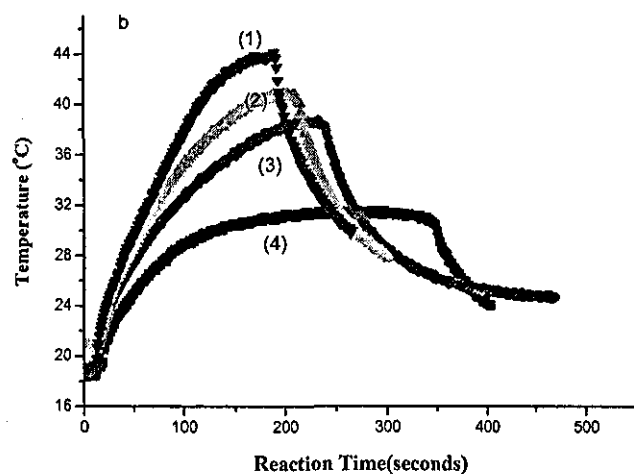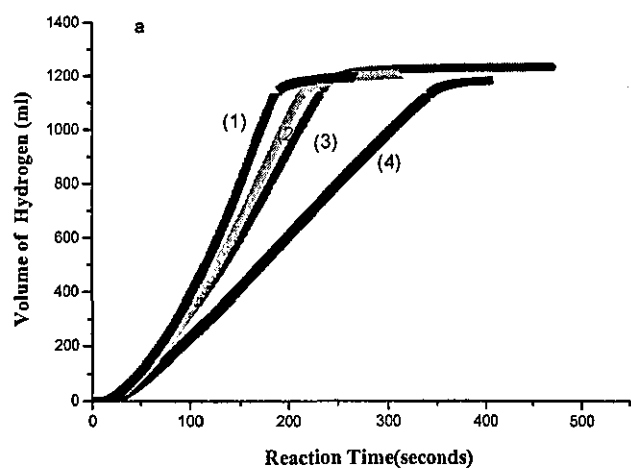
Figure 6.6 Hydrogen generation from the hydrolysis of NaBH$_4$ at various temperatures. The hydrolysis was conducted with an initial molality of NaBH4 of 1.32 mol kg^{-1}, in 10 ml of water with 0.3 g of ground catalyst with a mean diameter of 0.049 mm and with a stirring rate of 390 rpm. (a) Hydrogen production-time curves; (b) temperature-time curves.
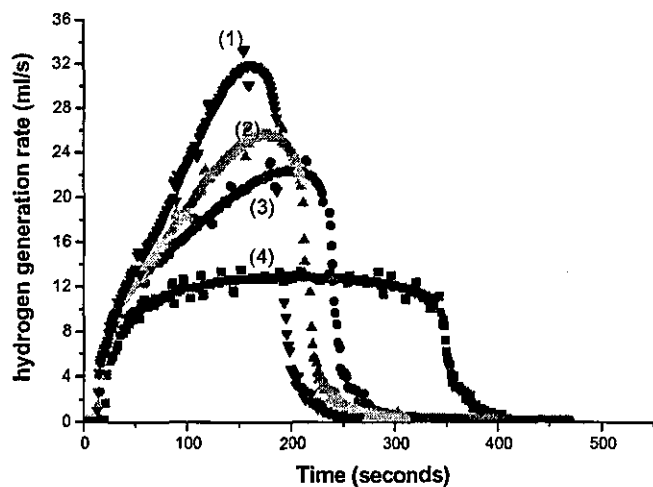
Figure 6.7 r_{H2} versus time at various temperatures, obtained by differentiation of Figure 6.6a.
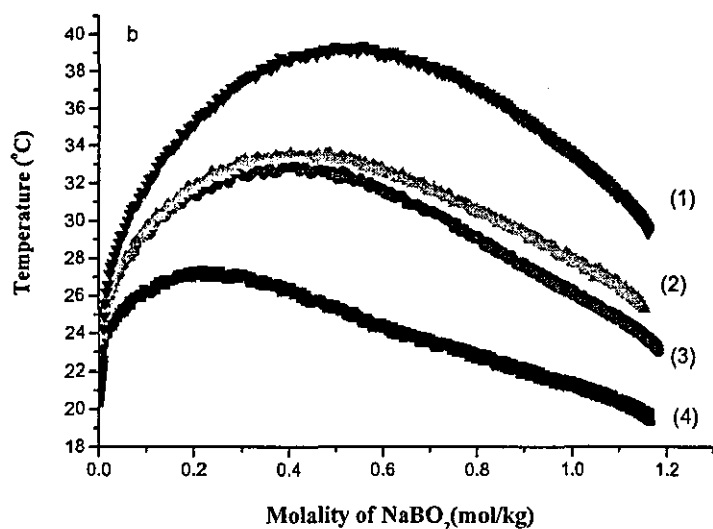

155
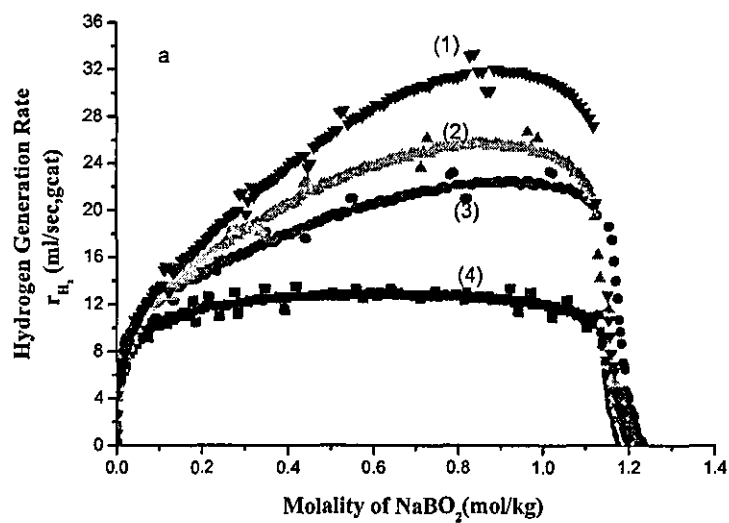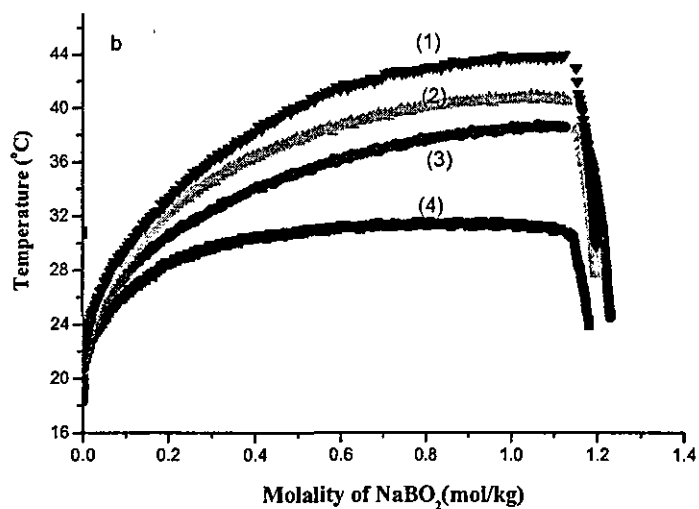
Figure 6.8 The rate of hydrogen generation versus $NaBO_2$ concentration (a) and temperature versus $NaBO_2$ concentration (b). They were transformed from Figure 6.7 and Figure 6.6b respectively.
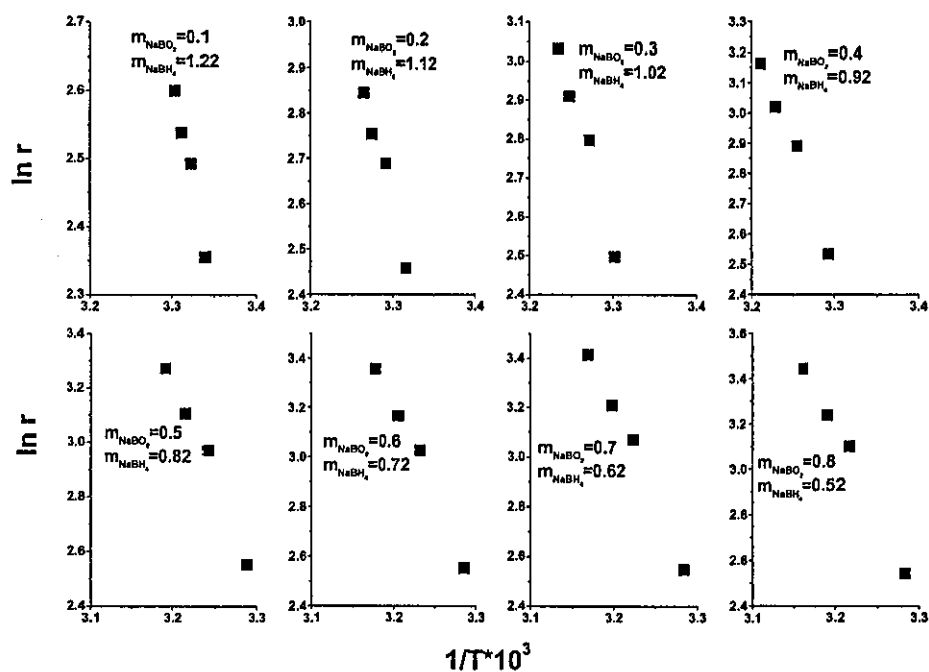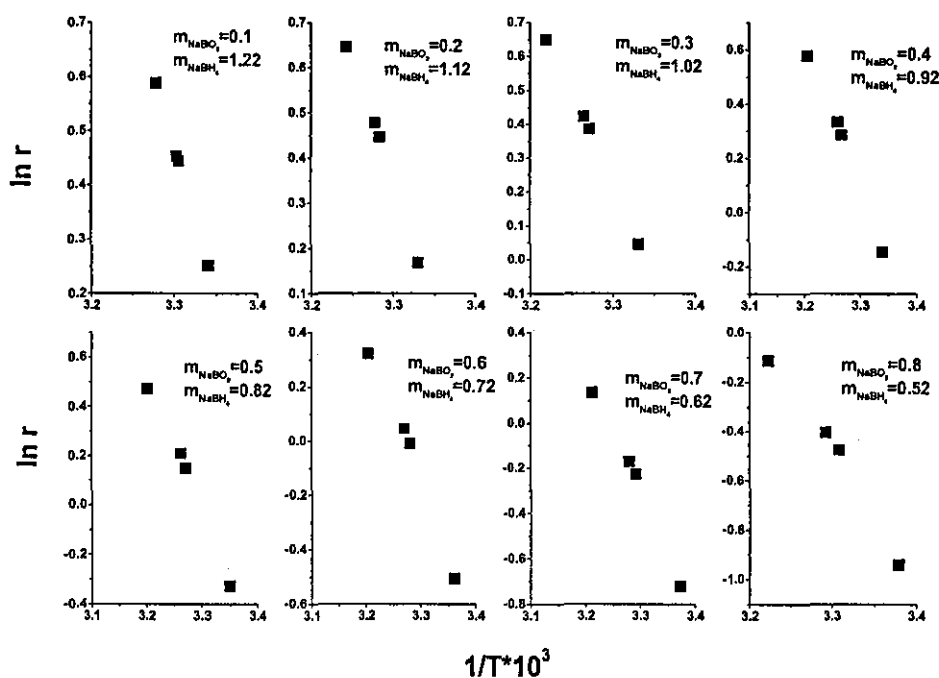

**Figure 6.9** $\ln r_{H2}$ versus 1/T derived from Figure 6.8.

156
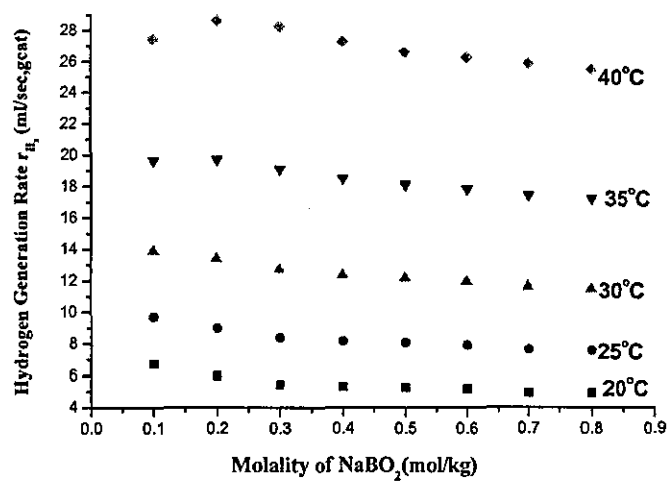
Figure 6.10 r_{H2} versus the extent of the reaction at various temperatures when the stirring rate was 390 rpm.
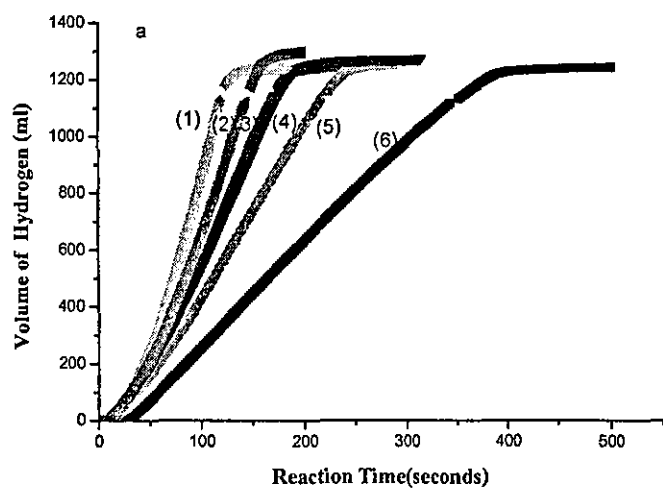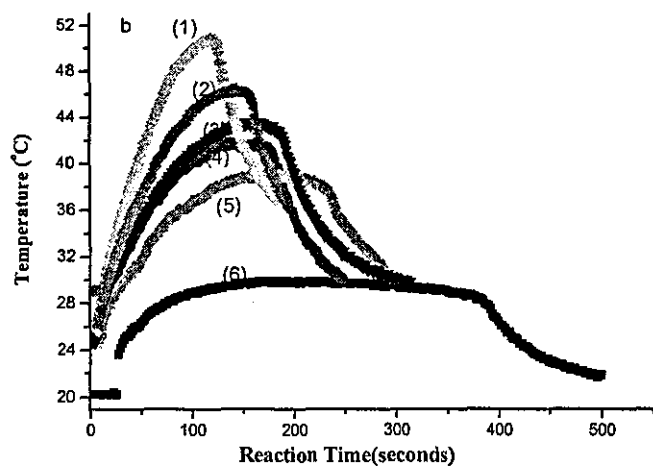
Figure 6.11 Hydrogen generation from the hydrolysis of NaBH₄ at various temperatures. The hydrolysis was conducted with an initial molality of NaBH₄ of 1.32 mol kg⁻¹, in 10 ml of water with 0.3 g of ground catalyst with a mean diameter of 0.049 mm and with a stirring rate of 650 rpm. (a) Hydrogen production-time curves; (b) Temperature-time curves.
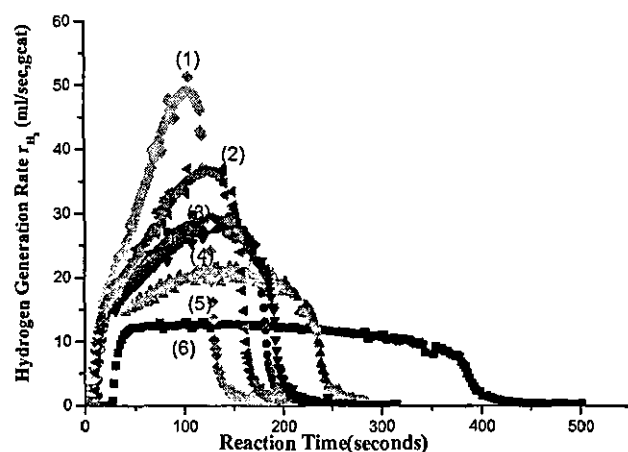
Figure 6.12 r_{H2} versus time at various temperatures, obtained by differentiation of Figure 6.11a.
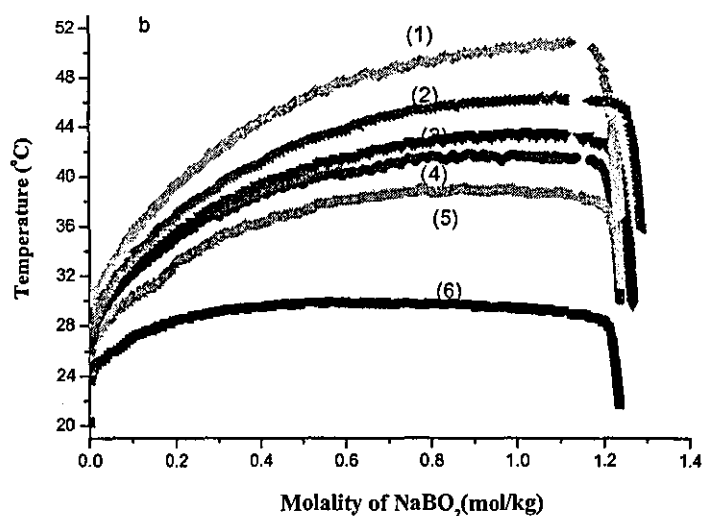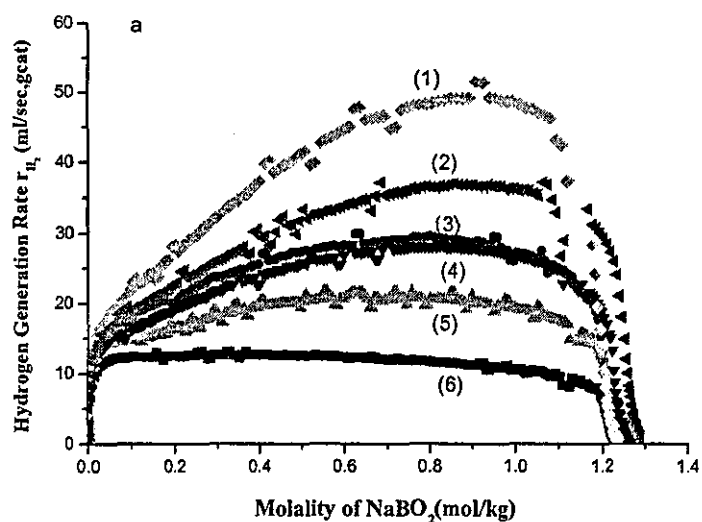
Figure 6.13 The rate of hydrogen generation versus NaBO₂ concentration (a) and temperature versus NaBO₂ concentration (b). They were transformed from Figure 6.12 and Figure 6.11b respectively.

159
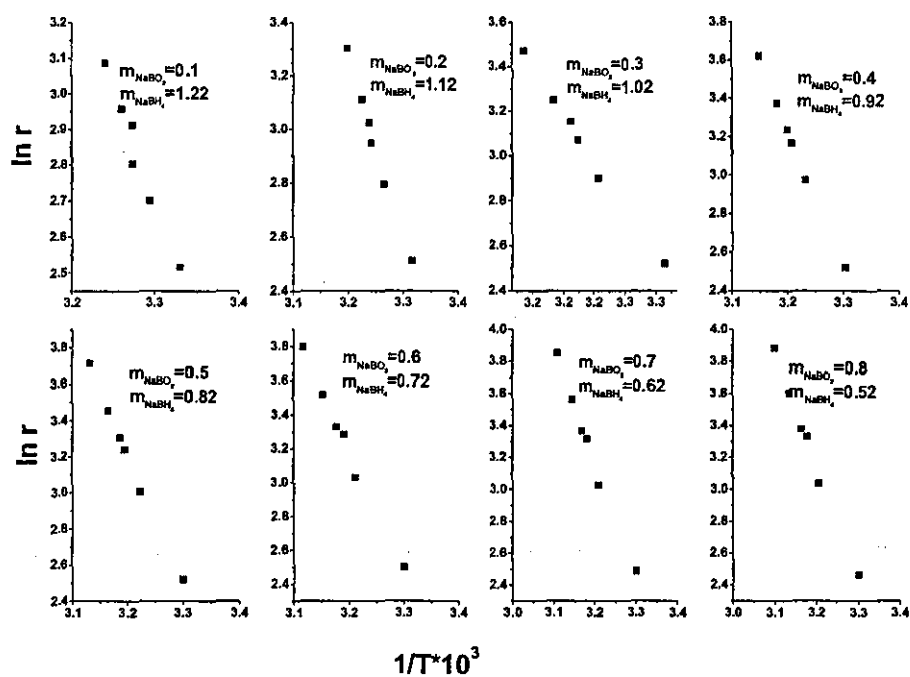
**Figure 6.14** $\ln r_{H2}$ and $1/T$ derived from Figure 6.13.
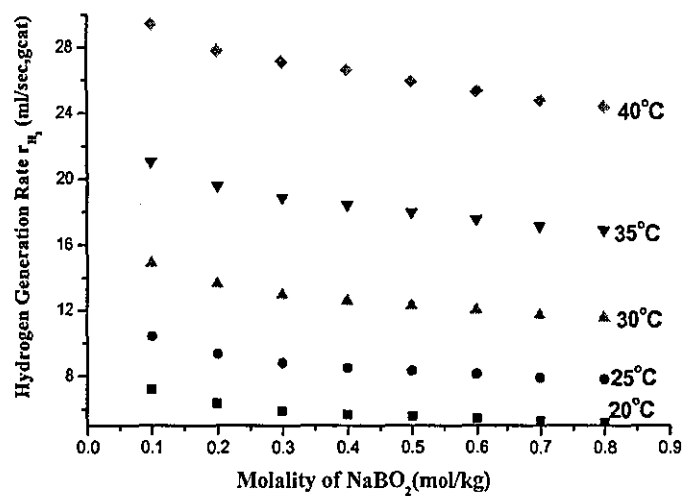
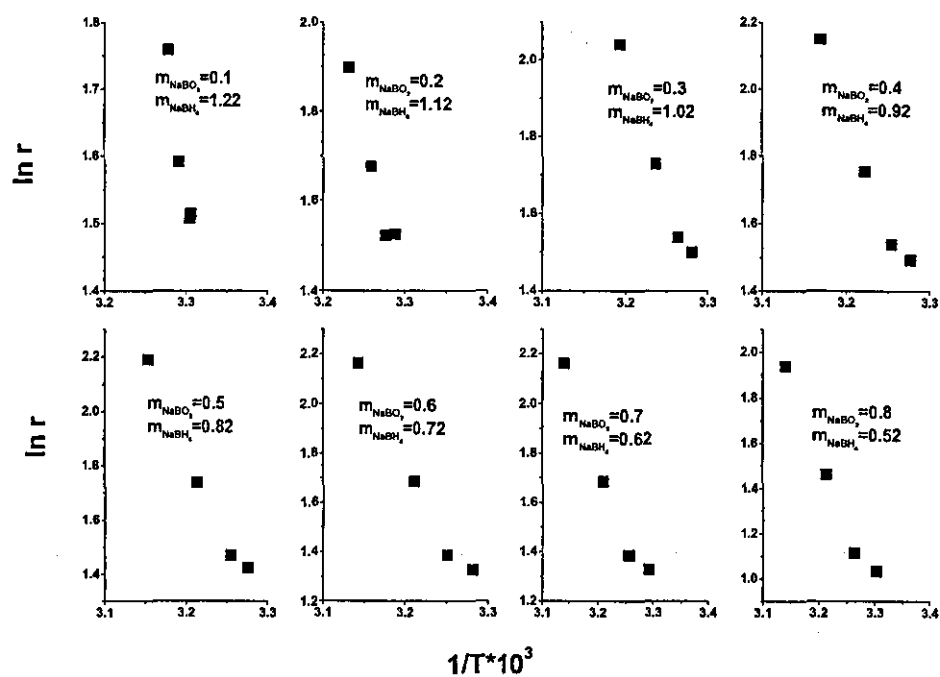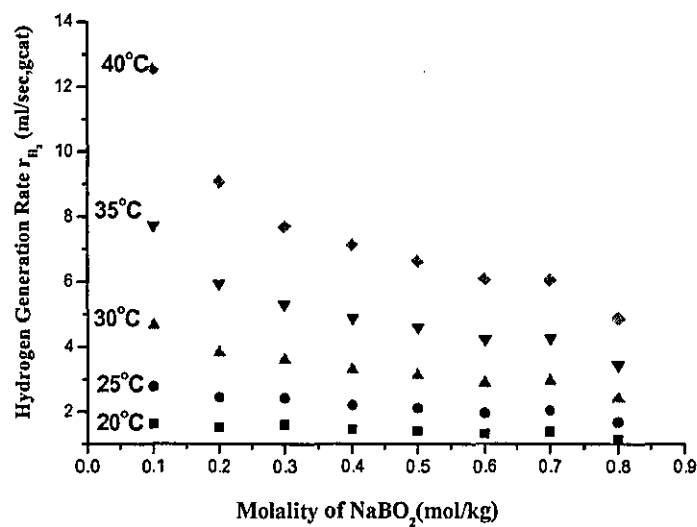**Figure 6.15** Reaction rate versus reaction extent at various temperatures when the stirring rate was 650 rpm.
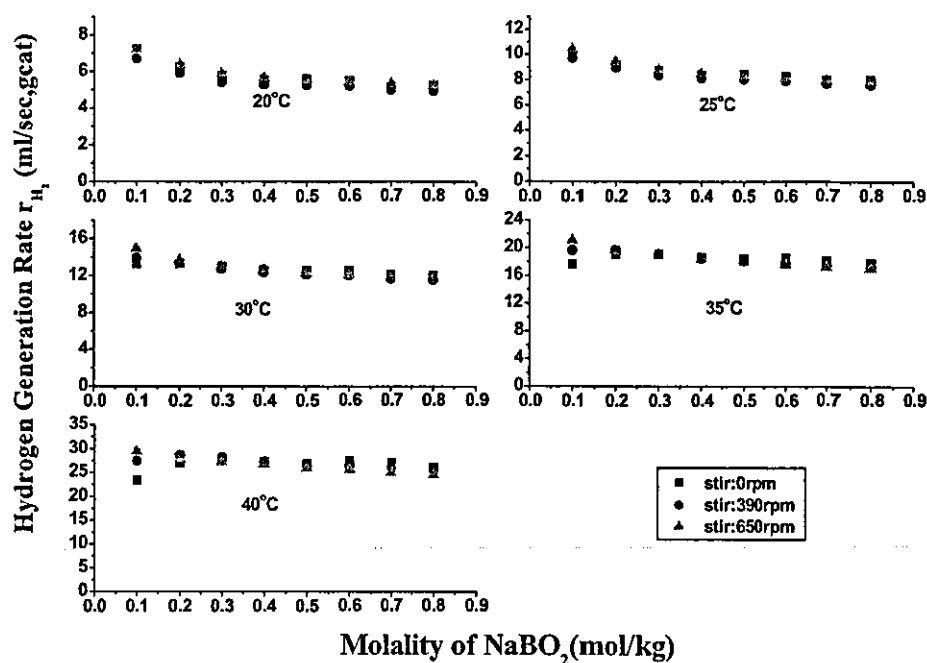
Figure 6.16 Comparison of the effect of stirring rate on reaction rate. The catalyst particles used had an average size of 0.049 mm. The reaction was conducted using 0.5g NaBH$_4$ in 10 ml of water.

In order to make a comparison, Figures 6.5, 6.10, and 6.15 were plotted together, as shown in Figure 6.16. At lower reaction temperatures, reaction rate is not affected significantly by stirring rate. At higher temperatures, reaction rate increases with an increase of stirring rate at the beginning of the reaction.

When the reaction temperature is low, reaction rate is low. Hence, it does not need a high rate of stirring in order to provide a high rate of mass transfer from the bulk fluid to the catalyst particles. When the reaction temperature increases, the reaction rate increases exponentially. In this case a high rate of mass transfer is required in order to provide NaBH$_4$ to the catalyst. Therefore the stirring rate, and thus the external mass transfer, is not significant at lower temperatures.

However, the stirring rate did not show any effect when the concentration of NaBO$_2$ was higher than 0.2 mol/kg, i.e. about 10% of NaBH$_4$ was hydrolysed. This may be due to the production of hydrogen gas, which agitated the reaction solution violently. The effect of hydrogen gas agitation made the effect of stirring rate on external mass transfer not

161

significant.

As shown in Figure 6.16, the difference between the reaction rates at above 30°C became obvious at a very early stage in the reaction. However, the difference between reaction rate at 390 rpm and 650 rpm was very small, less than 10%. Therefore, it can be concluded that 650 rpm is high enough to remove external diffusion limitation for the reaction. In the following work, the stirring rate was fixed at 650 rpm.

6.3 Internal diffusion

Internal diffusion refers to the mass transfer within a catalyst particle. It is affected mainly by the size of particle that is used. When the particle size is fine enough, the internal mass transfer limitation can be removed. In this section, a particle size is determined for which the internal mass transfer rate does not limit reaction rate. In order to investigate this, it is necessary to compare the reaction rate at various sizes of catalyst particle whilst the temperature and the $NaBH_4$ and $NaBO_2$ concentrations are fixed. Also, a sufficiently high stirring rate is employed, as per the results of section 6.2, so that the effects of external diffusion are removed.

Five different particle sizes were used for the investigation at a fixed concentration of $NaBH_4$ and stirring rate of 650 rpm. Figures 6.17 to 6.21 are $NaBH_4$ hydrolysis data when the catalyst particle diameter was 2 mm. Figures 6.22 to 6.26 are the experiments when the catalyst particle diameter was 0.60 mm. Figures 6.27 to 6.31 are the experiments when the catalyst particle diameter was 0.10 mm. Figure 6.32 to 6.36 are the experiments when the catalyst particle diameter was 0.05 mm. Figures 6.37 to 6.41 are the experiments when the catalyst particle diameter was 0.03 mm.
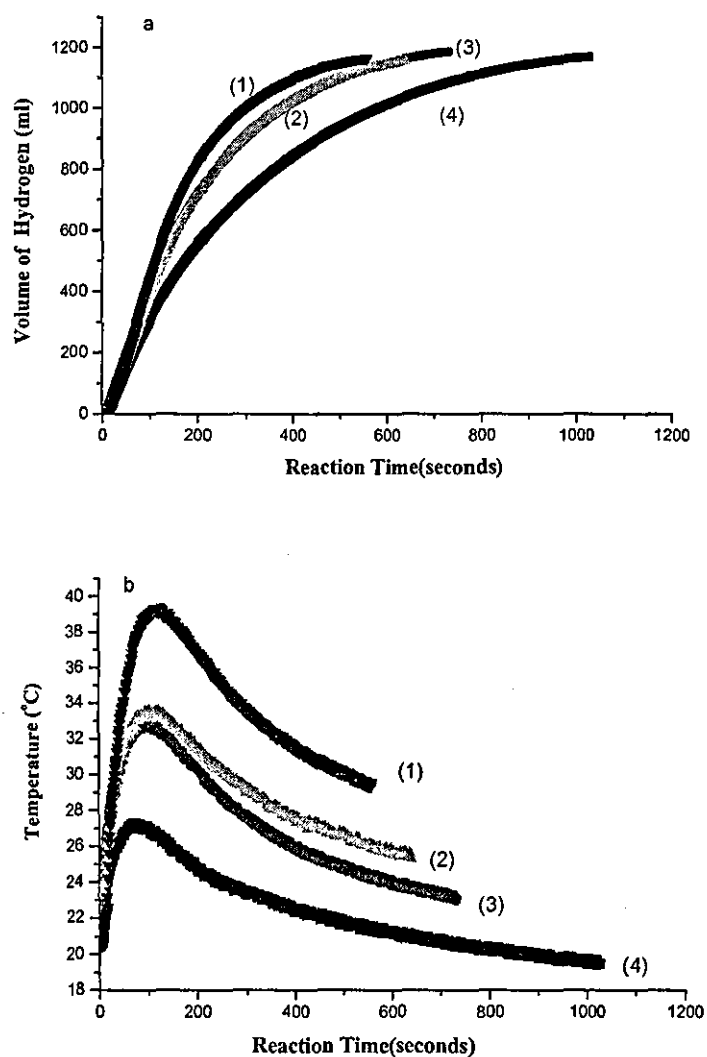
Figure 6.17 Hydrogen generation from the hydrolysis of NaBH$_4$ at various temperatures. The initial molality of NaBH4 was 1.32 mol kg^{-1}. The hydrolysis was performed in 10 ml of water with 0.3 g of catalyst with a mean diameter of 2 mm. (a) Hydrogen production-time curves; (b) Temperature-time curves.
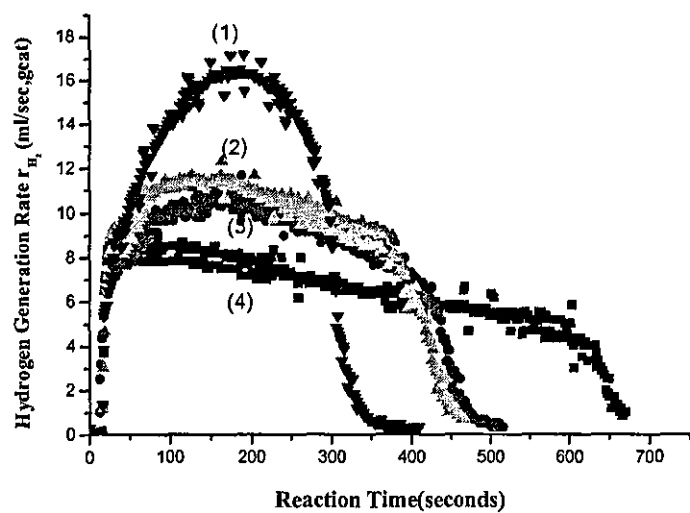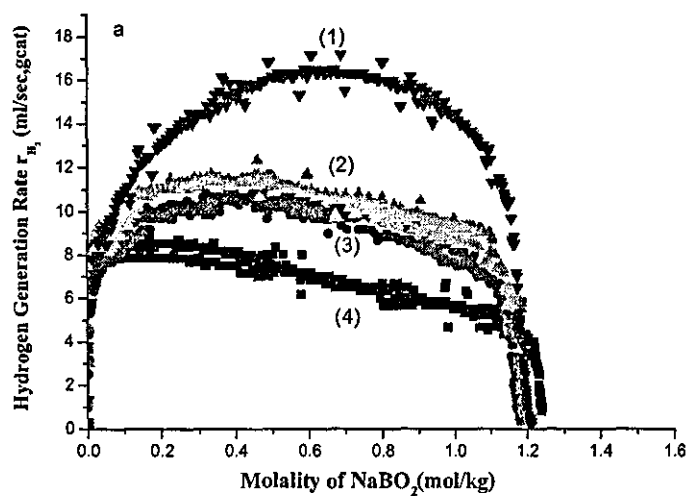
Figure 6.18 r_{H2} versus time at various temperatures by differentiation of Figure 6.17a.
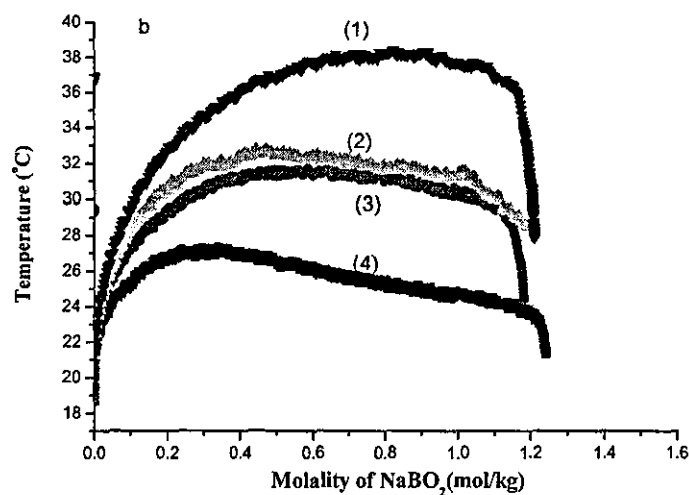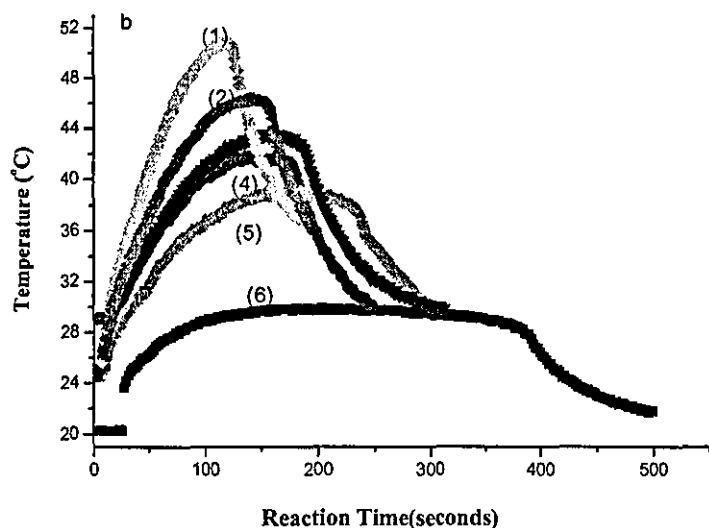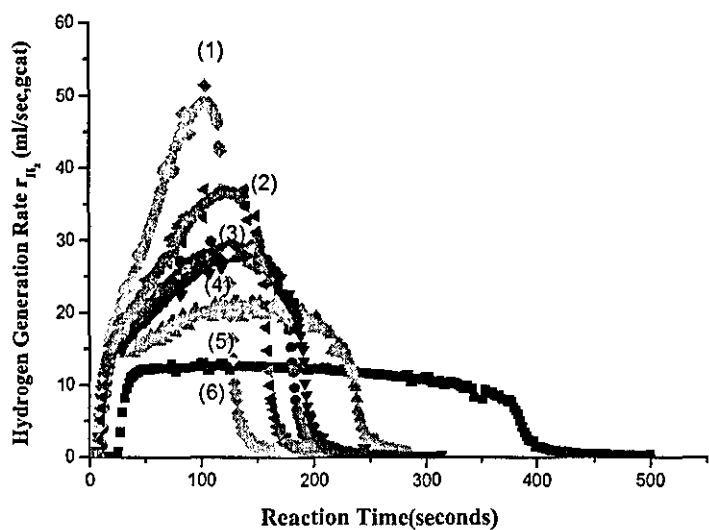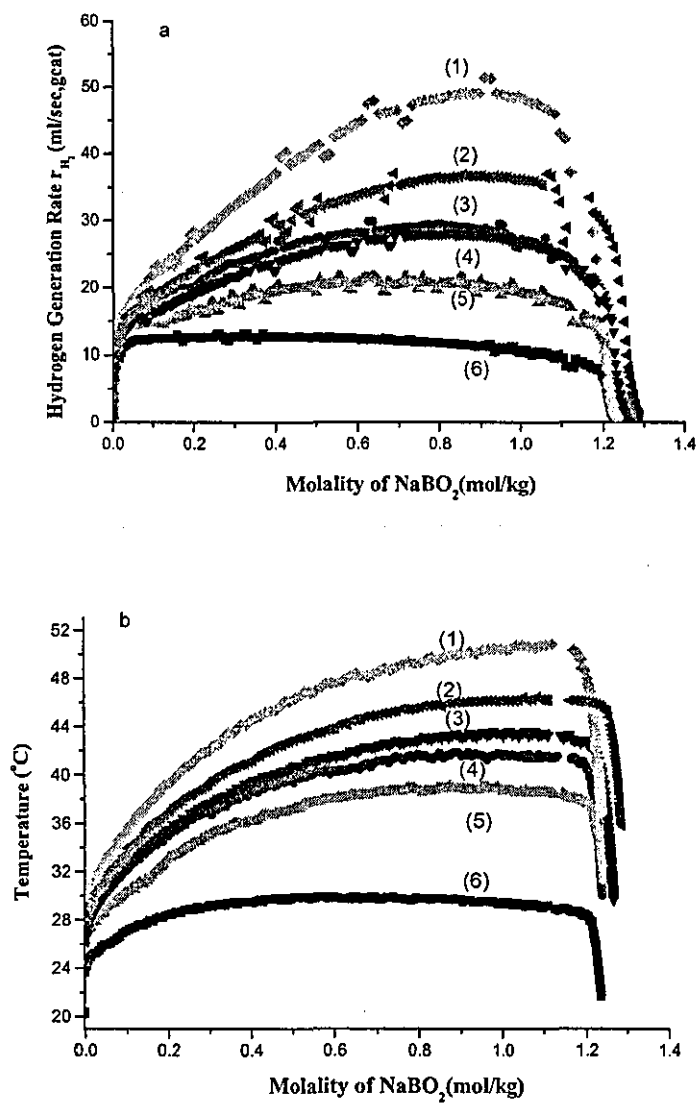

164
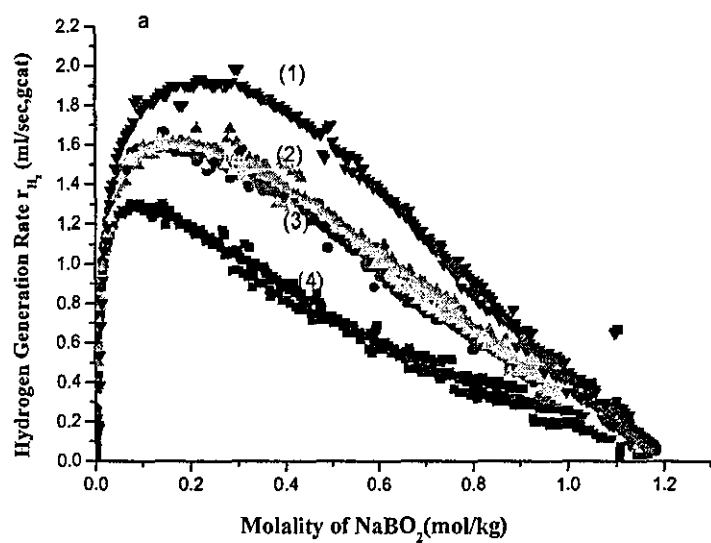
Figure 6.19 The rate of hydrogen generation versus $NaBO_2$ concentration (a) and temperature versus $NaBO_2$ concentration (b). They were transformed from Figure 6.18 and Figure 6.17b respectively.

Figure 6.20 $\ln r_{H2}$ and $1/T$ derived from Figure 6.19.

165
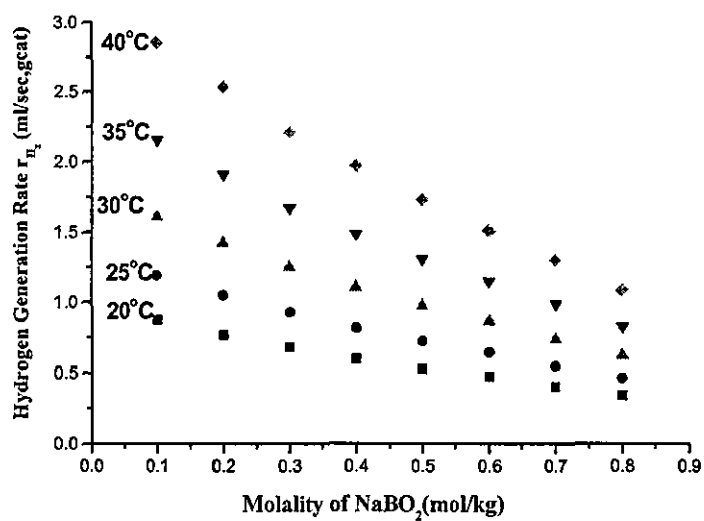
Figure 6.21 Reaction rate versus reaction extent at various temperatures when the catalyst particle size was 2 mm.
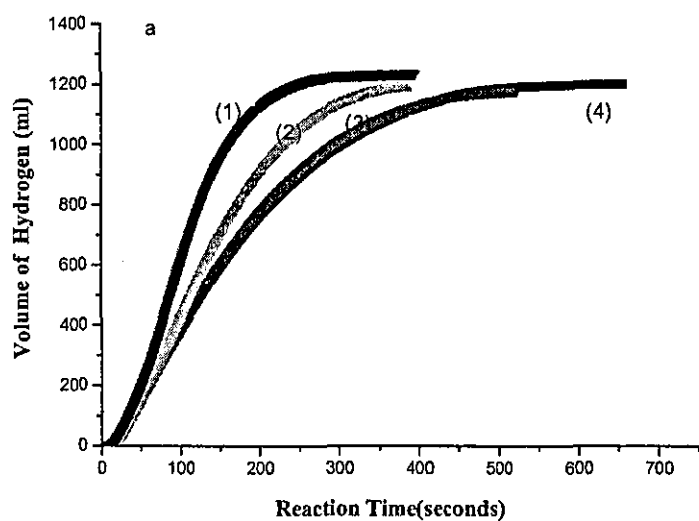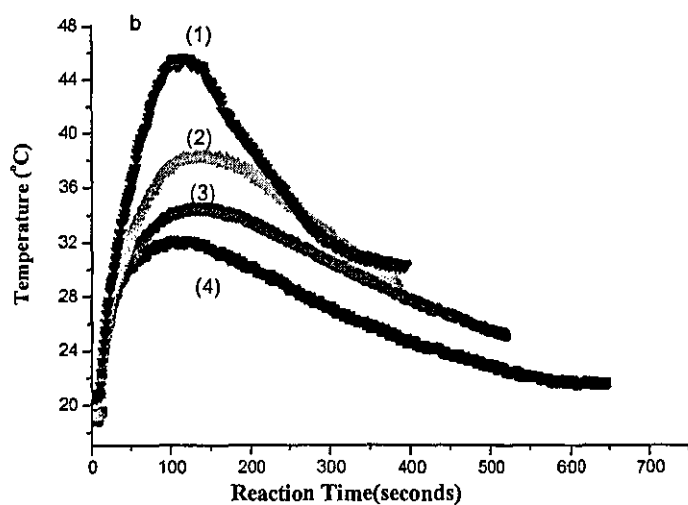
Figure 6.22 Hydrogen generation from the hydrolysis of $NaBH_4$ at various temperatures. The initial molality of $NaBH_4$ was 1.32 mol kg^{-1}. The hydrolysis was performed in 10 ml of water with 0.3 g of catalyst with a mean diameter of 0.55 mm. (a) Hydrogen production-time curves; (b) Temperature-time curves.
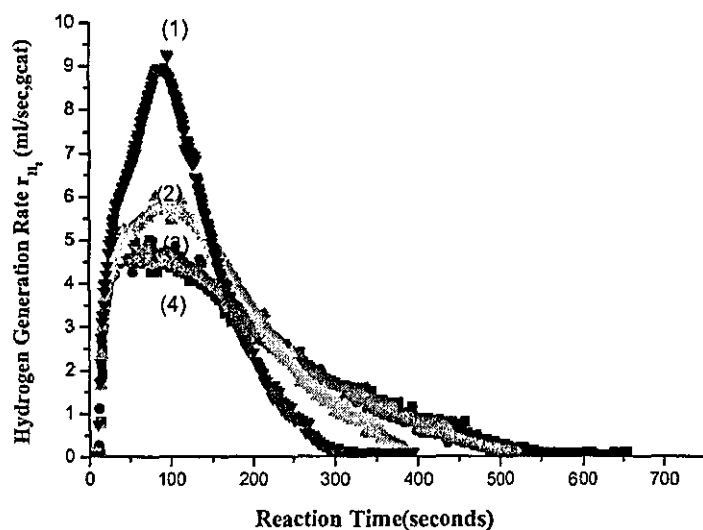
Figure 6.23 r_{H2} versus time at various temperatures by differentiation of Figure 6.22a.
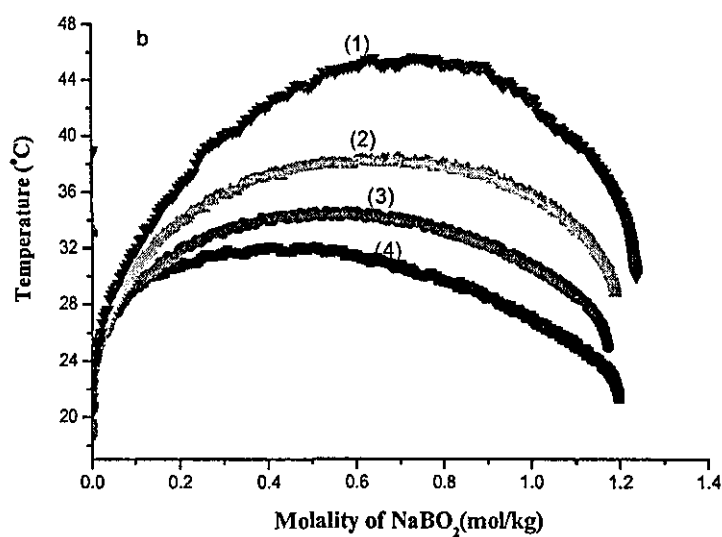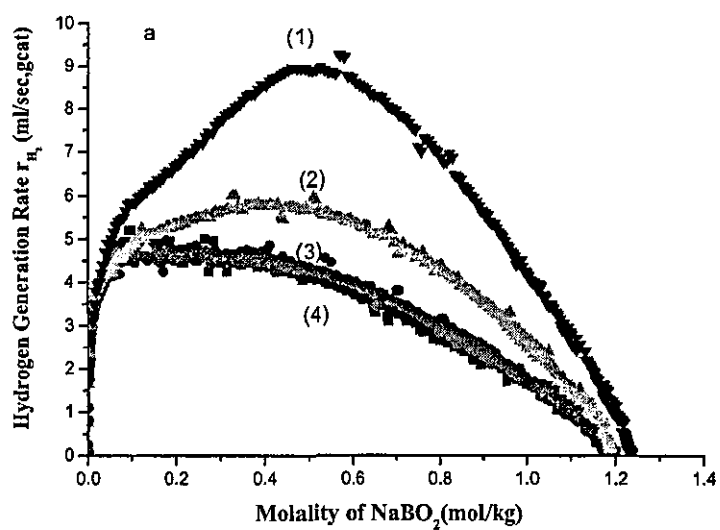
Figure 6.24 The rate of hydrogen generation versus NaBO₂ concentration (a) and temperature versus NaBO₂ concentration (b). They were transformed from Figure 6.23 and Figure 6.22b respectively.
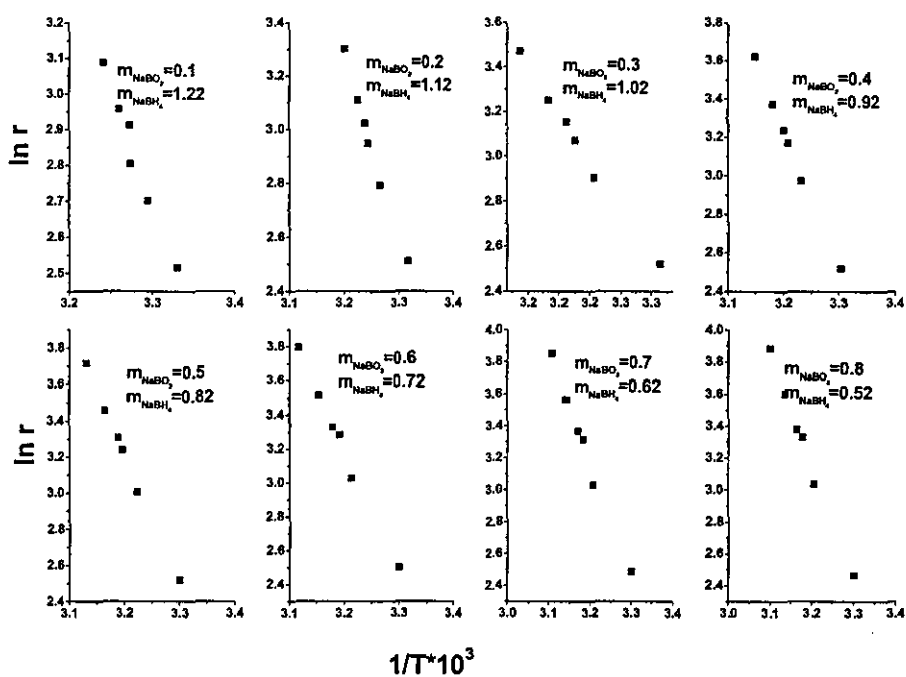
Figure 6.25 lnr_{H2} and 1/T derived from Figure 6.24.
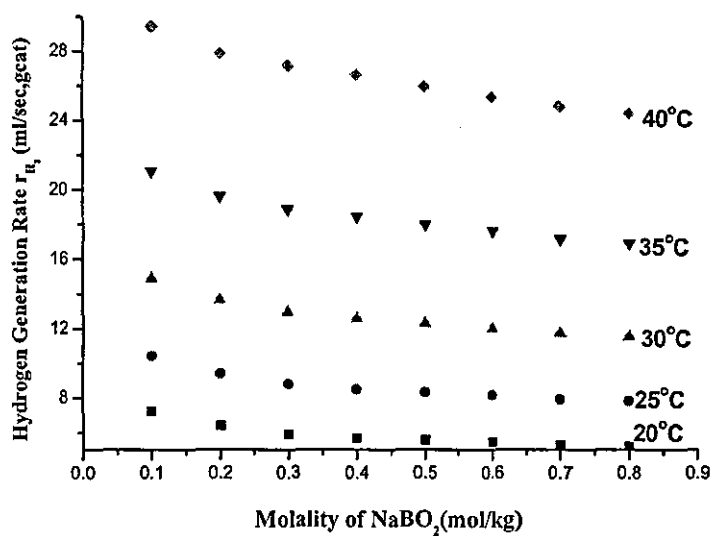

Figure 6.26 Reaction rate versus reaction extent at various temperatures when the catalyst particle size was 0.55 mm.
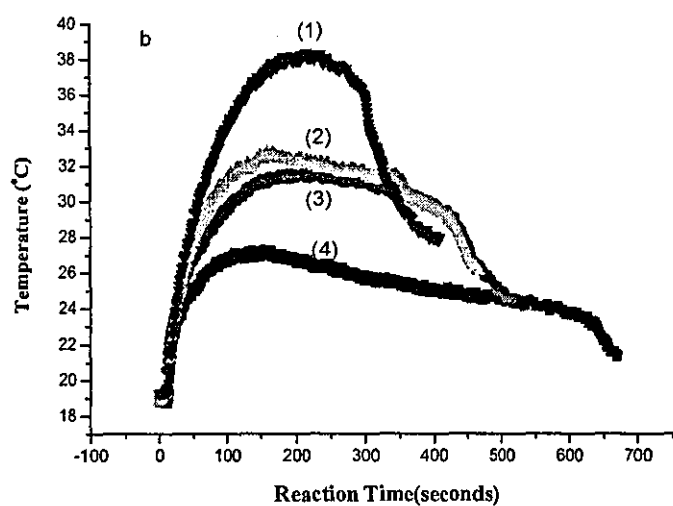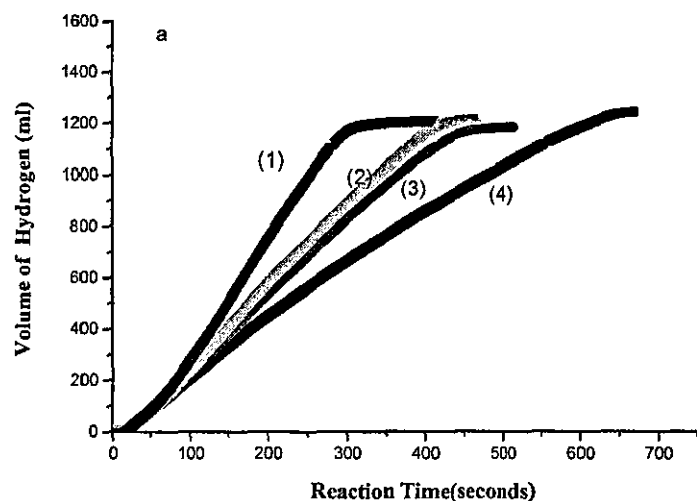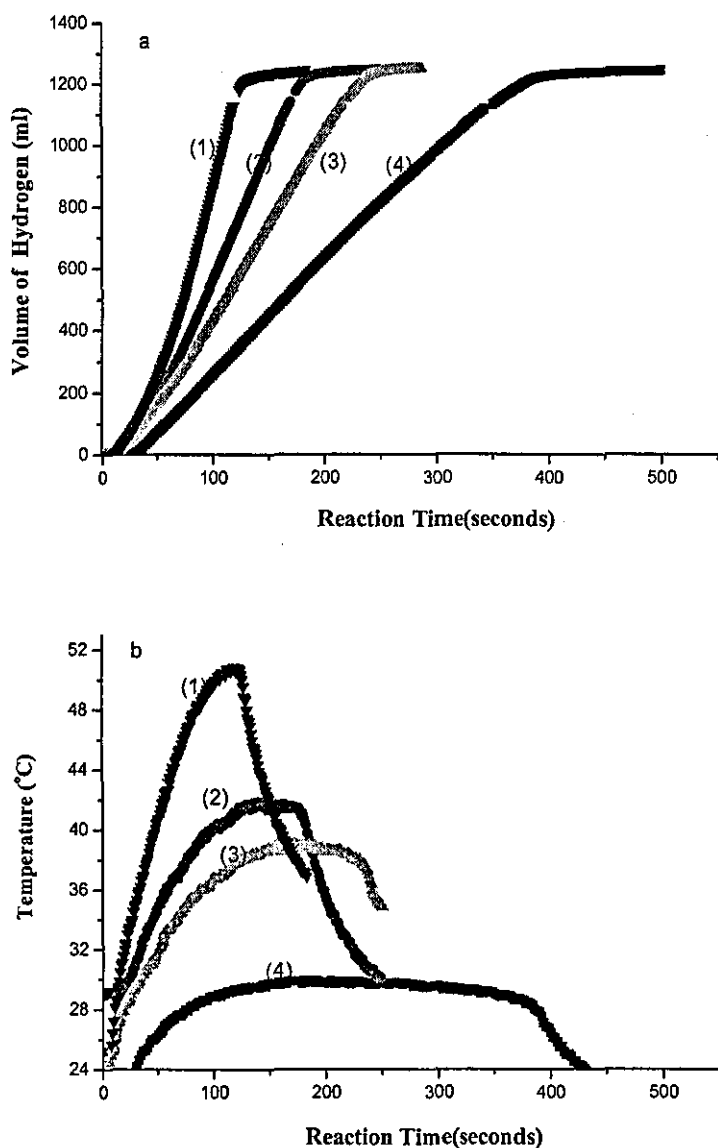
Figure 6.27 Hydrogen generation from the hydrolysis of NaBH₄ at various temperatures. The initial molality of NaBH₄ was 1.32 mol kg⁻¹. The hydrolysis was performed in 10 ml of water with 0.3 g of catalyst with a mean diameter of 0.098 mm. (a) Hydrogen production-time curves; (b) Temperature-time curves.
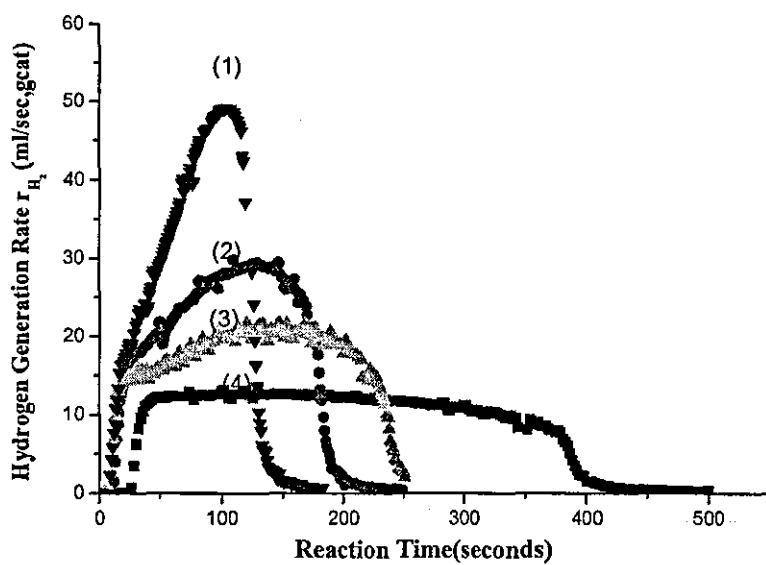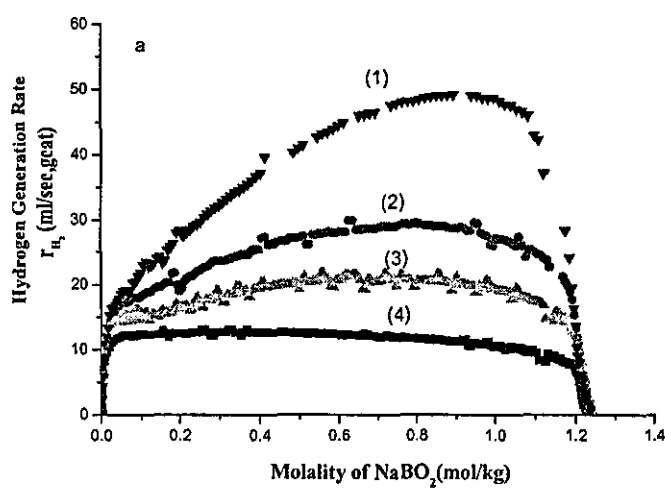
Figure 6.28 r_{H2} versus time at various temperatures by differentiation of Figure 6.27a.
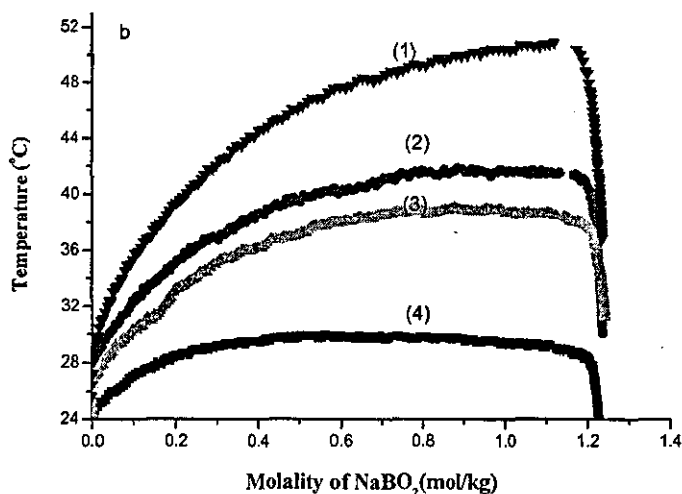

171

Figure 6.29 The rate of hydrogen generation versus NaBO₂ concentration (a) and temperature versus NaBO₂ concentration (b). They were transformed from Figure 6.28 and Figure 6.27b respectively.
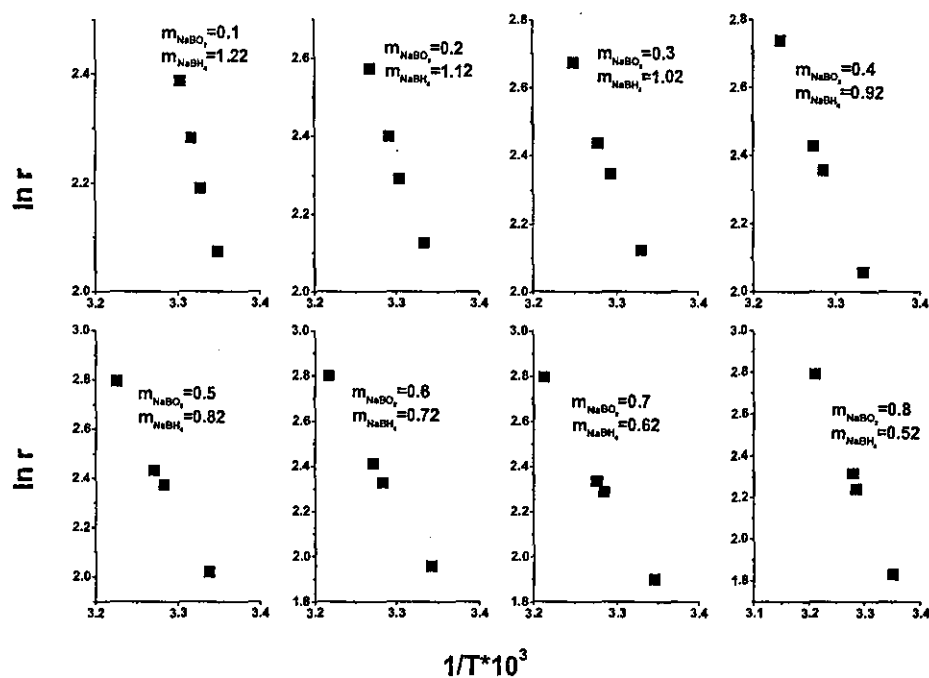
Figure 6.30 $\ln r_{H2}$ and $1/T$ derived from Figure 6.29.

172
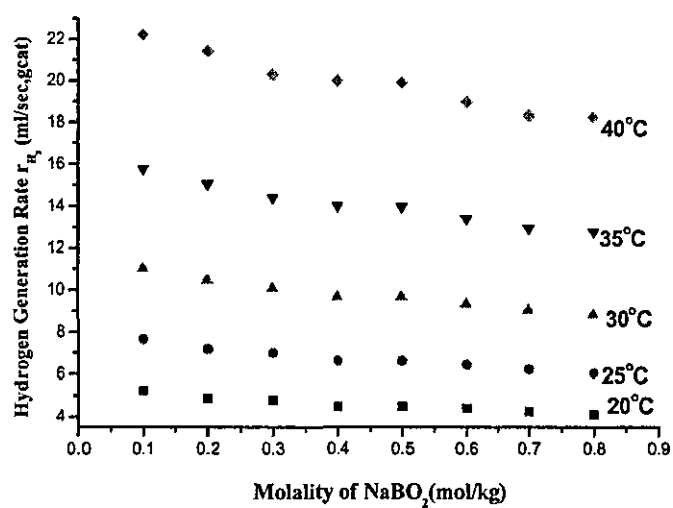
Figure 6.31 Reaction rate versus reaction extent at various temperatures when the catalyst particle size was 0.098 mm.

173
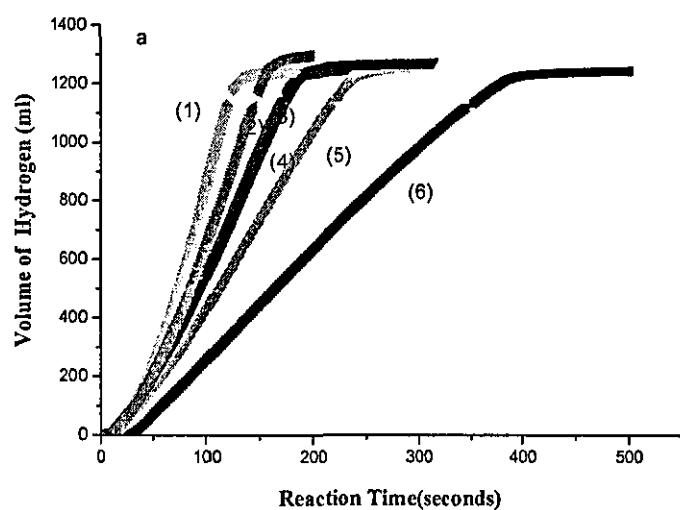
Figure 6.32 Hydrogen generation from the hydrolysis of NaBH$_4$ at various temperatures. The initial molality of NaBH$_4$ was 1.32 mol kg^{-1}. The hydrolysis was performed in 10 ml of water with 0.3 g of catalyst with a mean diameter of 0.049 mm. (a) Hydrogen production-time curves; (b) Temperature-time curves.

Figure 6.33 r_{H2} versus time at various temperatures by differentiation of Figure 6.32a

174

Figure 6.34 The rate of hydrogen generation versus NaBO₂ concentration (a) and temperature versus NaBO₂ concentration (b). They were transformed from Figure 6.33 and Figure 6.32b respectively.
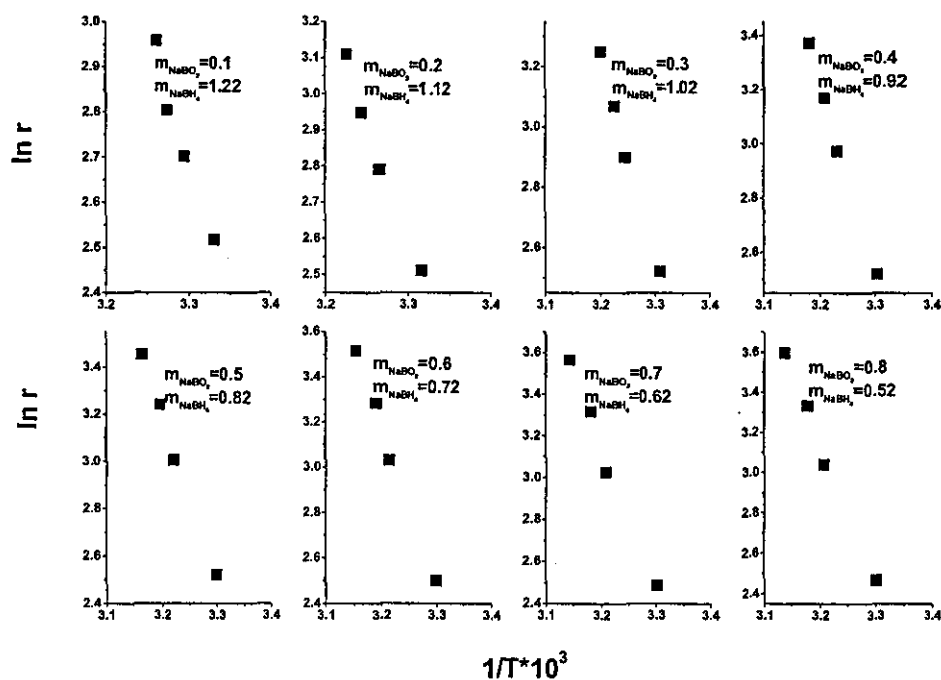
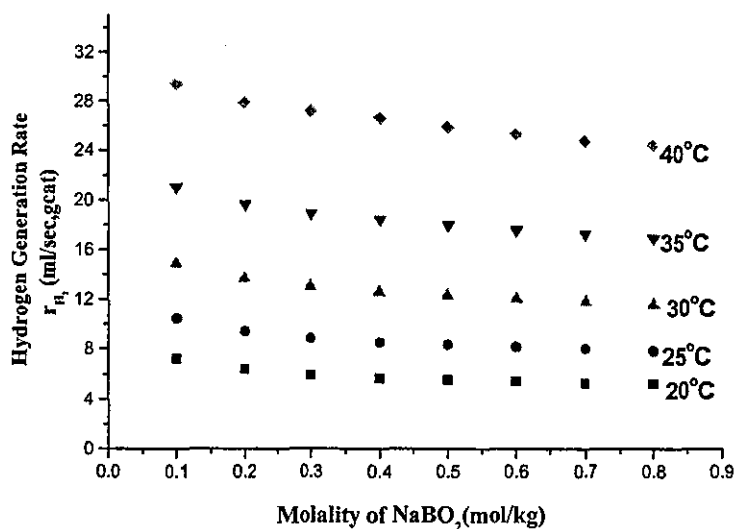**Figure 6.35** $\ln r_{H2}$ and 1/T derived from Figure 6.34.

Figure 6.36 Reaction rate versus reaction extent at various temperatures when the catalyst particle size was 0.049 mm.

Figure 6.37 Hydrogen generation from the hydrolysis of NaBH₄ at various temperatures. The initial molality of NaBH₄ was 1.32 mol kg⁻¹. The hydrolysis was performed in 10 ml of water with 0.3 g of catalyst with a mean diameter of 0.029 mm. (a) Hydrogen production-time curves; (b) Temperature-time curves.

Figure 6.38 r_{H2} versus time at various temperatures by differentiation of Figure 6.37a

Figure 6.39 The rate of hydrogen generation versus $NaBO_2$ concentration (a) and temperature versus $NaBO_2$ concentration (b). They were transformed from Figure 6.38 and Figure 6.37b respectively.

Figure 6.40 $\ln r_{H2}$ and $1/T$ derived from Figure 6.39.

179

Figure 6.41 Reaction rate versus reaction extent at various temperatures when the catalyst particle size was 0.029 mm.
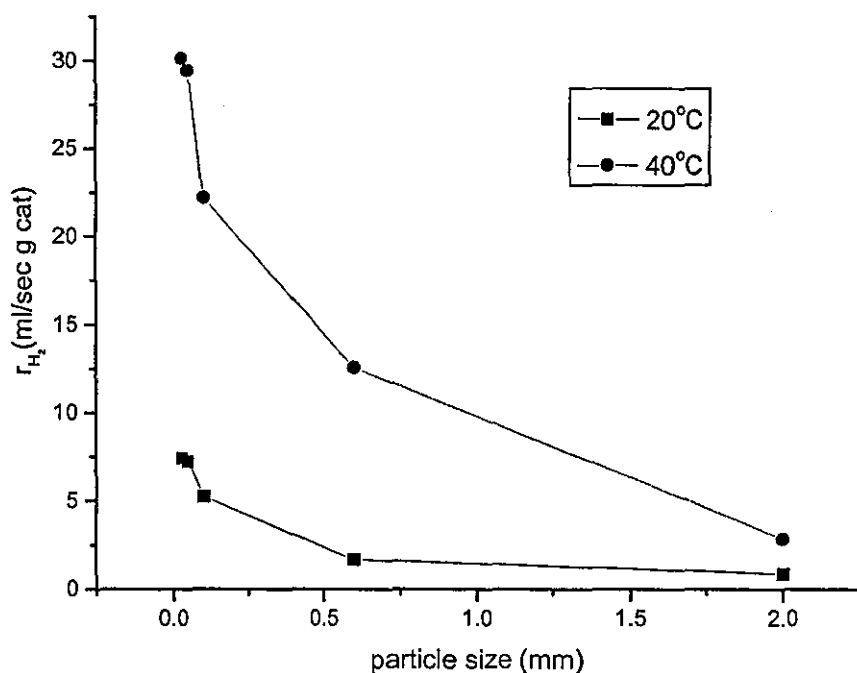
Figure 6.42 Comparison of the reaction rate at various temperatures for different catalyst particle sizes.

The reaction rates at various reaction temperatures for different particle sizes are compared in Figure 6.42. The reaction rates increased significantly with a decrease in

180

catalyst particle size. This suggests that the hydrolysis of NaBH$_4$ in the presence of a carbon supported ruthenium catalyst has a strong internal diffusion limitation when the catalyst particles are large. When the catalyst particle size is reduced to around 0.049 mm, the internal diffusion limitation is removed. This trend did not change with reaction temperature, as shown in Figure 6.42.

This indicates that the limiting effects of internal diffusion can be removed by using a catalyst particle size of less than 0.049 mm for the hydrolysis of NaBH$_4$ over a carbon supported ruthenium catalyst. Therefore, in the study of intrinsic kinetics that is reported in the next chapters, 0.049 mm catalyst particles and a stirring rate of 650 rpm are used.

6.4 Heat transfer effect

When the reaction is so fast that the heat released in the pellet cannot be removed rapidly enough to keep the pellet close to the temperature of the fluid, then non-isothermal effects intrude. In such a situation two different kinds of temperature effects may be encountered. One is within-particle ΔT. The other is film ΔT, in which the whole pellet may be hotter than the surrounding fluid.

Since fine particles are used in the study of intrinsic rate expressions, within particle ΔT can be ignored. The film ΔT can be calculated using equation (6.1) [1].

$$\Delta T_{film} = \frac{L(-r_{A,obs}''')(-\Delta H_r)}{h} \qquad (6.1)$$

Where ΔH_r is the reaction enthalpy change, L is the particle diameter, $-r_{A,obs}'''$ is the reaction rate per unit volume of catalyst, and h is the heat transfer coefficient of the surrounding fluid.

The heat transfer coefficient can be calculated using the following correlation [2].

$$Nu = 2 + 0.6\,\mathrm{Re}^{1/2}\,\mathrm{Pr}^{1/3} \qquad (6.2)$$

Where the dimensionless variables are defined as follows:

$$Nu = \frac{hd_p}{k_t}$$

$$Re = \frac{U\rho d_p}{\mu}$$

$$Pr = \frac{\mu C_p}{k_t}$$

where ρ = fluid density, kg/m^3

d_p = diameter of pellet, m

k_t = thermal conductivity, J/K.m.s

U = free-stream velocity, m/s

μ = fluid viscosity, Pa.s

Substituting the values of the above parameters for water, h can be obtained. By defining reaction rate and particle radius, the film temperature difference ΔT_f can be calculated. The calculation is shown in Figure 6.43 for different reaction rates and particle sizes.

As shown in Figure 6.43, ΔT_f depends on both the fluid flow rate around the catalyst particles and the reaction rate of NaBH$_4$. It increases with reaction rate and decreases with flow rate (stirring rate). Since the reaction rate is usually less than 2 g of NaBH$_4$ s^{-1} m^{-3}, the particle temperature varies from the fluid temperature by less than 1°C, even with no stirring. Thus it can be assumed that the film temperature is not significant.
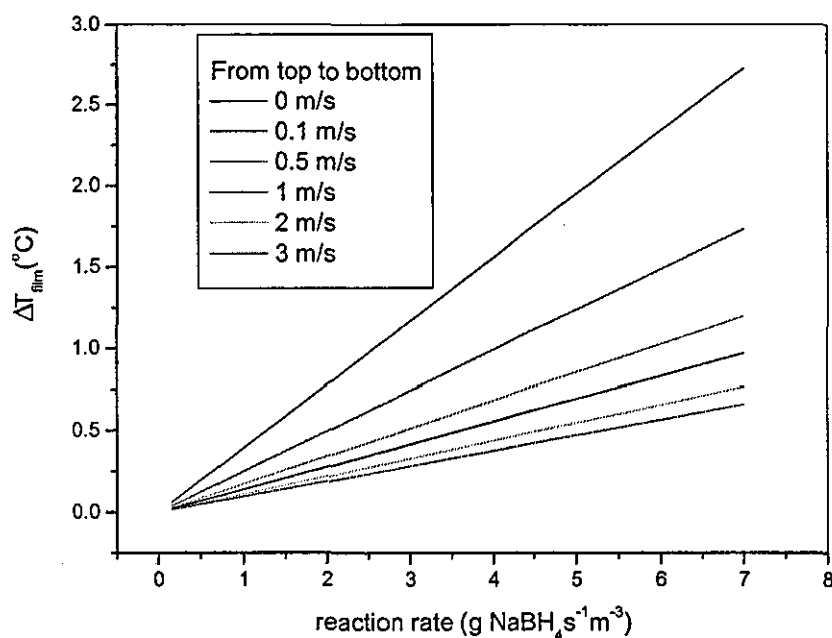
Figure 6.43 Dependence of the particle temperature on reaction rate and flow rate.

6.5 Conclusions

This chapter detailed the preparatory work that was necessary before beginning to investigate the intrinsic kinetics of $NaBH_4$ hydrolysis over a ruthenium catalyst, i.e. to negate the effects of heat and mass diffusion on the intrinsic kinetics. Three aspects of work have been studied: external diffusion, internal diffusion and heat effect. Through the work, the following conclusions have been drawn:

- When the stirring rate is greater than 650 rpm, the effects of external diffusion can be discounted.

- When the catalyst particle size is less than 0.049 mm, the effects of internal diffusion can be discounted.

- The film temperature difference and temperature gradients within particles are small enough to be ignored.

6.6 References

1. Levenspiel, O., *Chemical Reaction Engineering*. 1999, New York: John Wiley & Sons. 392-393.

2. Fogler, H.S., *Elements of Chemical Reaction Engineering*. 2006, New Jersey: Upper Saddle River: Pearson Education Inc. 774-775.

Chapter 7

The Effect of $NaBH_4$ and $NaBO_2$ on Intrinsic Kinetics

7.1 Introduction

In Chapter 6, studies were performed in order to determine the conditions that are required to allow the effects of mass and heat transfer on the intrinsic kinetics of the $NaBH_4$ reaction to be considered negligible. In this and subsequent chapters, the intrinsic kinetics are studied under these conditions. The ultimate objective is to obtain an intrinsic rate expression without diffusion limitations. The effects of $NaBH_4$ and $NaBO_2$ concentration are studied in this chapter and the effect of NaOH concentration is studied in the next chapter.

With the hydrolysis of $NaBH_4$, the concentration of $NaBH_4$ decreases and the concentration of $NaBO_2$ increases with time. Since $NaBO_2$ is a base it may affect the reaction rate of $NaBH_4$, as it is known that NaOH is used as a stabiliser for $NaBH_4$ in aqueous solution. Therefore, it is necessary to investigate both the effects of $NaBH_4$ and $NaBO_2$ concentration on the rate of the hydrolysis reaction.

7.2 Experimental Results

In order to investigate the effect of $NaBH_4$ concentration on the reaction rate, the temperature and $NaBO_2$ concentration must be fixed while the $NaBH_4$ concentration is varied. In order to investigate the effect of $NaBO_2$ on the reaction rate, the temperature and $NaBH_4$ concentration must be fixed while the $NaBO_2$ concentration is varied. The two factors can be investigated by designing one set of experiments as follows:

For each initial $NaBH_4$ concentration, several experiments are performed, each of which has a different initial temperature. Through this group of experiments, isothermal rate data can be derived for any $NaBO_2$ concentration as shown in last chapter. However, within this group of experiments, the concentrations of $NaBO_2$ and $NaBH_4$ depend on each other. They cannot vary independently since the initial $NaBH_4$ concentration is the same. In

order to vary $NaBH_4$ or $NaBO_2$ concentration, several groups of such experiments need to be conducted, with each group having a different initial $NaBH_4$ concentration. Within each group, the initial $NaBH_4$ concentration is the same but with a different initial reaction temperature.

Therefore, at a fixed $NaBO_2$ concentration the corresponding $NaBH_4$ concentration for each group is different. At a fixed $NaBH_4$ concentration the concentration of $NaBO_2$ is different.

In this work, six groups of experiments were conducted. Figures 7.1-7.24 show the six groups of hydrolysis experiments. The $V_{H2} \sim t$ was transformed to $r_{H2} \sim t$ by differentiation and to $r_{H2} \sim m_{NaBO2}$ by using equations (5.13) and (5.14). $\ln r_{H2} \sim 1/T$ was obtained by simultaneously measuring $r_{H2} \sim m_{NaBO2}$ and $T \sim m_{NaBO2}$.
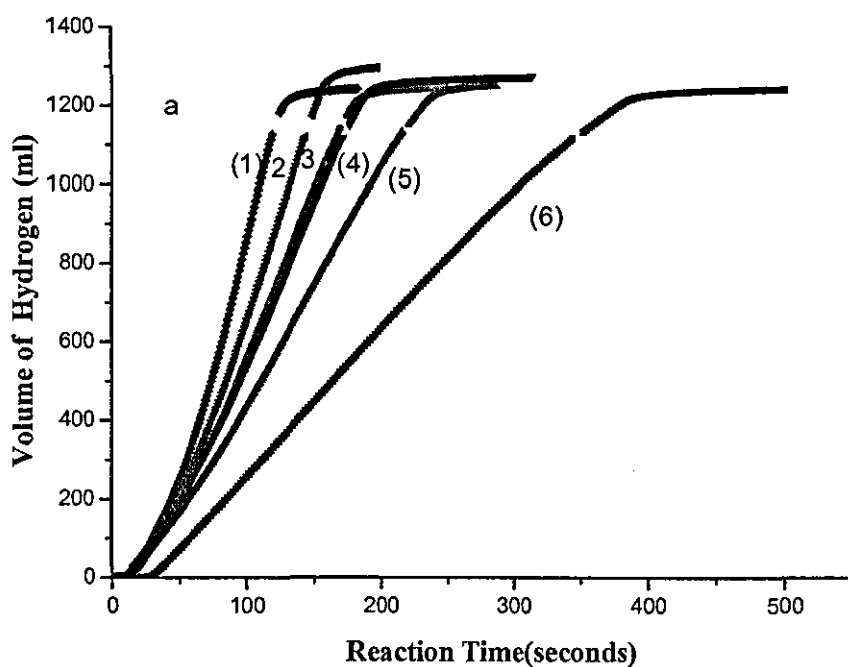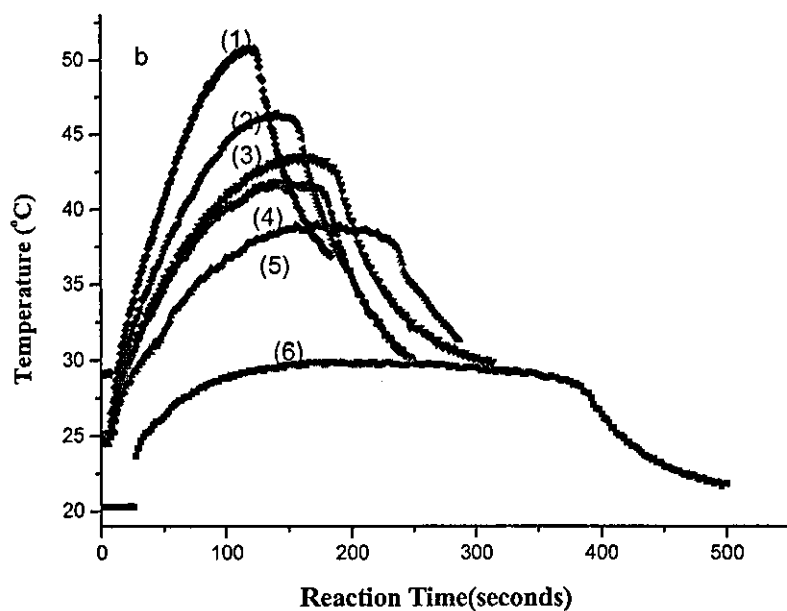
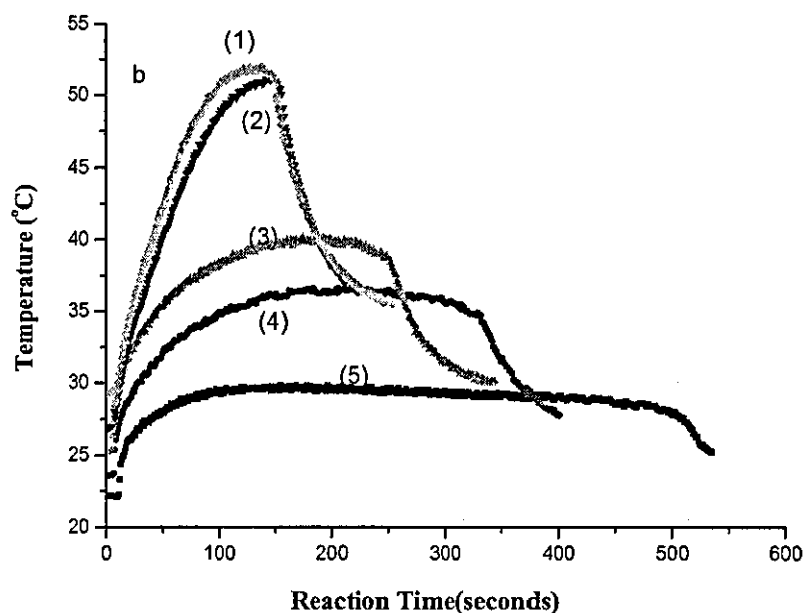**Figure 7.1** Hydrogen generation from the hydrolysis of $NaBH_4$ at various temperatures. The initial molality of NaBH4 was 1.32 mol kg^{-1}. The hydrolysis was performed in 10 ml of water with 0.3 g of catalyst with an average particle size of 0.049 mm. (a) Hydrogen production-time curves; (b) Temperature-time curves.
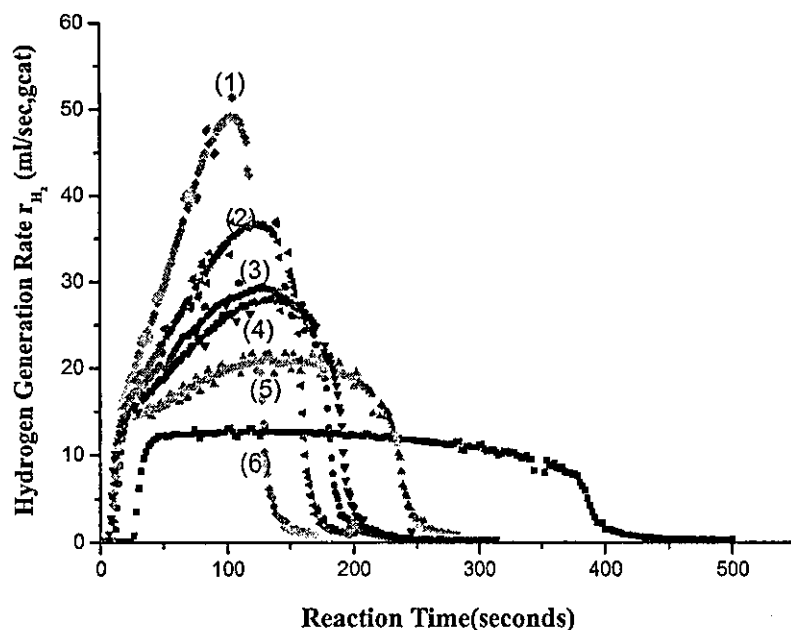
Figure 7.2 r_{H2} versus time from the hydrolysis of $NaBH_4$, which was transformed by differentiation of the curves in Figure 7.1a. Initial molality of $NaBH_4$ was 1.32 mol kg^{-1}.
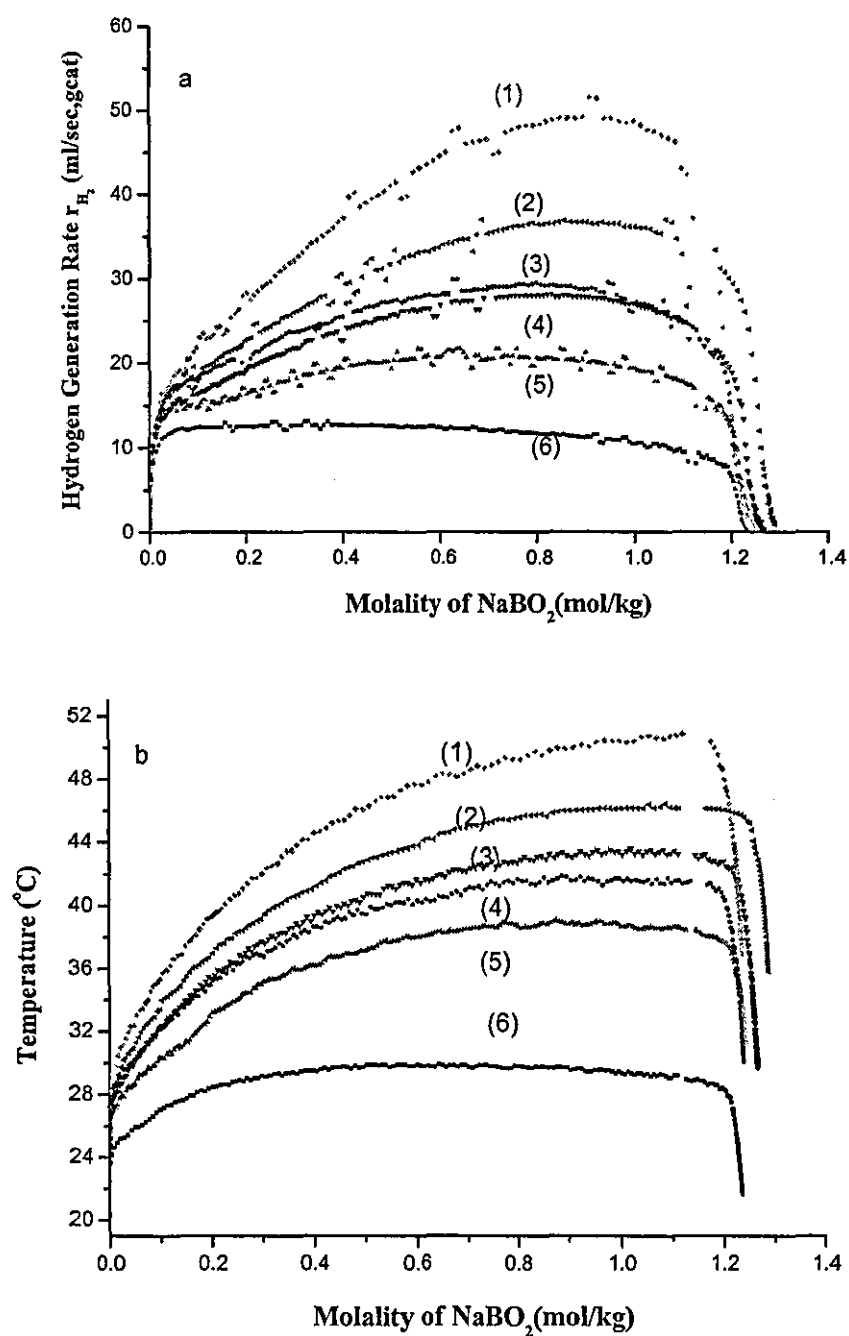
Figure 7.3 The rate of hydrogen generation versus $NaBO_2$ concentration (a) and temperature versus $NaBO_2$ concentration (b). They were transformed from Figure 7.2 and Figure 7.1b respectively. Initial molality of $NaBH_4$ was 1.32 mol kg^{-1}.
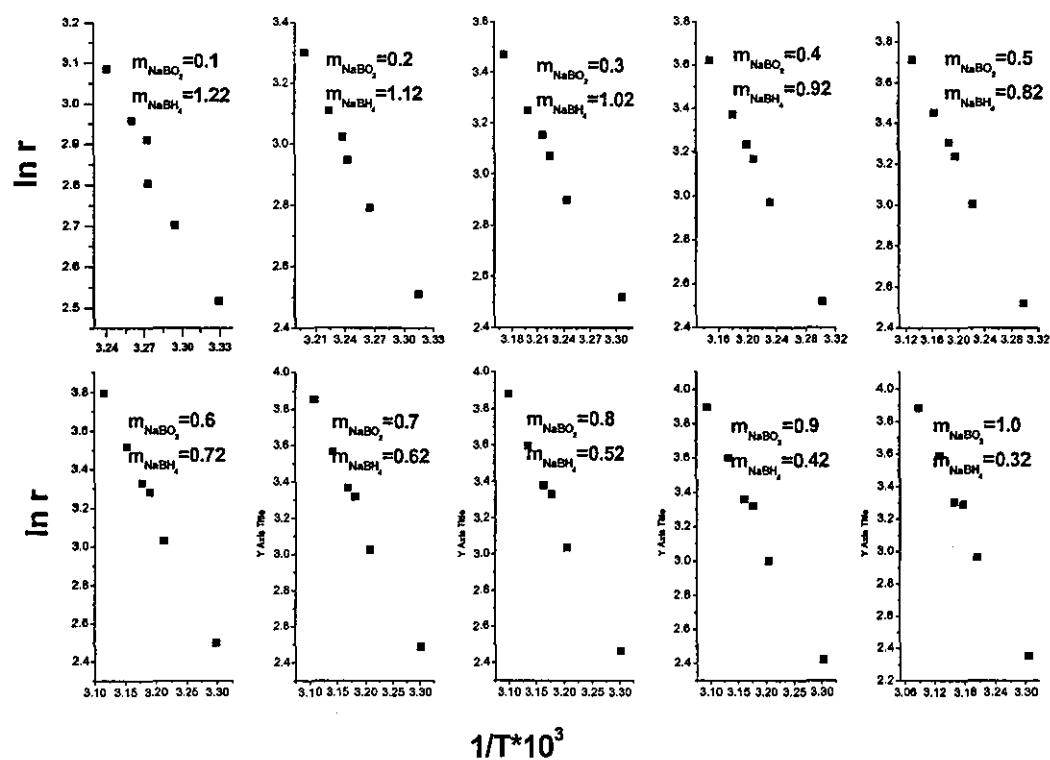
Figure 7.4 $\ln r_{H2}$ versus 1/T derived from Figure 7.3. Initial $NaBH_4$ molality was 1.32 mol kg^{-1}.
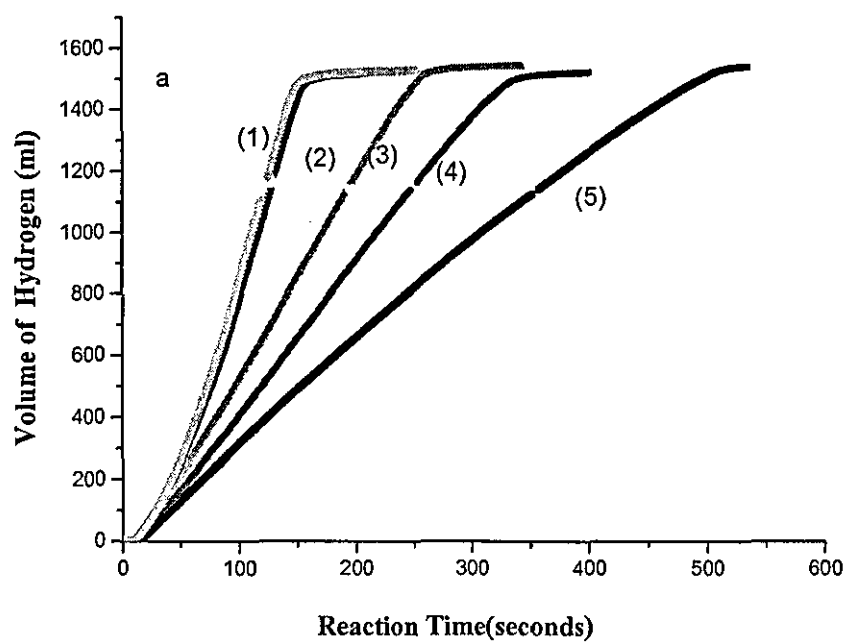
Figure 7.5 Hydrogen generation from the hydrolysis of $NaBH_4$ at various temperatures. The initial molality of NaBH4 was 1.59 mol kg^{-1}. The hydrolysis was performed in 10 ml of water with 0.3 g of catalyst with an average particle size of 0.049 mm. (a) Hydrogen production-time curves; (b) Temperature-time curves.
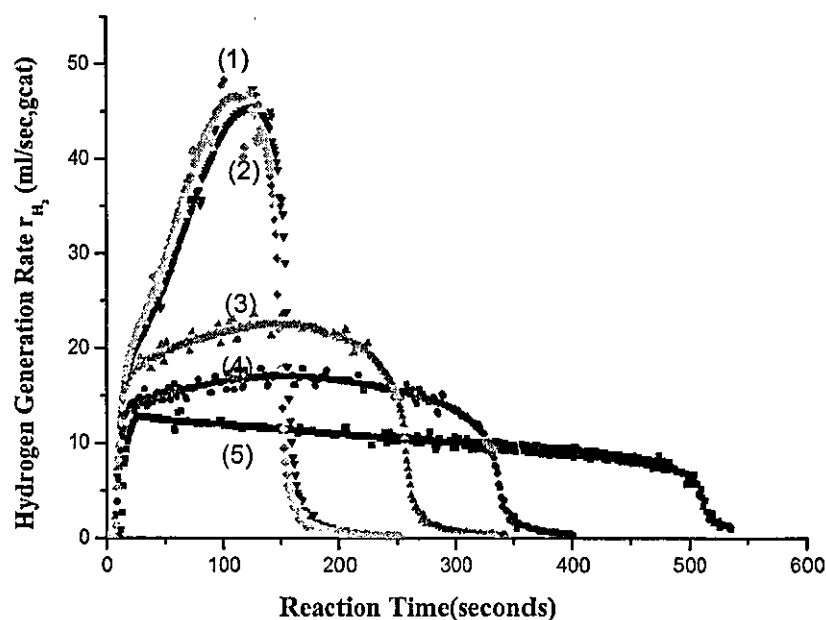

Figure 7.6 r_{H2} from the hydrolysis of $NaBH_4$, which was transformed from Figure 7.5a by differentiation. The initial molality of NaBH4 was 1.59 mol kg^{-1}.
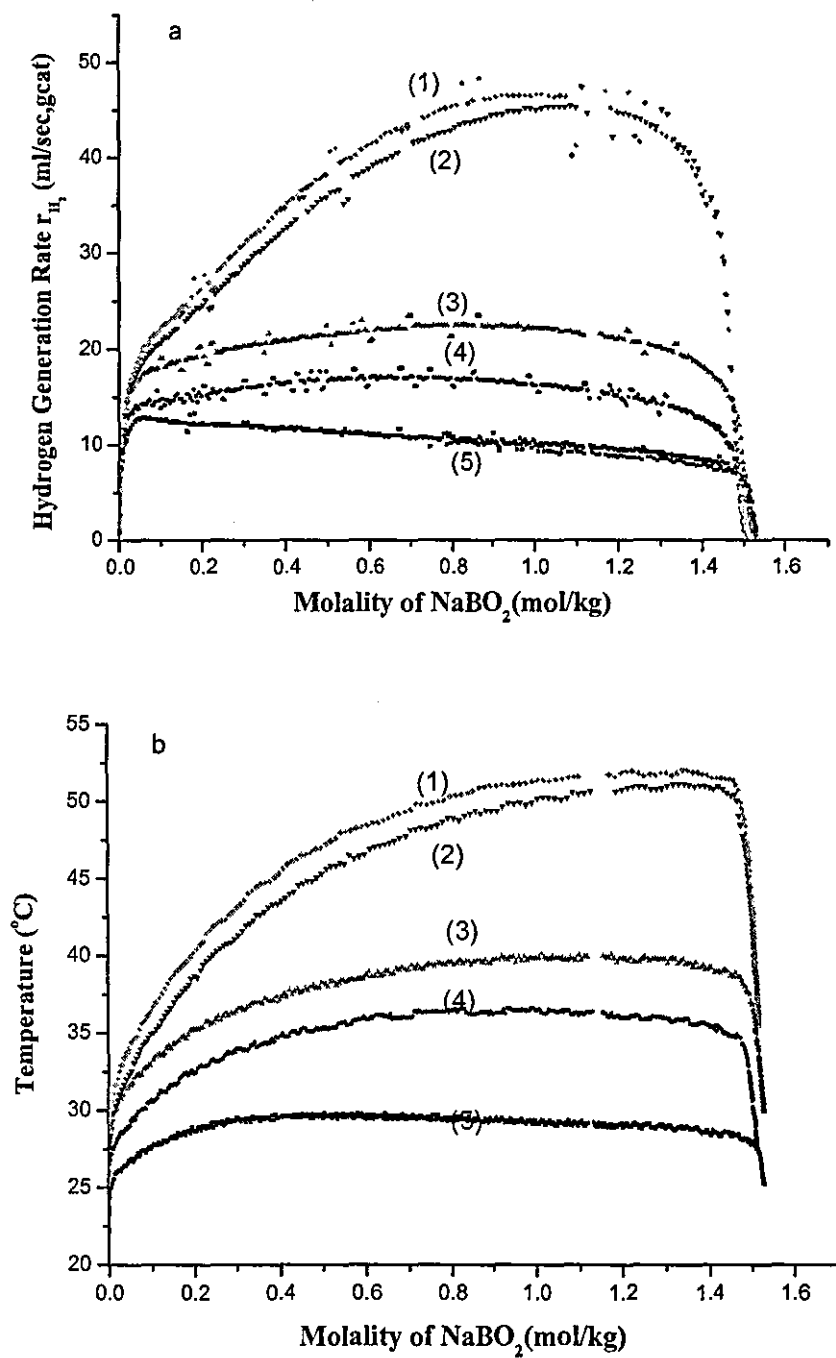
189

Figure 7.7 The rate of hydrogen generation (a) and reaction temperature (b) with NaBO$_2$ molality. They were transformed from Figure 7.6 and Figure 7.5b respectively. The initial molality of NaBH$_4$ was 1.59 mol kg^{-1}.
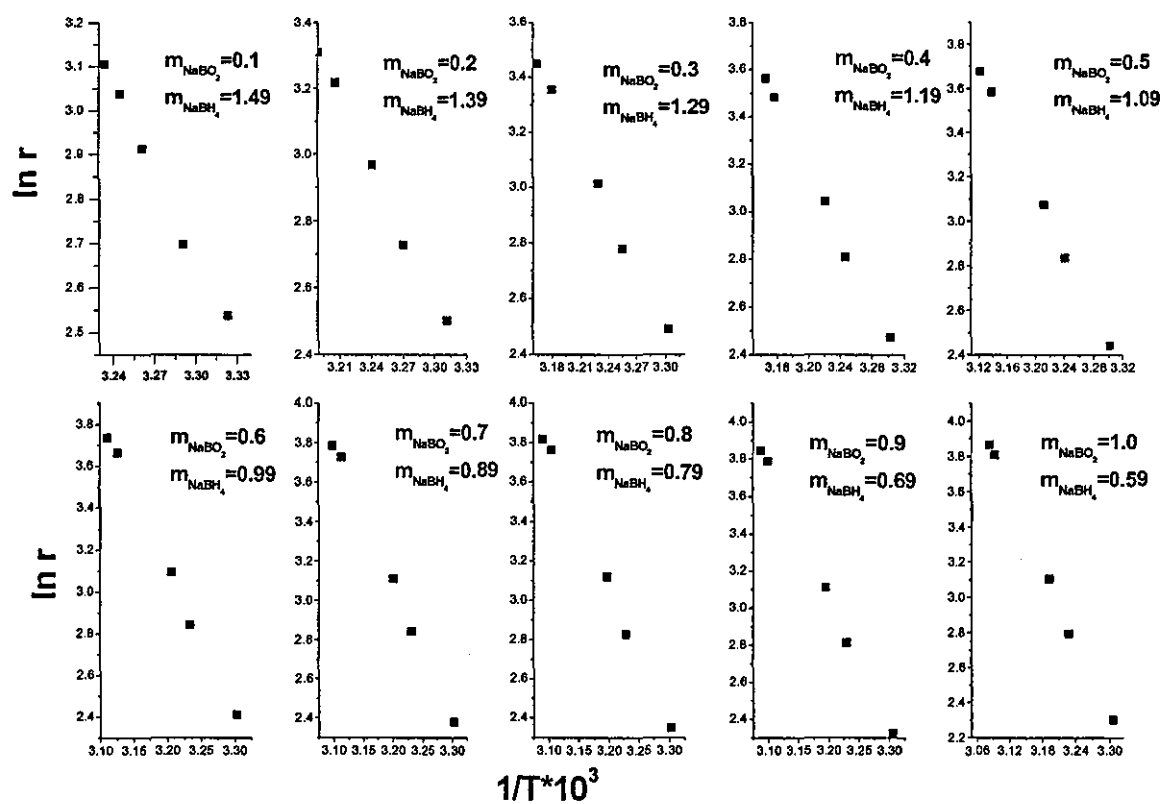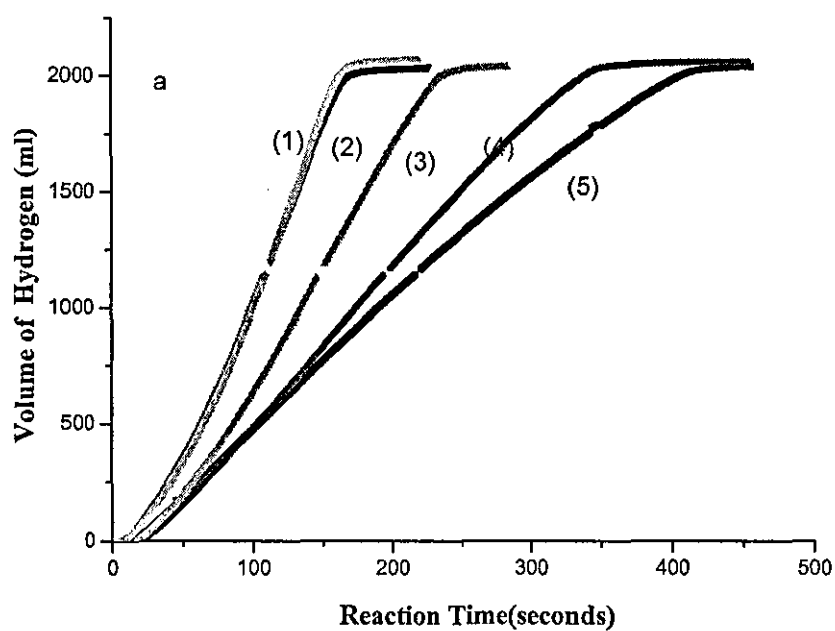
Figure 7.8 $\ln r_{H2}$ versus $1/T$ derived from Figure 7.7. Initial $NaBH_4$ molality was 1.59 mol kg^{-1}
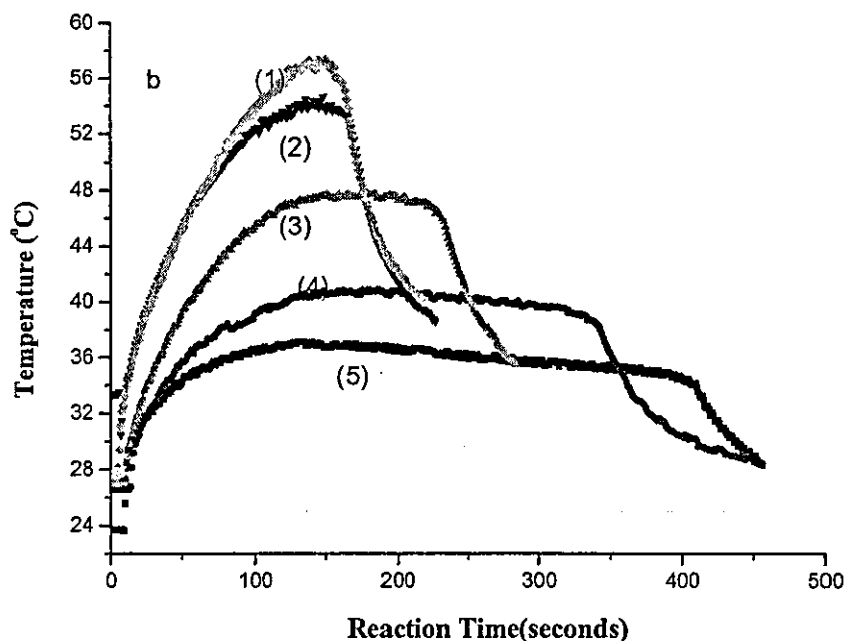
Figure 7.9 Hydrogen generation from the hydrolysis of $NaBH_4$ at various temperatures. The initial molality of NaBH4 was 2.11 mol kg^{-1}. The hydrolysis was performed in 10 ml of water with 0.3 g of catalyst of an average particle size of 0.049 mm. (a) Hydrogen production-time curves; (b) Temperature-time curves.
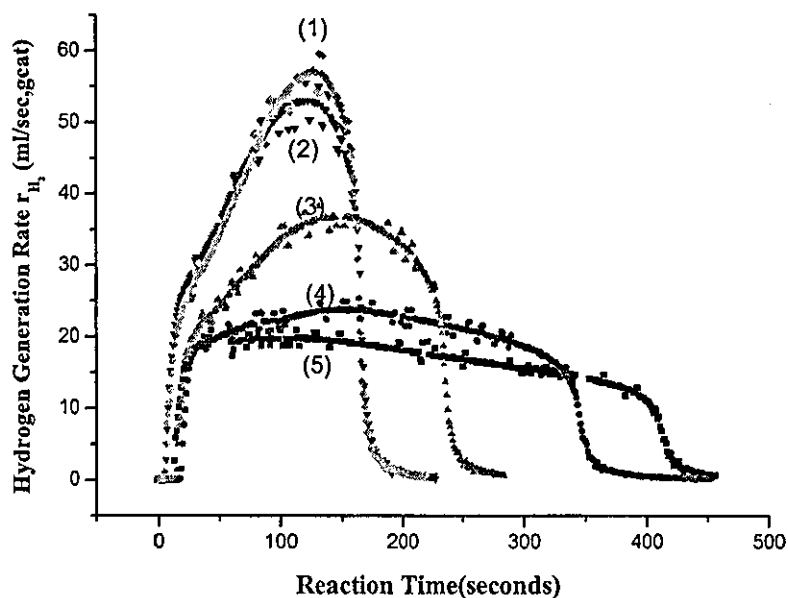

Figure 7.10 r_{H2} from the hydrolysis of $NaBH_4$, which was transformed from Figure 7.9a. The initial molality of NaBH4 was 2.11 mol kg^{-1}.
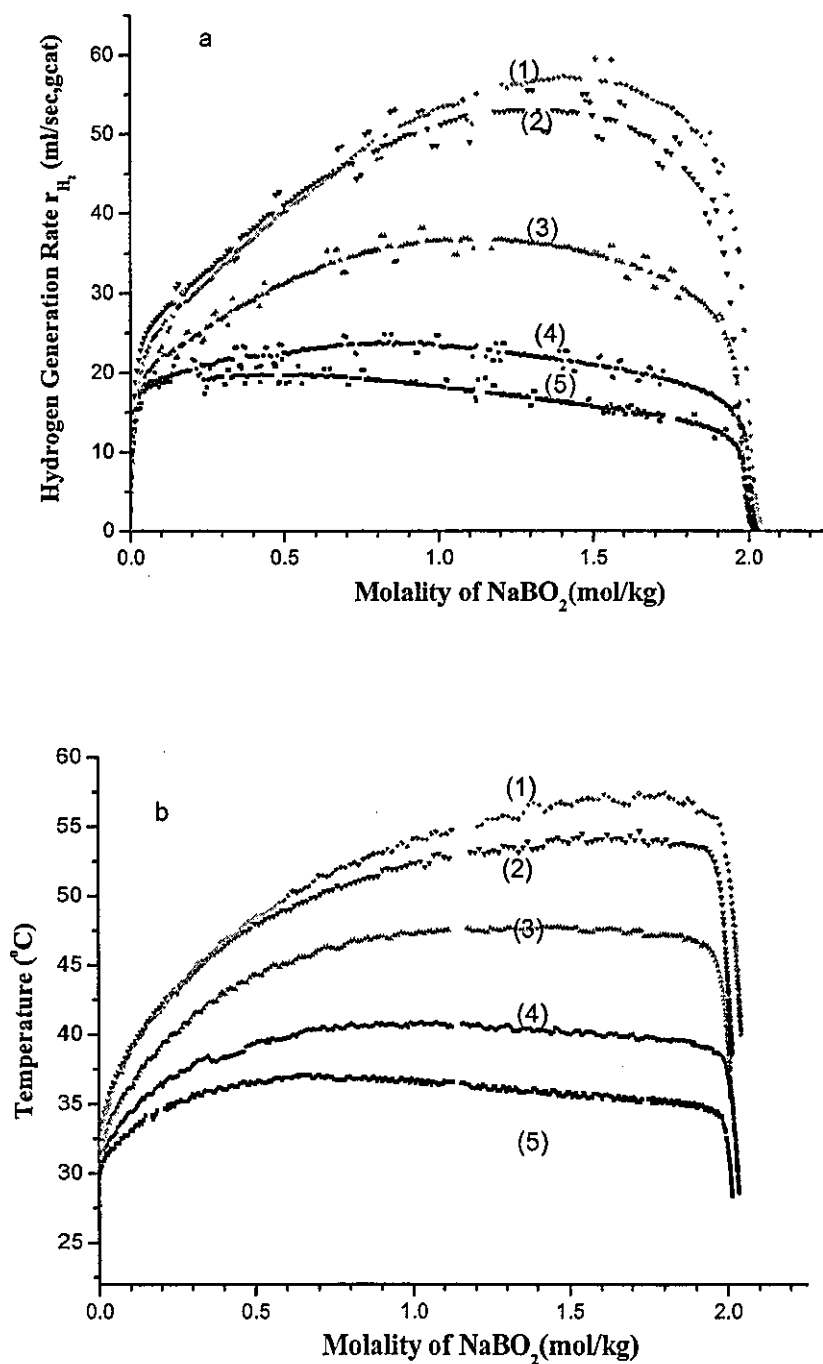
Figure 7.11 The rate of hydrogen generation (a) and reaction temperature (b) versus $NaBO_2$ molality. They were transformed from Figure 7.10 and Figure 7.9b respectively. The initial molality of $NaBH_4$ is 2.11 mol kg^{-1}.
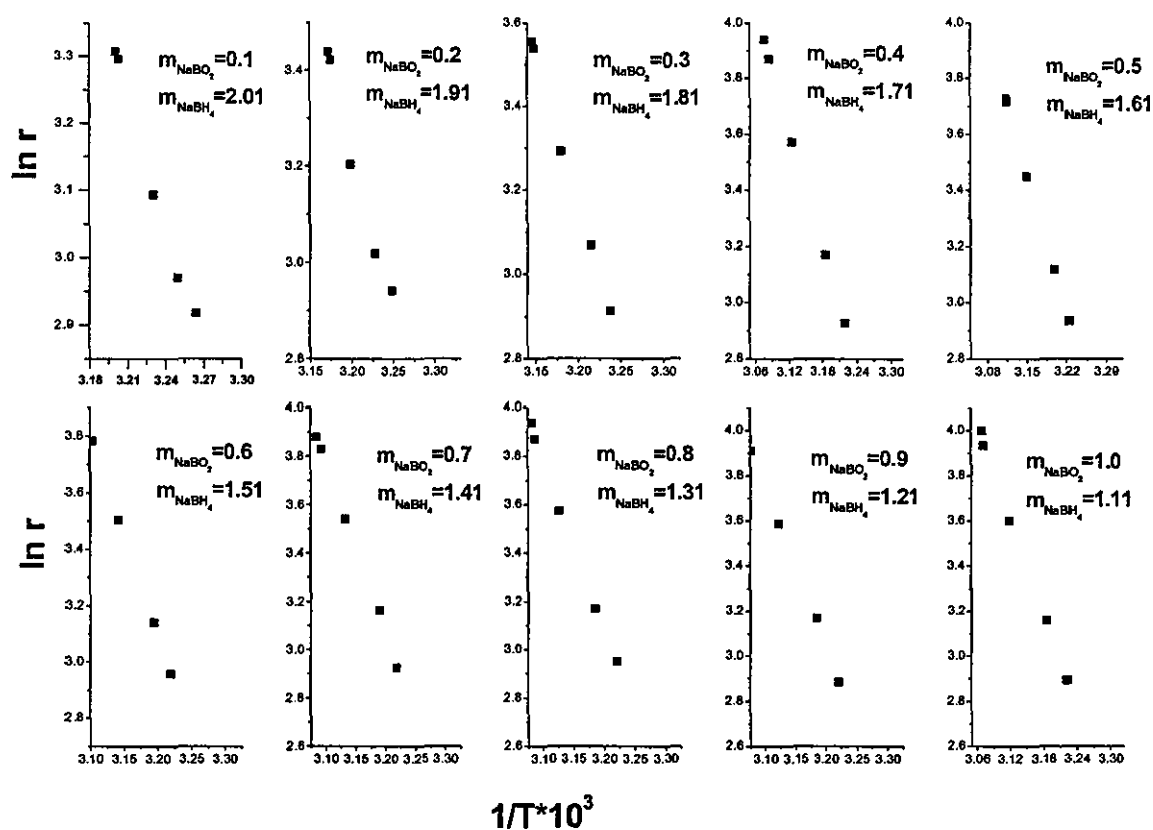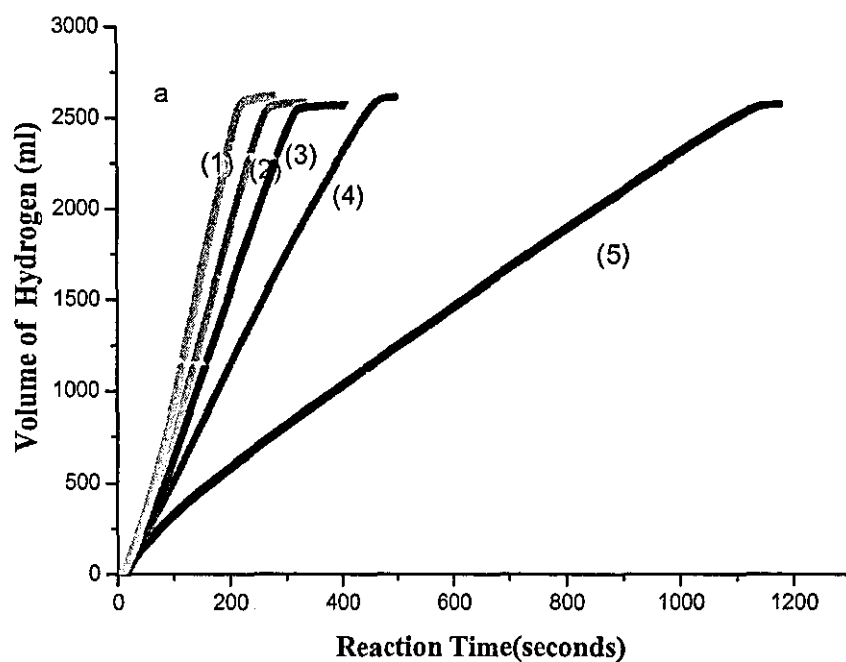
Figure 7.12 $\ln r_{H2}$ versus $1/T$ derived from Figure 7.11. Initial $NaBH_4$ molality was 2.11 mol kg^{-1}.

194

Figure 7.13 Hydrogen generation from the hydrolysis of $NaBH_4$ at various temperatures. The initial molality of NaBH4 was 2.64 mol kg^{-1}. The hydrolysis was performed in 10 ml of water with 0.3g of catalyst of an average particle size of 0.049 mm. (a) Hydrogen production-time curves; (b) Temperature-time curves.

Figure 7.14 The rate of hydrogen generation from the hydrolysis of $NaBH_4$, which was transformed from Figure 7.13a. Initial molality of NaBH4 was 2.64 mol kg^{-1}.

195

Figure 7.15 The rate of hydrogen generation (a) and reaction temperature (b) versus NaBO$_2$ molality. They were transformed from Figure 7.14 and Figure 7.13 b respectively. Initial molality of NaBH$_4$ is 2.64 mol kg^{-1}.

Figure 7.16 $\ln r_{H2}$ versus $1/T$ derived from Figure 7.15. Initial $NaBH_4$ molality was 2.64 mol kg^{-1}.
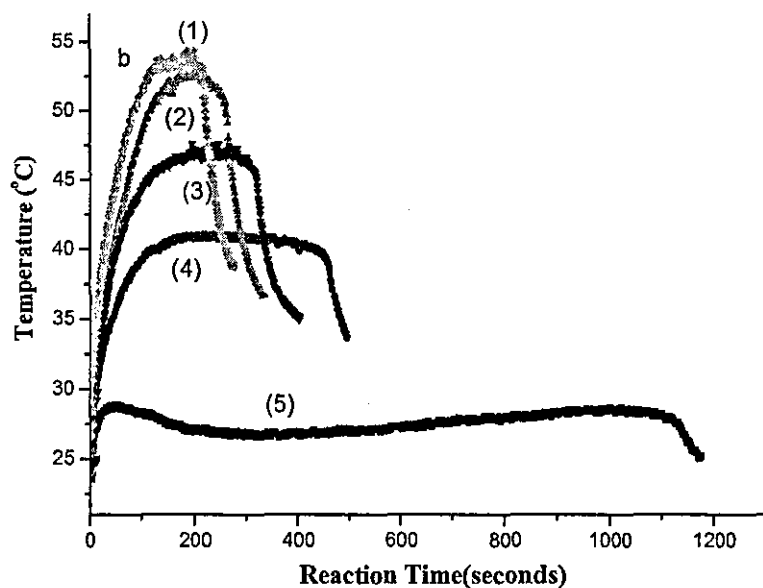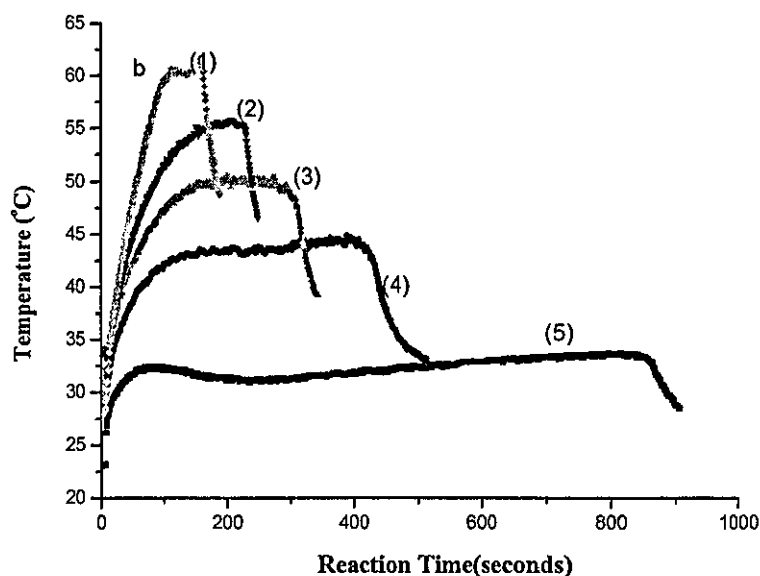
Figure 7.17 Hydrogen generation from the hydrolysis of $NaBH_4$ at various temperatures. The initial molality of NaBH4 was 3.17 mol kg^{-1}. The hydrolysis was performed in 10 ml of water with 0.3 g of catalyst of an average particle size of 0.049 mm. (a) Hydrogen production-time curves; (b) Temperature - time curves.
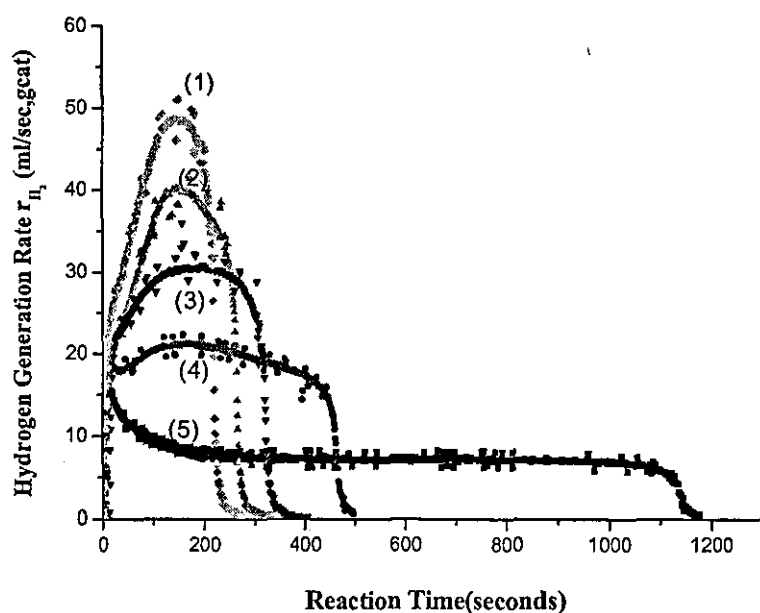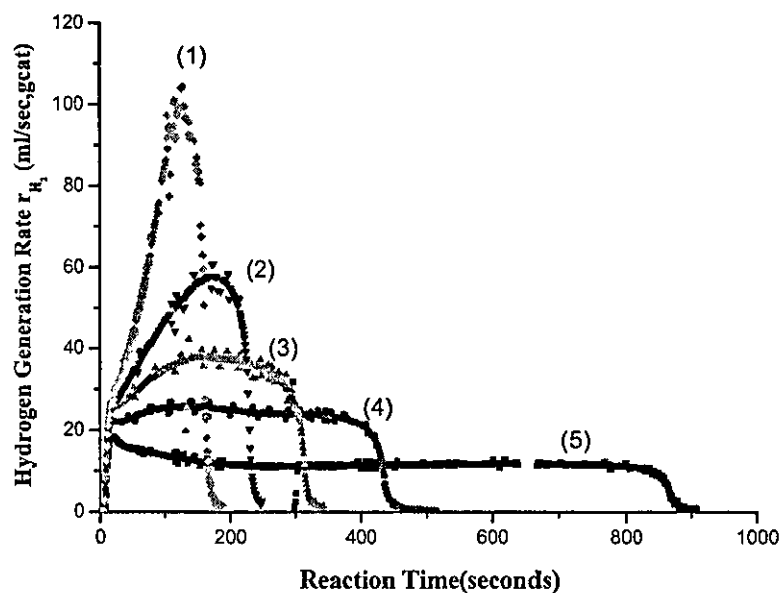

Figure 7.18 The rate of Hydrogen generation from the hydrolysis of $NaBH_4$, which was transformed from Figure 7.17a by differentiation. The initial molality of $NaBH_4$ was 3.17 mol kg^{-1}.
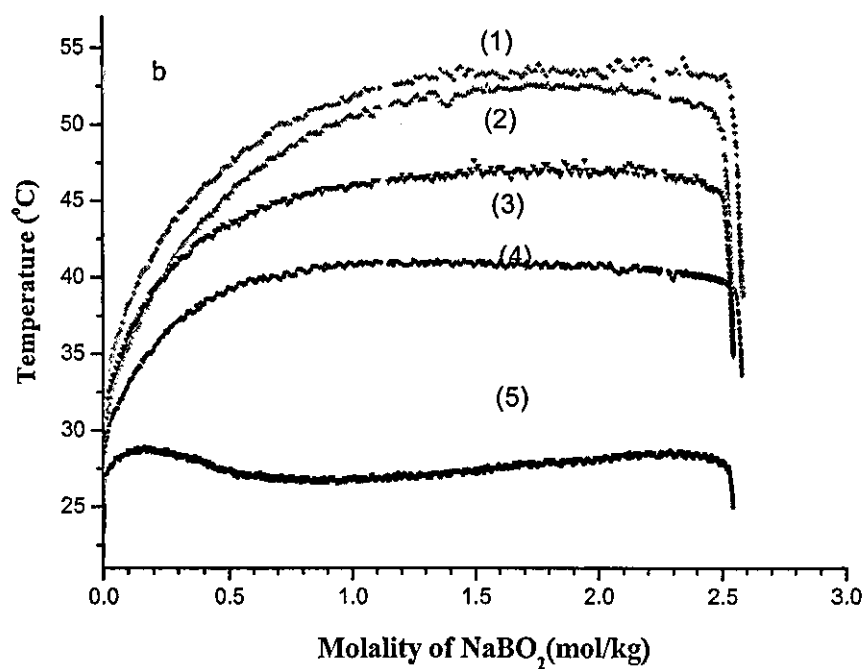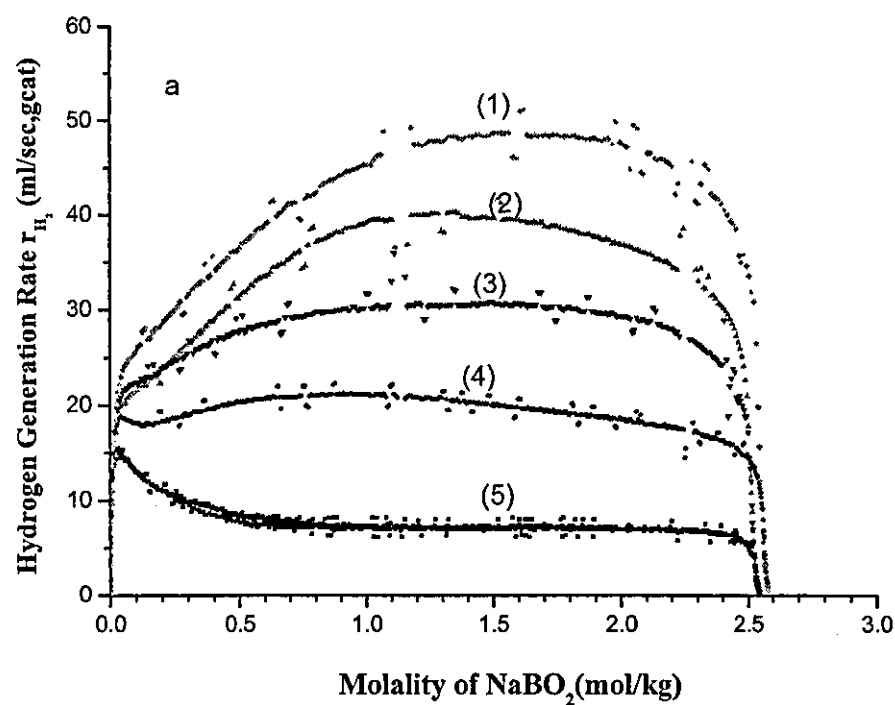
198

Figure 7.19 The rate of hydrogen generation (a) and reaction temperature (b) versus NaBO$_2$ molality. They were transformed from Figure 7.18 and Figure 7.17b respectively. Initial molality of NaBH$_4$ is 3.17 mol kg^{-1}.
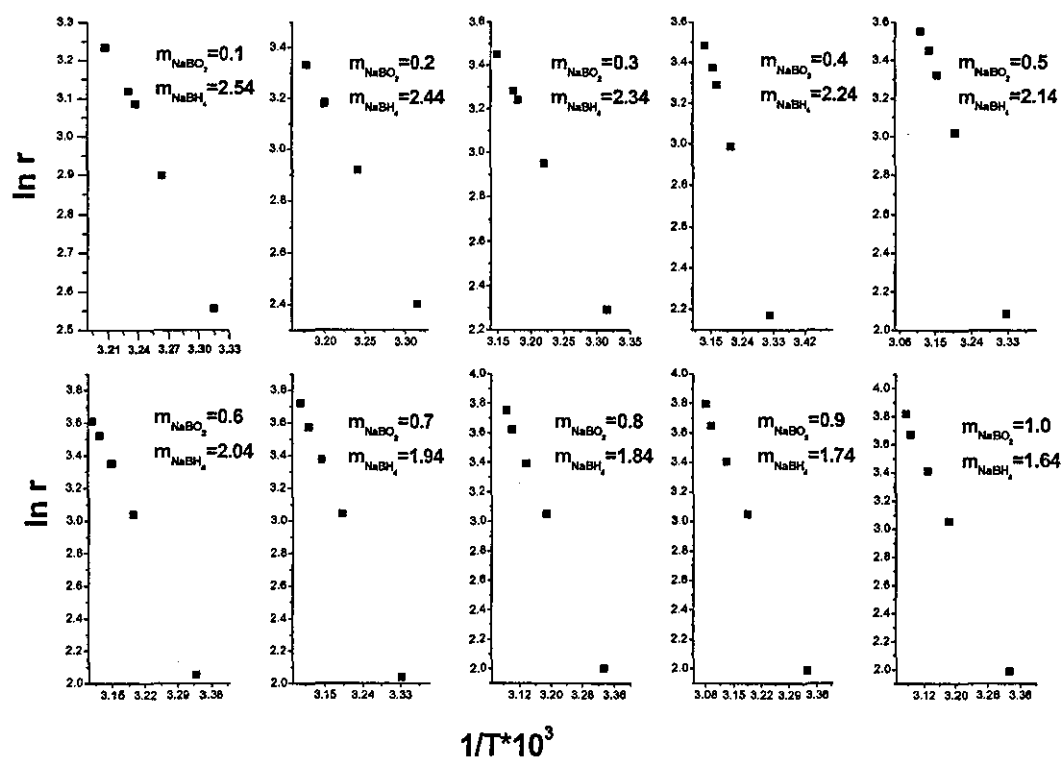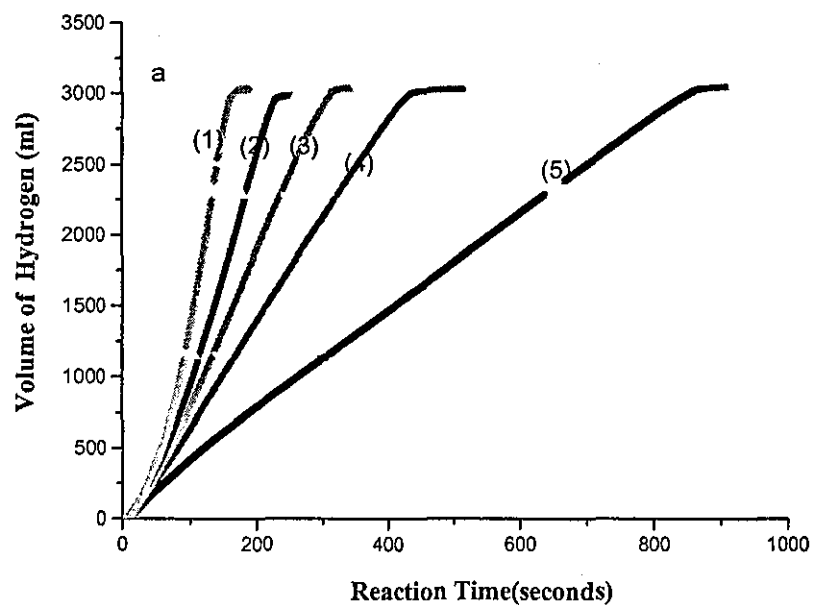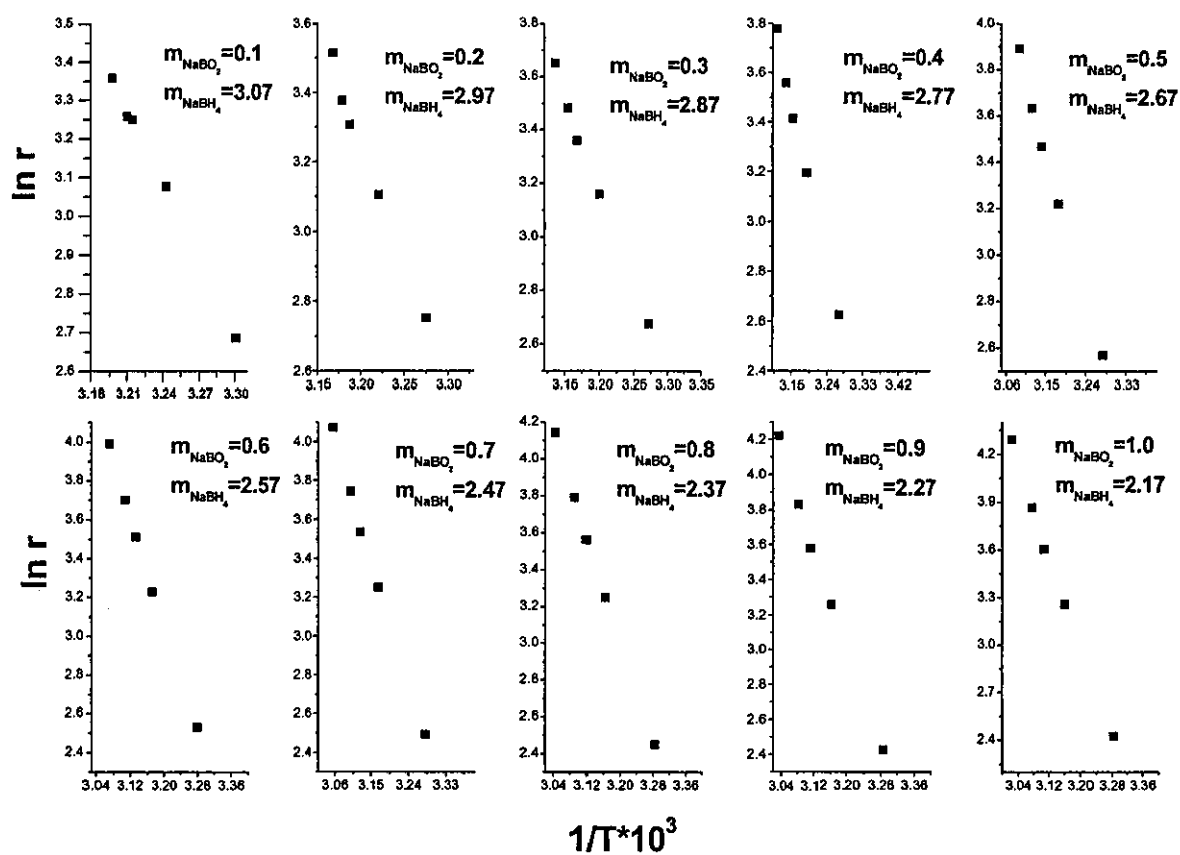
Figure 7.20 $\ln r_{H2}$ versus $1/T$ derived from Figure 7.19. Initial $NaBH_4$ molality was 3.17 mol kg^{-1}.
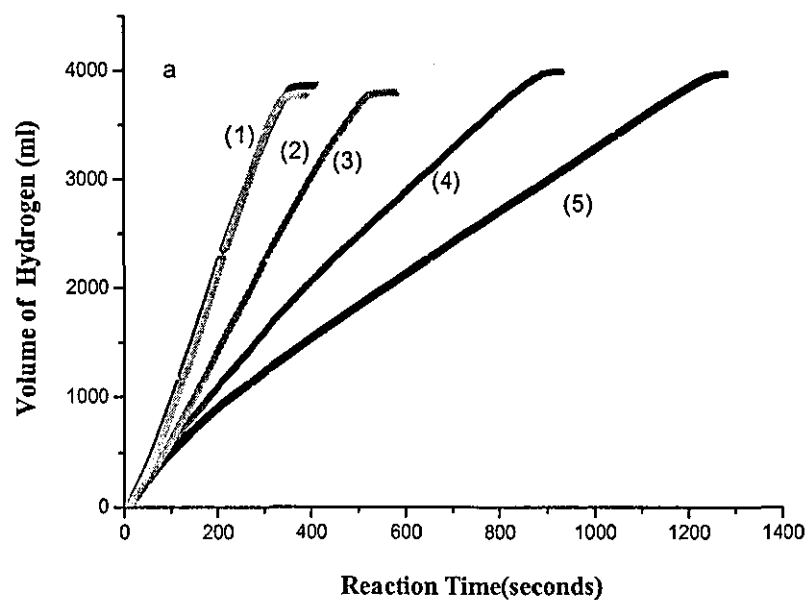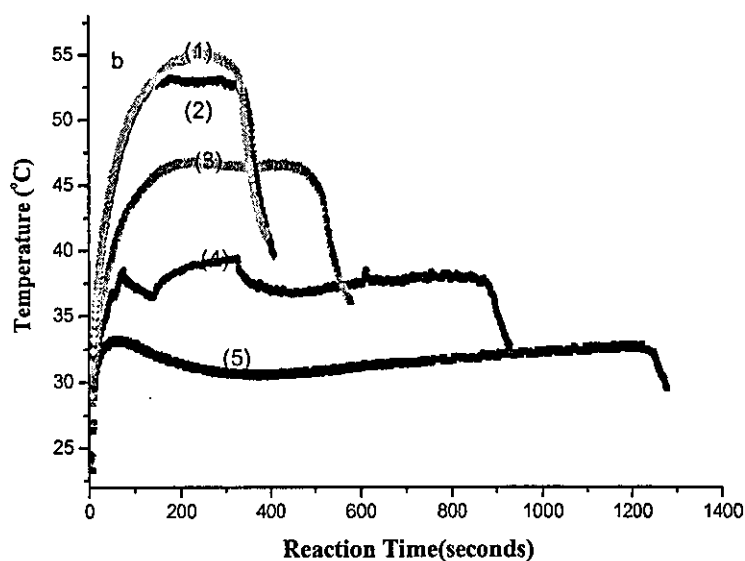
Figure 7.21 Hydrogen generation from the hydrolysis of NaBH₄ at various temperatures. The initial molality of NaBH4 was 3.97 mol kg⁻¹. The hydrolysis was performed in 10 ml of water with 0.3 g of catalyst of an average particle size of 0.049 mm. (a) Hydrogen production-time curves; (b) Temperature - time curves.
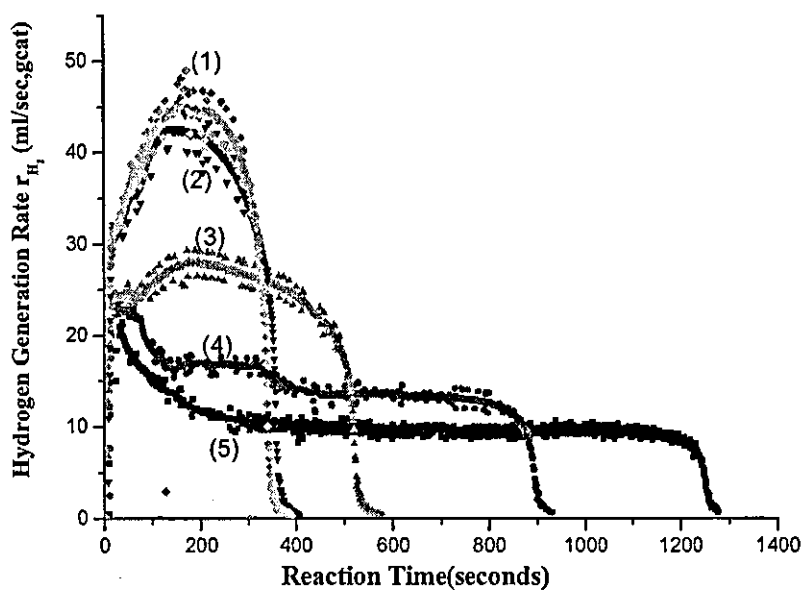
Figure 7.22 The rate of hydrogen generation from the hydrolysis of NaBH₄, which was transformed from Figure 7.21a by differentiation. The initial molality of NaBH4 was 3.97 mol kg⁻¹.

201
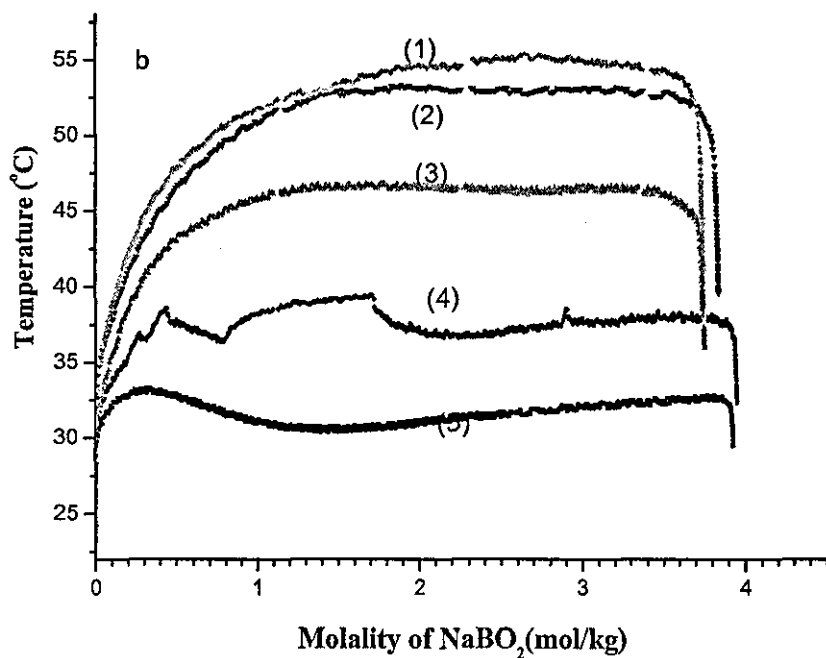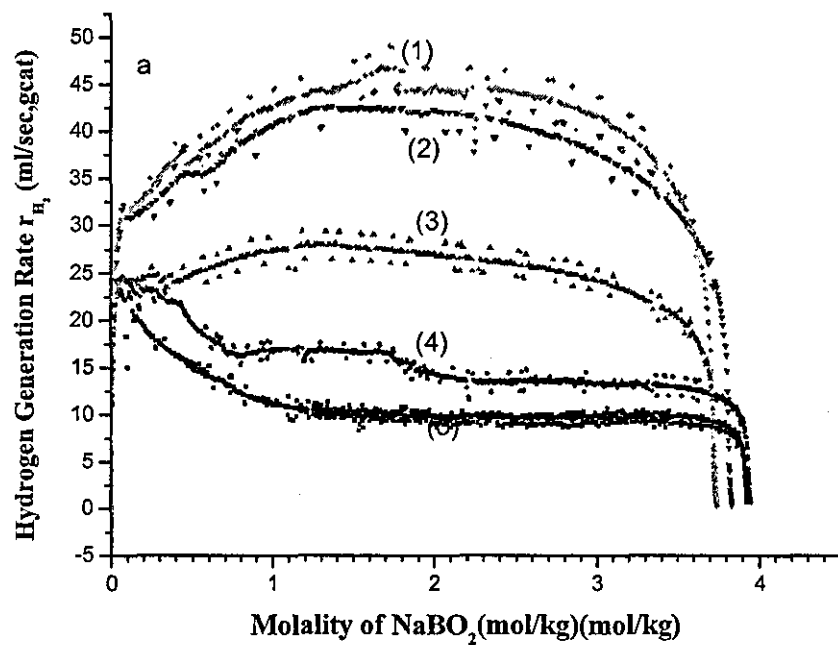
Figure 7.23 The rate of hydrogen generation (a) and reaction temperature (b) versus NaBO₂ molality. They were transformed from Figures 7.22 and 7.21b respectively. Initial molality of NaBH₄ is 3.97 mol kg⁻¹.

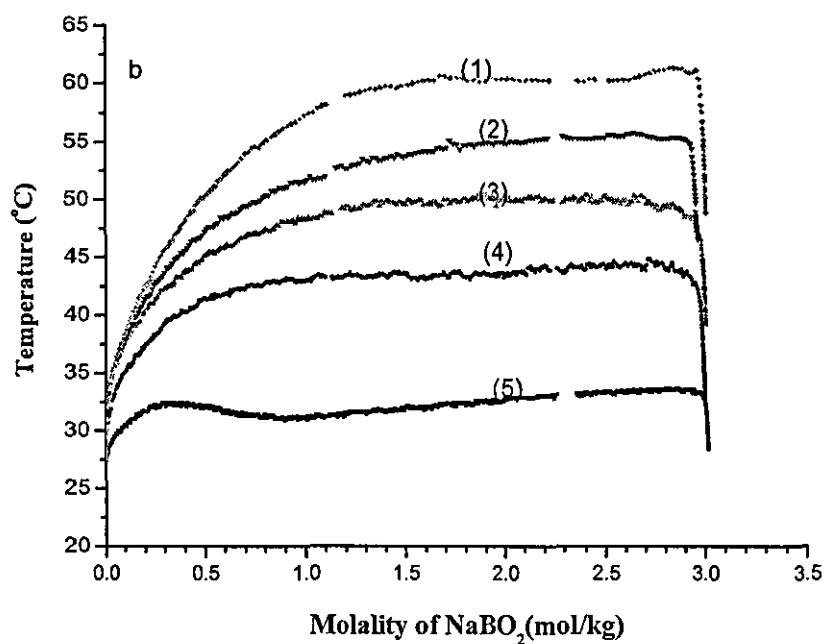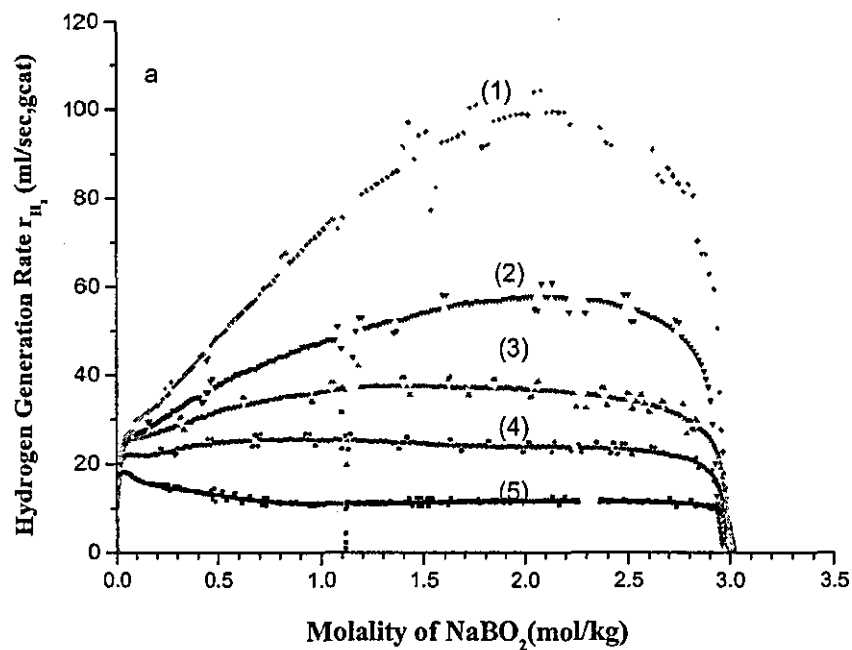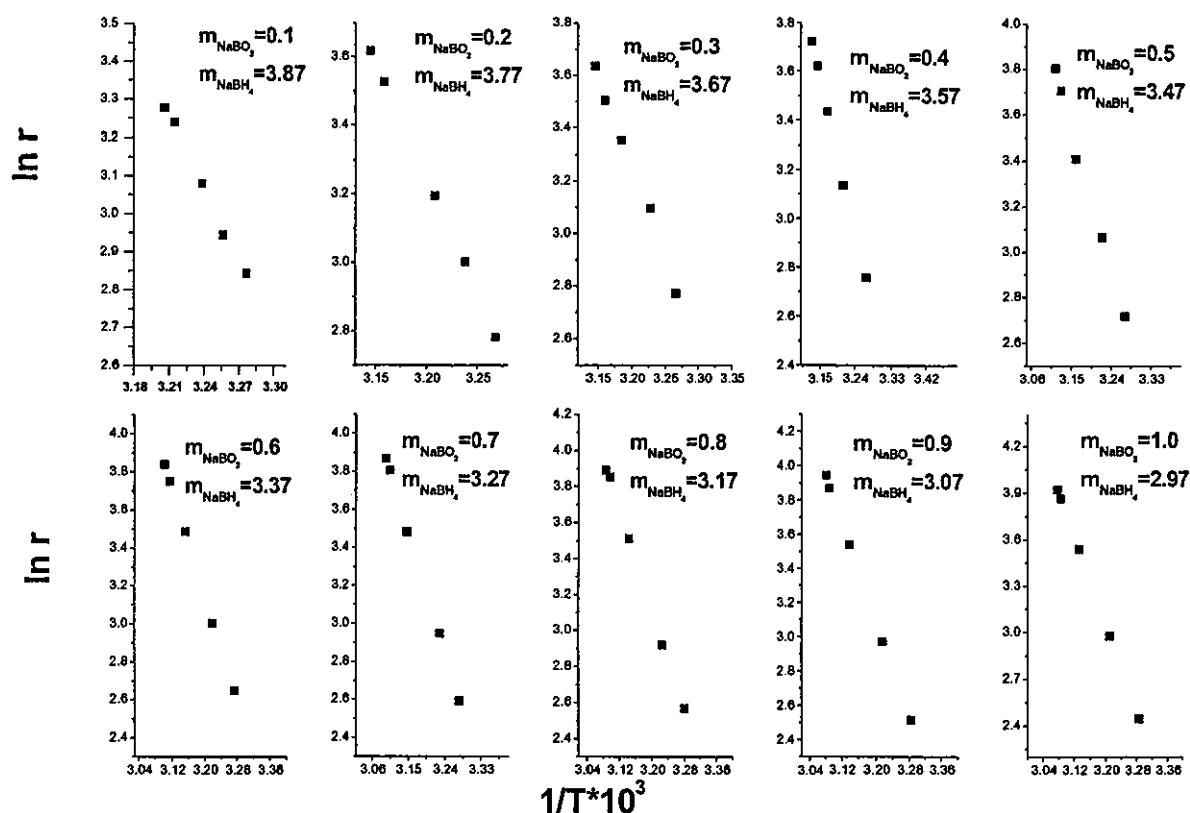**Figure 7.24** $\ln r_{H2}$ versus $1/T$ derived from Figure 7.23. Initial $NaBH_4$ molality was 3.97 mol kg^{-1}.

7.3 The effect of $NaBH_4$

It can be seen from Figures 7.4, 7.8, 7.12, 7.16, 7.20 and 7.24 that $\ln r_{H2}$ and $1/T$ had a good linear relationship. Because of this relationship, the reaction rate at any temperature can be obtained by interpolation. When the temperature and the molality of $NaBO_2$ are fixed, the change in reaction rate with $NaBH_4$ molality was obtained by interpolating the $\ln r_{H2} \sim 1/T$ curves in the relevant figures. The relationships thus obtained are shown in Figures 7.25 to 7.27 for three different temperatures.

As shown in Figures 7.25-7.27, the concentration of $NaBH_4$ had no effect on the rate of hydrogen generation for a fixed concentration of $NaBO_2$, regardless of a change in temperature. It can thus be concluded that the hydrolysis of $NaBH_4$ in the presence of a ruthenium catalyst is a zero-order reaction with regard to $NaBH_4$ concentration. There are

three main steps in the hydrolysis of $NaBH_4$ on a catalyst surface: adsorption of $NaBH_4$, reaction and desorption of H_2. The rate of Hydrogen generation is zero order with respect to $NaBH_4$, indicating that desorption of hydrogen from the catalyst surface is the rate-determining step.
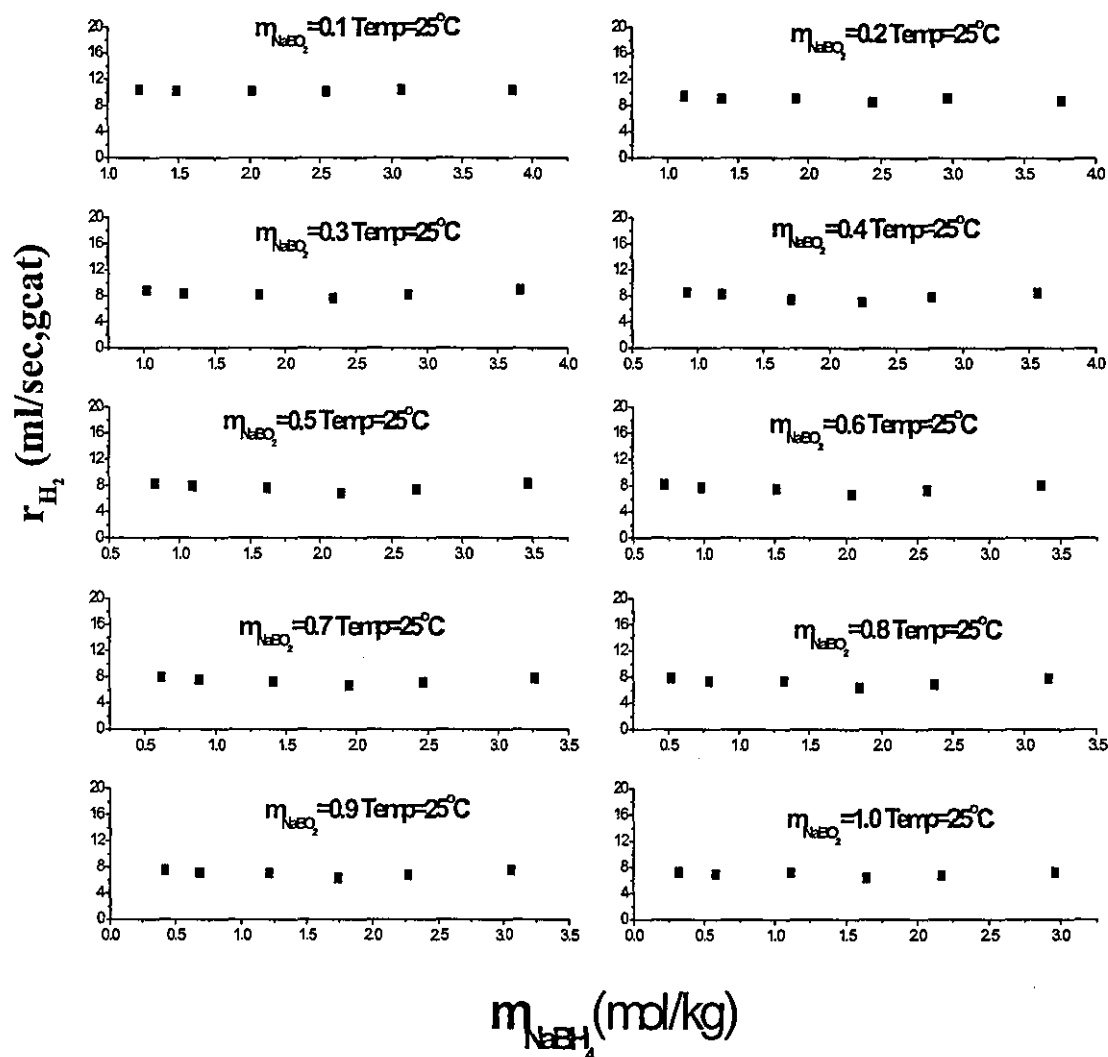
Figure 7.25 The relationship between r_{H2} and the molality of $NaBH_4$ at 25°C.
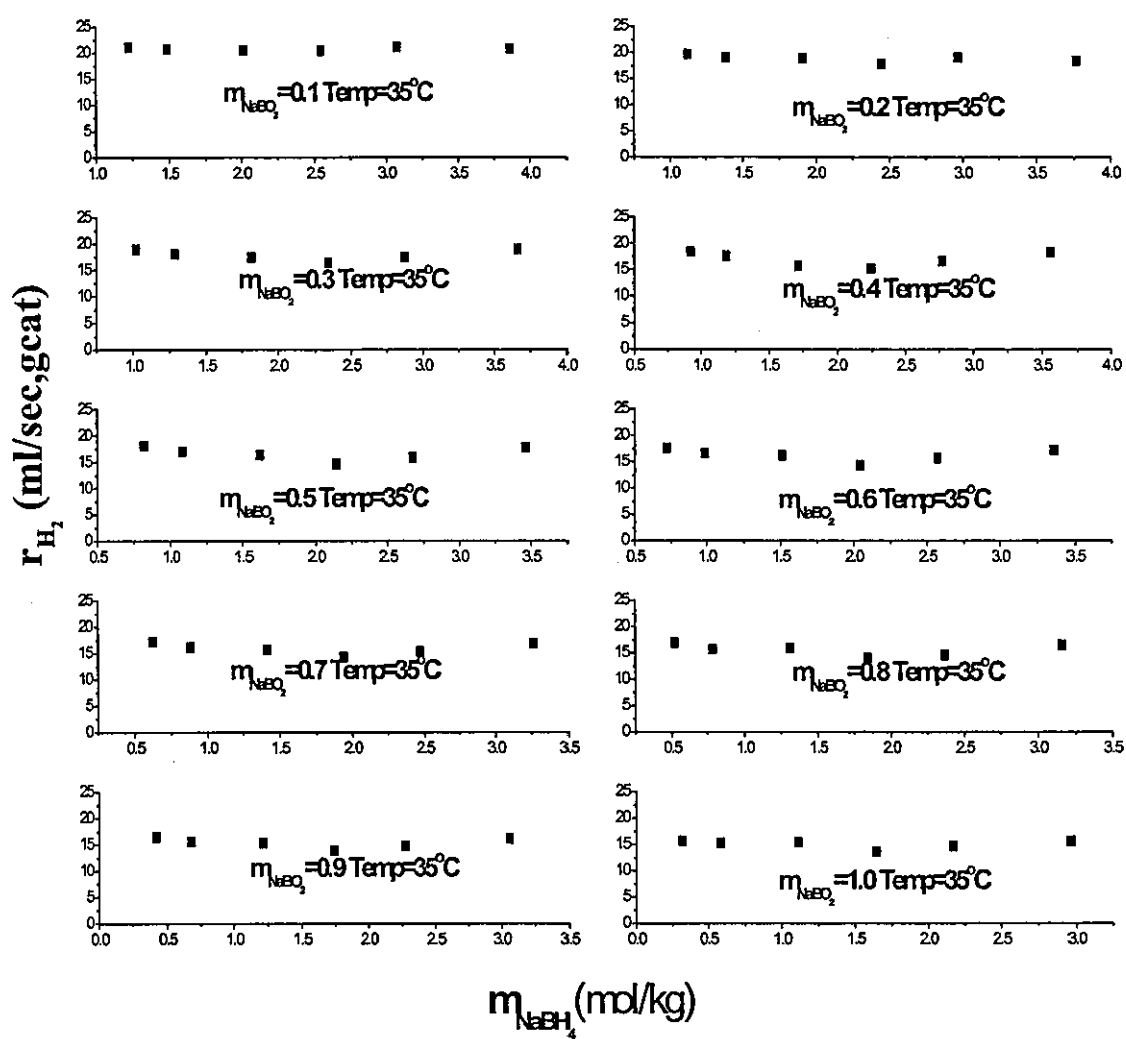
Figure 7.26 The relationship between r_{H2} and the molality of $NaBH_4$ at 35°C.

205
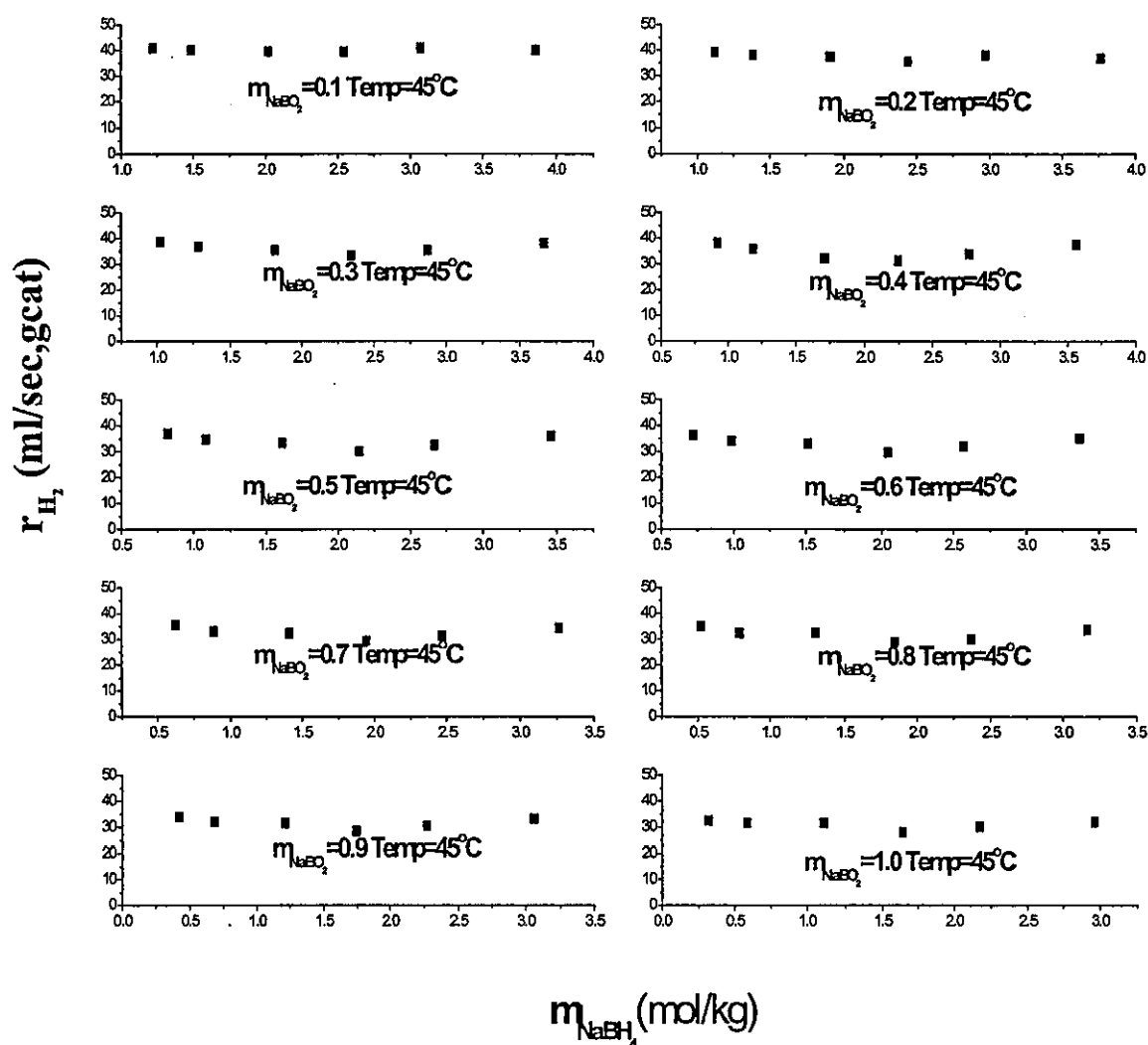
Figure 7.27 The relationship between r_{H2} and the molality of NaBH$_4$ at 45°C.

7.4 The effect of NaBO$_2$

The averages of the hydrogen generation rate for each NaBO$_2$ molality at different NaBH$_4$ molalities were taken from Figures 7.25-7.27 and plotted against the molality of NaBO$_2$ (shown in Figure 7.28). It can be seen that the reaction rate decreases at the earlier stages of the reaction with the increase of NaBO$_2$ concentration and the reaction rate levels off at later stages. Since NaBO$_2$ is a base, it suggests that the reaction intermediate involves the hydrogen ion.
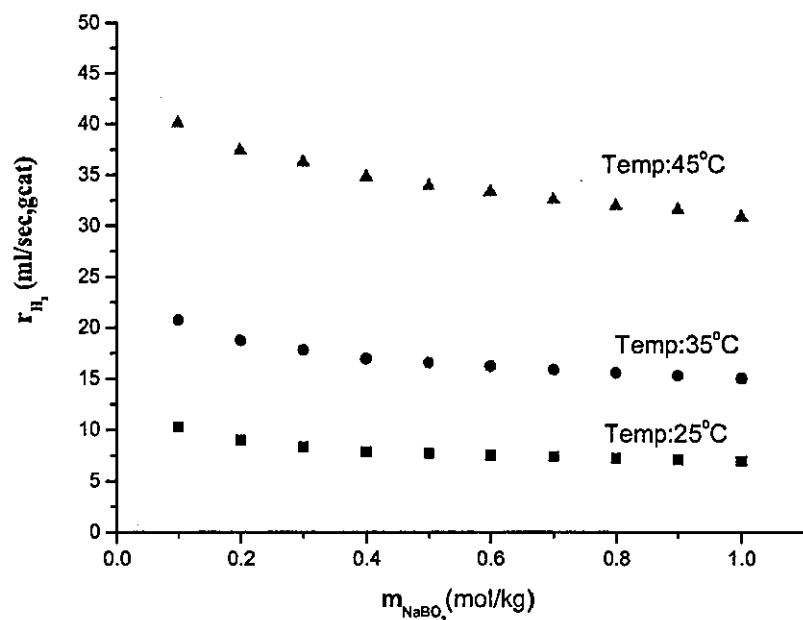
Figure 7.28 The relationship between r_{H2} and the molality of $NaBO_2$.

7.5 Conclusions

In this chapter, the effects of $NaBH_4$ and $NaBO_2$ concentration on the reaction rate have been studied. At a fixed temperature and $NaBO_2$ concentration, the reaction rate is zero order with respect to $NaBH_4$ concentration. At a fixed $NaBH_4$ concentration and temperature, the reaction rate decreases with an increase in $NaBO_2$ concentration.

Chapter 8

The Effect of NaOH on Intrinsic Kinetics and Rate Expression

8.1 Introduction

In Chapter 7, the dependence of reaction rate on the concentration of $NaBH_4$ and $NaBO_2$ was studied. It was found that the reaction is zero order with respect to $NaBH_4$ concentration but decreases steadily with an increase in $NaBO_2$ concentration. In this chapter, the effect of NaOH will be investigated.

In Chapter 2 it was shown that aqueous solutions of $NaBH_4$ are quite stable when maintained at a high pH value. In the absence of a catalyst, the half-life of $NaBH_4$ at room temperature can reach 1.5 years when the concentration of NaOH is 5% [1]. The effect of NaOH is thus an interesting aspect to the kinetics of $NaBH_4$.

8.2 Experimental Results

This chapter details an investigation into the effect of NaOH on the rate of hydrolysis of NaBH4 at various NaOH concentrations. The concentration of both $NaBH_4$ and $NaBO_2$ are fixed and the temperature is held constant. Since it has been shown that the reaction rate is independent of $NaBH_4$ concentration in Chapter 7, it is only necessary to compare rate data at fixed temperatures and $NaBO_2$ concentrations. The isothermal rate data was obtained by the method detailed in chapter 5.

Figures 8.1-8.25 show five sets of hydrolysis reactions in the presence of various NaOH concentrations, from 0.22% to 9.2%. In each set of experiments, five experiments were conducted with the same initial $NaBH_4$ concentration. The reaction rates at a fixed temperature were then derived from these experiments at various $NaBO_2$ molalities, as shown in Figures 8.5, 8.10, 8.15, 8.20 and 8.25.

Figure 8.1 Hydrogen generation from the hydrolysis of NaBH₄ at various temperatures. The initial molality of NaBH₄ was 1.32 mol kg^{-1}. The reaction was conducted in 10 ml of water with 0.3 g of catalyst with a mean particle size of 0.049 mm. The NaOH concentration was 0.22%. (a) Hydrogen production-time curves; (b) Temperature-time curves.

Figure 8.2 Rate of hydrogen generation from the hydrolysis of NaBH₄ at various temperatures, transformed from Figure 8.1a. The NaOH concentration was 0.22%.

Figure 8.3 The rate of hydrogen generation (a) and reaction temperature (b) with $NaBO_2$ molality. They were transformed from Figure 8.2 and Figure 8.1b. The initial molality of $NaBH_4$ was 1.32 mol kg^{-1}. NaOH concentration was 0.22%.
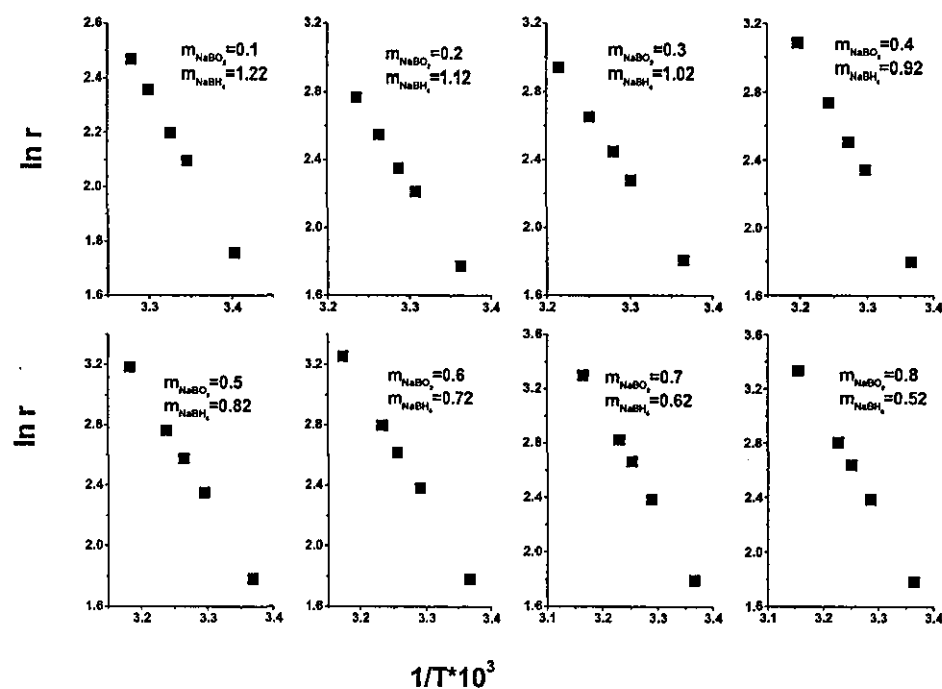
Figure 8.4 $\ln r_{H2}$ versus $1/T$ derived from Figure 8.3. The initial molality of $NaBH_4$ was 1.32 mol kg^{-1}. The NaOH concentration was 0.22%.

211
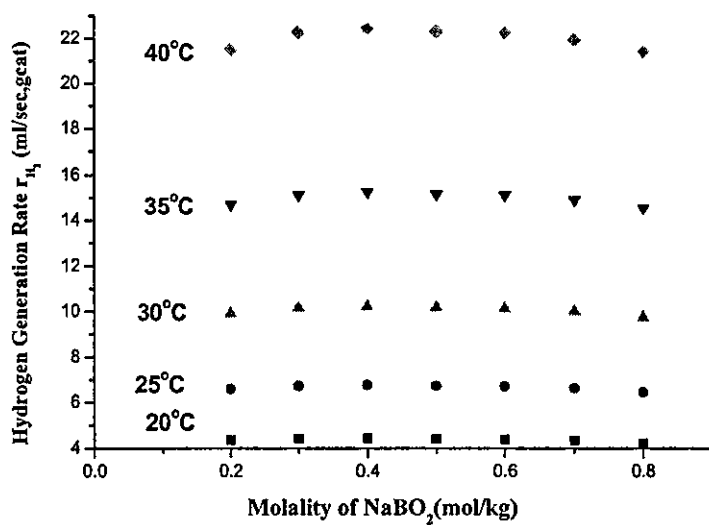
Figure 8.5 Reaction rate versus molality of $NaBO_2$ at various temperatures for NaOH =0.22%.
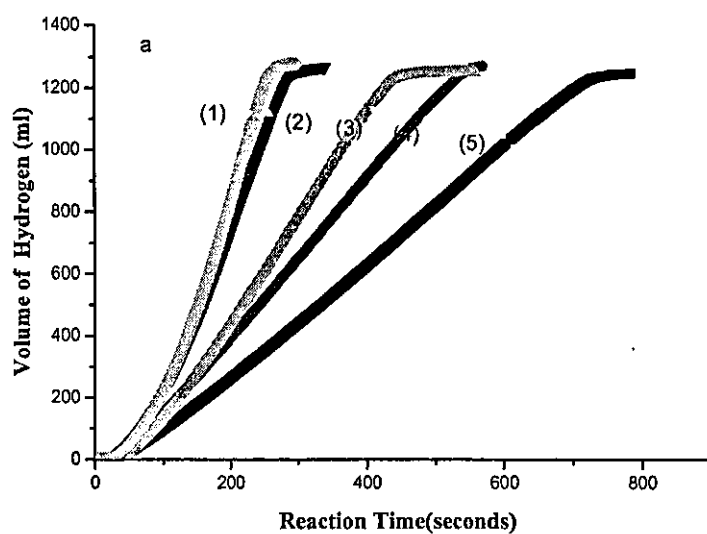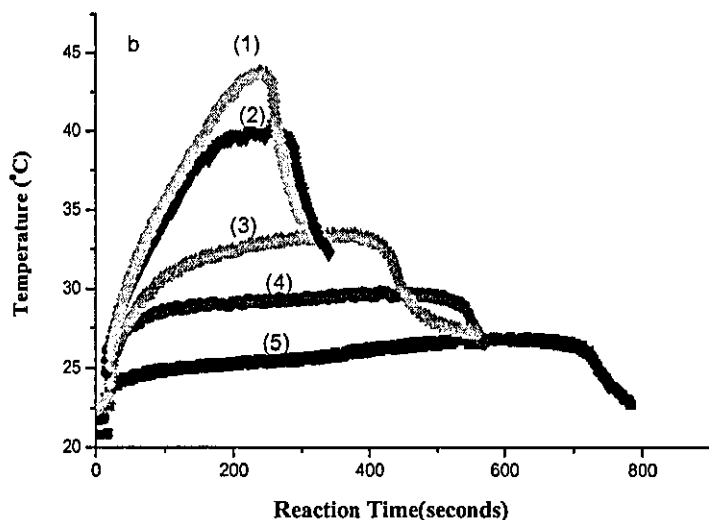
Figure 8.6 Hydrogen generation from the hydrolysis of $NaBH_4$ at various temperatures. The initial molality of NaBH4 is 1.32 mol kg^{-1}. The hydrolysis was performed in 10 ml of water with 0.3 g of catalyst with an average catalyst particle size of 0.049 mm. NaOH concentration was 0.43%. (a) Hydrogen production-time curves; (b) Temperature-time curves.
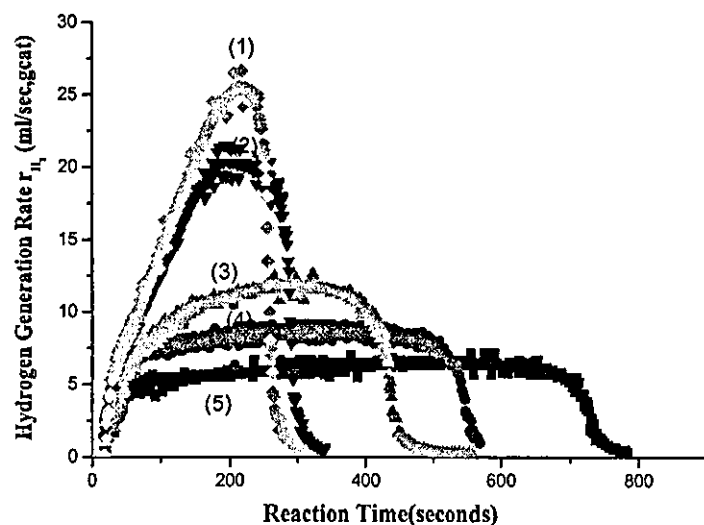
Figure 8.7 The rate of hydrogen generation from the hydrolysis of $NaBH_4$ at various temperatures, transformed from Figure 8.6a. NaOH concentration was 0.43%.

213
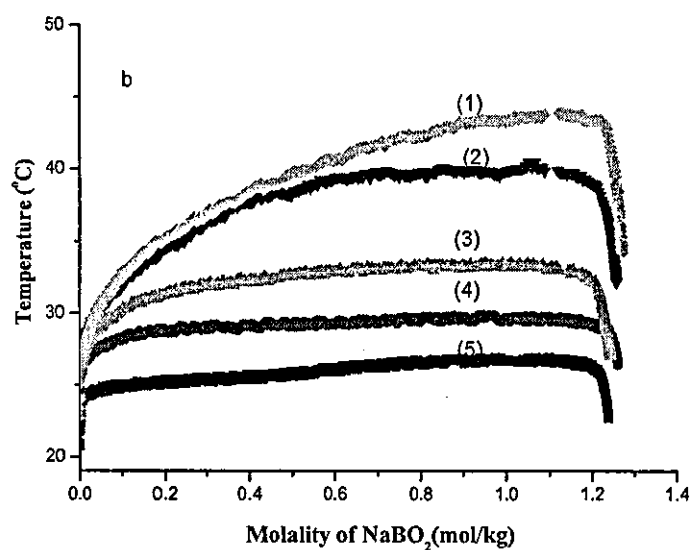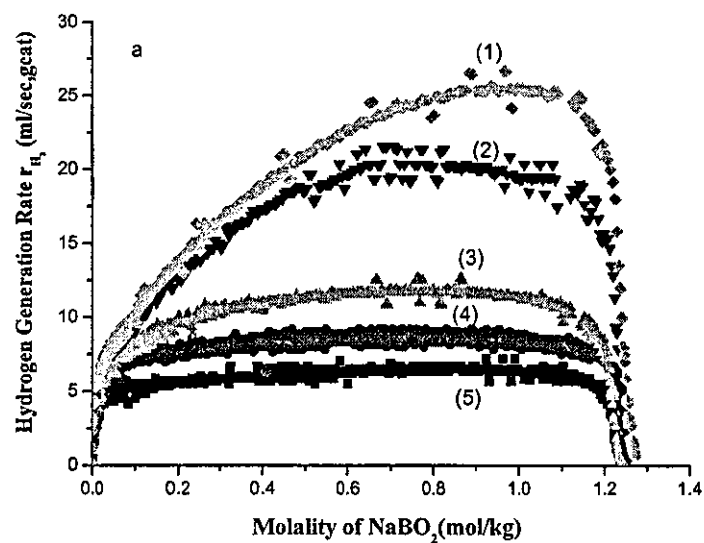
Figure 8.8 The rate of hydrogen generation (a) and reaction temperature (b) with $NaBO_2$ molality. They were transformed from Figure 8.7 and Figure 8.6b. Initial molality of $NaBH_4$ was 1.32 mol kg^{-1}. NaOH concentration was 0.43%.
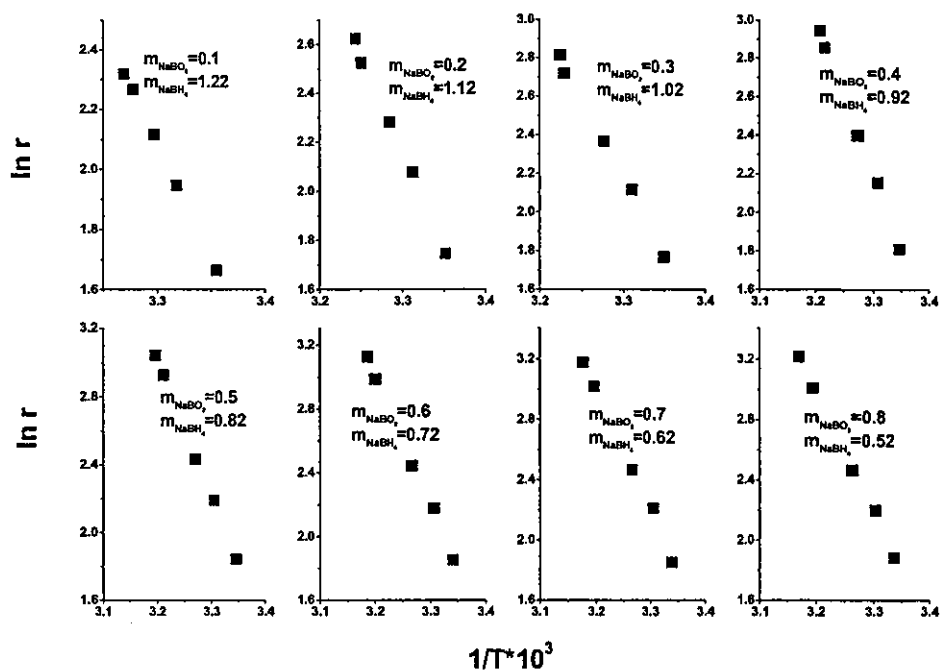
Figure 8.9 lnr_{H2} versus 1/T derived from Figure 8.8. Initial NaBH$_4$ molality was 1.32 mol kg^{-1}. NaOH concentration was 0.43%.
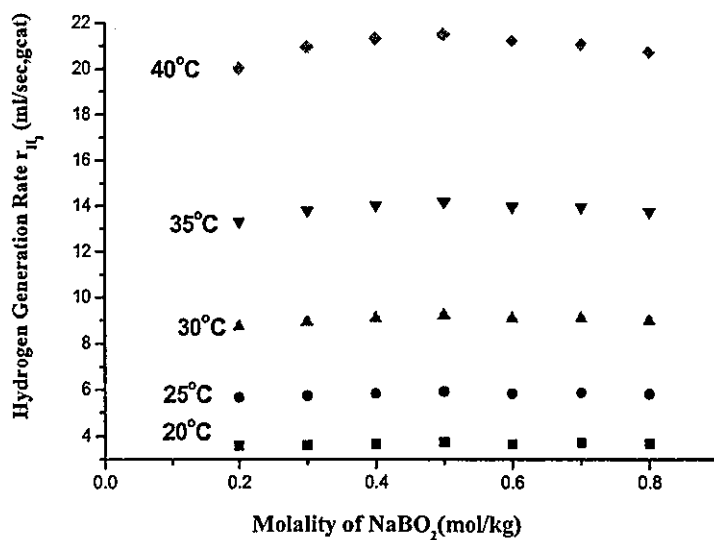
Figure 8.10 Reaction rate versus molality of NaBO$_2$ at various temperatures for NaOH =0.43%.
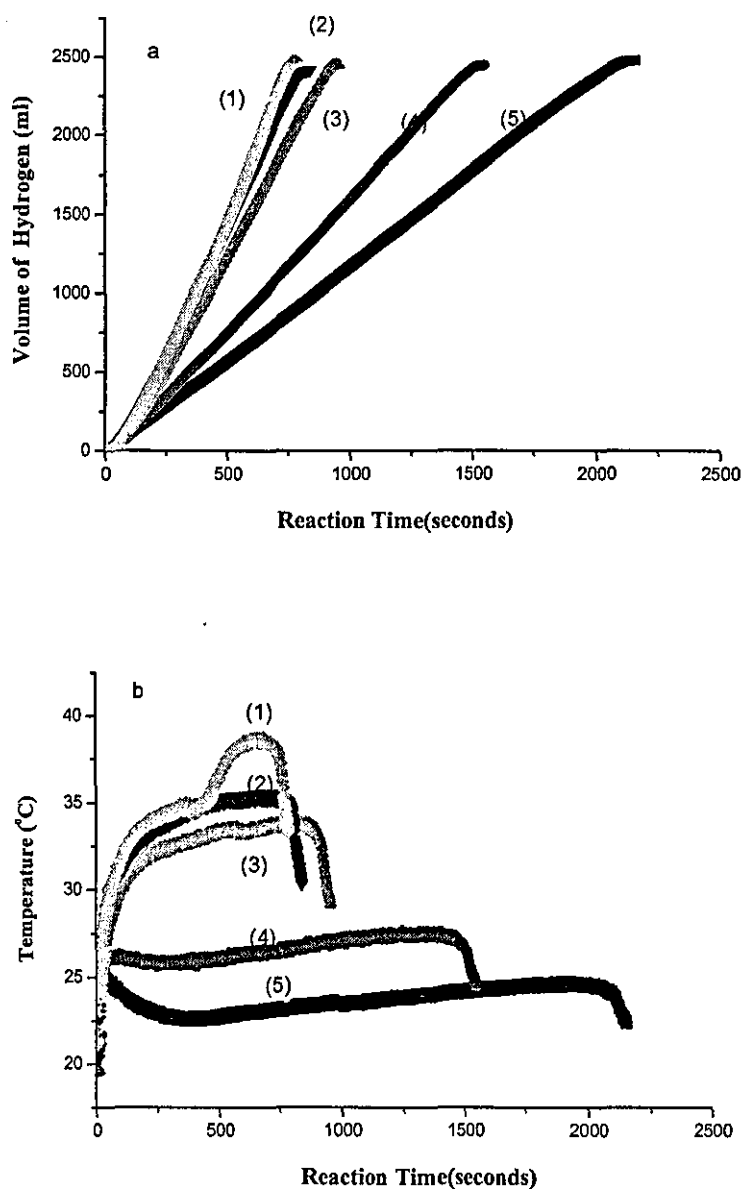
Figure 8.11 Hydrogen generation from the hydrolysis of NaBH₄ at various temperatures. The initial molality of NaBH4 was 2.64 mol kg⁻¹. The hydrolysis was performed in 10 ml of water with 0.3 g of catalyst with an average catalyst particle size of 0.049 mm. NaOH concentration was 2.8%. (a) Hydrogen production-time curves; (b) Temperature-time curves.
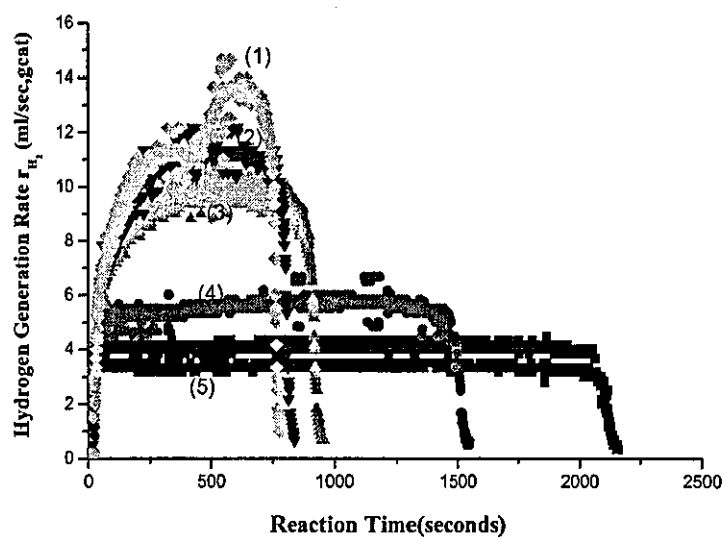
Figure 8.12 The rate of Hydrogen generation from the hydrolysis of NaBH₄ at various temperatures, transformed from Figure 8.11a. NaOH concentration was 2.8%.
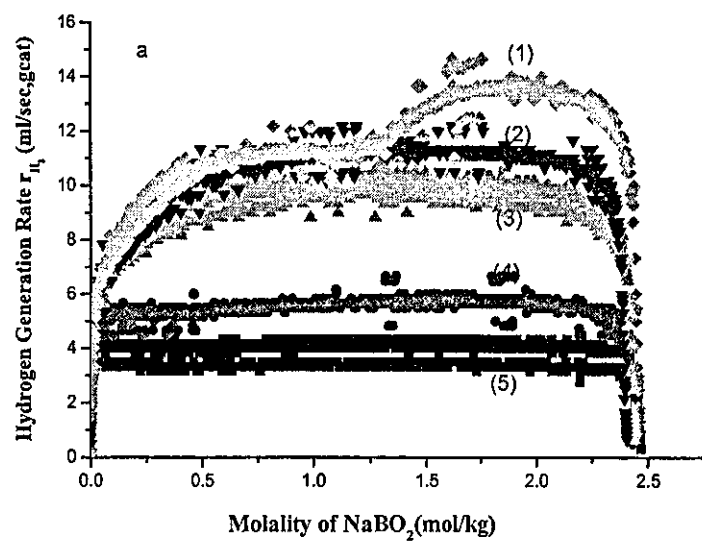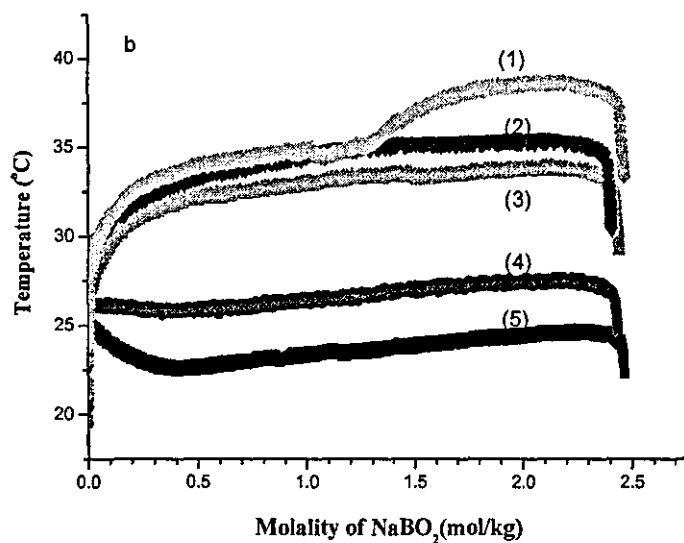
Figure 8.13 The rate of hydrogen generation (a) and reaction temperature (b) with $NaBO_2$ molality. They were transformed from Figure 8.12 and Figure 8.11b. NaOH concentration was 2.8%. The initial molality of $NaBH_4$ was 2.64 mol kg^{-1}.
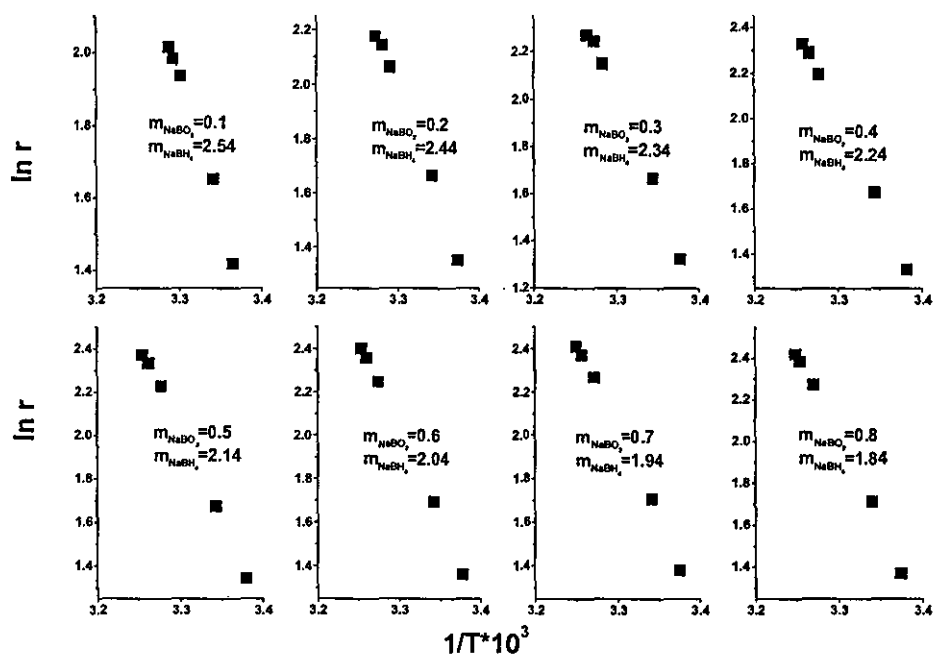
Figure 8.14 lnr~1/T derived from Figure 8.13. Initial $NaBH_4$ molality was 2.64 mol kg^{-1}. NaOH concentration was 2.8%

218
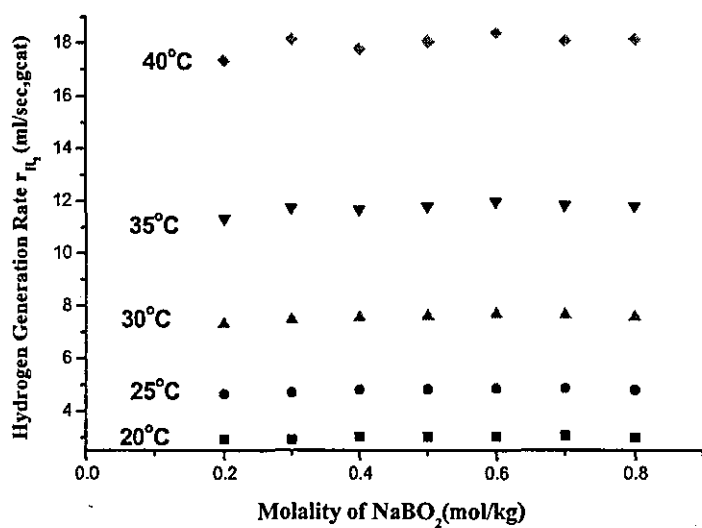
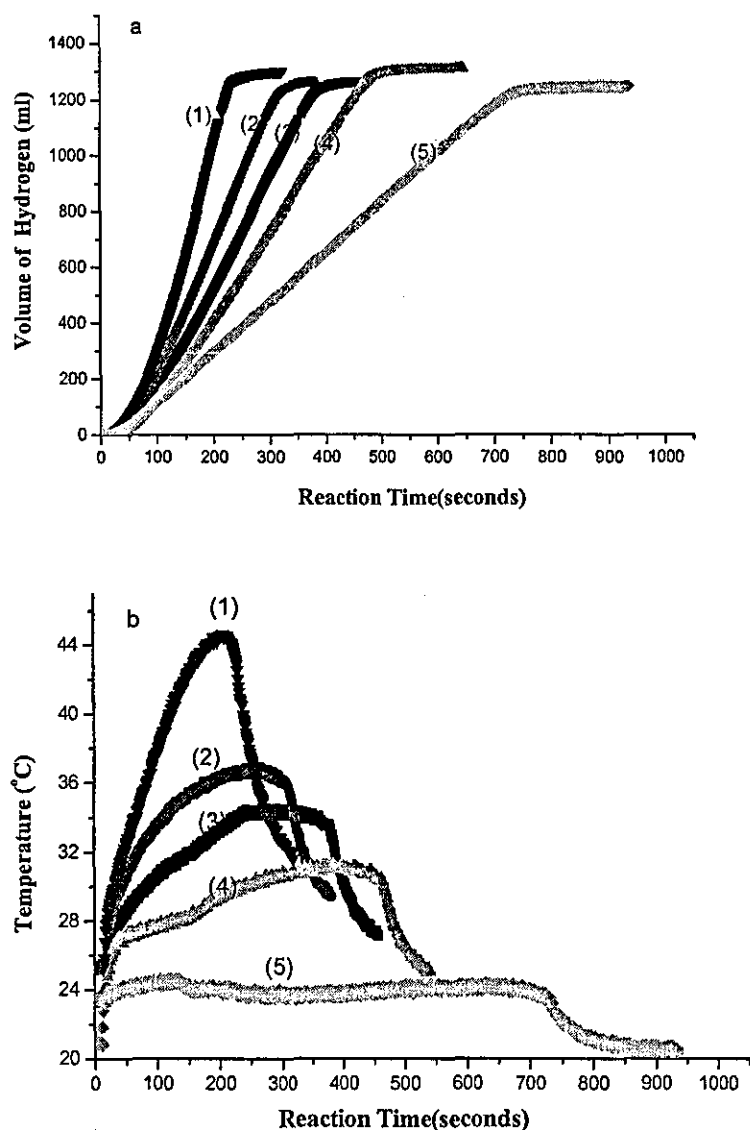**Figure 8.15** Reaction rate versus molality of $NaBO_2$ at various temperatures for NaOH =2.8%.
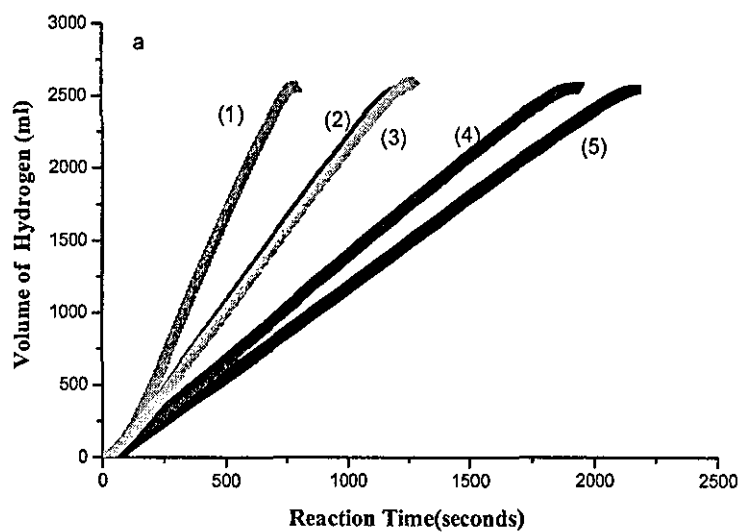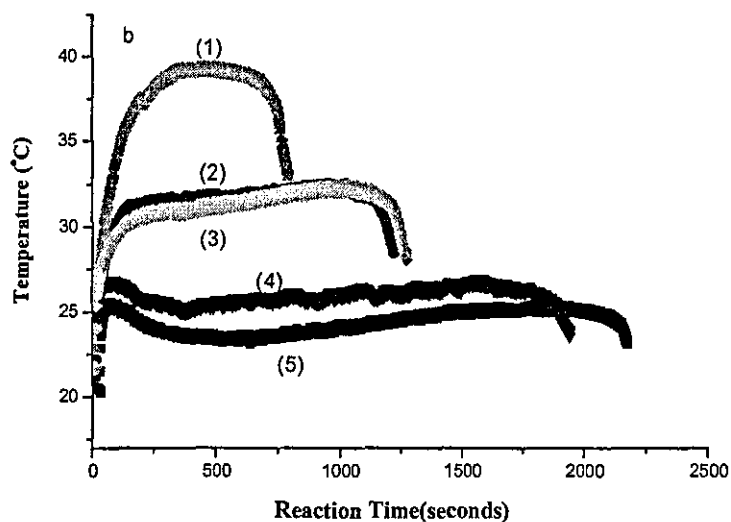
Figure 8.16 Hydrogen generation from the hydrolysis of NaBH₄ at various temperatures. The initial molality of NaBH4 was 2.64 mol kg⁻¹. The hydrolysis was performed in 10 ml of water with 0.3 g of catalyst with an average catalyst particle size of 0.049 mm. NaOH concentration was 4.8%. (a) Hydrogen production-time curves; (b) Temperature-time curves.
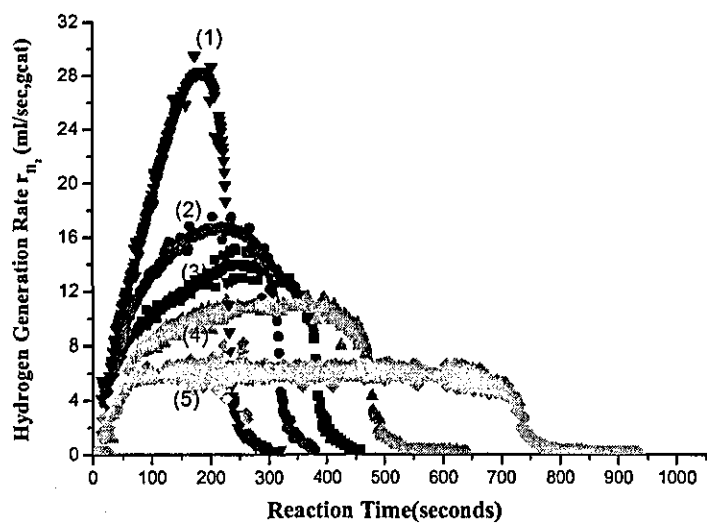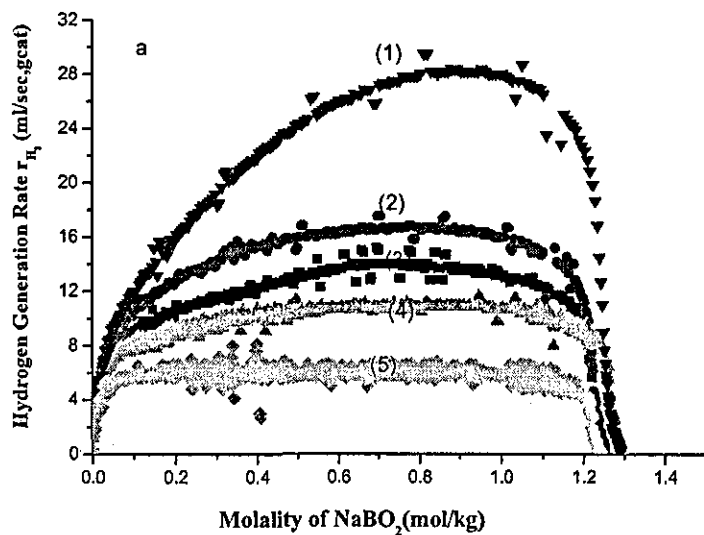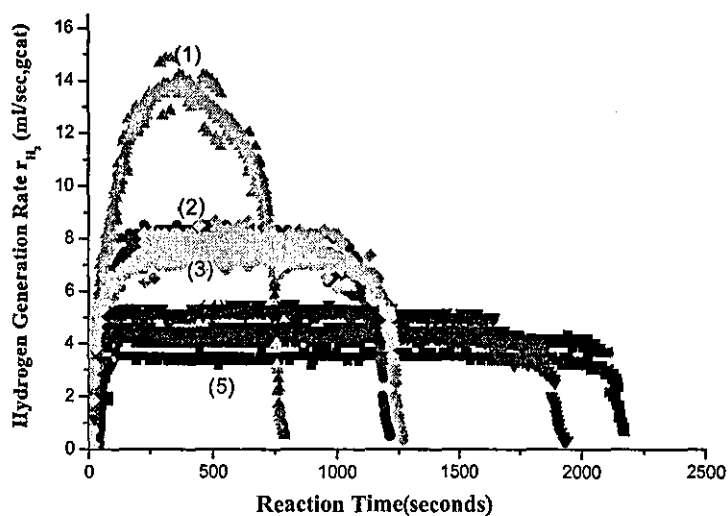

Figure 8.17 The rate of hydrogen generation from the hydrolysis of NaBH₄ at various temperatures, transformed from Figure 8.16a. NaOH concentration was 4.8%.
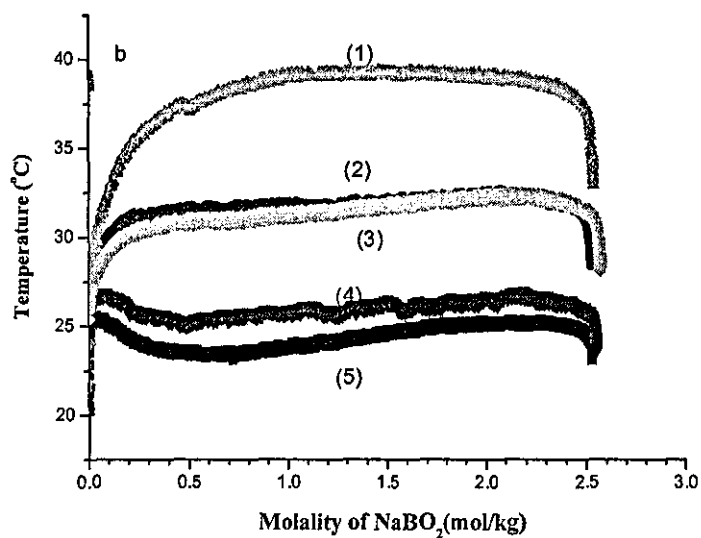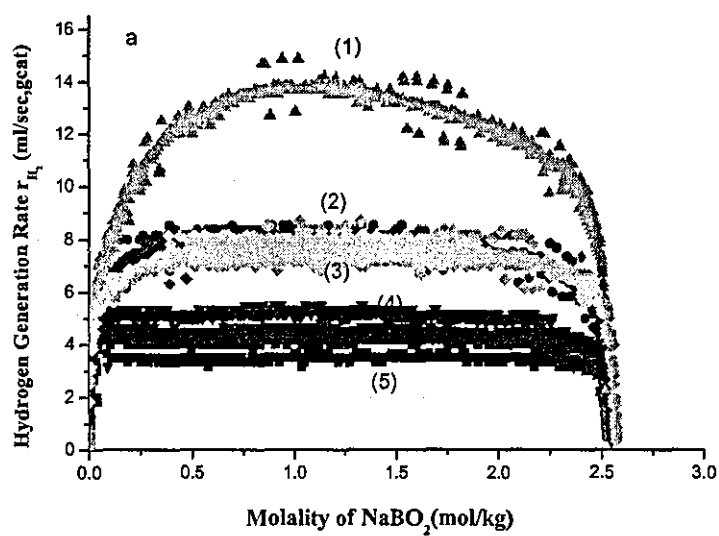
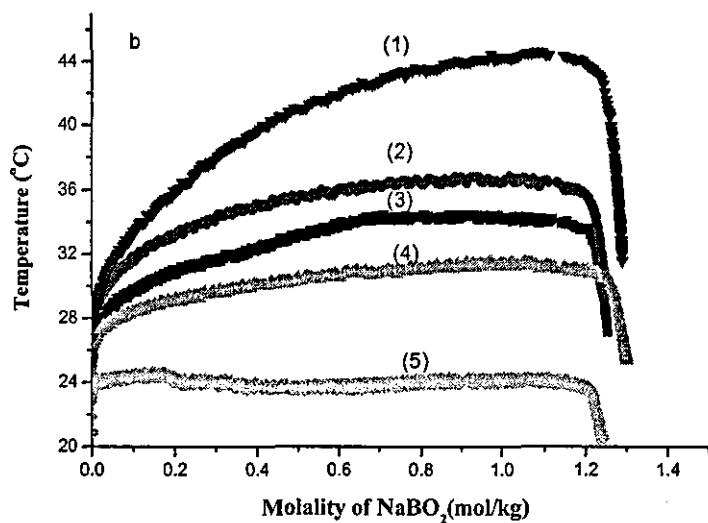**Figure 8.18** The hydrogen generation rate (a) and reaction temperature (b) with $NaBO_2$ molality. They were transformed from Figure 8.17 and Figure 8.16b. NaOH concentration was 4.8%. The initial molality of $NaBH_4$ was 2.64 mol kg^{-1}.
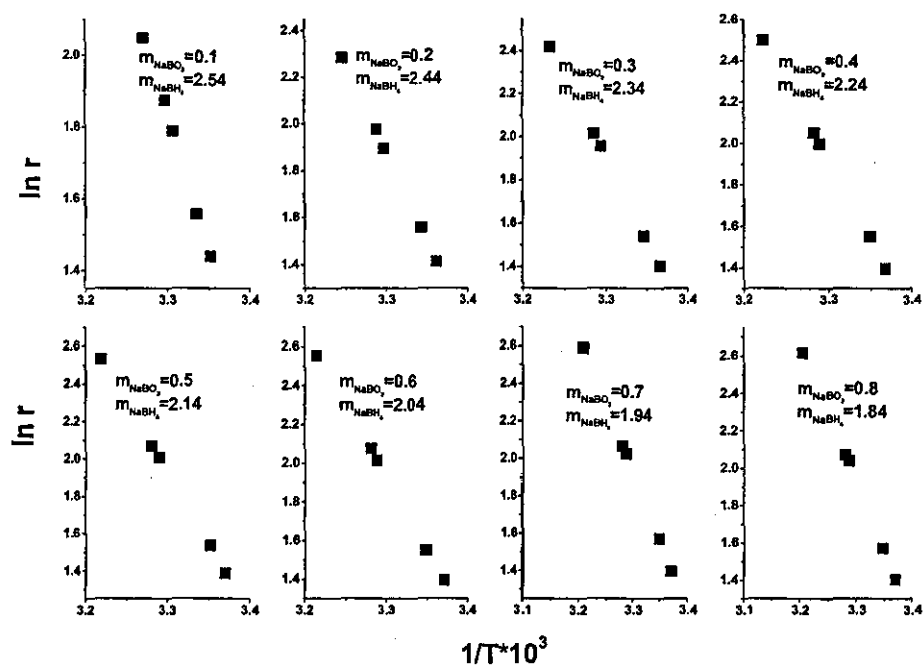
Figure 8.19 $\ln r_{H2} \sim 1/T$ derived from Figure 8.18. Initial $NaBH_4$ molality was 2.64 mol kg^{-1}. NaOH concentration was 4.8%
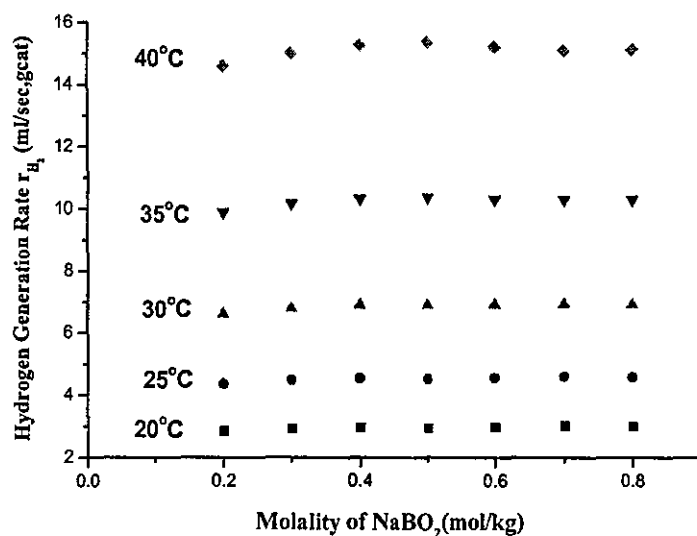
Figure 8.20 Reaction rate versus molality of $NaBO_2$ at various temperatures for NaOH =4.8%.

222
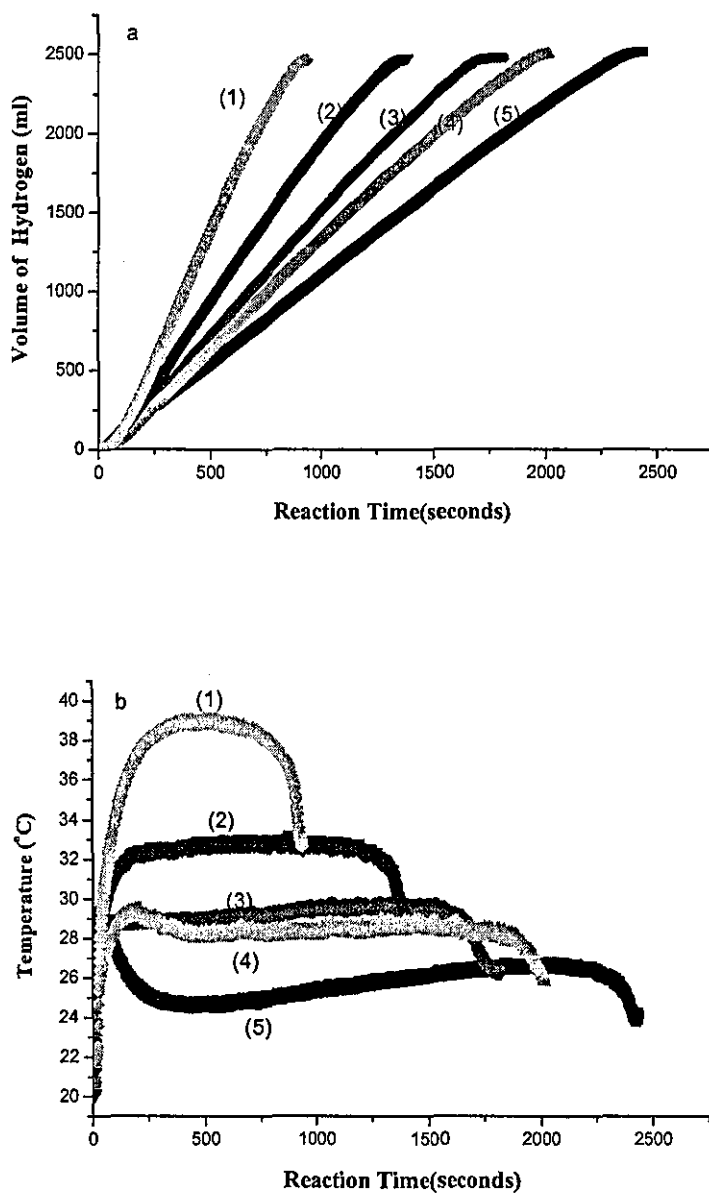
Figure 8.21 Hydrogen generation from the hydrolysis of NaBH₄ at various temperatures. The initial molality of NaBH4 was 2.64 mol kg⁻¹. The hydrolysis was performed in 10 ml of water with 0.3 g of catalyst with an average catalyst particle size of 0.049 mm. NaOH concentration was 9.2%. (a) Hydrogen production-time curves; (b) Temperature-time curves.
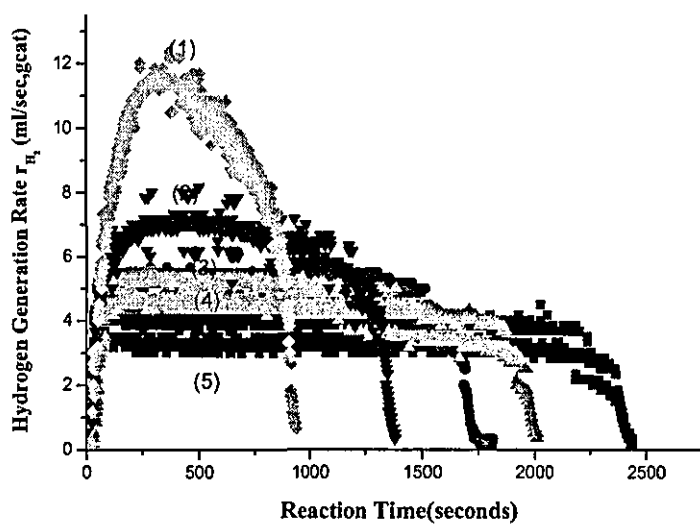
Figure 8.22 The rate of hydrogen generation from the hydrolysis of NaBH₄ at various temperatures, transformed from Figure 8.21a. NaOH concentration was 9.2%.

224
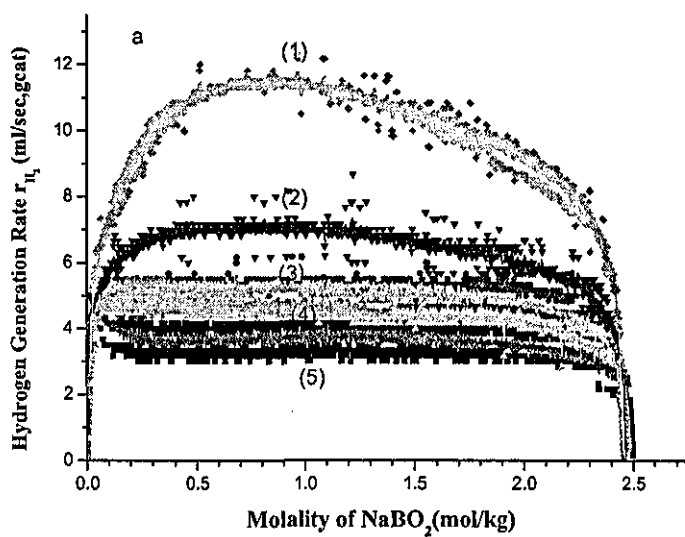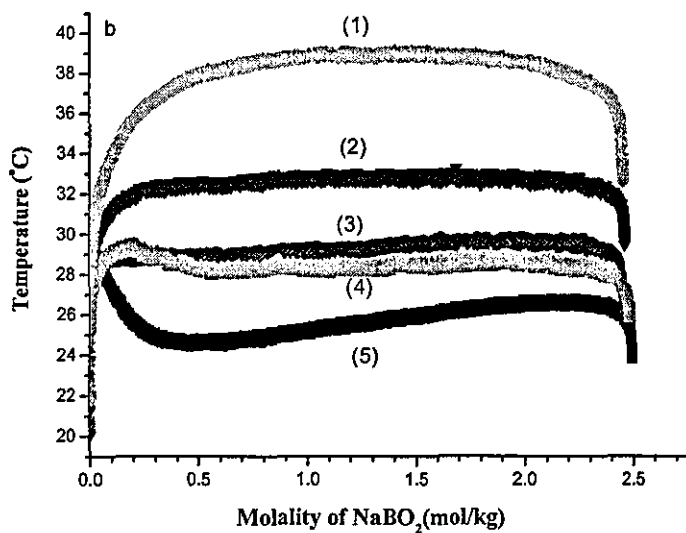
Figure 8.23 The rate of hydrogen generation (a) and reaction temperature (b) with $NaBO_2$ molality. They were transformed from Figure 8.22 and Figure 8.21b. NaOH concentration was 9.2%. The initial molality of $NaBH_4$ was 2.64 mol kg^{-1}.
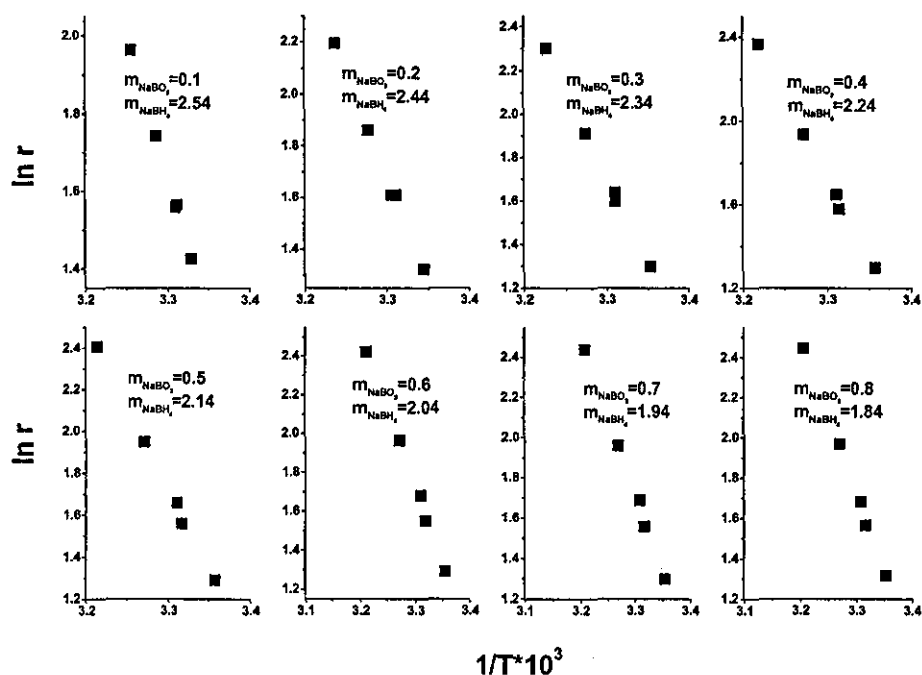
Figure 8.24 $\ln r_{H2} \sim 1/T$ derived from Figure 8.23. Initial $NaBH_4$ molality was 2.64 mol kg^{-1}. NaOH concentration was 9.2%.
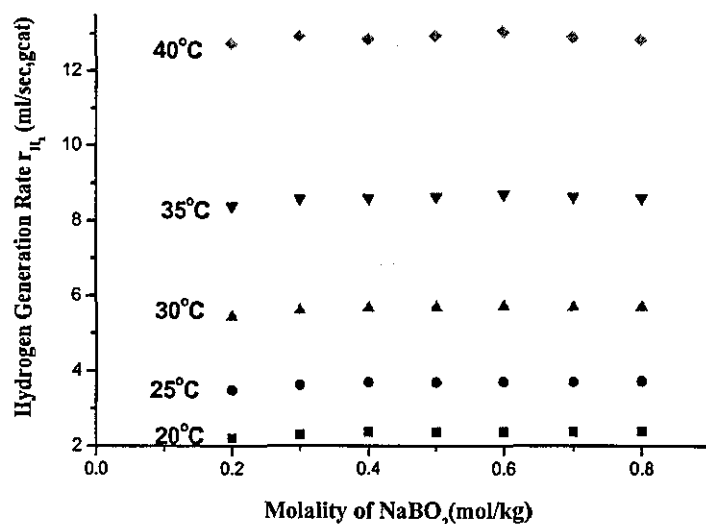
Figure 8.25 Reaction rate versus molality of $NaBO_2$ at various temperatures for NaOH =9.2%.

## 8.3 The effect of NaOH on the hydrolysis of $NaBH_4$

From Figures 8.5, 8.10, 8.15, 8.20 and 8.25, it can be seen that at a specific temperature, the reaction rate changes within a very small range in the presence of NaOH when compared with the rate in the absence of NaOH, which is shown in Figure 7.28. In the absence of NaOH, the pH value of the $NaBO_2$ solution changes significantly, moving from neutral (pH = 7) to strongly basic (pH = 12.5 according to the equilibrium $B(OH)_4^- = H_3BO_3 + OH^-$, K = 1.73 x 10^{-5}). The pH of the solution does not change significantly in the presence of NaOH due to the high concentration of OH^-. Since the basicity of the solution is stable in the presence of NaOH, it is consistent with the previous conclusion that the reaction is zero-order with respect to the concentration of $NaBH_4$.

8.4 Rate expressions

In this section, the final rate expression for the hydrolysis of $NaBH_4$ is derived. Since the reaction rate is zero order with respect to the concentration of $NaBH_4$, $NaBH_4$ should not be included in the rate expression. The rate is only related to the basicity of the solution and the reaction temperature.

In order to obtain the relationship between the reaction rate and the basicity of the solution, the rate of hydrogen generation r_{H2} was plotted against pOH. Here pOH is defined as $\ln 1/[OH^-]$. As shown in Figure 8.26, r_{H2} and pOH have a linear relationship.

226

The relationship between r_{H2} and pOH may thus be expressed by using equation (8.1).

$$r_{H2} = A \bullet pOH + B \qquad (8.1)$$

The parameters A and B for the linear equations at various temperatures and residual square root are given in Table 8.1.
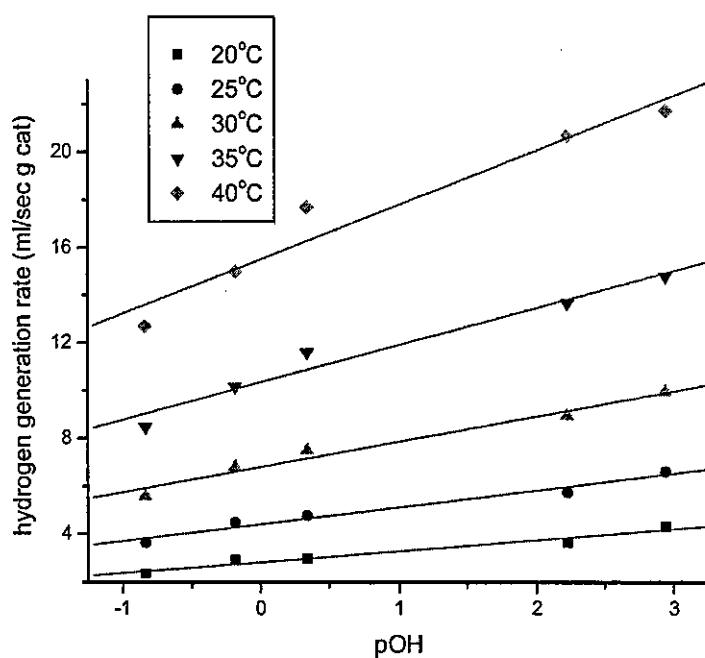
Figure 8.26 r_{H2} versus pOH and their linear regressions.

Table 8.1 The slopes and intercepts of the regressed equations in Figure 8.26.

Temperature ($^\circ$C)	A	B	Error (R^2)
20	0.4619	2.8219	0.98
25	0.7025	4.4118	0.99
30	1.0532	6.7987	0.99
35	1.5591	10.3340	0.98
40	2.2781	15.5020	0.97

It is shown clearly in Table 8.1 that both A and B change with temperature. To find the relationships between A and T and B and T, A and B are plotted against T as shown in

Figure 8.27. From the trend, both A and T and B and T have an exponential shape. Hence, they are regressed using an exponential equation. The final rate equation is given by equation (8.2).
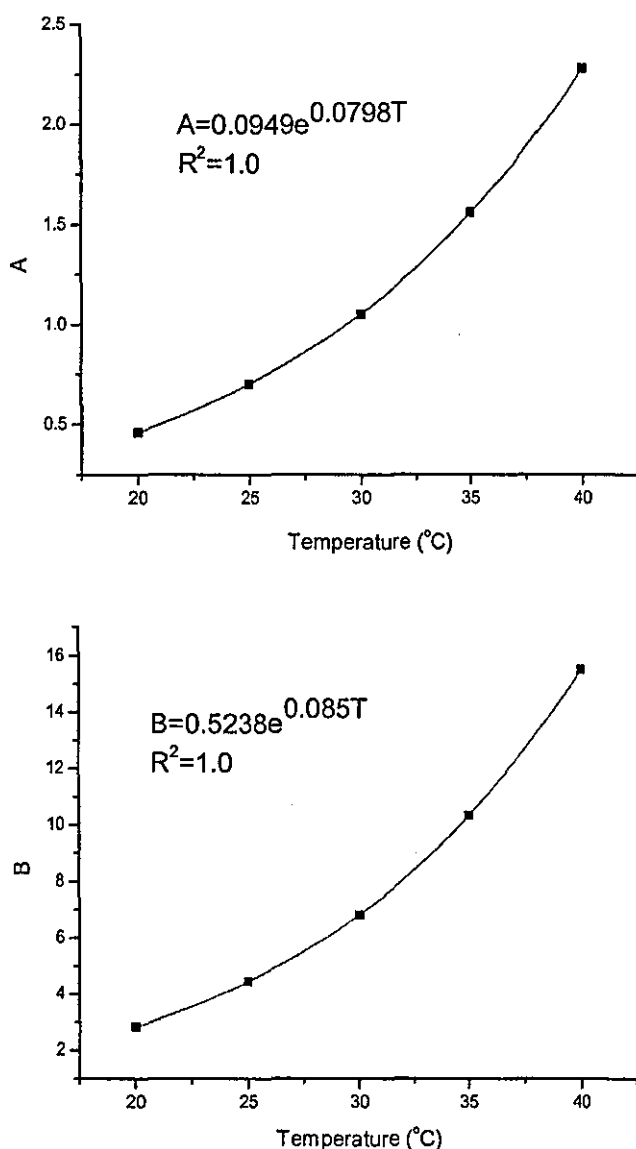
Figure 8.27 The regression of the coefficients of the rate expression.

$$r_{H2} = 0.0949e^{0.0798T} pOH + 0.5238e^{0.085T} \tag{8.2}$$

Equation (8.2) is the final rate expression for the hydrolysis of $NaBH_4$ in the presence of a carbon supported ruthenium catalyst. It is dependent on the basicity of the solution and the reaction temperature. The basicity is measured by pOH. Since pOH is the negative

logarithm of the OH⁻ ion concentration, the rate of hydrogen generation decreases with an increase in OH⁻ concentration. At the present stage, the physical meaning of the parameters A and B is not clear. However, they both change with temperature exponentially. This is reasonable for a chemical reaction. Since B increases more rapidly than A, the rate of hydrogen generation increases rapidly with an increase in temperature.

8.5 A Possible Reaction Mechanism for the Hydrolysis of NaBH₄
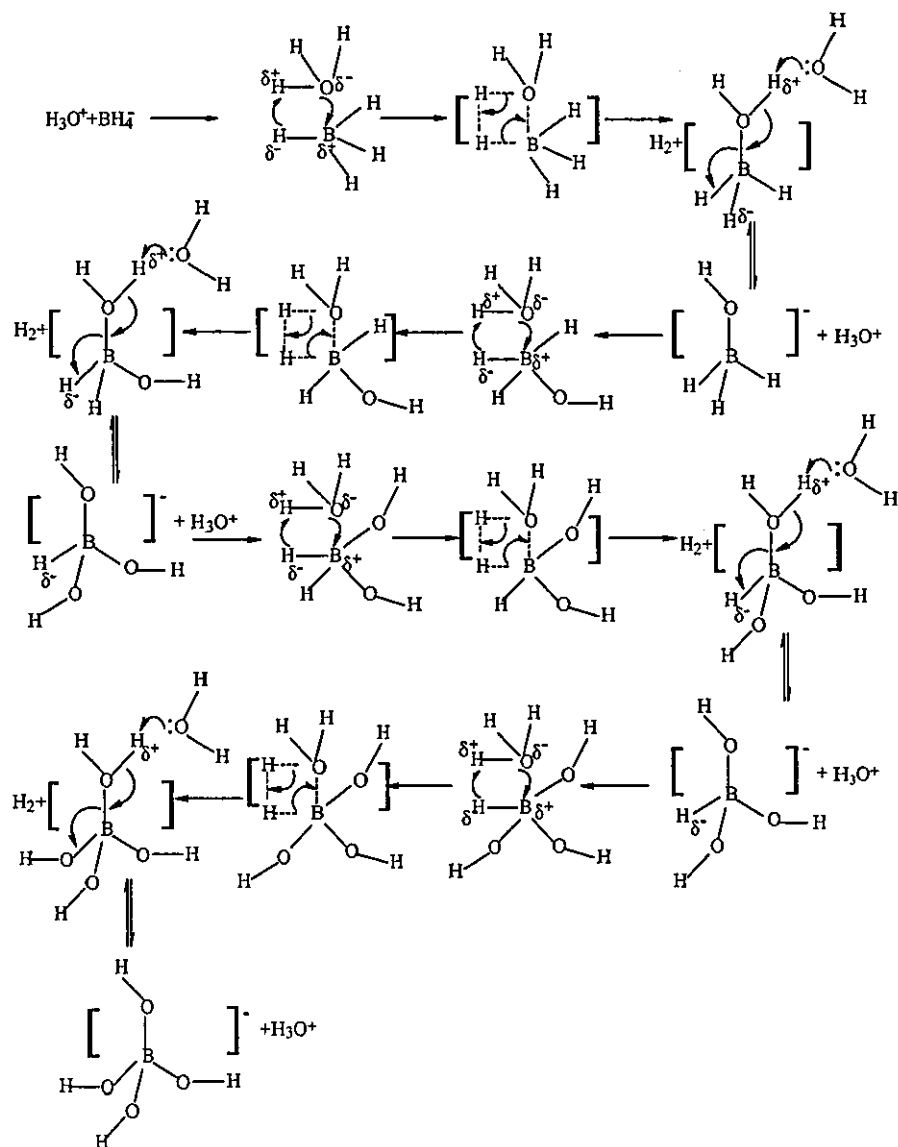
Figure 8.28 A possible mechanism for the hydrolysis of NaBH₄ over a metal catalyst.

The reason for this complicated dependence on temperature may be due to the reaction mechanism. The hydrolysis of NaBH₄ for releasing hydrogen must have involved the intermediate of H^+. When the basicity of the aqueous solution varies, the activation energy

and the pre-exponential factor for the Arrhenius form rate equation may also change. The mechanism may involve the steps shown in Figure 8.28. In the above mechanism, the hydrogen ion in the water (H_3^+O) attacks BH_4^-. Step by step, the hydrogen is replaced by OH^- from the water to form the generally accepted BO_2^- form in water: $B(OH)_4^-$.

8.6 Conclusions

In this chapter, experiments were conducted to investigate the effect of NaOH on the intrinsic kinetics of the hydrolysis of $NaBH_4$. The following conclusions can be drawn:

- The reaction rate depends strongly on the basicity of the solution. This may be due to the existence of acid intermediates in the reaction.

- The reaction rate can be expressed using the following equation, which correlates the reaction rate with the reaction temperature and the basicity of the solution.

$$r_{H2} = 0.0949e^{0.0798T} \, pOH + 0.5238e^{0.085T}$$

8.7 References

1.   Amendola, S.C., et al., *A safe, portable, hydrogen gas generator using aqueous borohydride solution and Ru catalyst.* International Journal of Hydrogen Energy, 2000. **25**: 969-975.

Chapter 9

Modelling Hydrogen Generation from the NaBH$_4$-NaOH-H$_2$O System for Big Catalyst Particles

9.1 Introduction

In Chapters 6-8, intrinsic kinetics were obtained to predict hydrogen evolution without heat and mass transfer limitation, where the catalyst particles that were used were very small. In practice, catalysts are particles of significant size in order to avoid large pressure drops. As shown in previous chapters, strong diffusion limitations occur when the catalyst particle size is at the level of practical accessibility such as 2 mm. The aim of this chapter is to model hydrogen generation from the NaBH$_4$-NaOH-H$_2$O system when catalyst particles of significant size are used. In the modelling, the mass transfer limitations are built into the overall kinetic equation.

Two situations are considered in the modelling. One is the isothermal hydrolysis of NaBH$_4$ aqueous solutions, the other is the non-isothermal reaction. The non-isothermal reaction is more practical since this can reduce system complexity by controlling the system temperature.

9.2 Model Construction

9.2.1 General description

The hydrolysis of NaBH$_4$ is an exothermic reaction and the heat that is generated will accelerate the reaction. The faster the reaction proceeds, the higher the temperature is raised. However, the temperature cannot exceed the boiling point of the solution because water begins to evaporate and the extra heat from the reaction will contribute to phase change rather than to an increase in temperature. Evaporation of water from the solution will cause the pOH of the solution to increase, resulting in a reduction of the reaction rate. In the following, the calculation is described in detail.

9.2.2 Overall kinetics for the hydrolysis of NaBH$_4$

In Chapter 8, the intrinsic kinetics expression (as given by equation (5.16)) was obtained

231

by investigating fine catalyst particle size in which the mass and heat transfer effects have been removed.

$$r_{H2} = 0.0949e^{0.0798T} \, pOH + 0.5238e^{0.085T} \qquad (5.16)$$

When particle size is increased, internal mass transfer is no longer negligible. This is taken into account by using an effectiveness factor η as reviewed in Chapter 5. For a zero-order reaction, the Thiele modulus ϕ is defined by equation (9.1)[1].

$$\phi = L\sqrt{\frac{k'}{2D_e C_{As}}} \qquad (9.1)$$

Where k' is the reaction rate constant based on the volume of total catalyst particles, D_e is the effective diffusivity of reactant in the catalyst particles, L is the characteristic length of a catalyst particle and C_{As} is the surface concentration of the reactant on the catalyst particles.

The rate data in the research is based on the weight of catalyst particles, which is related to k' by equation (9.2).

$$k\rho_c = k' \qquad (9.2)$$

Where k is the rate constant based on the weight of catalyst, and ρ_c is the density of the catalyst.

In the case of strong diffusion limitation ($\phi > 4$ or $\eta < 0.25$), effectiveness factor η and Thiele modulus have the following relationship [1]:

$$\eta = \frac{1}{\phi} \qquad (9.3)$$

Substitute equation (9.1) into equation (9.3) and L = R/2 for a cylindrical catalyst particle (R is the radius of the cylinder), yielding

$$\eta = \frac{2}{R}\sqrt{\frac{2D_e C_{As}}{k'}} \qquad (9.4)$$

232

Rearrange equation (9.4), yielding

$$D_e = \frac{\eta^2 R^2 k}{8 C_{As}}$$ (9.5)

The effectiveness factor η can be measured experimentally using the rate data for 2 mm cylindrical catalyst particles and the rate data for 0.049 mm catalyst particles in which there is effectively no diffusion limitation as shown in Chpater 6. The effective diffusivity can be then calculated using equation (9.5). It should be noted that the rate data used for the calculation should be based on the rate in regard to $NaBH_4$. Equation (9.6) can be used for the transformation of rate data in regard to hydrogen volume, to the rate data in regard to $NaBH_4$.

$$r_{H_2} = \frac{dV_{H_2}}{dt} = \frac{d(n_{H_2} RT_0 / P_0)}{dt} = \frac{d(n_{NaBH_4} RT_0 / 4P_0)}{dt} = \frac{RT_0}{4P_0} r_{NaBH_4}$$ (9.6)

After obtaining the value of effective diffusivity experimentally, effectiveness factor can be then calculated using equation (9.4) at any concentration and temperature. Hence, reaction rate with diffusion limitation can be calculated.

9.2.3 Heat transfer coefficient and heat loss

The heat loss of the reactor is the heat transfer from reactor to environment. The heat transfer can be calculated using equation (9.7).

$$Q = K_t S \Delta T_m$$ (9.7)

where K_t is the overall heat transfer coefficient, S is the heat transfer area, and ΔT_m is the average temperature difference.

The overall heat transfer coefficient can be calculated using equation (9.8).

$$\frac{1}{k} = \frac{x}{k_w} + \frac{1}{\alpha_A} + \frac{1}{\alpha_B}$$ (9.8)

where x is the thickness of the reactor wall, k_w is the thermal conductivity of the wall materials, α_A is the convective heat transfer coefficient of the fluid in the reactor and α_B is

the convective heat transfer coefficient of the air outside the reactor.

Fluid in the reactor is extensively stirred. Therefore, the convective heat transfer coefficient of the reaction fluid can be calculated using equation (9.9) [2].

$$Nu = 0.023 \, \mathrm{Re}^{0.8} \, \mathrm{Pr}^{0.4} \qquad (9.9)$$

where Nu is the Nusselt number, Re is Reynolds number and Pr is the Prandtl number. They are defined as follows:

$$Nu = \frac{\alpha L}{\lambda}$$

$$\mathrm{Re} = \frac{du\rho}{\mu}$$

$$\mathrm{Pr} = \frac{v}{\kappa}$$

where λ is the thermal conductivity of the fluid, η is the viscosity of the fluid, ρ is the density of the fluid, κ is the thermal diffusivity (which is equal to $\lambda/(\rho c_p)$), c_p is the specific heat capacity, L is the appropriate dimension and v is the kinematic viscosity of the fluid.

When the reactor is assumed to be in air, the air is in a natural convection state. The heat transfer coefficient can be calculated using equation (9.10) [3].

$$Nu = Nu_0 + Ra^{1/4} \left(\frac{f_4(\mathrm{Pr})}{5} \right)^{1/4} \qquad (9.10)$$

For a sphere, $Nu_0 = \pi$, and for a horizontal cylinder, $Nu_0 = 0.36\pi$. $f_4(\mathrm{Pr})$ in equation (9.10) is defined by equation (9.11).

$$f_4(\mathrm{Pr}) = \left[1 + \left(\frac{0.5}{\mathrm{Pr}} \right)^{9/16} \right]^{-16/9} \qquad (9.11)$$

Ra in equation (6.12) is the Rayleigh number. It is defined by equation (9.12).

234

$$Ra = \frac{g\xi\Delta Tl^{3}}{\nu\kappa} \tag{9.12}$$

where ξ is the coefficient of expansion of the fluid (per Kelvin), ΔT is the temperature difference between the surface and the bulk fluid, g is the acceleration due to gravity and l is the appropriate dimension (for a sphere or horizontal cylinder, $l = \pi D/2$. D is the diameter)

9.2.4 Calculation procedure

At the beginning of the calculation the following data is input. The other calculations are described in the next section.

T_0: ambient temperature

P_0: atmospheric pressure (assumed to be 101325 Pa)

t: time (initialised to be 0)

dW_{NaBH4}: differential amount of $NaBH_4$ that reacts at each step

w_{NaOH} : NaOH concentration (wt%)

W_{H_2O} : initial mass of water (g)

W_{NaBH_4} : initial mass of $NaBH_4$ (g)

The initial molality of $NaBH_4$ is calculated using equation (9.13).

$$m_{NaBH_4} = \frac{W_{NaBH_4}}{W_{H_2O}} \tag{9.13}$$

The heat generated when dW_{NaBH4} reacts can be calculated using equation (9.14).

$$Q = \frac{dW_{NaBH_4}}{37.84}\Delta H \tag{9.14}$$

where ΔH is the enthalpy change of the hydrolysis reaction of $NaBH_4$, which is 285 kJ mol^{-1}. Heat loss Q' in dt can be calculated using the equations in section 9.2.3. Temperature change of the solution is calculated using equation (9.15)

$$\Delta T = \frac{Q - Q'}{c_p W_{H_2O}}$$ (9.15)

where c_p is the heat capacity of the solution. The temperature of the solution is obtained using equation (9.16)

$$T = T + \Delta T$$ (9.16)

If T is greater than boiling point of the solution, T is given the value of the boiling point and the heat Q is in its entirety used to evaporate water, which can be calculated using equation (9.17).

$$\Delta W_{H_2O} = \frac{Q}{\Delta H_{evp}}$$ (9.17)

where ΔH_{evp} is the enthalpy change of water evaporation. The water remaining in the system after dW_{NaBH4} is obtained by equation (9.18)

$$W'_{H_2O} = W_{H_2O} - \Delta W_{H_2O}$$ (9.18)

The hydrogen that is generated when dW_{NaBH4} has reacted can be calculated using equation (9.19).

$$\Delta V_{H_2} = \frac{4 \Delta W_{NaBH_4}}{37.84} R T_0 / P_0$$ (9.19)

The by-product $NaBO_2$ that is produced when dW_{NaBH4} has reacted is calculated using equation (9.20)

$$dW_{NaBO_2} = (dW_{NaBH_4} / 37.84) \times 66.22$$ (9.20)

where 66.22 is the molecular weight of $NaBO_2$. The concentration of $NaBO_2$ in the system can be calculated using equation (9.21)

$$m_{NaBO_2} = \frac{W_{NaBO_2} / 66.22}{W_{H_2O}}$$ (9.21)

236

where W_{NaBO_2} is the accumulated amount of $NaBO_2$ in the solution. Equation (9.22) is used to calculate the OH^- concentration in the solution after obtaining the concentration of $NaBO_2$.

$$[OH^-] = \frac{-(m_{NaOH} + K) + \sqrt{(m_{NaOH} + K)^2 + 4Km_{NaBO_2}}}{2} + m_{NaOH} \qquad (9.22)$$

where $[OH^-]$ is the concentration of OH^- in the solution, and K is the equilibrium constant for the BO_2^- ions in water $(B(OH)_4^-)$: $B(OH)_4^- = H_3BO_3 + OH^-$. $K = 1.74 \times 10^{-5}$. After obtaining the OH^- concentration, pOH can be then calculated by using the definition (pOH $= -\ln[OH^-]$).

Intrinsic reaction rate can be then calculated using equation (5.16). Actual reaction rates can be calculated using equation (9.23).

$$r_{H_2} \text{ (real)} = r_{H_2} \text{ (instrinsic)} \eta W_{cat} \qquad (9.23)$$

where W_{cat} is the mass of catalyst. The reaction rate in terms of $NaBH_4$ can be obtained using equation (9.6).

The time dt needed to reacting dW_{NaBH4} can be then calculated using equation (9.24).

$$dt = \frac{dW_{NaBH_4}}{r_{NaBH_4} \text{ (real)}} \qquad (9.24)$$

The above procedure is repeated until all the $NaBH_4$ is reacted. In the following, two cases are discussed: isothermal reaction and non-isothermal reaction.

9.3 Results and Discussion

9.3.1 Determination of effective diffusivity of $NaBH_4$ in catalyst particles

The effective diffusivity of $NaBH_4$ in big catalyst particles, D_e, was determined experimentally using equation (9.5). The same procedure as in Chapters 6-8 was used in this chapter to derive isothermal reaction rates for fine catalyst particles and 2 mm x 3 mm catalyst particles. Figures 9.1 and 9.2 show the rate and temperature for fine and large particles respectively. The rate data for various $NaBO_2$ molalities and temperatures for the

two sizes of catalyst particles are listed in Tables 9.1-9.6. The measured effective diffusivities for temperatures from 25-75°C are given in the last column of the tables.
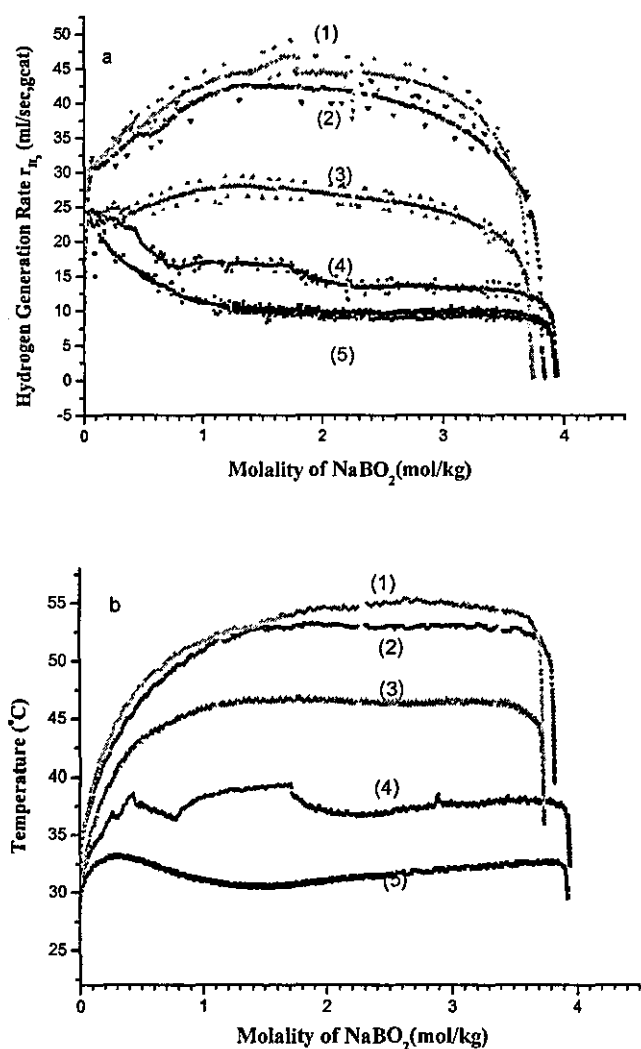
Figure 9.1 Rate of hydrogen generation for the hydrolysis of NaBH₄ at various temperatures when fine catalyst particles (0.049 mm) were used. The initial molality of NaBH₄ was 3.97 mol kg⁻¹. The hydrolysis was performed in 10 ml of water, using 0.3 g of catalyst. (a) Hydrogen production-time curves; (b) Temperature - time curves.
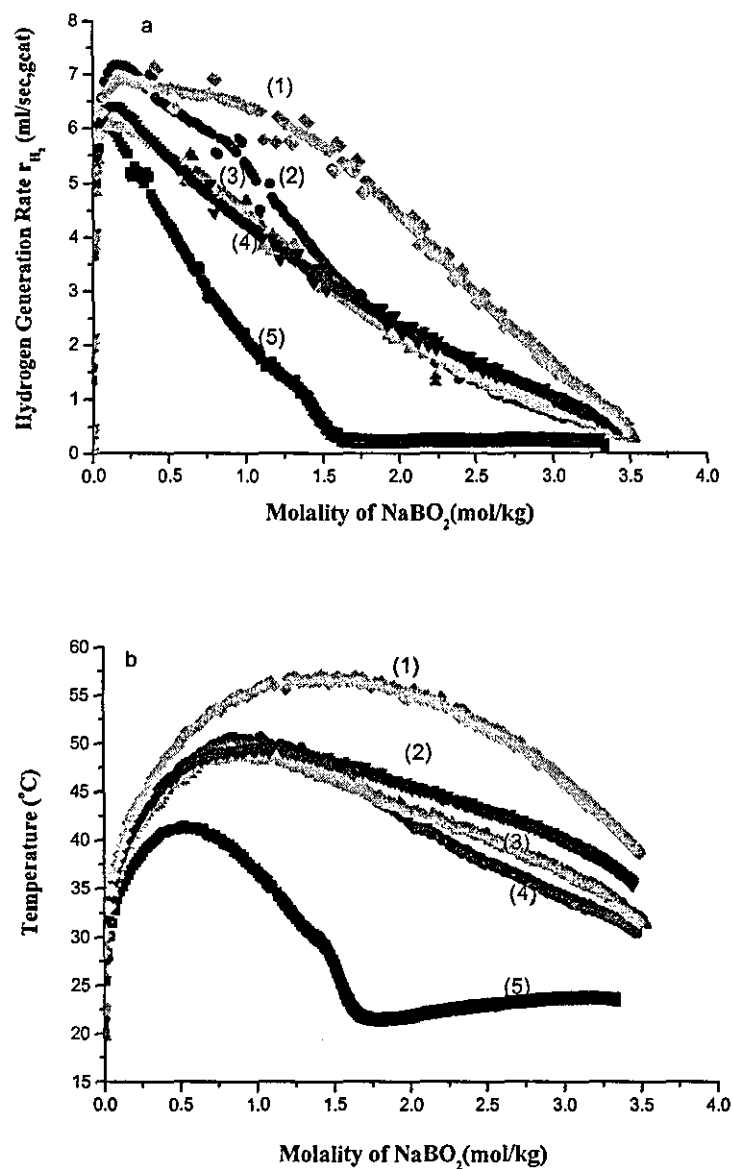
Figure 9.2 Rate of hydrogen generation for the hydrolysis of $NaBH_4$ at various temperatures when the catalyst was in the form of 2 mm x 3 mm cylinders. The initial molality of $NaBH_4$ was 3.97 mol kg^{-1}. The hydrolysis was performed in 10 ml of water, (a) Hydrogen production-time curves; (b) Temperature - time curves.

Table 9.1 Derivation of effective diffusivity D_e at 25°C.

m_{NaBO2} (mol kg^{-1})	r_{H2} (m^3/s gcat) (fine catalyst)	r_{NaBH4} (mol /s m^{3}cat) (fine catalyst)	C_{NaBH4} (mol/m^3)	r_{H2} (m^3/s gcat) (2mm catalyst)	η ($r_{H2\ 2mm\ cat}/r_{H2}$ fine cat)	D_e (m^2/s)
0.25	11.05	241.13	3715.00	2.34	0.21	3.65E-10
0.50	8.77	191.41	3465.00	1.66	0.19	2.48E-10
1.00	6.80	148.42	2965.00	0.95	0.14	1.23E-10
1.50	6.34	138.42	2465.00	0.46	0.07	3.65E-11
2.00	6.18	134.81	1965.00	0.31	0.05	2.18E-11
2.50	6.08	132.70	1465.00	0.31	0.05	2.94E-11
2.75	5.89	128.46	1215.00	0.33	0.06	4.17E-11
3.00	5.27	115.05	965.00	0.29	0.06	4.63E-11

Table 9.2 Derivation of effective diffusivity D_e at 35°C.

m_{NaBO2} (mol kg^{-1})	r_{H2} (m^3/s gcat) (fine catalyst)	r_{NaBH4} (mol /s m^{3}cat) (fine catalyst)	C_{NaBH4} (mol/m^3)	r_{H2} (m^3/s gcat) (2mm catalyst)	η ($r_{H2\ 2mm\ cat}/r_{H2}$ fine cat)	D_e (m^2/s)
0.25	21.00	458.44	3715.00	4.18	0.20	6.12E-10
0.50	16.58	361.90	3465.00	3.08	0.19	4.51E-10
1.00	13.74	299.98	2965.00	1.84	0.13	2.27E-10
1.50	12.85	280.40	2465.00	1.10	0.09	1.04E-10
2.00	12.60	275.11	1965.00	0.83	0.07	7.63E-11
2.50	12.62	275.35	1465.00	0.77	0.06	8.77E-11
2.75	12.07	263.41	1215.00	0.78	0.06	1.12E-10
3.00	10.88	237.52	965.00	0.72	0.07	1.35E-10

Table 9.3 Derivation of effective diffusivity D_e at 45°C.

m_{NaBO2} (mol kg^{-1})	r_{H2} (m^3/s gcat) (fine catalyst)	r_{NaBH4} (mol /s m^{3}cat) (fine catalyst)	C_{NaBH4} (mol/m^3)	r_{H2} (m^3/s gcat) (2mm catalyst)	η ($r_{H2\ 2mm\ cat}/r_{H2\ fine\ cat}$)	D_e (m^2/s)
0.25	38.35	837.07	3715.00	7.20	0.19	9.92E-10
0.50	30.12	657.42	3465.00	5.49	0.18	7.88E-10
1.00	26.58	580.06	2965.00	3.42	0.13	4.06E-10
1.50	24.89	543.35	2465.00	2.49	0.10	2.76E-10
2.00	24.59	536.78	1965.00	2.09	0.08	2.47E-10
2.50	25.00	545.75	1465.00	1.81	0.07	2.44E-10
2.75	23.65	516.29	1215.00	1.73	0.07	2.84E-10
3.00	21.47	468.52	965.00	1.67	0.08	3.66E-10

Table 9.4 Derivation of effective diffusivity D_e at 55°C.

m_{NaBO2} (mol kg^{-1})	r_{H2} (m^3/s gcat) (fine catalyst)	r_{NaBH4} (mol /s m^{3}cat) (fine catalyst)	C_{NaBH4} (mol/m^3)	r_{H2} (m^3/s gcat) (2mm catalyst)	η ($r_{H2\ 2mm\ cat}/r_{H2\ fine\ cat}$)	D_e (m^2/s)
0.25	67.50	1473.35	3715.00	11.98	0.18	1.56E-09
0.50	52.76	1151.57	3465.00	9.44	0.18	1.33E-09
1.00	49.37	1077.46	2965.00	6.12	0.12	6.98E-10
1.50	46.33	1011.28	2465.00	5.39	0.12	6.94E-10
2.00	46.07	1005.54	1965.00	4.96	0.11	7.41E-10
2.50	47.54	1037.52	1465.00	4.04	0.08	6.38E-10
2.75	44.50	971.25	1215.00	3.66	0.08	6.78E-10
3.00	40.63	886.70	965.00	3.67	0.09	9.38E-10

Table 9.5 Derivation of effective diffusivity D_e at 65°C.

m_{NaBO2} (mol kg^{-1})	r_{H2} (m^3/s gcat) (fine catalyst)	r_{NaBH4} (mol /s m^{3}cat) (fine catalyst)	C_{NaBH4} (mol/m^3)	r_{H2} (m^3/s gcat) (2mm catalyst)	η ($r_{H2\ 2mm\ cat}/r_{H2}$ fine cat)	D_e (m^2/s)
0.25	114.91	2508.01	3715.00	19.36	0.17	2.40E-09
0.50	89.41	1951.38	3465.00	15.73	0.18	2.18E-09
1.00	88.40	1929.40	2965.00	10.57	0.12	1.16E-09
1.50	83.13	1814.29	2465.00	11.13	0.13	1.65E-09
2.00	83.16	1814.99	1965.00	11.18	0.13	2.09E-09
2.50	87.00	1898.86	1465.00	8.58	0.10	1.58E-09
2.75	80.64	1760.10	1215.00	7.43	0.09	1.54E-09
3.00	74.04	1615.99	965.00	7.71	0.10	2.27E-09

Table 9.6 Derivation of effective diffusivity D_e at 75°C.

m_{NaBO2} (mol kg^{-1})	r_{H2} (m^3/s gcat) (fine catalyst)	r_{NaBH4} (mol /s m^{3}cat) (fine catalyst)	C_{NaBH4} (mol/m^3)	r_{H2} (m^3/s gcat) (2mm catalyst)	η ($r_{H2\ 2mm\ cat}/r_{H2}$ fine cat)	D_e (m^2/s)
0.25	189.72	4140.75	3715.00	30.42	0.16	3.58E-09
0.50	146.98	3207.98	3465.00	25.44	0.17	3.47E-09
1.00	153.08	3341.24	2965.00	17.70	0.12	1.88E-09
1.50	144.21	3147.47	2465.00	22.04	0.15	3.73E-09
2.00	145.09	3166.79	1965.00	24.07	0.17	5.54E-09
2.50	153.79	3356.68	1465.00	17.47	0.11	3.69E-09
2.75	141.23	3082.56	1215.00	14.47	0.10	3.33E-09
3.00	130.36	2845.29	965.00	15.52	0.12	5.23E-09

It can be seen from Tables 9.1-9.6 that the effectiveness factor is much less than 0.25. Therefore, the reaction of $NaBH_4$ is in the regime of strong diffusion limitation when the catalyst particles are 2 mm in size. It is thus reasonable that effective diffusivity can be calculated using equation (9.4). D_e depends both on the concentration of by-product $NaBO_2$ and on temperature. D_e was found to decrease with the increase of $NaBO_2$ and level off with a further increase of the concentration. The reason for this may be due to the blockage of catalyst pores. $NaBO_2$ may be saturated in the vicinity of the reaction site on the surface of the catalyst's pores.

The dependence of D_e on temperature can be described using equation (9.25).

$$D_e = D_{e0}e^{-E/RT} \tag{9.25}$$

where D_{e0} is the pre-exponential factor, and E is the activation energy for diffusion. Take the logarithm of both sides, yielding

$$\ln D_e = \ln D_{e0} - \frac{E}{RT} \tag{9.26}$$

$\ln D_e$ was plotted against $1/T$ at various $NaBO_2$ concentrations as shown in Figure 9.3. It can be seen that a good linear relationship between $\ln D_e$ and $1/T$ was obtained, indicating the applicability of equation (9.26). The E/R and $\ln D_{e0}$ values in equation (9.26) derived from Figure 9.3 are listed in Table 9.7. The relationships between $\ln D_{e0}$ and m_{NaBO2} and E/R and m_{NaBO2} are plotted in Figures 9.4 and 9.5 respectively. For the convenience of calculation, the curves were fitted using an index function with the form $f(x) = A-BC^x$, where A, B and C are parameters. They were determined using a least-square method. The resulting equations are (9.27) and (9.28) respectively. The choice of index is due to the characteristics of chemical reactions.

$$E/R = 10770.5 - 8196.3 \times 0.40^{m_{NaBO2}} \tag{9.27}$$

$$\ln D_{e0} = 12.0 - 23.9 \times 0.42^{m_{NaBO2}} \tag{9.28}$$
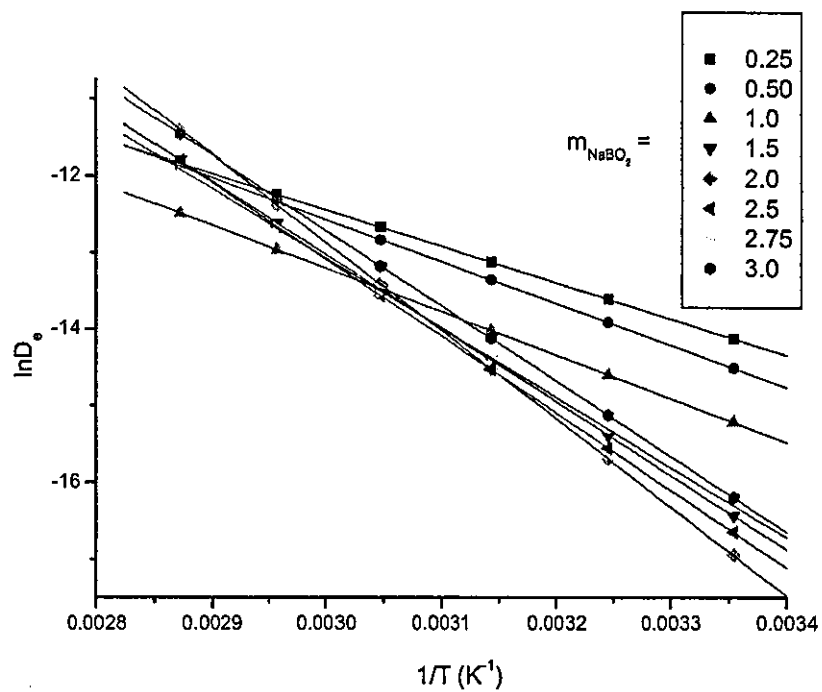
Figure 9.3 $\ln D_e$ versus $1/T$ at various $NaBO_2$ concentrations.

Table 9.7 Parameters for diffusion equation obtained from Figure 9.3.

m_{NaBO2} (mol/kg)	E/R	$\ln D_{e0}$	Regression Residue
0.25	4740.1	1.7689	1.0
0.5	5472.1	3.8386	1.0
1	5669.2	3.7944	1.0
1.5	9604	15.779	1.0
2	11494	21.606	1.0
2.5	10032	16.999	1.0
2.75	9089.1	14.187	1.0
3	9812.8	16.717	1.0

Figure 9.4 $\ln D_{e0}$ versus the molality of $NaBO_2$, m_{NaBO2}.
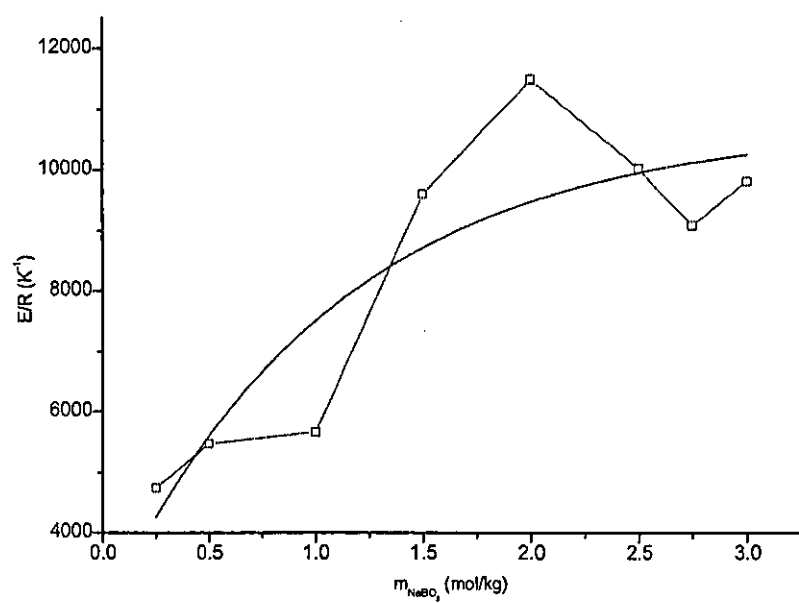
Figure 9.5 E/R versus the molality of $NaBO_2$, m_{NaBO2}.

9.3.2 Heat loss from a round-bottom flask to the surrounding environment

In this section, the heat transfer coefficient is estimated so that the model can be verified experimentally. The reactor is in an open laboratory, surrounded by air. Two situations are considered here.

Reaction solution properties (50°C) [4]:

$\rho = 979$ kg/m³; $c_p = 4.20$ kJ/(kg K); $\eta = 4.20 \times 10^{-4}$ N s/m²; $\nu = 3.75 \times 10^{-7}$ m²/s; $\lambda = 0.668$ W/(m K); Pr = 2.29.

Substitute the above properties into equation (9.9), yielding

$$\alpha_A = 0.023 \left(\frac{du\rho}{\mu} \right)^{0.8} \text{Pr}^{0.4} \frac{\lambda}{L} = 2162.5 \text{ W/(m}^2 \text{ K)}$$

Air properties (25°C) [4]:

$\rho = 1.16$ kg/m³; $c_p = 1.007$ kJ/(kg K); $\eta = 184.6 \times 10^{-7}$ N s/m²; $\nu = 15.89 \times 10^{-6}$ m²/s; $\lambda = 26.3 \times 10^{-3}$ W/(m K); $\kappa = 2.5 \times 10^{-6}$ m²/s; Pr = 0.707.

It is assumed that the round-bottom flask is a sphere and the surrounding temperature is constant at 25°C. A sphere has a characteristic length $L = \pi D/2 = 0.10$ m. The Rayleigh number is

$$Ra = \frac{g\xi(T_s - T_b)L^3}{\nu\kappa} = \frac{9.81 \times 3.22 \times 10^{-3} \times 45 \times 0.0785^3}{16.9 \times 10^{-6} \times 24.0 \times 10^{-6}} = 3.50 \times 10^6$$

Because Ra is less than 10^9, the flow of air on the surface of the reactor is laminar and the heat transfer coefficient is calculated using equation (9.10), where $\text{Nu}_0 = 3.14.$, $f_4(\text{Pr}) = 0.342$. Substitute the above value into equation (9.10), yielding

$\alpha_B = 6.64$ W/(m² K).

Glass properties:

$\rho = 2.50 \times 10^3$ kg/m³; $c_p = 480$ kJ/(kg K); $\lambda = 15.1 \times 10^{-3}$ W/(m K); $\kappa = 3.91 \times 10^{-6}$ m²/s.

The thermal conductivity of the reactor material is 100 W/(m² K). It can be seen that the

thermal transfer resistance is mainly due to air. Therefore, the conductive heat loss is about 6.64 $W/(m^2 K)$.

9.3.3 Modelling the isothermal generation of hydrogen

The first case to study in order to verify the model is that of the generation of hydrogen in an isothermal reaction when large catalyst particles are used. Figures 9.6-9.8 show the model prediction and experimental results for isothermal reactions at $25°C$, $30°C$, and $40°C$ respectively. The extent of the reaction was indicated by the production of $NaBO_2$. The experimental data are consistent with the model prediction.

Unlike fine catalyst particles, with which there is no diffusion limitation, large particles saw a rapid decrease in reaction rate. The same trend occurred regardless of the temperature change. This indicates that the hydrolysis of $NaBH_4$ does not proceed in zero-order reaction with regard to the concentration of $NaBH_4$. This is consistent with theoretical prediction [1].
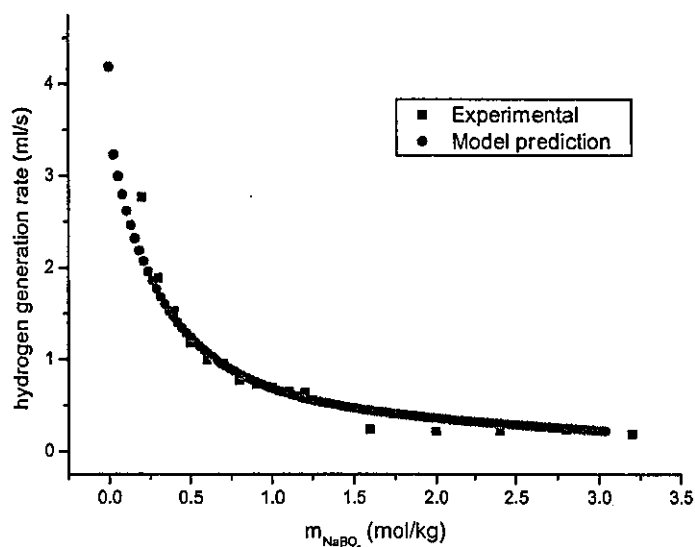
Figure 9.6 Comparison between experimental and model prediction. Reaction temperature $=20°C$, NaOH = 0, catalyst = 3g, $NaBH_4$ 1.5g in 10g of water.
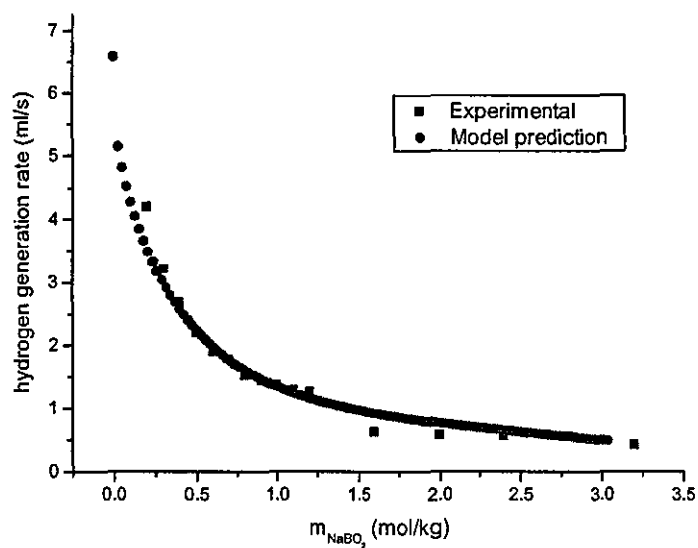
Figure 9.7 Comparison between experimental and model prediction. Reaction temperature =30°C, NaOH = 0, catalyst = 3g with a particle size of 2 mm x 3 mm, NaBH$_4$ 1.5g in 10g of water.
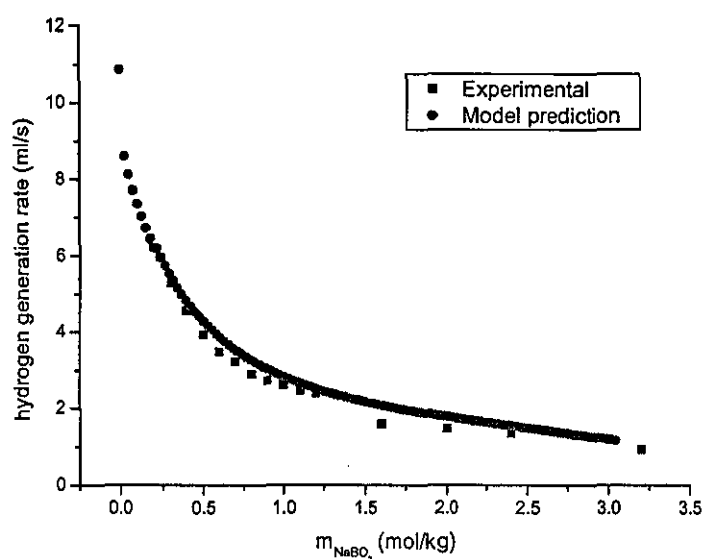
Figure 9.8 Comparison between experimental and model prediction. Reaction temperature =40°C, NaOH = 0, catalyst = 3g with a particle size of 2 mm x 3 mm, NaBH$_4$ 1.5g in 10g of water.

9.3.4 Modelling the non-isothermal generation of hydrogen

Figure 9.9 shows results from the non-isothermal generation of hydrogen. The reaction was conducted in a round-bottom flask in air, hence the heat loss is due to mainly the heat transfer from the reactor wall to the air. As can be seen from Figure 9.9, non-isothermal hydrolysis proceeded with an auto-acceleration at around 80 seconds. This is due to the temperature increase resulting from retained heat, since this was not dispersed to the air around the fast at a sufficient rate. The experimental results and model prediction are in good agreement. This supports the validity of the model.
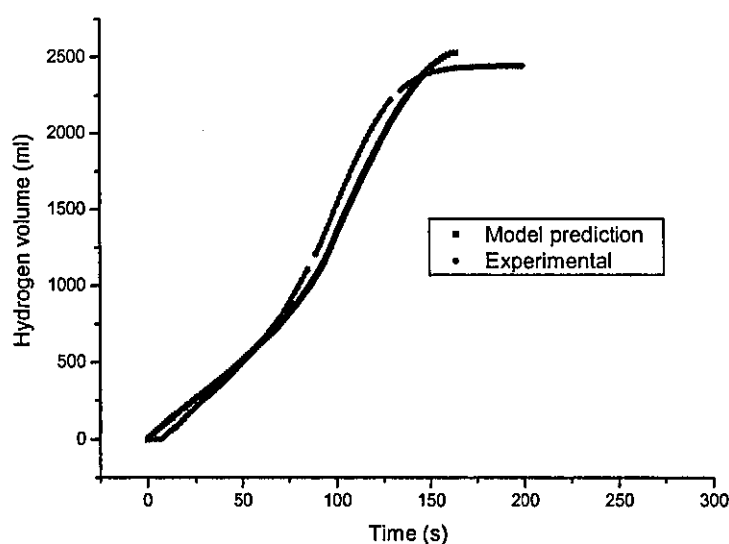
Figure 9.9 Comparison between experimental and model prediction for a non-isothermal reaction. NaOH = 0, catalyst = 3g with a particle size of 2 mm x 3 mm, $NaBH_4$ = 1.0g in 10g of water.

9.4 Conclusions

In this chapter, heat and mass transfer were built into the intrinsic rate expression obtained in Chapter 8 through use of the Thiele modulus. The effective diffusivity of $NaBH_4$ in catalyst pores was experimentally measured. The model was then validated through both isothermal and non-isothermal hydrolysis of $NaBH_4$. From the study, the following conclusions can be reached:

- When large catalyst particles are used, strong diffusion limitation is observed for the hydrolysis of $NaBH_4$, which can be seen from the very low efficiency factor

that was obtained experimentally.

- The effective diffusivity of $NaBH_4$ in catalyst pores depends on both the temperature and the concentration of $NaBO_2$. The dependence on the latter may be due to local saturation of $NaBO_2$ in the vicinity of active sites of the catalyst surface.

- In the region of diffusion limitation, reaction order to $NaBH_4$ is not zero-order. The reaction rate decreases rapidly with a decrease in $NaBH_4$ concentration.

- After combining intrinsic kinetics with diffusion limitation, heat generation and water evaporation, the model can be used to predict hydrogen generation from the hydrolysis of $NaBH_4$. The validation of the model has been performed for both isothermal and non-isothermal hydrolysis.

9.5 References

1. Levenspiel, O., *Chemical Reaction Engineering*. 3rd ed. 1999, New York: John Wiley & Sons. 389-390.

2. Hewitt, G.F., Shires, G.L., and Bott, T.R., *Process Heat Transfer*. 1994, Boca Raton: CRC Press. 104-105.

3. Hewitt, G.F., Shires, G.L., and Bott, T.R., *Process Heater Transfer*. 1994, Boca Raton: CRC Press. 108-115.

4. Hewitt, G.F., Shires, G.L., and Bott, T.R., *Process Heat Transfer*. 1994, Boca Raton: CRC Press. Appendix.

Chapter 10

Conclusions and Future Work

10.1 Conclusions

Hydrogen storage is an ongoing problem for hydrogen economy. The use of metal hydrides is the most promising and constitutes a significant area of focus for world research into hydrogen storage. An attempt in this thesis has been made to glean insights into the use of the hydrolysis of sodium borohydride for hydrogen storage. This thesis has been centred around the two issues relating to the use of $NaBH_4$: the maximum concentration and the rate of hydrogen generation.

The maximum concentration of $NaBH_4$ in its hydrolysis system was studied in Chapters 3 and 4 using a thermodynamic approach, in the presence or absence of NaOH.

- The relationship between solubility and temperature was derived thermodynamically based on the equality of chemical potential of a solute in its solution and in its solid state as shown below:

$$\ln m_{\pm} = -\frac{\Delta H^{\circ}_{m,B}}{v_{\pm}RT} + \frac{\Delta S^{\circ}_{m,B}}{v_{\pm}R} - \ln \gamma_{\pm} \quad \text{(no NaOH)}$$

$$\ln m_{\pm,B} + \ln \frac{\gamma'_{\pm}}{\gamma_{\pm}} = -\frac{\Delta H^{0}_{m,B}}{2RT} + \left(\frac{\Delta S^{0}_{m,B}}{2RT} - \ln \gamma_{\pm} \right) \quad \text{(with NaOH)}$$

- The solubility of $NaBH_4$ was obtained by analysis of the phase diagram of the $NaBH_4$-$NaOH$-H_2O system.

- The solubility of $NaBO_2$ was obtained by analysis of the phase diagram of the $NaBO_2$-$NaOH$-H_2O system, which was derived from the phase diagram of the Na_2O-B_2O_3-H_2O system by setting Na_2O:B_2O_3 = 1:1.

251

- The value of $\dfrac{\gamma'_\pm}{\gamma_\pm}$ in the presence of NaOH was calculated from phase diagrams using the hydration analysis method.

- By plotting the left hand side of the equations against 1/T, the equations when NaOH is absent are

$$\ln m_{\text{NaBH}_4} = -\frac{1982.3}{T} + 9.47$$

$$\ln m_{\text{NaBO}_2} = -\frac{2912.9}{T} + 11.37$$

- The equations when NaOH is present are

$$\ln m_{\pm, Na\text{BH}_4} + \ln \frac{\gamma'_\pm}{\gamma_\pm} = -\frac{1920.2}{T} + 9.3$$

$$\ln m_{\pm, Na\text{BO}_2} + \ln \frac{\gamma'_\pm}{\gamma_\pm} = -\frac{3008.5}{T} + 11.7$$

- From the thermodynamic modelling and experimental validation of the model, the maximum concentration of sodium borohydride is determined mainly by the solubility of the by-product $NaBO_2$ at a given reaction temperature and concentration of NaOH. The maximum concentration increases with an increase in reaction temperature and decreases with an increase in NaOH concentration.

The rate of hydrogen generation was studied in Chapters 5-9. Chapters 5-8 determined experimentally the intrinsic kinetic expression for the hydrolysis and in Chapter 9 the overall kinetic model was established and validated experimentally.

Four factors were examined that affect the intrinsic rate of hydrogen generation: temperature, NaOH concentration, $NaBH_4$ concentration and $NaBO_2$ concentration. The following conclusions were drawn.

- The rate of $NaBH_4$ hydrolysis is strongly dependent on the basicity of the solution

and the reaction temperature.

- The rate of hydrolysis is zero- order with respect to the concentration of $NaBH_4$.

- The rate of hydrolysis rate can be expressed using the following equation:

$$r_{H2} = 0.0949e^{0.0798T} \, pOH + 0.5238e^{0.085T}$$

- When large catalyst particles are used, the rate of reaction is limited by significant pore diffusion effects. The magnitude of these effects is dependent upon both the reaction temperature and the concentration of $NaBO_2$.

- A kinetic model that combines both the intrinsic kinetic rates and diffusion limitations has been validated experimentally using isothermal and non-isothermal reactions.

10.2 Future Work

This thesis has focused on the understanding of the sodium borohydride hydrolysis reaction, specifically relating to the effects of concentration and temperature. There are several directions in which the present research could be extended.

10.2.1 The Transformation of Sodium Metaborate to Sodium Borohydride

Recycling sodium metaborate back to sodium borohydride is essential in order to facilitate practical usage of this method of hydrogen storage. In Chapter 2, possible routes for this transformation were proposed. Experimental work needs to be undertaken in order to refine the required operating conditions for the proposed processes.

10.2.2 Application of the Hydrogen Generation System to Fuel Cells

A fuel cell is a device that continuously converts the chemical energy of the hydrogen and oxygen reaction into electric energy needed to drive motors. When the hydrogen generated from the hydrolysis of $NaBH_4$ is used in fuel cells, a detailed design should be produced in order to improve the observed energy density. This design might include the utilisation of the water produced from the fuel cell system, the design of a suitable feeding system for $NaBH_4$, and the design of a suitable reactor for controlled generation of hydrogen. Modelling work is also necessary in order to predict the efficiency of the

system.

10.2.3 Development of High Efficiency Catalysts for the Hydrolysis of NaBH$_4$

Development of high efficiency catalysts for the hydrolysis of NaBH$_4$ is another aspect of work that could be performed, since this can improve the conversion efficiency of NaBH$_4$. One possible route is to develop a new catalyst, another would be to develop a new carrier for an existing metal catalyst.

Intrinsic kinetics of NaBH$_4$ hydrolysis over carbon

supported ruthenium

Y Shang[1], R Chen[1], G Jiang[2]

[1]Department of Aeronautic and Automotive Engineering, Loughborough University, Loughborough,

Leicestershire LE11 3TU, UK

[2]School of Mechanical, Materials and Manufacturing Engineering, University of Nottingham,

Nottingham NG7 2RD, UK

Abstract

Hydrolysis of sodium borohydride (NaBH$_4$) is a promising route for on-board hydrogen generation. Carbon supported ruthenium is one of the most efficient catalysts. This paper presents an investigation of the intrinsic kinetics for the hydrolysis of NaBH$_4$ over the catalyst. For kinetic analysis, a new experimental method was designed to obtain isothermal rate data from non-isothermal hydrolysis. It was found that the hydrolysis reaction is a zero-order reaction with respect to NaBH$_4$ concentration. The hydrolysis rate decreased with an increase of the basicity of NaBH$_4$ aqueous solution.

Key Words

Sodium borohydride, intrinsic kinetics, hydrolysis, ruthenium

1. Introduction

On-board hydrogen generation is one of the challenging problems for the application of hydrogen energy to automobiles. Many methods have been designed to meet the challenge, including pyrolysis of metal hydrides (e.g. LiH, MgH_2),[1] hydrogen release from hydrogen adsorption materials (e.g. carbon nanotubes),[2] compressed hydrogen tanks,[3] and hydrolysis of metal hydrides.[4] Among these methods, hydrolysis of $NaBH_4$ has attracted attention due to its stability and the convenience of hydrogen production and relatively high energy density.[4-8]

The hydrolysis of $NaBH_4$ is shown in Scheme 1. One mole of $NaBH_4$ produces four moles of hydrogen, half of which is extracted from water. A catalyst is necessary for an efficient hydrolysis. The catalysts for borohydride hydrolysis include acids,[9] metal halides such as $NiCL_2$, $CoCl_2$,[10] and the most efficient transition metal catalysts.[10]

$$NaBH_4 + 2H_2O = NaBO_2 + 2H_2O$$
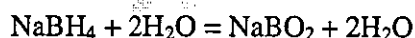
Scheme 1. The hydrolysis of sodium borohydride

Acid catalysis is now well understood. However, the kinetics for metal catalysis has little been investigated. Metal catalysts are often supported on carriers for practical applications. The catalyst particles have a porous structure. Complex heat and mass transfer processes are involved in the heterogeneous catalytic reaction, which frequently impact upon the overall performance of a heterogeneous catalytic reaction. For rational design of a chemical reactor for on-board hydrogen generation, the first step is to get intrinsic rate expression and then heat and mass transfer effects are built into the intrinsic rate expression to obtain an overall rate expression.

Accurate kinetic rate equations can seldom be extracted from data obtained under the influence of significant heat and/or mass transport limitations. Thus it is important that the rate data obtained from kinetic runs be acquired in the regime of kinetic control.

In a heterogeneous catalytic reaction, heat removal is a difficult factor to overcome in order to obtain

isothermal rate data. A number of different batch reactors have been designed. The main consideration

for design an experiment to obtain isothermal rate data is to remove heat generated efficiently by

minimizing the contact time for reaction mixture and catalyst in one cycle such as the well-known

Carberry reactor.[11] However, the method will not work for studying the hydrolysis of NaBH$_4$ since

NaBH$_4$ hydrolysis has a significant rate at higher temperatures even without the presence of a catalyst.

Another difficulty is to separate the effects of NaBH$_4$ and NaBO$_2$, since the two materials always comes

together during the reaction.

In this work, instead of making an effort to control reaction temperature precisely and attempting to

separate the effects of NaBH$_4$ and NaBO$_2$, an alternative method was developed. This approach does not

involve a new reactor design, but uses a new method of analyzing the non-isothermal rate data to obtain

isothermal rate data. This paper reports an investigation of the intrinsic kinetics of NaBH$_4$ hydrolysis

over ruthenium catalyst using this method.

2. Experimental

2.1 Data analysis method

The rate for any reaction can be expressed approximately using equation (1).

$$r = Ae^{-E/RT}C^{\alpha} \tag{1}$$

where r is the reaction rate, E is the activation energy, R is the universal gas constant, T is the

temperature, C is the concentration of reactant, α is the reaction order, and A is the pre-exponential

factor. To deriving isothermal rate data from non-isothermal reaction, take logarithms of both sides,

yielding

$$\ln r = \ln A + \alpha \ln C - \frac{E}{RT} \tag{2}$$

Since A and α are constants for a specific reaction, ln$r$ against 1/T will have a linear relationship when

C is fixed. Several runs can be performed with the same initial NaBH$_4$ concentration but with a different

initial reaction temperature, and then a series of hydrogen release curves can be obtained. At a given

$NaBO_2$ concentration m_{NaBO2}, reaction rates and the corresponding reciprocal temperatures ($1/T$) are plotted the result should be linear, with a slope corresponding to $-E/R$, and an intercept on the y axis of $\ln A + \alpha \ln C$. After determination of equation, reaction rate at temperature T can be determined using equation (2) at m_{NaBO2}.

If several groups of the above experiments are performed, and each group has a different initial $NaBH_4$ concentration, reaction rate at m_{NaBO2} can be determined in each group for temperature T. Since initial $NaBH_4$ concentration in each group is different, $NaBH_4$ concentrations at m_{NaBO2} are different. Therefore, isothermal rate data for temperature T is obtained.

2.2 Experimental procedure

2.2.1 Materials

Sodium borohydride ($NaBH_4$), and sodium hydroxide ($NaOH$) were both purchased from Sigma-Aldrich, with a purity of 98.0% (wt) and 99.9 % (wt) respectively. $NaBH_4$ was used without further purification. Ruthenium on carbon was purchased from Johnson Matthey. The catalyst contained 3% (wt) ruthenium. It had a cylindrical shape with a size of $\phi 2$ mm x 3 mm.

2.2.2 Catalyst Grinding

The catalyst particles must be fine enough so that internal diffusion can be neglected. In this study, the catalyst was ground using a pestle and mortar and then sieved using a set of sieves with different mesh apertures (Fisher Scientific Ltd). Eight different sieves were stacked on top of each other, and the average diameters of the catalyst particles trapped in each sieve were assumed to match the average aperture sizes of the two adjacent sieves. The catalyst size obtained were 550 μm, 98 μm, 49 μm and 29 μm respectively.

2.2.3 Experimental rig

The measurement of the concentration of $NaBH_4$ is rather difficult due to its hydrolysis even at room temperature. In this study, a method for measuring the hydrogen volume with time was used, since hydrogen volume and $NaBH_4$ concentration can be related using the stoichiometric coefficients in the Scheme 1.

A schematic diagram for the experimental set-up is shown in Figure 1. The rig consisted of three parts: the reaction system, a sytem to monitor temperature and a system to measure the volume of hydrogen that is generated. The reaction system consists of a three-port reactor and a magnetic stirrer, a water bath that was used to adjust reaction temperature and a feeding system. One side-port of the reactor was equipped with a thermocouple and another side-port was connected to the water replacement system. The middle port of the reactor was used to site a feeding funnel. Since $NaBH_4$ can be hydrolysed even at room temperature when contacting water, a special feeding system was used as shown in Figure 3. $NaBH_4$ and catalyst were added to the reactor first and then water was added through the feeding system to the reactor. Once the chemicals come into contact, hydrogen is produced and the amount that was generated was recorded.

The volume of hydrogen that was produced was measured using a water replacement system. The water replacement system consisted of a graduated cylinder full of water and a water reservoir that was used to immerse the cylinder. A container was placed onto an electronic balance. Before starting the experiment, the water in the reservoir was filled to such a level that any extra water would overflow from the cylinder through a slope into the container on the balance. The electronic balance was connected to a computer using a standard RS232 connector. Software provided by the balance manufacturer was used to record the time and the weight of the water displaced from the cylinder. The time interval for recording the weight was one second. Both the software and the electronic balance were purchased from A & D Company Ltd. (UK).

In order to monitor the temperature of the reaction system, a thermocouple was put into a side port of the reactor. This K-type thermocouple was connected to a data logger, which transferred the information to a computer. The data logger and the thermocouple were purchased from Pico Company Ltd (UK).

Before conducting the experiment, the reactor was cleaned using distilled water and then dried in an oven for 24 hours. After the temperature was stable, the reactor was put into the water bath with a fixed amount of catalyst inside. A pre-determined amount of $NaBH_4$ powder was then put into the reactor. After all these were ready, the cork of the feeding funnel was opened to let the water flow into the

reactor to start the hydrolysis. The water that was displaced by the hydrogen production and the overall

reaction temperature were both monitored by using the computer. When calculating the reaction rate, the

saturated vapour pressure at room temperature was considered.

The amount of catalyst that was used was based on the convenience of reaction control. Reaction rate

for heterogeneous catalysis is proportional to the mass of catalyst. The rate data is based on unit mass of

catalyst.

Figure 1 A schematic experimental set-up for the research of NaBH$_4$ hydrolysis kinetics.

3. Results and Discussion

3.1 Removal of diffusion limitation

Figure 2 shows the comparison of the hydrogen generation rate using three different stirring rates (0

rpm, 390 rpm, and 650 rpm) at three different temperatures (20°C, 30°C, and 40°C). At each temperature

and stirring rate, hydrogen generation rate decreased rapidly with the proceeding of the hydrolysis. The

reaction rate increased steadily with the increase of the reaction temperature from 20°C to 40°C. At any

reaction temperature, the stirring rate showed little effect when the concentration of NaBO$_2$ was greater

than 0.2 mol/kg, which corresponded to the hydrolysis of 10% of NaBH$_4$. However, stirring rate showed

some effect on initial stages of the hydrolysis. At 20°C, initial reaction rate did not change significantly

with stirring rate. This situation changed at higher temperatures. At 30°C, reaction rate was 13.2 ml/sec

gcat when there was no stirring. It increased to 13.9 ml/sec gcat for a stirring rate of 390 rpm and 14.9

ml/sec gcat for a stirring rate of 650 rpm. At 40°C, initial reaction rate was 23 ml/sec gcat when there

was no stirring. It increased to 27.5 ml/sec g cat for a stirring rate of 390 rpm and to 28.5 ml/sec gcat for

a stirring rate of 650 rpm.
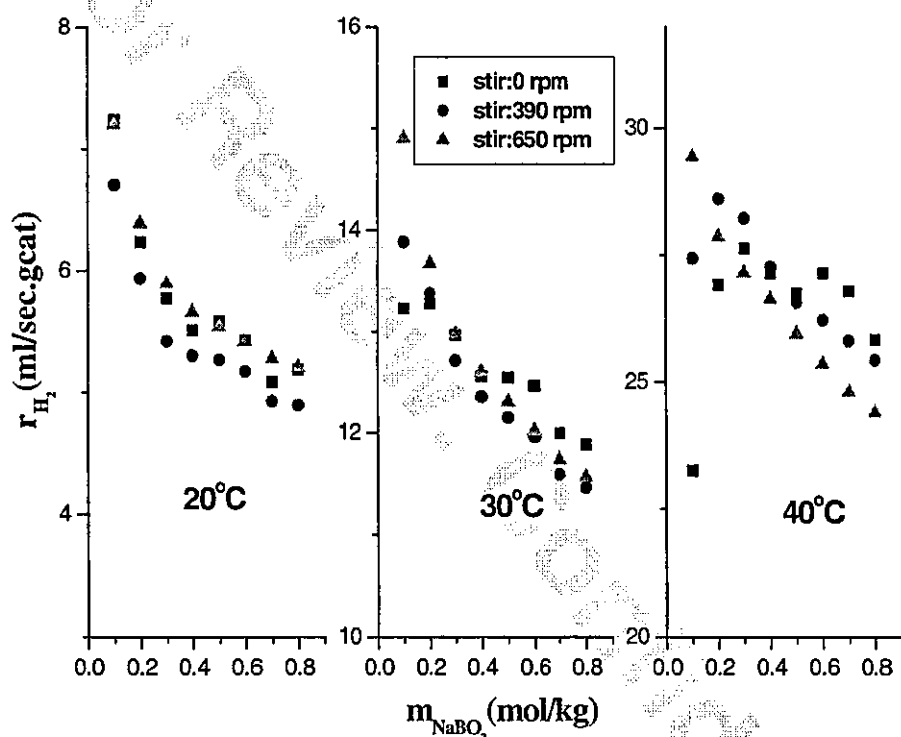
Figure 2 Comparison of the effect of stirring rate on reaction rate. The catalyst particles used had an

average size of 0.049 mm. The reaction was conducted using 0.5g NaBH$_4$ in 10 ml of water.

When the reaction temperature is low, reaction rate is low. Hence, it does not need a high rate of

stirring in order to provide a high rate of mass transfer from the bulk fluid to the catalyst particles.

Therefore the stirring rate, and thus the external mass transfer, is not significant at lower temperatures.

At the other hand, the hydrogen gas produced agitated the reaction solution violently. The effect of

hydrogen gas agitation made the effect of stirring rate on external mass transfer not significant. When

the reaction temperature increases, the reaction rate increases exponentially. In this case a high rate of

mass transfer is required in order to provide NaBH$_4$ to the catalyst. Therefore, stirring rate has a

significant effect on hydrogen generation rate especially at early stages of the hydrolysis. With the

agitation effect of the hydrogen gas produced, the role of stirring rate becomes less important. However, the difference between reaction rate at 390 rpm and 650 rpm was very small, less than 10%, even at early stages. Therefore, it can be concluded that 650 rpm is high enough to remove external diffusion limitation for the reaction. In the following work, the stirring rate was fixed at 650 rpm.

Internal diffusion refers to the mass transfer within a catalyst particle. It is affected mainly by the size of particle that is used. When the particle size is fine enough, the internal mass transfer limitation can be removed. It is thus necessary to determine the particle size for which the internal mass transfer rate does not limit reaction rate. In order to investigate this, it is necessary to compare the reaction rate at various sizes of catalyst particle whilst the temperature and the $NaBH_4$ and $NaBO_2$ concentrations are fixed. Also, a sufficiently high stirring rate is employed, as per the results of Figure 2, so that the effects of external diffusion are removed.
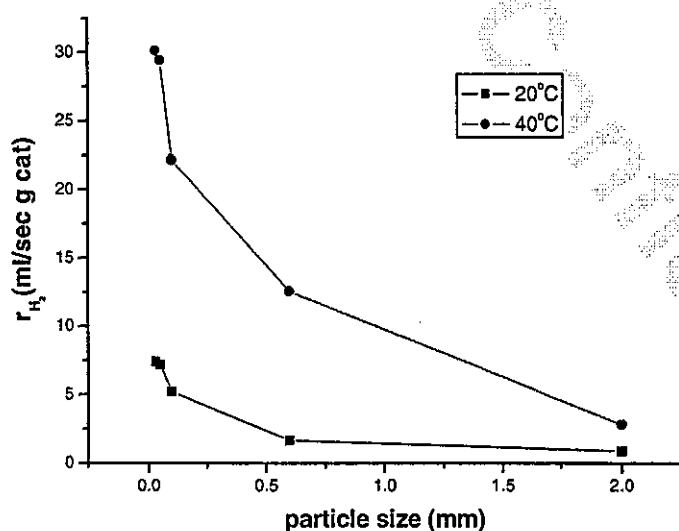
Figure 3 Comparison of the reaction rate at various temperatures for different catalyst particle sizes. The reaction was performed using 0.5 g $NaBH_4$ in 10 ml of water.

The reaction rates at various reaction temperatures for different particle sizes are compared in Figure 3 for two temperatures (20°C and 40°). At both temperatures, the reaction rate increased significantly with a decrease in catalyst particle size. This suggests that the hydrolysis of $NaBH_4$ in the presence of a carbon supported ruthenium catalyst has a strong internal diffusion limitation when the catalyst particles

are large. When the catalyst particle size is reduced to around 0.049 mm, the internal diffusion limitation is removed. This trend did not change with reaction temperature, as shown in Figure 3.

This indicates that the limiting effects of internal diffusion can be removed by using a catalyst particle size of less than 0.049 mm for the hydrolysis of $NaBH_4$ over a carbon supported ruthenium catalyst. Therefore, in the study of intrinsic kinetics, 0.049 mm catalyst particles and a stirring rate of 650 rpm are used.

3.2 Effect of $NaBO_2$ and $NaBH_4$ concentrations

Figure 4 shows the dependence of hydrogen generation rate on $NaBH_4$ concentration at three different temperatures for three different $NaBO_2$ molalities. The rate of hydrogen generation for a fixed concentration of $NaBO_2$ did not vary significantly with the change of the concentration of $NaBH_4$. This trend did not change at different temperatures. This indicates that the hydrolysis of $NaBH_4$ does not depend on $NaBH_4$ concentration, i.e. it is a zero-order reaction with regard to $NaBH_4$ concentration.

There are three main steps in the hydrolysis of $NaBH_4$ on a catalyst surface: adsorption of $NaBH_4$, hydrolysis reaction of $NaBH_4$ on catalyst surface and desorption of H_2 from the catalyst surface. The rate of hydrogen generation is zero order with respect to $NaBH_4$, indicating that desorption of hydrogen from the catalyst surface is the rate-determining step.

The dependence of hydrogen generation rate on the concentration of $NaBO_2$ at different temperatures is shown in Figure 5. At the earlier stages of the reaction, the reaction rate decreased with the increase of $NaBO_2$ concentration and the reaction rate leveled off at later stages. Since $NaBO_2$ is a base, it indicates that the hydrolysis reaction involves the hydrogen ion.
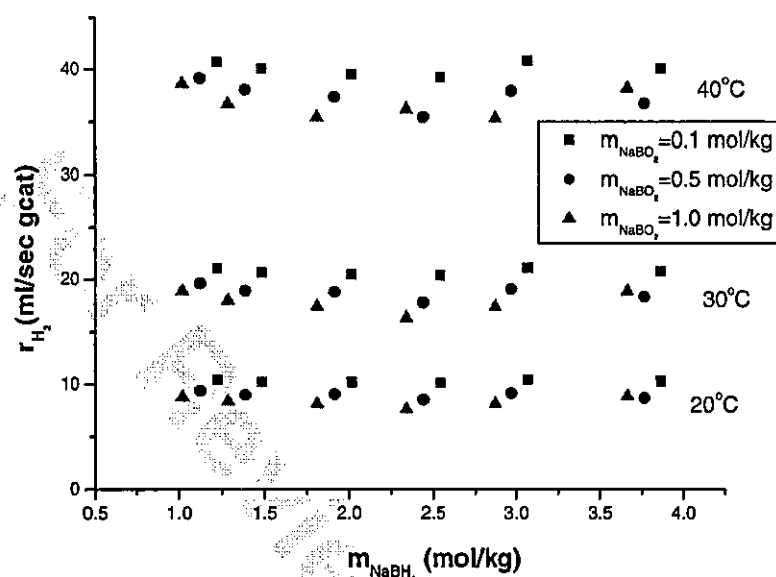
Figure 4 Hydrogen generation rate versus the molality of $NaBH_4$.
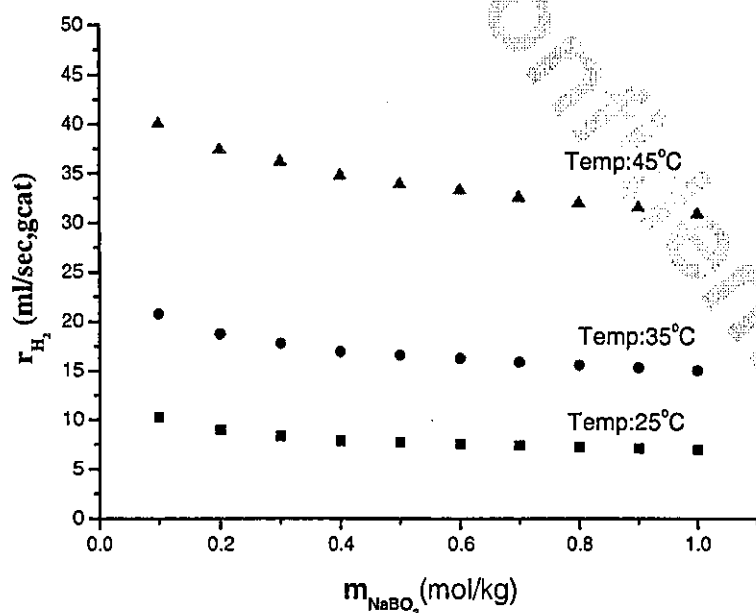
Figure 5 The relationship between r_{H2} and the molality of $NaBO_2$.

3.3 Effect of NaOH concentration

Since hydrogen generation rate depends on the concentration of base and NaOH is often used as a

stabilizer for $NaBH_4$ aqueous solutions, it is thus interesting to investigate the dependence of hydrogen

generation rate on NaOH concentration. It has been shown that the reaction rate was independent of

$NaBH_4$ concentration in previous sections. Therefore, it is only necessary to compare rate data at fixed

temperatures and $NaBO_2$ concentrations. Figure 6 shows the dependence of reaction rate on NaOH

concentrations at 20°C and 40°C.
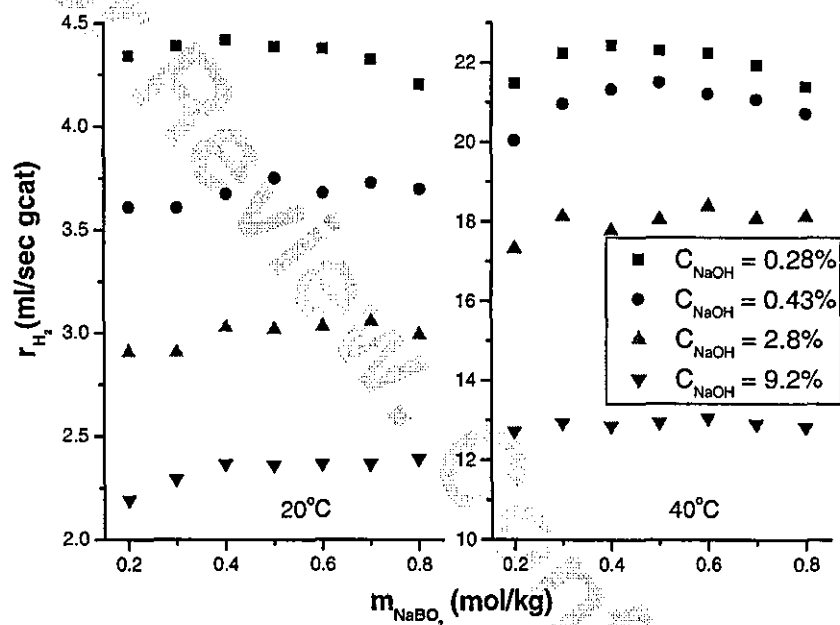
Figure 6 Reaction rate versus molality of $NaBO_2$ at 20°C and 40°C for various NaOH concentrations.

At both temperatures, with the increase of NaOH concentration, reaction rate decreased rapidly. For

example, at 20°C, the hydrogen generation rate decreased from 4.3 ml/sec gcat at a NaOH concentration

of 0.28% to about 2.3 ml/sec g cat when the concentration of NaOH increased to 9.2%. However, at a

specific temperature, the reaction rate changed within a very small range in the presence of NaOH when

compared with the rate in the absence of NaOH, which is shown in Figure 5. In the absence of NaOH,

the pH value of the $NaBO_2$ solution changes significantly, moving from neutral (pH = 7) to strongly

basic (pH = 12.5 according to the equilibrium $B(OH)_4^- = H_3BO_3 + OH^-$, K = 1.73 x 10^{-5}). The pH of the

solution does not change significantly in the presence of NaOH due to the high concentration of OH^-.

Since the basicity of the solution is stable in the presence of NaOH, it is consistent with the previous

conclusion that the reaction is zero-order with respect to the concentration of $NaBH_4$.

3.4 Intrinsic rate expression

Since the reaction rate is zero order with respect to the concentration of $NaBH_4$, $NaBH_4$ should not be included in the rate expression. The rate is only related to the basicity of the solution and the reaction temperature. In order to obtain the relationship between the reaction rate and the basicity of the solution, the rate of hydrogen generation r_{H2} was plotted against pOH. Here pOH is defined as $ln1/[OH^-]$. As shown in Figure 7, r_{H2} and pOH had a linear relationship. The relationship between r_{H2} and pOH may thus be expressed by using equation (3).

$$r_{H2} = A \cdot pOH + B \qquad\qquad (3)$$

The parameters A and B for the linear equations at various temperatures and residual square root are given in Table 1.
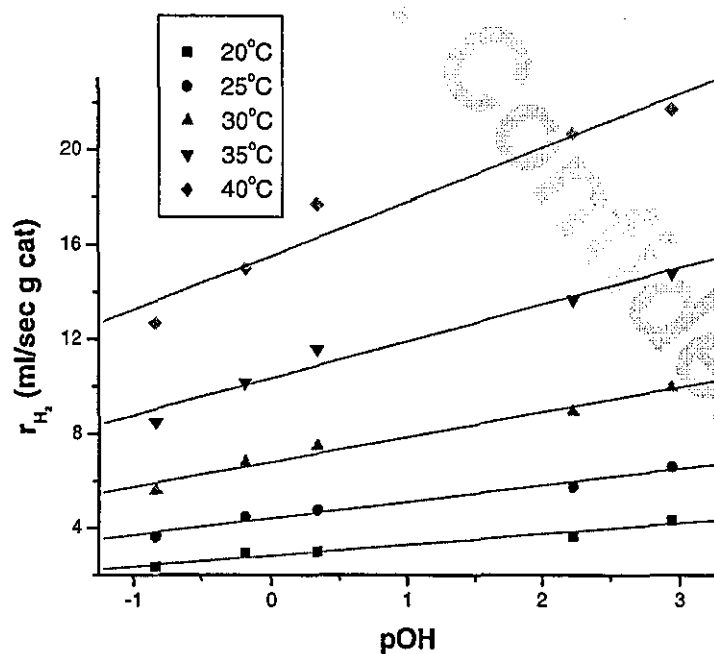
Figure 7 r_{H2} versus pOH and their linear regressions.

Table 1 The values of A and B of the regressed equations in Figure 7.

Temperature (°C)	A	B	Error (R^2)
20	0.4619	2.8219	0.98
25	0.7025	4.4118	0.99
30	1.0532	6.7987	0.99
35	1.5591	10.3340	0.98
40	2.2781	15.5020	0.97

It is shown clearly in Table 4 that both A and B change with temperature. They were regressed using an exponential equation. The final rate equation is given by equation (4).

$$r_{H2} = 0.0949e^{0.0798T} pOH + 0.5238e^{0.085T} \tag{4}$$

Equation (4) is the final rate expression for the hydrolysis of $NaBH_4$ in the presence of a carbon supported ruthenium catalyst. It is dependent on the basicity of the solution and the reaction temperature. The basicity is measured by pOH. Since pOH is the negative logarithm of the OH^- ion concentration, the rate of hydrogen generation decreases with an increase in OH^- concentration. At the present stage, the physical meaning of the parameters A and B is not clear. However, they both change with temperature exponentially. This is reasonable for a chemical reaction. Since B increases more rapidly than A, the rate of hydrogen generation increases rapidly with an increase in temperature.

The reason for this complicated dependence on temperature may be due to the reaction mechanism. The hydrolysis of $NaBH_4$ for releasing hydrogen must have involved the intermediate of H^+. When the basicity of the aqueous solution varies, the activation energy and the pre-exponential factor for the Arrhenius form rate equation may also change.

4. Conclusions

The intrinsic kinetics for the hydrolysis of $NaBH_4$ over ruthenium on carbon catalyst has been investigated in this paper. Since $NaBH_4$ can be hydrolysed rapidly at higher temperatures even in the absence of a catalyst, the traditional design for obtaining isothermal rate data will not work well by minimising contact time between catalyst and $NaBH_4$ solution. A new method for data analysis has been

established in this research for obtaining isothermal rate data through non-isothermal reactions. The method was then applied to get isothermal rate data. The following conclusions can be drawn:

- When catalyst particle size reduced to less than 0.049 mm, internal mass transfer limitation can be neglected.

- The hydrolysis of $NaBH_4$ over ruthenium catalyst is zero-order to $NaBH_4$ concentration.

- The reaction rate depends strongly on the basicity of the solution. This may be due to the existence of acid intermediates in the reaction. It also strongly depends on reaction temperature.

References

(1)   Grochala, W.; Edwards, P. P. *Chemical Reviews* **2004**, *104*, 1283-1315.

(2)   Bououdina, M.; Grant, D.; Walker, G. *International Journal of Hydrogen Engergy* **2006**, *31*, 177-182.

(3)   Irani, R. S. *MRS Bulletin* **2002**, *27*, 680-682.

(4)   Wu, C.; Zhang, H.; Yi, B. *Catalysis Today* **2004**, *93-95*, 477-483.

(5)   Richardson, B. S.; Birdwell, J. F.; Pin, F. G. *Journal of Power Sources* **2005**, *145*, 21-29.

(6)   Krishnan, P. K.; Yang, T. H.; Lee, W. Y.; Kim, C. S. *Journal of Power Sources* **2005**, *143*, 17-23.

(7)   Kojima, Y.; Suzuki, K.-I.; Fukumoto, K.; Kawai, Y.; Kimbara, M.; Nakanishi, H.; Matsumoto, S. *Journal of Power Sources* **2004**, *125*, 22-26.

(8)   Amendola, S.; Onnerud, P.; Kelly, M. T.; Binder, M. *Talanta* **1999**, *49*, 267-277.

(9)   Davis, R. E.; Bromels, E.; Kibby, C. L. *Journal of American Chemical society* **1962**, *84*, 885-892.

(10)   Kaufman, C. M.; lousiana State University and Agricultural and Mechamical College, 1981, p 166.

(11)   Weekman, V. W. *AIChE Journal* **1974**, *20*, 833-840.

Modeling of the hydrolysis of NaBH$_4$ over carbon supported ruthenium

◈scholarONE™
Manuscript Central

Modeling of the hydrolysis of NaBH₄ over carbon

supported ruthenium

Y Shang[1], R Chen[1], G Jiang[2]

[1]Department of Aeronautic and Automotive Engineering, Loughborough University, Loughborough,

Leicestershire LE11 3TU, UK

[2]School of Mechanical, Materials and Manufacturing Engineering, University of Nottingham,

Nottingham NG7 2RD, UK

Abstract

The hydrolysis of sodium borohydride over carbon supported ruthenium catalyst has been shown an

effective route for on-board hydrogen generation. After obtaining the intrinsic kinetics in the previous

work, mass transfer and heat effect was taken account in this paper. Effective diffusivity of sodium

borohydride aqueous solution in catalyst particles was measured experimentally. The effectiveness

factor was then correlated with temperature and $NaBO_2$ concentration. Non-iosthermal hydrolysis of

sodium borohydride was calculated using the model by incorporation of mass and heat effects into

intrinsic kinetic equation. Good agreements were achieved between model and experimental results.

Key words

Sodium borohydride, overall kinetics, hydrolysis, ruthenium, effectiveness factor

1. Introduction

The hydrolysis of $NaBH_4$ over ruthenium catalyst is a promising way for on-board hydrogen generation. In the previous paper,[1] intrinsic kinetics for the hydrolysis was obtained. In practice, catalyst particles are of significant size in order to avoid large pressure drops. Strong diffusion limitations occur when the catalyst particle size is at the level of practical accessibility.

The hydrolysis of $NaBH_4$ is a strong exothermic reaction. About 285 kJ heat was generated for hydrolysis of one mole.[2,3] The heat generated, if not removed effectively, will increase the reaction temperature. The increase in reaction temperature will lead to an increase in reaction rate. When the reaction temperature increases up to the boiling point of the solution, water will be evaporated, leading to the increase of $NaBO_2$ concentration. The increase in its concentration results in a higher basicity of the reaction system, which will slow down the reaction rate. For calculation of the hydrogen generation, the heat effect must be taken into account.

The aim of this paper is to model hydrogen generation from $NaBH_4$-H_2O system when large catalyst particles are used. In the modeling, the mass transfer limitations and heat effect are built into the intrinsic kinetic equation. Non-isothermal reaction was then calculated using the model since it can reduce system complexity by controlling the system temperature.

2. Model construction

2.1 Effectiveness factor

The hydrolysis of $NaBH_4$ over ruthenium catalyst is a zero-order reaction. The intrinsic kinetics is given by equation (1), which was obtained by investigating reaction rate over very fine catalyst particle size in which the mass and heat transfer effects have been removed.

$$r_{H2} = 0.0949e^{0.0798T} \, pOH + 0.5238e^{0.085T} \tag{1}$$

where r_{H2} is hydrogen generation rate, T is the temperature and pOH is defined as the negative logarithm of OH^- concentration. When the size of catalyst particles is increased, internal mass transfer is no longer negligible. This is taken into account by using an effectiveness factor η, the ratio of actual to intrinsic

reaction rates. Effectiveness factor is often correlated with Thiele modulus. For a zero-order reaction, the Thiele modulus ϕ is defined by equation (2).[4]

$$\phi = L\sqrt{\frac{k'}{2D_e C_{As}}} \qquad (2)$$

were k' is the reaction rate constant based on the volume of total catalyst particles, D_e is the effective diffusivity of reactant in the catalyst particles, L is the characteristic length of a catalyst particle and C_{As} is the surface concentration of the reactant on the catalyst particles.

The rate data is often based on the weight of catalyst particles, which is related to k' by equation (3).

$$k\rho_c = k' \qquad (3)$$

where k is the rate constant based on the weight of catalyst, and ρ_c is the density of the catalyst. In the case of strong diffusion limitation ($\phi > 4$ or $\eta < 0.25$), effectiveness factor η and Thiele modulus have the relationship shown in equation (4).[4]

$$\eta = \frac{1}{\phi} \qquad (4)$$

Substitute equation (2) into equation (4) and $L = D/4$ for a cylindrical catalyst particle (D is the diameter of the cylinder), yielding

$$\eta = \frac{4}{D}\sqrt{\frac{2D_e C_{As}}{k'}} \qquad (5)$$

In the study, the volume of hydrogen is measured against time. According to the volume of hydrogen produced, the concentration of $NaBH_4$ in the solution can be calculated, which is regarded as the concentration of $NaBH_4$ on the surface of catalyst particles C_{As}. D_e can be measured experimentally. Therefore, effectiveness factor η is known. The actual hydrogen generation rate is the product of intrinsic rate and η. Equation (6) can be used for the transformation of rate data in regard to hydrogen volume, to the rate data in regard to $NaBH_4$.

$$r_{H_2} = \frac{dV_{H_2}}{dt} = \frac{d(n_{H_2} RT_0 / P_0)}{dt} = \frac{d(n_{NaBH_4} RT_0 / 4P_0)}{dt} = \frac{RT_0}{4P_0} r_{NaBH_4} \qquad (6)$$

where V_{H2} is the volume of hydrogen, n_{H2} is the moles of hydrogen, R is the universal gas constant, T_0 is

the room temperature, P_0 is the atmosphere pressure, t is reaction time, n_{NaBH4} is the moles of $NaBH_4$

when reaction time is t, and r_{NaBH4} is the hydrolysis rate based on the change of $NaBH_4$.

2.2 Calculation procedure for taking account of heat effect

At the beginning of the calculation the following data is input.

T_0: ambient temperature.

P_0: atmospheric pressure.

t: time (initialised to be 0).

dW_{NaBH4}: differential amount of $NaBH_4$ that reacts at each step.

w_{NaOH} : NaOH concentration (wt%).

W_{H_2O} : initial mass of water (g).

W_{NaBH_4} : initial mass of $NaBH_4$ (g).

Initial molality of $NaBH_4$ is calculated using equation (7).

$$m_{NaBH_4} = \frac{W_{NaBH_4}}{W_{H_2O}}$$ (7)

Heat generated when dW_{NaBH4} reacts is calculated using equation (8)

$$Q = \frac{dW_{NaBH_4}}{37.84} \Delta H$$ (8)

where ΔH is the enthalpy change of the hydrolysis reaction of $NaBH_4$, which is 285 kJ mol^{-1}. Heat loss

Q' in dt is calculated using equation (9).

$$Q' = KS\Delta T_m$$ (9)

where K is the overall heat transfer coefficient from the reactor to environment, S is the total heat

transfer area and ΔT_m is the average temperature difference between environment and the reactor.

Temperature change of the solution is calculated using equation (10)

$$\Delta T = \frac{Q - Q'}{c_p W_{H_2O}}$$ (10)

where c_p is the heat capacity of the solution. The temperature of the solution is calculated using equation (11)

$$T = T + \Delta T \tag{11}$$

If T is greater than boiling point of the solution, T is given the value of the boiling point and the heat Q is in its entirety used to evaporate water, which is calculated using equation (12).

$$\Delta W_{H_2O} = \frac{Q}{\Delta H_{evp}} \tag{12}$$

where ΔH_{evp} is the enthalpy change of water evaporation. The water remaining in the system after dW_{NaBH4} is obtained by equation (13)

$$W'_{H_2O} = W_{H_2O} - \Delta W_{H_2O} \tag{13}$$

The hydrogen that is generated when dW_{NaBH4} has reacted is calculated using equation (14).

$$\Delta V_{H_2} = \frac{4\Delta W_{NaBH_4}}{37.84} RT_0 / P_0 \tag{14}$$

The by-product $NaBO_2$ that is produced when dW_{NaBH4} has reacted is calculated using equation (15)

$$dW_{NaBO_2} = (dW_{NaBH_4} / 37.84) \times 66.22 \tag{15}$$

where 66.22 is the molecular weight of $NaBO_2$, and 37.84 is the molecular weight of $NaBH_4$. The concentration of $NaBO_2$ in the system is calculated using equation (16)

$$m_{NaBO_2} = \frac{W_{NaBO_2} / 66.22}{W_{H_2O}} \tag{16}$$

where W_{NaBO_2} is the accumulated amount of $NaBO_2$ in the solution. Equation (17) is used to calculate the OH$^-$ concentration in the solution after obtaining the concentration of $NaBO_2$.

$$[OH^-] = \frac{-(m_{NaOH} + K) + \sqrt{(m_{NaOH} + K)^2 + 4Km_{NaBO_2}}}{2} + m_{NaOH} \tag{17}$$

where [OH$^-$] is the concentration of OH$^-$ in the solution, and K is the equilibrium constant for the BO_2^- ions in water ($B(OH)_4^-$) : $B(OH)_4^- = H_3BO_3 + OH^-$. $K = 1.74 \times 10^{-5}$. pOH can be then calculated by using the definition: pOH = -ln[OH$^-$].

Intrinsic reaction rate is calculated using equation (1). Actual reaction rates can then be calculated using equation (18).

$$r_{H_2}(\text{real}) = r_{H_2}(\text{instrinsic})\eta W_{cat} \qquad (18)$$

where W_{cat} is the mass of catalyst. The reaction rate in terms of $NaBH_4$ is calculated using equation (6). The time dt needed to reacting dW_{NaBH4} can be then calculated using equation (19).

$$dt = \frac{dW_{NaBH_4}}{r_{NaBH_4}(\text{real})} \qquad (19)$$

The calculation is continued until the amount of $NaBH_4$ left is less than 0.1% of the initial amount.

3. Experimental section

3.2 Materials

The catalyst ruthenium supported on carbon was purchased from Johnson Mattwey. The original size was 3 mm x ϕ2 mm. Sodium borohydride was purchased from Sigma-Aldrich, which had a purity of 98%. It was used without any further purification. For measurement of diffusivity, the catalyst was grounded using mortar and pestle and sieved into an average size of 0.049 mm.

3.1 Measurement of effective diffusivity

The effectiveness factor η was measured using the rate data for 2 mm cylindrical catalyst particles and 0.049 mm catalyst particles in which diffusion limitations is not significant. The effective diffusivity De was calculated using equation (20), which is obtained by re-arranging equation (6).

$$D_e = \frac{\eta^2 R^2 k}{8C_{As}} \qquad (20)$$

3.2 Measurement of hydrogen generation rate

Hydrogen generation rate was measured using water replacement method. The rig was described in detail in the previous paper.[1] For non-isotheral hydrogen generation, the reaction flask was placed in air. Hydrogen volume was then measured against time.

4. Results and discussion

4.1 Effective diffusivity

The measured effective diffusivity with the change of temperature and the molality of $NaBO_2$ is shown in Figure 1. D_e depends both on the molality of $NaBO_2$ and temperature. At fixed molality of $NaBO_2$, D_e increased rapidly with temperature. At a molality of m_{NaBO2} of 0.25 mol/kg, D_e increased from 3.65 x 10^{-10} m^2/s to 35.8 x 10^{-10} m^2/s when the temperature increased from 25°C to 75°C. At a lower temperature, D_e decreased rapidly with the increase of the molality of $NaBO_2$ at first and then leveled off with a further increase of the concentration. The reason for this may be due to the blockage of catalyst pores. $NaBO_2$ was saturated in the vicinity of the reaction site on the surface of the catalyst's pores. When the temperature became higher, D_e did not change significantly with the increase of the molality of $NaBO_2$. At higher temperature, dissolution process became faster, and hence local $NaBO_2$ may not be saturated as it produced. This resulted in a constant D_e regardless of the change of the molality of $NaBO_2$ when the temperature was 75°C.
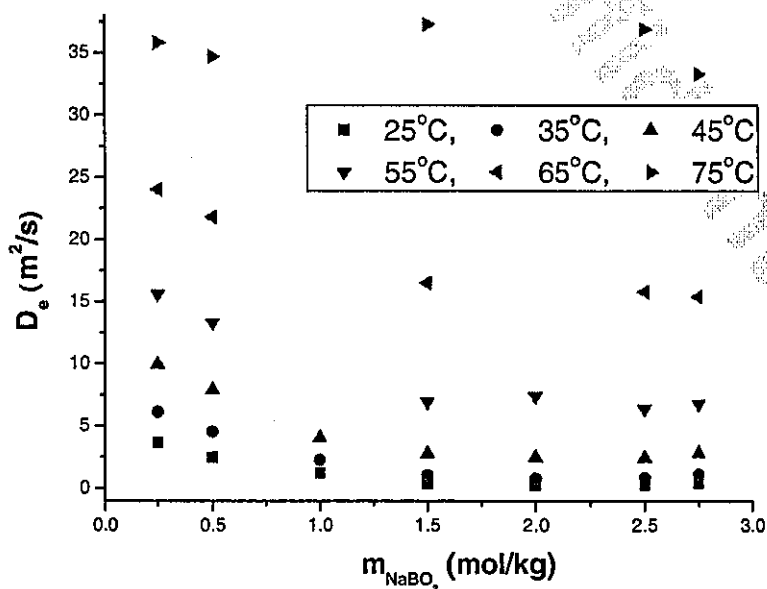
Figure 1. Effective diffusivity versus the molality of $NaBO_2$ and temperature.

The dependence of D_e on temperature can be described using equation (21).

$$D_e = D_{e0}e^{-E/RT} \qquad\qquad (21)$$

where D_{e0} is the pre-exponential factor, and E is the activation energy for diffusion. Take the logarithm of both sides, yielding

$$\ln D_e = \ln D_{e0} - \frac{E}{RT} \tag{22}$$

$\ln D_e$ was plotted against $1/T$ at various $NaBO_2$ concentrations as shown in Figure 2. It can be seen that a good linear relationship between $\ln D_e$ and $1/T$ was obtained, indicating the applicability of equation (21). The E/R and $\ln D_{e0}$ values in equation (22) derived from Figure 2 are listed in Table 1.

For the convenience of calculation, the data in Table 1 were fitted using an index function. The resulting equations are given in equations (23) and (24) respectively. The choice of index was due to the characteristics of chemical reactions.

$$E/R = 10770.5 - 8196.3 \times 0.40^{m_{NaBO2}} \tag{23}$$

$$\ln D_{e0} = 12.0 - 23.9 \times 0.42^{m_{NaBO2}} \tag{24}$$
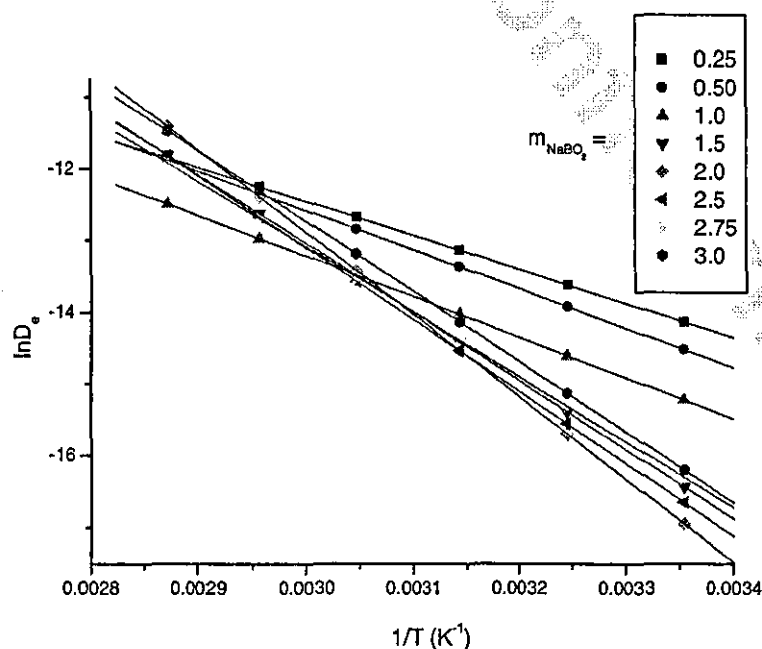
Figure 2 $\ln D_e$ versus $1/T$ at various $NaBO_2$ concentrations.

Table 1 Parameters for diffusion equation obtained from Figure 1.

m_{NaBO2} (mol/kg)	E/R	lnD_{e0}	Regression Residue
0.25	4740.1	1.7689	1.0
0.5	5472.1	3.8386	1.0
1	5669.2	3.7944	1.0
1.5	9604	15.779	1.0
2	11494	21.606	1.0
2.5	10032	16.999	1.0
2.75	9089.1	14.187	1.0
3	9812.8	16.717	1.0

4.2 Modelling of the generation of hydrogen

Figure 3 shows the comparison between experimental hydrogen generation from the non-isothermal generation of hydrogen and model calculation. The reaction was conducted in a round-bottom flask in air. Hence the heat loss is due to mainly the heat transfer from the reactor wall to the air. The overall heat transfer coefficient from the reaction to the air was estimated to be about 6.6 $W/(m^2 K)$.[5-7] In the experiment, hydrogen generation was finished within 150 seconds from the 10% $NaBH_4$ solution. It was in quite agreement with the model estimation of 160 seconds. As can be seen from Figure 3, both of the hydrolysis curves had an inflexion point at around 80 seconds (about 40% of $NaBH_4$ was consumed), which indicated the maximum hydrogen generation rate. The reason for the auto-acceleration was due to the maximum temperature at this point. The temperature began to increase resulting from retained heat, since this was not dispersed to the air around the fast at a sufficient rate. When the temperature reached the maximum, heat loss rate reached the maximum too due to the maximum temperature difference between reactor wall and surrounding air. With the increase of $NaBO_2$ concentration, reaction rate decreased, leading to the decrease of reaction temperature. The model predicted both the overall hydrolysis time and the maximum hydrolysis rate. This supported the validity of the model.
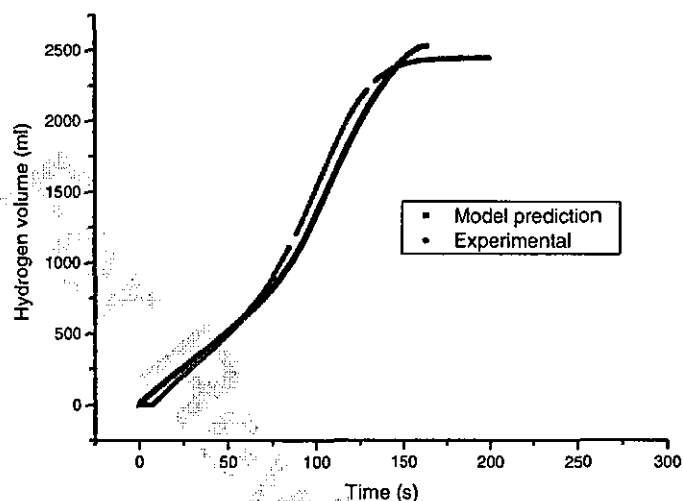
Figure 3 Comparison between experimental and model prediction for a non-isothermal reaction. NaOH = 0, catalyst = 3g with a particle size of 2 mm x 3 mm, NaBH$_4$ = 1.0g in 10g of water.

5. Conclusions

In this paper, heat and mass transfer were built into the intrinsic rate expression through the use of the Thiele modulus. The effective diffusivity of NaBH$_4$ in catalyst pores was experimentally measured. The model was then validated through both isothermal and non-isothermal hydrolysis of NaBH$_4$. From the study, the following conclusions can be reached:

- When large catalyst particles are used, strong diffusion limitation is observed for the hydrolysis of NaBH$_4$, which can be seen from the very low efficiency factor that was obtained experimentally.

- The effective diffusivity of NaBH$_4$ in catalyst pores depends on both the temperature and the concentration of NaBO$_2$. The dependence on the latter may be due to local saturation of NaBO$_2$ in the vicinity of active sites of the catalyst surface.

- In the region of diffusion limitation, reaction order to NaBH$_4$ is not zero-order. The reaction rate decreases rapidly with a decrease in NaBH$_4$ concentration.

- After combining intrinsic kinetics with diffusion limitation, heat generation and water evaporation, the model can be used to predict hydrogen generation from the hydrolysis of

NaBH$_4$. The validation of the model has been performed for both isothermal and non-isothermal hydrolysis.

References

(1)   Shang, Y.; Chen, R.; Jiang, G. *Energy and Fuels* **2007**, *submitted*.

(2)   Hua, D.; Hanxi, Y.; Xinping, A.; Chuansin, C. *International Journal of Hydrogen Energy* **2003**, *28*, 1095-1100.

(3)   Davis, R. E.; Bromels, E.; Kibby, C. L. *Journal of American Chemical society* **1962**, *84*, 885-892.

(4)   Levenspiel, O. *Chemical Reaction Engineering*; 3rd ed.; John Wiley & Sons: New York, 1999.

(5)   Hewitt, G. F.; Shires, G. L.; Bott, T. R. *Process Heat Transfer*; CRC Press: Boca Raton, 1994.

(6)   Hewitt, G. F.; Shires, G. L.; Bott, T. R. *Process Heater Transfer*; CRC Press: Boca Raton, 1994.

(7)   Hewitt, G. F.; Shires, G. L.; Bott, T. R. *Process Heat Transfer*; CRC Press: Boca Raton, 1994.

Intrinsic kinetics of NaBH$_4$ hydrolysis over carbon supported ruthenium

Hydrogen Storage via the Hydrolysis of NaBH₄ Basic Solution: Optimization of NaBH₄ Concentration

Y. Shang* and R. Chen

Department of Aeronautical and Automotive Engineering, Loughborough University, Loughborough, Leicestershire LE11 3NW, United Kingdom

Generation of hydrogen via the hydrolysis of sodium borohydride (NaBH₄) solution in the presence of metal catalysts is a promising method for hydrogen storage. The concentration of NabH₄ should be as high as possible in order to improve energy density. On the other hand, NaBO₂ is produced after the hydrolysis of NaBH₄. When the NaBH₄ concentration is high enough, NaBO₂ will precipitate from the solution, which would block the active sites of the catalysts and bring about the complexity of solution transportation. This paper addressed the issue through thermodynamic modeling. A mathematical model was derived first using the equality of chemical potential of the solute in solution and in its solid state. The parameters in the model were determined using phase-diagram analysis and hydration analysis of the NaBH₄–NaOH–H₂O and NaBO₂–NaOH–H₂O systems. The optimal concentration of NaBH₄ in the hydrogen-generation system was then calculated and a comparison of the modeling results with experimental data, which were in good agreement, was given.

1. Introduction

Interest in hydrogen as a fuel has grown dramatically, and many advances in hydrogen production and utilization technologies have been made. However, hydrogen-storage technologies must be significantly advanced if a hydrogen-based energy system, particularly in the transportation sector, is to be established. At the present time, the main obstacle in the way of transition to a hydrogen economy is the absence of a practical means for hydrogen storage. For years, the goal of researchers has been to develop a high-density hydrogen-storage system that can release hydrogen at temperatures lower than 100 °C. A hydrogen economy will flourish when adequate storage technology exists, allowing people to tap and trade regional, renewable power sources. This cache of stored energy will offer viability to the full range of local and global renewable energy sources.

For a hydrogen-storage system to be put into practical use, the energy density must reach a high level. For example, U.S. Department of Energy recommended that an energy density of 6.5% and 62 kg m⁻³ must be achieved in order for a hydrogen-storage system to be the appropriate weight and size to facilitate a fuel-cell vehicle driving a distance of 560 km. Storing hydrogen is somewhat difficult because of its low density and low critical temperature. Currently, there are a number of technologies available for hydrogen storage, such as high-pressure cylinder, liquification, adsorption on high surface carbon materials, and metal hydrides.

It is believed that metal hydrides are a safe and promising way to store hydrogen. Various metal hydrides have been used via direct pyrolysis or hydrolysis methods. In the area of pyrolysis, LiBH₄ and NaAlH₄ have attracted great attention.[1]

The temperature for pyrolysis is still too high for practical usage in the transportation sector, whereas the hydrolysis route is safer and easier to handle. In this respect, NaBH₄ has been extensively studied, as shown in Scheme 1. The only byproduct, sodium metaborate, is water soluble and environmentally benign. The reaction is very fast in the presence of a catalyst, and there is no need to supply external heat for the reaction to occur. It is reported that Millennium Cell has designed a portable hydrogen-gas generator using an aqueous borohydride solution.[2] Looking for efficient catalysts for the hydrolysis is an aspect of the use of the NaBH₄ hydrolysis system.[3–6]

The concentration of NaBH₄ in the hydrolysis system is an important issue for practical usage. To improve the energy density of the system, the concentration of NaBH₄ should be as high as possible. However, when the concentration is too high, the byproduct sodium metaborate precipitates from the solution, which blocks the active sites of the catalyst and thus reduces the life of the catalyst. Precipitation of the byproduct would also bring about problems in solution transportation, such as blockage of the piping system. However, little attention has been paid to NaBH₄ concentration for hydrogen generation.

In a previous paper,[7] NaBH₄ concentration was studied and optimized in the case of neat solution through thermodynamic modeling. In practice, 1–10% NaOH is used to stabilize the solution.[8–10] In this paper, thermodynamic modeling is used to

*To whom correspondence should be addressed. E-mail: y.shang@lboro.ac.uk. Phone: 0044-1509-235690.

(1) Zuttel, A.; Wenger, P.; Rentsch, S.; Sudan, P.; Mauron, P.; Emmenegger, C. *J. Power Sources* 2003, *118*, 1–7.

(2) Amendola, S. C.; Sharp-Goldman, S. L.; Janjua, M. S.; Spencer, N. C.; Kelly, M. T.; Petillo, P. J.; Binder, M. *Int. J. Hydrogen Energy* 2000, *25*, 969–975.
(3) Wu, C.; Zhang, H.; Yi, B. *Catal. Today* 2004, *93–95*, 477–483.
(4) Kim, J.-H.; Lee, H.; Han, S.-C.; Lee, J.-Y. *Int. J. Hydrogen Energy* 2004, *29*, 263–267.
(5) Kojima, Y.; Suzuki, K.-I.; Fukumoto, K.; Kawai, Y.; Kimbara, M.; Nakanishi, H.; Matsumoto, S. *J. Power Sources* 2004, *125*, 22–26.
(6) Krishnan, P. K.; Yang, T. H.; Lee, W. Y.; Kim, C. S. *J. Power Sources* 2005, *143*, 17–23.
(7) Shang, Y.; Chen, R.; Thring, R. *World J. Eng.* 2005, *2*, 1–9.
(8) Kreevoy, M. M.; Jacobson, R. W. *Ventron Alembic* 1979, *15*, 2–3.

Scheme 1. Hydrolysis Reaction of Sodium Borohydride

$$NaBH_4 + 2H_2O \longrightarrow NaBO_2 + 4H_2$$
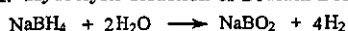
optimize the concentration of $NaBH_4$ in the presence of NaOH. The modeling results are then compared with experimental data.

2. Thermodynamic Model for A Three-Component Solution

When solute B is dissolved into water in the presence of a third component A, that is, solute B is dissolved in A's solution, the chemical potential of B in the solution is equal to the chemical potential in its solid state in equilibrium, considering that the solution of A is the environment.

For an electrolyte $A_{\nu_+}B_{\nu_-}$, where ν_+ is the number of cations and ν_- is the number of anions, the chemical potential for the electrolyte in its aqueous solution can be expressed using eq 1.

$$\mu = \mu^0 + \nu_\pm RT \ln \gamma_\pm m_\pm \qquad (1)$$

where the standard chemical potential μ^0 of the electrolyte is the chemical potential in a solution of unit activity on the molality scale, R is the universal gas constant (8.314 J mol⁻¹ K⁻¹), T is the temperature (K), and the mean ionic molality $m_\pm$ and mean ionic activity coefficient $\gamma_\pm$ are defined as

$$m_\pm = (m_+^{\nu_+} m_-^{\nu_-})^{1/\nu\pm} = m(\nu_+^{\nu_+}\nu_-^{\nu_-})^{1/\nu\pm} \qquad (2)$$

$$\gamma_\pm = (\gamma_+^{\nu_+}\gamma_-^{\nu_-})^{1/\nu\pm} \qquad (3)$$

$$\nu_\pm = \nu_+ + \nu_- \qquad (4)$$

On the basis of the equality of the chemical potential of a species in solution and in the solid state, we obtain eq 5.

$$\mu_B^\bullet(s) = \mu_B^0 + \nu_\pm RT \ln \gamma_{\pm,B}' m_{\pm,B} \qquad (5)$$

where $\mu_B^\bullet(s)$ is the chemical potential of solute B in its solid state and $\gamma_{\pm,B}'$ is the mean activity coefficient of B in A's solution. Rearranging eq 5 gives

$$\ln m_{\pm,B} = \frac{\mu_B^\bullet(s) - \mu_B^0}{\nu_\pm RT} - \ln \gamma_{\pm,B}' \qquad (6)$$

The difference of the chemical potentials in eq 6 is the molar Gibbs energy change of the solute from its solid state to the unit activity in its solution on a molality scale, which is further related to other thermodynamic functions.

$$\Delta G_{m,B}^0 = \mu_B^0 - \mu_B^\bullet(s) = \Delta H_{m,B}^0 - T\Delta S_{m,B}^0 \qquad (7)$$

where $\Delta G_{m,B}^0$, $\Delta H_{m,B}^0$, and $\Delta S_{m,B}^0$ are the molar Gibbs energy change, molar enthalpy change, and molar entropy change of B for the dissolution of one mole of solid-state solute to unit activity in solution, respectively. Substituting eq 7 into eq 6 gives the relationship between solubility and temperature.

$$\ln m_{\pm,B} = -\frac{\Delta H_{m,B}^0}{\nu_\pm RT} + \frac{\Delta S_{m,B}^0}{\nu_\pm R} - \ln \gamma_{\pm,B}' \qquad (8)$$

For both $NaBH_4$ and $NaBO_2$, $\nu_\pm = 2$. When this value is substituted into eq 8, the relationship between the solubility of $NaBH_4$ and $NaBO_2$ in NaOH solution is obtained.

$$\ln m_{\pm,B} = -\frac{\Delta H_{m,B}^0}{2RT} + \frac{\Delta S_{m,B}^0}{2R} - \ln \gamma_{\pm,B}' \qquad (9)$$

When NaOH is not present, the activity coefficient of $NaBH_4$ and $NaBO_2$, $\gamma_{\pm,B}$, can be considered as being constant with temperature in its saturated solution.[7] However, it is shown in the following section that the activity coefficient of $NaBH_4$ and $NaBO_2$ in the presence of NaOH, $\gamma_{\pm,B}'$, is not constant when temperature changes. This may be due to the fact that the effective water needed to dissolve the salts in NaOH solution is affected significantly by the temperature because of the interactions between NaOH ions with the noneffective water.[11] To determine the parameters, we modified eq 9 by adding $-\ln \gamma_{\pm,B}$ to both sides.

$$\ln m_{\pm,B} - \ln \gamma_{\pm,B} = -\frac{\Delta H_{m,B}^0}{2RT} + \frac{\Delta S_{m,B}^0}{2RT} - \ln \gamma_{\pm,B}' - \ln \gamma_{\pm,B} \qquad (10)$$

Rearranging eq 9 gives

$$\ln m_{\pm,B} + \ln \frac{\gamma_{\pm,B}'}{\gamma_{\pm,B}} = -\frac{\Delta H_{m,B}^0}{2RT} + \left(\frac{\Delta S_{m,B}^0}{2RT} - \ln \gamma_{\pm,B}\right) \qquad (11)$$

Because $\Delta H_{m,B}^0$ and $\Delta S_{m,B}^0$ can be considered as being constant when the temperature range is not large, the left-hand side of eq 11 and $1/T$ have a linear relationship. The parameters can be determined by plotting $\ln m_{\pm,B} + \ln(\gamma_{\pm,B}'/\gamma_{\pm,B})$ against $1/T$ at several known solubilities. The ratio of the activity coefficient in the presence of NaOH, $\gamma_{\pm,B}'$, to the activity coefficient in the absence of NaOH, $\gamma_{\pm,B}$, can be calculated using the hydration analysis method.[11-13] Hence, the solubility of the salts at any temperatures can be calculated using eq 11 after obtaining the parameters.

3. Solubility Data of NaBH₄ and NaBO₂ in NaOH Aqueous Solutions

3.1. Solubility Data for NaBH₄ in NaOH Aqueous Solutions.
The solubilities for $NaBH_4$ in NaOH aqueous solutions are not available directly in the literature. However, the phase diagram of the $NaBH_4$–$NaOH$–H_2O system is available.[14] For the convenience of calculation, the triangle phase diagram in the literature is transformed into a rectangular phase diagram, as shown in Figure 1.

For different temperatures, the solubility line consists of smooth parts and inflection points. In the smooth part, one crystalline form coexists with solution. A different smooth part has a different crystalline form. At the inflection point between two of the smooth parts, the two different crystalline forms coexist with the solution. The inflection point between the two smooth parts is called the invariant point, because the composition and temperature are fixed. For example, at invariant point 1 in Figure 1, crystalline states $NaBH_4 \cdot 2H_2O$ and $NaBH_4$ coexist with $NaBH_4$ in NaOH aqueous solutions. The temperature of the invariant point is 0 °C. The composition is 22.5% NaOH, 22.3% NaBH4, and 55.2% water. There are seven invariant points in total, as shown by points 1−7 in the figure.

The line for 0 °C, line a, is divided into three parts by invariant points 1 and 2. Before point 1, the solution is saturated with the crystalline state $NaBH_4 \cdot 2H_2O$. At point 1, crystalline states $NaBH_4 \cdot 2H_2O$ and $NaBH_4$ exist simultaneously. With the increase in NaOH concentration, the crystalline state becomes

(9) Suda, S.; Sun, Y.-M.; Liu, B.-H. *Appl. Phys. A: Mater. Sci. Process.* **2001**, *72*, 209−212.

(10) Hua, D.; Hanxi, Y.; Xinping, A.; Chuansin, C. *Int. J. Hydrogen Energy* **2003**, *28*, 1095−1100.

(11) Eysseltova, J. *Coll. Czech. Chem. Commun.* **1994**, *59*, 2351−2356.

(12) Eysseltova, J. *Coll. Czech. Chem. Commun.* **1994**, *59*, 126−137.

(13) Nyvlt, J.; Eysseltova, J. *Coll. Czech. Chem. Commun.* **1994**, *59*, 1911−1921.
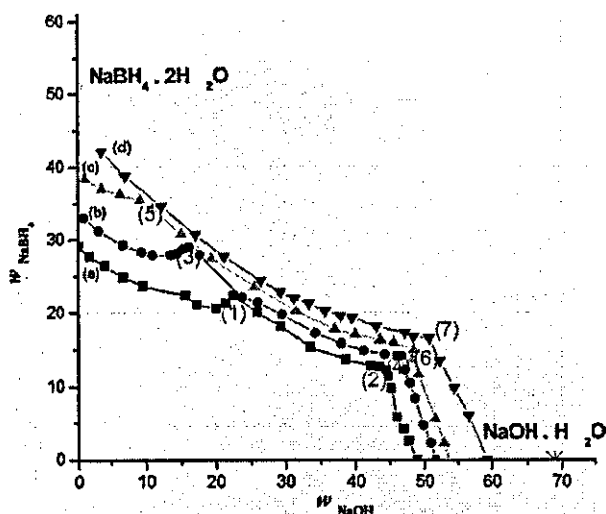
(14) Gmelins, L. *Handb. Anorg. Chem.* **1974**, 21.

Figure 1. Phase diagram for the NaBH₄−NaOH−H₂O system at (a) 0, (b) 18, (c) 30, and (d) 50 °C.

NaBH₄. NaOH arrives at its saturated state at point 2 and precipitates together with NaBH₄ in the state of hydrated crystal NaOH·H₂O. After point 2, NaBH₄ is no longer saturated, and the solution saturated with NaOH has NaOH·H₂O as the equilibrium solid state until no NaBH₄ exists in the system.

At 18 and 30 °C, the situations are similar to that at 0 °C except for the invariant point compositions. At 50 °C, there is only one invariant point, point 7. Before point 7, the solution coexists with the crystalline state NaBH₄. After point 7, the solution coexists with the crystalline state NaOH·H₂O. At point 7, the solution coexists with the two crystalline states NaOH· H₂O and NaBH₄.

To do the calculation, we regressed the smooth parts in Figure 1 at each temperature to mathematical equations.

3.2. Solubility Data for NaBO₂ in NaOH Aqueous Solutions. There are no systematic solubility data available for the NaBO₂−NaOH−H₂O ternary system. However, the phase diagram for the Na₂O−B₂O₃−H₂O system is available in the literature.[15] The solubility data for NaBO₂−NaOH−H₂O system can be achieved from this phase diagram when the ratio of Na₂O to B₂O₃ equals 1:1 using eqs 12 and 13.

$$w_{NaBO_2} = \frac{w_{B_2O_3}}{M_{B_2O_3}} 2M_{NaBO_2} \tag{12}$$

$$w_{NaOH} = \left(\frac{w_{Na_2O}}{M_{Na_2O}} - \frac{w_{B_2O_3}}{M_{B_2O_3}} \right) 2M_{NaOH} \tag{13}$$

where M_{NaBO_2} and M_{NaOH} are the molecular masses of NaBO₂ and NaOH, respectively. The obtained phase diagram is shown in Figure 2. The interpretation of Figure 2 is the same as that for Figure 1. The phase diagram was then regressed using mathematical equations in order to perform calculations.

4. Hydration Analysis for $\gamma'_{\pm,B}/\gamma_{\pm,B}$

The hydration analysis method is used to calculate $\gamma'_{\pm,B}/\gamma_{\pm,B}$. Hydration analysis is a method of analyzing the solubility data to explain the ionic processes in a ternary saturated solu-

(15) Mellor, J. W. *Supplement to Mellor's Comprehensive Treatise on Inorganic and Theoretical Chemistry*; Longman: London, 1980; Vol. 5, Boron−Oxygen Compounds.
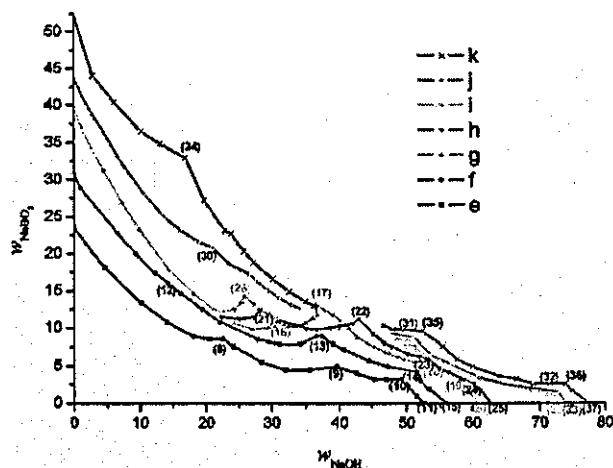
Figure 2. Phase diagram for the NaBO₂−NaOH−H₂O system at (e) 30, (f) 45, (g) 56, (h) 60, (i) 64, (j) 80, and (k) 100 °C.
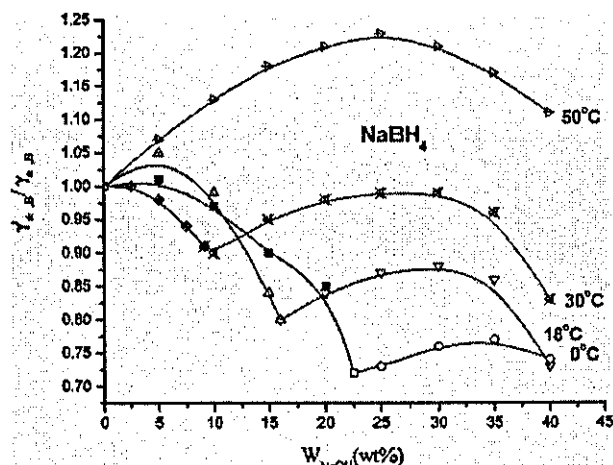
Figure 3. $\gamma'_{\pm,B}/\gamma_{\pm,B}$ for the NaBH₄−NaOH−H₂O system.
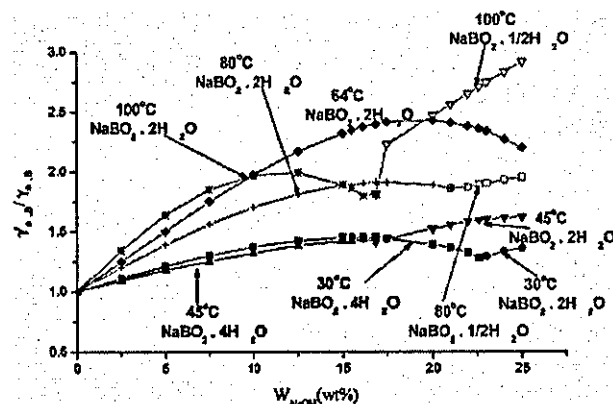
Figure 4. $\gamma'_{\pm,B}/\gamma_{\pm,B}$ for the NaBO₂−NaOH−H₂O system.

tion.[11,12,16] Detailed methods can be found in the literature. Equation 14 is used to calculate the ratio.

$$\frac{\gamma'_{\pm}}{\gamma_{\pm}} = \frac{x_{H_2O}}{x_{H_2O} - P} \tag{14}$$

where x_{H_2O} is the mole fraction of water in solution, and P is

(16) Stokes, R. H.; Robinson, R. A. *J. Am. Chem. Soc.* **1948**, *70*, 1870−1878.
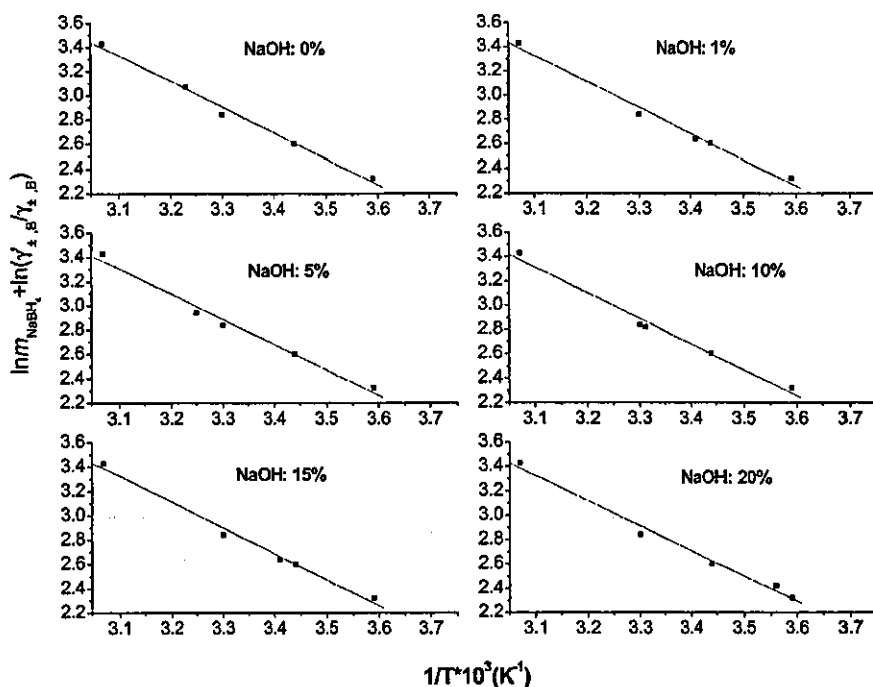
Figure 5. Relationship between ln m_B and $(1/T)$ for NaBH₄ in NaOH solution.

given by eq 15.

$$P = \frac{n_{H_2O}^0 n_{NaB}^0 - n_{H_2O}^0 \sqrt{n_{NaB}^2 + n_{NaB} n_{NaOH}}}{n_{NaB}^0 (n_{H_2O} + n_{NaB} + n_{NaOH})} \quad (15)$$

where n_{H_2O} is the number of moles of water in solution, n_{NaB} is the number of moles of NaBH₄ or NaBO₂ in solution, and n_{NaOH} is the number of moles of NaOH in solution.

In the phase diagram for NaBH₄–NaOH–H₂O or NaBO₂–NaOH–H₂O, each NaOH concentration corresponds to a NaBH₄ or NaBO₂ concentration for a specific temperature. The weight percentage of water is 100% minus the sum of the NaBH₄ or NaBO₂ concentration and NaOH concentration. The values of n_{H_2O}, n_{NaB}, and n_{NaOH} in eq 15 can thus be calculated. The values of $n_{H_2O}^0$ and n_{NaB}^0 can be obtained by setting $w_{NaOH} = 0$. The ratio of $\gamma'_{\pm,B}/\gamma_{\pm,B}$ is calculated using eq 14 and is shown in Figures 3 and 4 for NaBH₄ and NaBO₂, respectively.

## 5. Determination of Model Parameters

After obtaining the mathematical forms for NaBH₄ solubility in NaOH solution and $\gamma'_{\pm,B}/\gamma_{\pm,B}$ for the NaBH₄–NaOH–H₂O system, we can calculate the parameters for NaBH₄ in eq 11 by plotting ln $m_{\pm,B}$ + ln($\gamma'_{\pm,B}/\gamma_{\pm,B}$) against $1/T$. The parameters for NaBO₂ in eq 11 can be obtained in a similar way. Linearity was achieved when plotting ln $m_{\pm,B}$ + ln($\gamma'_{\pm,B}/\gamma_{\pm,B}$) against $(1/T)$, as shown in Figures 5 and 6 for NaBH₄ and NaBO₂, respectively.

In Figures 5 and 6, the slope of the line represents $-(\Delta H_{m,B}^0/2RT)$ and the intercept represents $(\Delta S_{m,B}^0/2R)$ − ln $\gamma_{\pm,B}$. The values of $\Delta H_{m,B}^0$ and $(\Delta S_{m,B}^0/2R)$ − ln $\gamma_\pm$ at various NaOH concentrations are calculated as shown in Tables 1 and 2 for NaBH₄ and NaBO₂, respectively.

As shown in Tables 1 and 2, the values are very close. This is reasonable, because the change is from solid state of the salts

to 1 mol kg⁻¹ of its solution without the presence of NaOH. Substituting the parameters into eq 10, gives

$$\ln m_{\pm,B} + \ln \frac{\gamma'_{\pm,B}}{\gamma_{\pm,B}} = -\frac{1920.2}{T} + 9.3 \quad (16)$$

for NaBH₄

$$\ln m_{\pm,B} + \ln \frac{\gamma'_{\pm,B}}{\gamma_{\pm,B}} = -\frac{3008.5}{T} + 11.7 \quad (17)$$

for NaBO₂.

It should be noted that in order to get the relationship between m_B and T from eqs 16 and 17, the presence of common ions must be considered when calculating the mean activity coefficient of mixed electrolytes.[17] In both NaBH₄–NaOH–H₂O and NaBO₂–NaOH–H₂O, the common ion is Na⁺. The mean activity coefficient $m_\pm$ is calculated using eq 18.

$$m_\pm = (m_{Na^+} m_{B^-})^{1/2} = [(m_{NaB} + m_{NaOH})m_{NaB}]^{1/2} \quad (18)$$

where m_{NaB} represents the molality of NaBH₄ or NaBO₂, m_{Na^+} is the molality of sodium ion, m_{B^-} is the molality of BH₄⁻ ion or BO₂⁻, and m_{NaOH} is the molality of NaOH.

To get the relationship between m_B and T at a specific NaOH concentration, the value of $\gamma'_{\pm,B}/\gamma_{\pm,B}$ must be determined at the NaOH concentration. As shown in Figures 3 and 4, the value has a range with the temperature. In this work, the average value was taken and then plotted against NaOH concentration to regress into mathematical equations so that the value of

(17) Alberty, S. *Physical Chemistry*, 3rd ed.; John Wiley & Sons: New York, 2001.
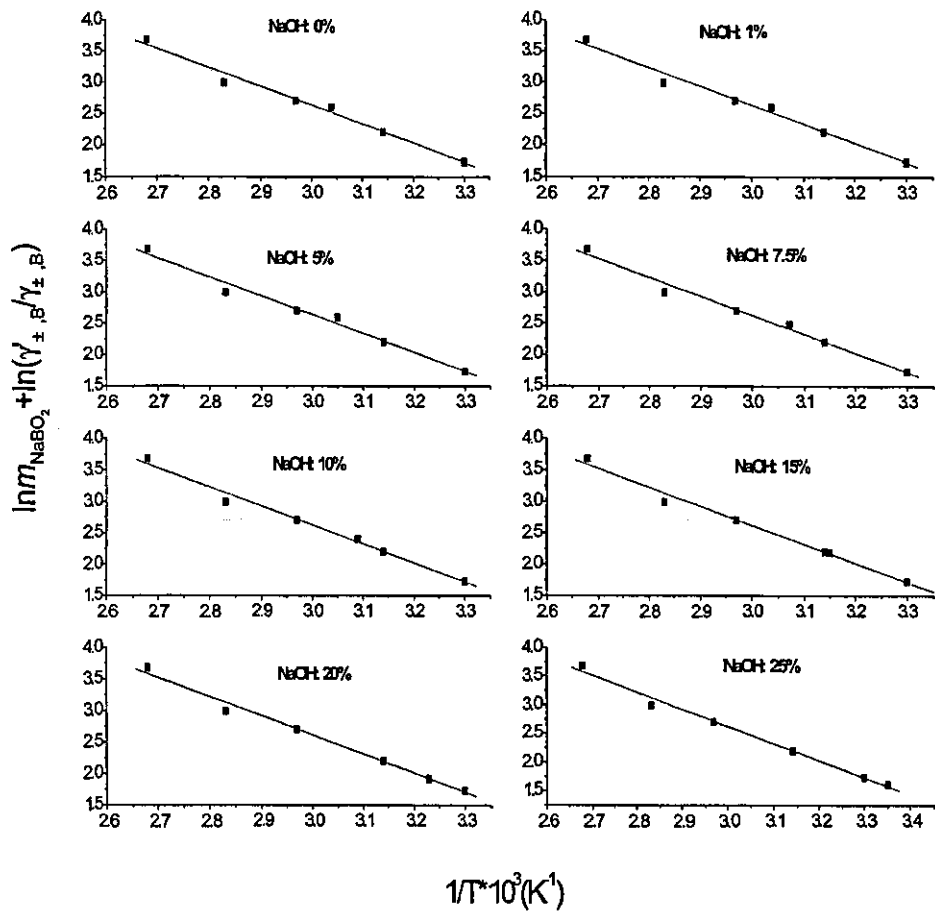
$$1/T*10^3(K^{-1})$$

Figure 6. Relationship between ln m_B and $(1/T)$ for $NaBO_2$ in NaOH solution.

Table 1. Values of the Parameters for $NaBH_4$ at Various NaOH Concentrations

w_{NaOH}	$\Delta H^0_{m,NaBH_4}/2R$ (K^{-1})	$\Delta S^0_{m,NaBH_4}/2R - \ln\gamma'_\pm$	$\Delta H^0_{m,NaBH_4}$ (kJ mol^{-1})
0	1935.6	9.3275	32.2
1	1886.9	9.1485	31.4
5	1890.2	9.1581	31.4
10	1910.4	9.2237	31.8
15	1954.6	9.3755	32.6
20	1943.3	9.3534	32.2
average	1920.2	9.2645	32.0

Table 2. Values of the Parameters for $NaBO_2$ at Various NaOH Concentrations

w_{NaOH}	$\Delta H^0_{m,NaBO_2}/2R$ (K^{-1})	$\Delta S^0_{m,NaBO_2}/2R - \ln\gamma'_\pm$	$\Delta H^0_{m,NaBO_2}$
0	3007.2	11.66	50.0
1	3006.8	11.659	50.0
5	2997.9	11.635	49.8
7.5	3009.9	11.661	50.0
10	3012.0	11.664	50.1
15	3021.9	11.687	50.2
20	3026.6	11.7	50.3
25	2985.5	11.582	49.6
average	3008.5	11.656	50.0

$\gamma'_{\pm,B}/\gamma_{\pm,B}$ can be estimated at any NaOH concentration. The regressed equations are given as eqs 19 and 20.

$$\gamma'_\pm/\gamma_\pm = 0.97 \tag{19}$$

$$\gamma'_\pm/\gamma_\pm = -0.0015w^2_{NaOH} + 0.07w_{NaOH} + 1.0 \tag{20}$$

where w_{NaOH} is the weight percentage of NaOH in $NaBH_4$ aqueous solution.

6. Optimization of $NaBH_4$ Concentration

The solubility of $NaBH_4$ in NaOH solution can be obtained by simultaneously solving eqs 15, 18, and 19; the solubility of $NaBO_2$ in NaOH solution can be obtained by simultaneously solving eqs 17, 18, and 20. The amount of water (g) contained in the saturated solution containing 1 mole of $NaBH_4$ is calculated using eq 21.

$$W_1 = \frac{1000}{m_{NaBH_4}} \tag{21}$$

The amount of water (g) contained in the saturated solution containing 1 mole of $NaBO_2$ or the weight of water needed to dissolve 1 mole of $NaBO_2$ is calculated using eq 22.

$$W_2 = \frac{1000}{m_{NaBO_2}} \tag{22}$$

The amount of water (g) needed to react with 1 mole of $NaBH_4$ is calculated using eq 23.

$$W_3 = 4M_{H_2O} \tag{23}$$

The maximum concentration of $NaBH_4$ in the hydrolysis system is determined by the maximum value between W_1 and $(W_2 + W_3)$.

The comparison between W_1 and $(W_2 + W_3)$ was calculated and is shown in Figure 7.
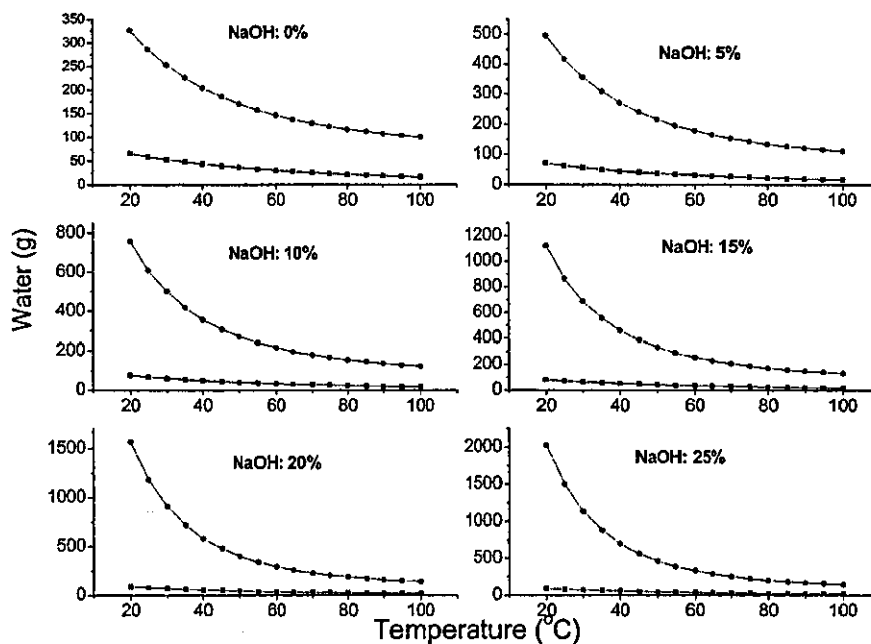
Figure 7. Quantity of water needed to dissolve 1 mole of NaBO₂ and to react with 1 mole of NaBH₄ (●) compared with the quantity of water contained in saturated NaBH₄ solution (■).
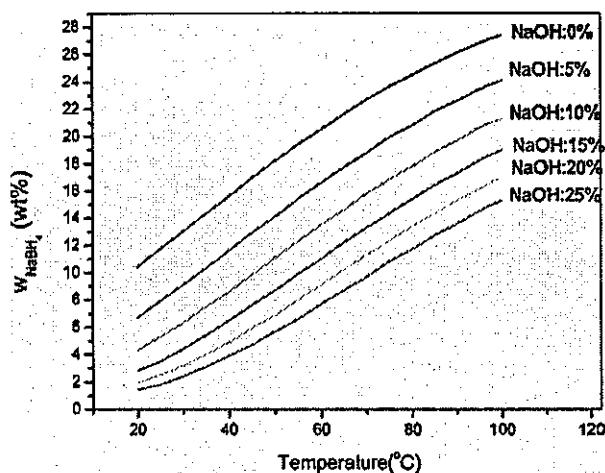
Figure 8. Calculated maximum concentration of NaBH₄ in the hydrolysis system.

Figure 9. Comparison between the calculated and experimental concentrations of NaBH₄ when sodium metaborate is deposited from the system.

It can be seen that the amount of water needed to dissolve 1 mole of NaBO₂ and to react with 1 mole of NaBH₄ is much greater than that in the saturated NaBH₄ solution. Therefore, the maximum concentration of NaBH₄ in the hydrolysis system is determined by ($W_2 + W_3$). The amount of NaOH (g) in the solution containing 1 mole of NaBH₄ is

$$W_{\text{NaOH}} = \frac{w_{\text{NaOH}}(M_{\text{NaBH}_4} + W_2 + W_3)}{(100 - w_{\text{NaOH}})} \qquad (24)$$

where w_{NaOH} is the weight percentage of NaOH. Equation 24 is transformed into eq 25 in order to calculate the maximum concentration of NaBH₄ w (wt %).

$$w = \frac{M_{\text{NaBH}_4}}{M_{\text{NaBH}_4} + W_{\text{NaOH}} + W_2 + W_3} \qquad (25)$$

The maximum concentration of NaBH₄ calculated using eq 25

is shown in Figure 8 for various NaOH concentrations. It can be seen that the maximum concentration increases with an increase in temperature but decreases with an increase in NaOH concentration.

7. Comparison of the Modeling Results with Experimental Data

The NaBH₄ concentration at which NaBO₂ precipitates from the hydrolysis system was measured experimentally. A series of NaBH₄ solutions were prepared in 5 mL glass vials (the NaBH₄ powder was purchased from Aldrich). The liquid level was then marked. To accelerate its hydrolysis, we put a small amount of catalyst into the solutions and conducted the reaction at an elevated temperature (the catalyst was ruthenium supported on carbon, which was purchased from Johnson Matthew Ltd.). After the reaction was finished (no hydrogen coming out), some water was added to the marked level of the vials, and the glass

vials were then sealed and put into an oven at a predetermined temperature. After 24 h, the glass vials were examined visually to see the precipitate from the solution. The minimum solution concentration that had precipitate was considered to be the maximum concentration of $NaBH_4$ solution at that temperature (the oven temperature).

Solutions with 1 and 5% NaOH were used as the reaction medium. The experimentally measured concentrations at which $NaBO_2$ precipitated were plotted together with the modeling results, as shown in Figure 9, using temperature on the Celsius scale. The experimental results are in good agreement with the model predictions.

8. Conclusions

A thermodynamic modeling method was adopted to calculate the maximum concentration of $NaBH_4$ in the presence of NaOH and then experimentally validated for a hydrogen storage system. The maximum concentration of $NaBH_4$ in the hydrolysis system is determined by the amount of water needed to dissolve the byproduct $NaBO_2$ and react with $NaBH_4$, which increases with the increase in reaction temperature and decreases with the increase in NaOH concentration in the system.

Semiempirical Hydrogen Generation Model Using Concentrated Sodium Borohydride Solution

Yinghong Shang* and Rui Chen

*Department of Automotive and Aeronautical Engineering, Loughborough University,
Loughborough, Leicestershire LE11 3TU, United Kingdom*

The characteristics of hydrogen generation from concentrated sodium borohydride ($NaBH_4$) solutions were studied in this paper because of its potential application in hydrogen storage. The hydrolysis was conducted over a carbon-supported ruthenium catalyst, and the hydrogen generated was measured using a computer-monitored water replacement method. The effects of the hydrolysis temperature, NaOH concentration, $NaBH_4$ concentration, and the byproduct, sodium metaborate, on hydrogen generation behavior have been investigated. An empirical model was proposed to represent the hydrogen-generation rate.

Introduction

Sodium borohydride ($NaBH_4$) reacts with water to produce pure hydrogen and a byproduct, sodium borate. The advantages and benefits of hydrogen generation from this hydrolysis reaction are well-known. It is the least expensive metal hydride commercially available, and it is safe to use, handle, and store. It requires no or limited equipment investment for the system implementation of the reaction. The byproduct of the reaction is in the form of an aqueous solution; therefore, it is easy to be removed from the system. Also, the hydrogen-storage densities of the system with an optimized design can meet the technical target of 6% hydrogen capacity (mass %) set by U.S. Department of Energy (DOE).[1,2] $NaBH_4$ has thus been proposed to be an effective hydrogen-storage medium for a wide variety of applications in both distributed power generation and transportation applications. Recently, extensive research has been performed using $NaBH_4$ aqueous solution for hydrogen supply, and the results have been reported by a number of publications.[3–7]

$NaBH_4$ solutions are unstable since the self-hydrolysis reactions can occur at low pH conditions. Such instabilities can be significantly improved if the pH of the solution is maintained above a level of 9.[8] One of the most convenient methods for achieving such a pH level is to use sodium hydroxide, NaOH, as the solution stabilizer. When such a stabilized solution is used for hydrogen generation, a selected metal catalyst is needed to accelerate the reaction.

To use $NaBH_4$ to generate hydrogen for power systems such as fuel cells, it is essential to control the rate of hydrogen evolution from its aqueous solutions. The reaction rate is affected by the hydrolysis temperature, NaOH concentration, $NaBH_4$ concentration, and the byproduct, sodium metaborate. The effects of the reaction temperature and $NaBH_4$ concentration have been studied elsewhere for dilute solutions.[9–11] However, few systematic reports have so far been found for the investigation of the effects of these factors on hydrogen generation from a concentrated $NaBH_4$ solution. It is therefore the goal of this research to identify these effects.

Kinetic Experimental Study

Chemical Materials. The chemical materials used in this study were all of reagent grade and were supplied by Sigma Aldrich Company, Ltd. Both the sodium borohydride ($NaBH_4$) powder and sodium metaborate ($NaBO_2$) powder have a purity of 98%. The ruthenium catalyst used to accelerate the hydrolysis of $NaBH_4$ was purchased from Johnson Matthew Ltd. It had 3% ruthenium supported on carbon and was in a pellet form with a diameter of 2 mm. The stabilizer, NaOH, used in the $NaBH_4$ solution was supplied by Sigma Aldrich Company, Ltd. It had a purity of 99.998%.

Hydrogen Generation. Figure 1 shows a schematic diagram of the experimental setup. The rig consists mainly of a three-port reactor (1), a water bath (3) that was used to adjust reaction temperature, a water replacement system (6) that was used to measure the volume of the hydrogen generated, and a replaced water measurement system (7–9).

There are three ports on the reactor. The left-hand port was equipped with a thermometer to continuously monitor the temperature of the reactor. The right-hand port was used to guide the generated hydrogen gas into the to the water replacement system. The middle port was connected to the water addition funnel which contains 10 mL of the reaction medium.

* To whom correspondence should be addressed. E-mail: y.shang@lboro.ac.uk.

(1) Zuttel, A. *Mater. Today* **2003,** 24–33.

(2) Zuttel, A. *Naturwissenschaften* **2004,** *91,* 157–172.

(3) Amendola, S.; Onnerud, P.; Kelley, M. T.; Binder, M. *Talanta* **1999,** *49,* 267–277.

(4) Amendola, S. C.; Ortega, J. V.; Wu, Y. (Millennium Cell, Inc., Eatontown, NJ). Processes for synthesizing borohydride compounds. U.S. Patent 6,670,444, 2003.

(5) Amendola, S. C.; Sharp-Goldman, S. L.; Janjua, M. S.; Spencer, N. C.; Kelley, M. T.; Petillo, P. J.; Binder, M. *Int. J. Hydrogen Energy* **2000,** *25* 969–975.

(6) Kojima, Y.; Suzuki, K.-i.; Fukumoto, K.; Kawai, Y.; Kimbara, M.; Nakanishi, H.; Matsumoto, S. *J. Power Sources* **2004,** *125* 22–26.

(7) Kim, J.-H.; Lee, H.; Han, S.-C.; Kim, H.-S.; Song, M.-S.; Lee, J.-Y. *Int. J. Hydrogen Energy* **2004,** *29* 263–267.

(8) Kreevoy, M. M.; Jacobson, R. W. *Ventron Alembic* **1979,** *15,* 2–3.

(9) Davis, R. E.; Bromels, E.; Kibby, C. L. *J. Am. Chem. Soc.* **1962,** *84,* 885–892.

(10) Davis, R. E.; Swain, C. G. *J. Am. Chem. Soc.* **1960,** *82* 5949–5950.

(11) Kaufman, C. M. *Catalytic Generation of Hydrogen from the Hydrolysis of Sodium Borohydride: Application in a Hydrogen/Oxygen Fuel Cell*; Louisiana State University and Agricultural and Mechanical College: Baton Rouge, LA, 1981; p 166.
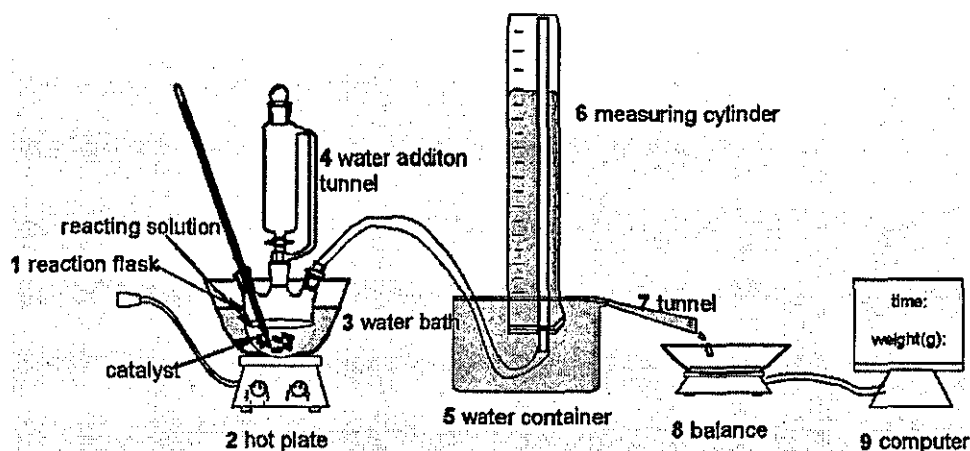
Figure 1. Schematic diagram for the experimental setup.

Table 1. Hydrogen Generation from NaBH₄ Solution under Various Conditions

run	NaBH₄ (g)	NaBH₄ molality (mol/kg)	temp (°C)	NaOH (wt %)	measured H₂ (mL)	calcd H₂ (mL)	% of theoretical yield	initial H₂ generation rate (mL/min)
1	0.55	1.45	26	0	1315.4	1426.7	92.2	278.3
2	0.75	1.98	26	0	1869.7	1945.5	92.5	391.7
3	0.98	2.59	26	0	2470.6	2542.1	97.2	563.3
4	1.14	3.01	26	0	2865.9	2957.1	96.9	658.3
5	1.28	3.38	26	0	3216.4	3320.3	96.9	738.3
6	1.70	4.49	26	0	4194.4	4409.7	95.1	978.3
7	0.54	1.43	42	0	1175.3	1196.9	98.2	703.3
8	0.96	2.54	42	0	2569.6	2619.9	98.1	1400.3
9	1.71	4.52	42	0	4279.6	4409.7	97.1	2500.3
10	2.00	5.29	42	0	5035.9	5187.9	97.1	2770.7
11	0.50	1.32	42	1	1175.3	1196.9	98.2	501.3
12	1.01	2.67	42	1	2569.6	2619.9	98.1	1360
13	1.70	4.49	42	1	4279.6	4409.7	97.1	247.5
14	2.00	5.28	42	1	5035.9	5187.9	97.1	2659.0
15	0.48	1.27	60	1	1230.1	1245.1	98.8	1400.3
16	1.00	2.64	60	1	2430.8	2594.0	93.7	2678.3
17	1.29	3.41	60	1	3231.6	3346.2	96.6	3396.7
18	1.67	4.41	60	1	4000.4	4331.9	93.4	4479.2
19	0.50	1.32	42	5	1236.6	1297.0	95.3	442.1
20	1.04	2.75	42	5	2520.0	2697.7	93.4	1050.7
21	1.70	4.49	42	5	4173.3	4409.7	94.7	1890.9
22	1.98	5.23	42	5	4962.4	5136.0	96.6	2248.8
23	0.53	1.40	60	5	1374.8	1374.8	100.0	1280.2
24	0.95	2.51	60	5	2357.9	2542.1	92.8	2209.8
25	1.29	3.41	60	5	3189.8	3346.2	95.3	2934.2
26	1.65	4.36	60	5	4028.7	4280.0	94.1	3705.9
27	0.50	1.32	60	0	1232.1	1297.0	94.9	1371.0
28	0.50	1.32	60	7	1198.5	1297.0	92.4	1004.0
29	0.50	1.32	60	10	1292.0	1297.0	99.6	901.5

The water replacement system consisted of a graduated cylinder full of water and a water container that was used to submerge the cylinder. Before the experiment was started, the water in the container was filled to such a level that any extra water could flow out of it from the slope into the container on the balance. The replaced water measurement system consisted of a container and an electronic balance that was connected with a computer using a standard RS232 connector.

Before starting the experiment, the reactor was cleaned using distilled water then dried, and the water in the water bath was electrically heated using the hot plate (2) to a stabilized predefined temperature. The reactor containing 3 g of catalyst was put into the water bath. A predetermined amount of NaBH₄ powder was then put into the reactor. When the system was ready, the cork of the feeding funnel was turned on to let the contained water or the NaOH solution flow into the reactor to start the hydrolysis. The water replaced by the hydrogen produced was then monitored using the computer.

Semiempirical Model

When the kind and amount of catalyst is fixed, the reaction rate of NaBH₄ hydrolysis is affected by the reaction temperature, the NaOH concentration, the NaBH₄ concentration, and the byproduct, sodium metaborate. During the experiment, the volume of hydrogen was measured at 20 °C. Table 1 summarized the experimental results. The theoretical quantity of the hydrogen generation in the table was calculated using the $PV = nRT$ relationship taking into account the saturated vapor pressure (which is 3400 Pa at 20 °C).

Figure 2 shows typical hydrogen generation behaviors at 42 °C. The water supplied into the system was 10 mL in volume and it contained 5% NaOH. Four NaBH₄ concentrations were tested: (1) 0.5, (2) 1.04, (3) 1.7, and (4) 1.98 g. Figure 2a shows the accumulated hydrogen production, and Figure 2b shows the hydrogen generation rate. Similarly, Figure 3 shows typical hydrogen generation behaviors at 60 °C under the same NaOH
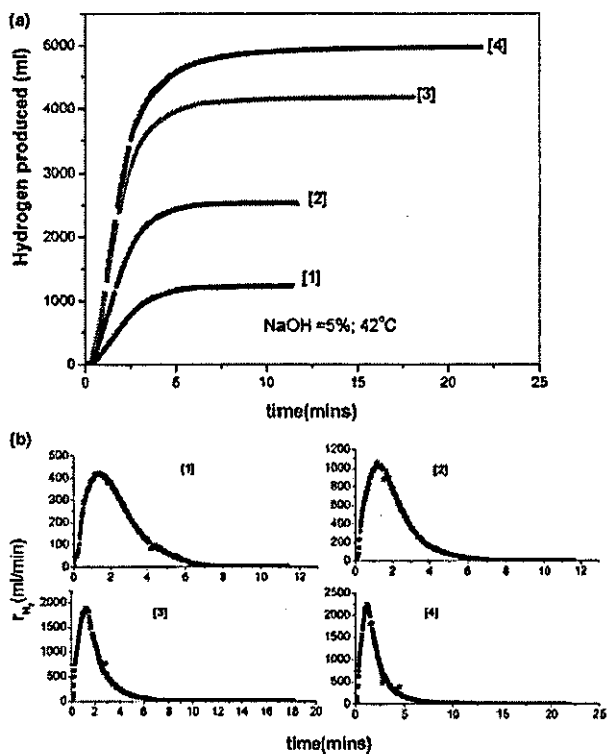
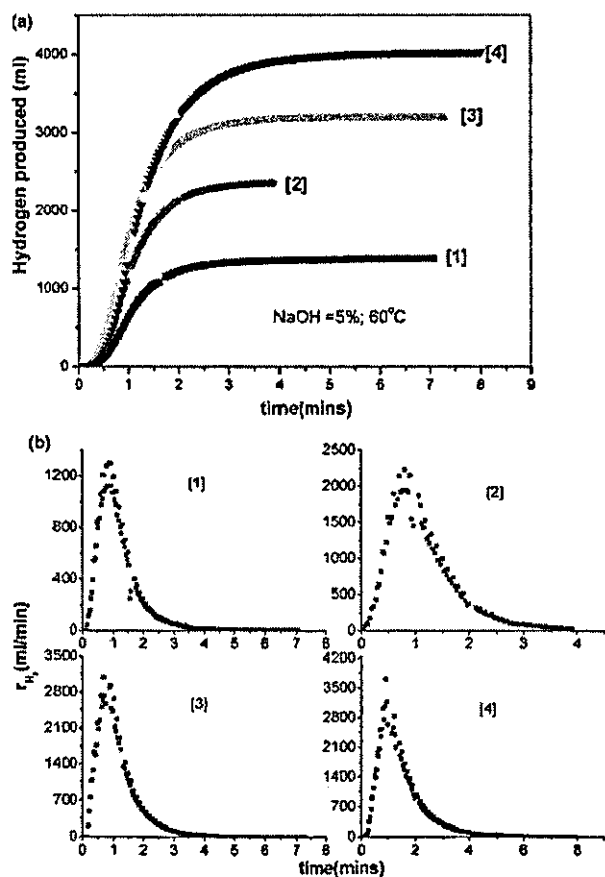**Figure 2.** Hydrogen generation by hydrolysis of NaBH₄ at 42 °C.

Figure 3. Hydrogen generation by hydrolysis of NaBH₄ at 60 °C.

and NaBH₄ concentrations. It can be seen that the rate of hydrogen generation increased quickly to a maximum value in

the first one minute or so and then decreased until no hydrogen can be further produced. The amount of hydrogen produced increased as the NaBH₄ concentration increased.

The hydrolysis of a concentrated NaBH₄ solution in the presence of solid catalyst is a complicated process. In the literature, nonconsistent mechanisms were reported, and the study was conducted in dilute solutions. The reaction mechanism in the presence of metal catalysts is still not clear. Second, the activity coefficient data of NaBH₄ in concentrated solutions is not available. Third, pore diffusion resistance exists for such a large catalyst particle. The diffusion may not only involve the BH_4^- ion but also the product, hydrogen gas.

Theoretically, the maximum reaction rate occurs at the beginning of the reaction since the concentration of the reactant is the highest. However, the maximum reaction rate was delayed because of the pore diffusion resistance. The size of the catalyst has a significant effect on the extent of this delay. The size influences will be further studied.

However, it is impossible to use pure precious metal catalyst powder without any support and configuration in practice. It has to be supported by a substrate. In this paper, for the convenience of calculation, it is assumed that the maximum hydrogen generation rate was the initial value of hydrogen generation rate. The error caused by this assumption needs to be verified further in the future work.

From runs 1–26, it can be observed that hydrogen generation rate increased with the increase of NaBH₄ concentration at a fixed temperature and NaOH concentration. The rate can thus be expressed using eq 1

$$r_{H_2} \approx m_{NaBH_4}^\alpha \qquad (1)$$

where r_{H_2} is the rate of hydrogen generation in milliliters per minute, m_{NaBH_4} is the molality of NaBH₄, and α is the apparent reaction order.

From runs 15, 23, and 27–29, it can be observed that hydrogen generation rate decreased linearly with the increase of NaOH concentration at a fixed NaBH₄ concentration and temperature. A rate expression in which the NaOH concentration appears in the denominator could explain this dependency, as shown in eq 2[12]

$$r_{H_2} \approx \frac{1}{1 + k_1 w_{NaOH}} \qquad (2)$$

where w_{NaOH} is the concentration of NaOH in weight percent and k_1 is a proportional constant.

In a combination of eqs 1 and 2, the rate law of hydrogen generation from a basic NaBH₄ solution can be expressed using eq 3, where k is another proportional constant

$$r_{H_2} = \frac{k m_{NaBH_4}^\alpha}{1 + k_1 w_{NaOH}} \qquad (3)$$

The equation may be rationalized as follows: when no NaOH is added, the hydrogen-generation rate is proportional to the molality of NaBH₄ in the solution. k is the hydrolysis rate constant, measuring the hydrogen-generation rate from the solutions with a unity molality of NaBH₄. This is understandable since the reaction sites increase with the increase of the concentration of NaBH₄. When NaOH is added to the solution but its concentration is fixed, the denominator is a constant.

(12) Fogler, H. S. *Elements of Chemical Reaction Engineering*, 3rd ed.; Prentice Hall: Upper Saddle River, NJ, 2000; pp 622–623.
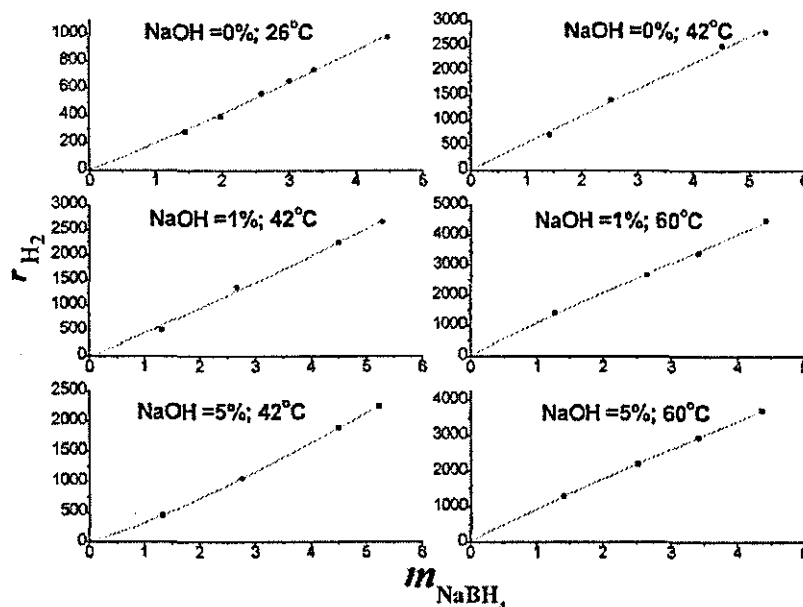
Figure 4. Regression of initial hydrogen generation rate with the molality of NaBH₄.

Table 2. Parameters Determined at Various Temperatures and NaOH Concentrations

temp (°C)	NaOH concentration (%)	$k/(1+k_1 w_{NaOH})$	α
26	0	193.0	1.08
42	0	538.8	1.00
42	1	452.2	1.09
60	1	1030.8	1.00
42	5	318.0	1.18
60	5	931.1	0.94

$k/(1 + k_1 w_{NaOH})$ now becomes less than k, indicating that the reaction rate constant becomes smaller, and thus hydrogen is generated in a slower rate. Hydrogen generation from the hydrolysis involves hydrogen ion. The addition of NaOH makes the concentration of hydrogen ion smaller resulting in a lower hydrogen-generation rate. In the following, the features of the parameters were studied.

In eq 3, $k/(1 + k_1 w_{NaOH})$ is a constant at a fixed temperature and NaOH concentration. The parameters $k/(1 + k_1 w_{NaOH})$ and α in eq 3 can then be determined by regressing the maximum hydrogen-generation rate and the initial NaBH₄ concentration using a power function. The curves obtained are shown in Figure 4, and the parameters determined are listed in Table 2.

It can be seen from Table 2 that the order of the reaction with respect to NaBH₄ concentration α equals 1. To determine parameters k and k_1, eq 3 was transformed into eq 4

$$\frac{1}{r_{H_2}} = \frac{1}{k m_{NaBH_4}} + \frac{k_1}{k} \frac{w_{NaOH}}{m_{NaBH_4}} \qquad (4)$$

Therefore, a plot of $1/r_{H_2}$ versus w_{NaOH}/m_{NaBH_4} should yield a straight-line graph, whereby the intercept on the y axis is $1/k m_{NaBH_4}$ and the slope is k_1/k, from which both k and k_1 may be determined.

In Figures 5 and 6, the regressed lines at 42 and 60 °C are shown. Good linearity justified eq 4. The values of k and k_1 yielded are listed in Table 3. It can be seen that k increased significantly from 530.1 to 1043.5 when the temperature increased from 42 to 60 °C. However, k_1 did not change significantly with NaBH₄ concentration and temperature. From
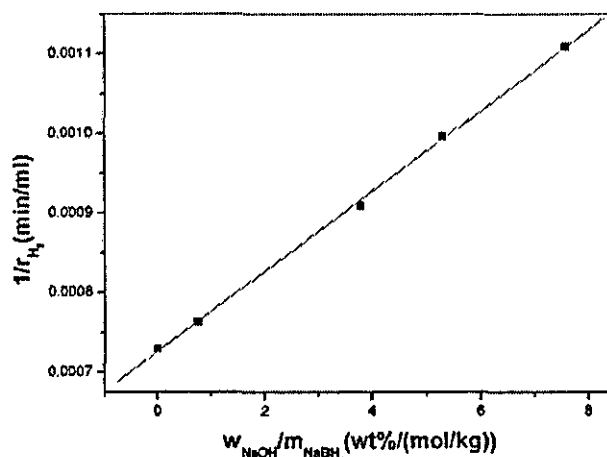

Figure 5. Relationship between w_{NaOH}/m_{NaBH_4} against the reverse hydrogen-generation rate at 60 °C when the NaBH₄ concentration is 1.32 mol/kg.

the above study, the empirical relationship (eq 3) is good enough to describe the effect of NaOH concentrations, temperatures, and NaBH₄ concentrations.

The change of rate constant with temperature can be expressed using the Arrhenius equation (eq 5)

$$k = Ae^{-E/RT} \qquad (5)$$

where E is the apparent activation energy, R is the universal gas constant, and T is the reaction temperature. The values of E and A were estimated by substituting the k values at 42 and 60 °C into eq 5, where $A = 7.47 \times 10^8$ and $E = 37.3$ kJ/mol.

To integrate eq 3, the relationship between r_{H_2} and m_{NaBH_4} (eq 6) was substituted

$$r_{H_2} = \frac{dV_{H_2}}{dt} = \frac{d(n_{H_2}RT_0/P_0)}{dt} = \frac{d(4n_{NaBH_4}RT_0/P_0)}{dt} = \frac{d(4m_{NaBH_4}w_{H_2O}RT_0/P_0)}{dt} \qquad (6)$$
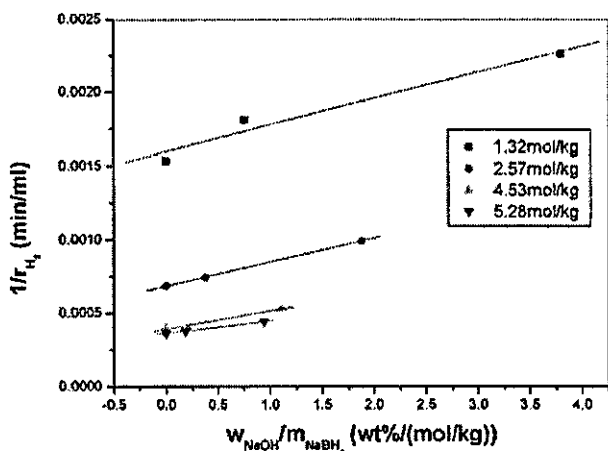
Figure 6. Relationship between w_{NaOH}/m_{NaBH_4} against the reverse hydrogen-generation rate at 42 °C at various $NaBH_4$ concentrations.
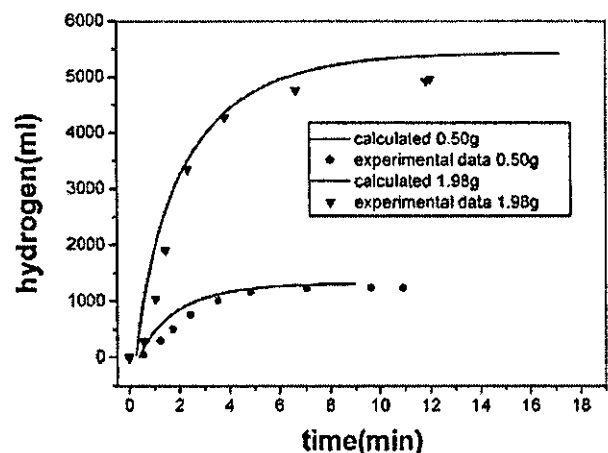

Figure 7. Comparison between experimental data and calculated hydrogen generation for the hydrolysis of 0.5 and 1.98 g of $NaBH_4$ in 10 mL of water at 42 °C when the NaOH concentration was 5%.

Table 3. Parameters Determined at Various Temperatures and $NaBH_4$ Concentrations

$NaBH_4$ molality (mol/kg)	temp (°C)	k	k_1
1.32	60	1043.5	0.052
1.32	42	473.5	0.084
2.75	42	531.6	0.086
4.49	42	571.1	0.069
5.32	42	520.7	0.044

where V_{H_2} is the volume of hydrogen produced, T_0 and P_0 are the temperature and pressure, respectively, at which the hydrogen was measured, n_{H_2} is the number of moles of hydrogen produced, n_{NaBH_4} is the number of moles of $NaBH_4$ consumed when n_{H_2} is produced, m_{NaBH_4} is the molality of $NaBH_4$, w_{H_2O} is the mass of water in the solution in kilogram, and t is time.

Substitution of the values of A and E and integration of eq 3 allows the hydrogen produced with time to be calculated. The calculated results and experimental data are shown in Figure 7 for the hydrolysis of 0.5 and 1.98 g $NaBH_4$ at 42 °C when the concentration of NaOH was 5%. The discrepancy occurred mainly at the initial stage. This may be caused by the transportation effect that results in a later occurrence of the maximum hydrogen-generation rate. Moreover, since the byproduct, $NaBO_2$, is a strong base, it has an effect similar to that of NaOH and slows down the rate of hydrogen generation at later stages.
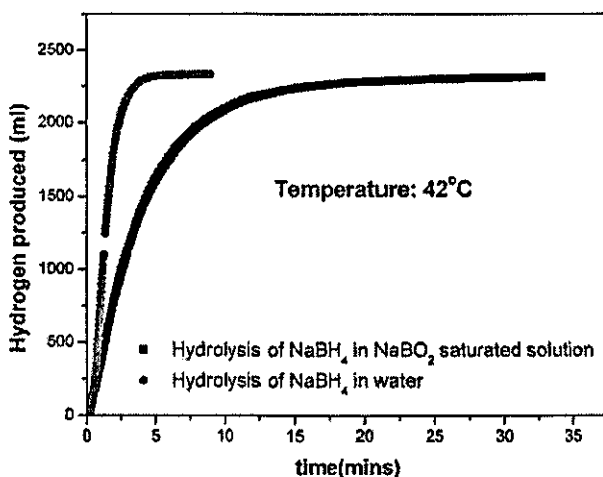

Figure 8. Comparison of the hydrogen production by hydrolysis of $NaBH_4$ in a saturated $NaBO_2$ solution and in water at 42 °C.
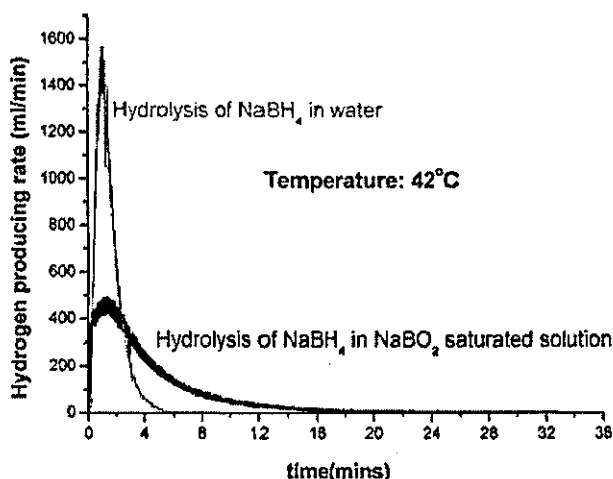

Figure 9. Comparison of the hydrogen-producing rate by hydrolysis of $NaBH_4$ in saturated $NaBO_2$ solution and in water at 42 °C.

Effects of $NaBO_2$

The production of $NaBO_2$ has the same effect as that of adding NaOH since it is a strong base. In addition to depressing the hydrogen generation rate, $NaBO_2$ may have other effects because of its limited solubility. When $NaBO_2$ is saturated in the reaction system, it will precipitate from the solution. In this section, the effect of the $NaBO_2$ precipitation on the hydrogen-generation rate was studied. To this end, a saturated $NaBO_2$ solution was used instead of pure water. The saturated $NaBO_2$ solution was put into the reaction containing $NaBH_4$ and catalyst mixture to allow $NaBH_4$ to hydrolyze.

The hydrolysis of $NaBH_4$ in saturated $NaBO_2$ solutions at 42 °C was compared with the corresponding hydrolysis in water. As shown in Figures 8 and 9, the hydrogen-generation rate was significantly depressed when an $NaBO_2$-saturated solution was used as the reaction medium. Since the reaction medium was a saturated $NaBO_2$-solution, $NaBO_2$ precipitated from the solution as soon as the hydrolysis started. The decrease of the hydrogen-generation rate was most probably the result of the blockage of the catalyst by the precipitated $NaBO_2$. This suggests that the concentration of $NaBH_4$ in the hydrolysis system is limited by the solubility of $NaBO_2$ in water. The concentration of $NaBH_4$ should not be high enough to produce a saturated $NaBO_2$ solution.

Conclusions

In this work, the kinetic features of hydrogen generation from the hydrolysis of a concentrated $NaBH_4$ solution have been investigated. The hydrogen-generation rate increases with the increase of temperature and $NaBH_4$ concentration. However, the addition of NaOH slows down the rate. When the byproduct $NaBO_2$ is saturated in the solution, the hydrogen generation rate is significantly depressed. From the present work, the following can be concluded.

The hydrolysis of $NaBH_4$ is first order to the concentration of $NaBH_4$, which indicates that the hydrogen-generation rate is directly proportional to the $NaBH_4$ concentration.

The reaction temperature has no significant effect on the depression of the hydrogen-generation rate by NaOH.

The depression of hydrogen generation rate when $NaBO_2$ is saturated in the reaction system was most probably the result of its blockage of the catalyst active sites.
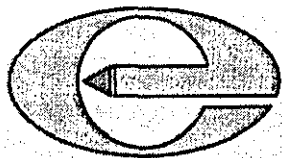
Hydrolysis of sodium borohydride-a potential compact hydrogen storage method

Y. Shang, R. Chen* and R. Thring

Department of Aeronautical and Automotive Engineering, Loughborough University, Loughborough,
Leicestershire LE 11 3TU, UK.
* Corresponding author: E-mail: r. chen@lboro.ac.uk.

Abstract

Hydrogen is the only universal fuel that can power almost everything from spaceships to automobiles. The main problems are how to generate hydrogen from renewable resources and how to store it in a manageable form since hydrogen has the minimum density among all the gases. At the present time, the lack of practical storage methods has hindered the more widespread use of the renewable and environmentally friendly hydrogen fuels. Research so far has proven that the use of the hydrolysis of sodium borohydride ($NaBH_4$) is one of the most promising methods of hydrogen storage. However, there are two main barriers for its commercialisation. One is how to improve its energy density. The other is how to recycle the by-product sodium metaborate ($NaBO_2$). In this paper, a detailed review is given of the production, hydrolysis and applications of sodium borohydride, as well as the routes for transformation of sodium metaborate back to sodium borohydride.

Key words: Hydrogen storage, Sodium borohydride, Sodium metaborate, Hydrolysis

1. Introduction

With the progress of human society and the population growth, the use of energy and the exploitation of energy resources has expanded rapidly. A good supply of energy has become an indispensable factor for economiy development. The history of humanity is in fact the history of the availability and utilization of energy. Each revolution in new energy utilization brings significant progress in human society.

In ancient times, people were able to use the power of water to drive watermills for grinding grain and the power of wind energy for pumping water and driving ships. The beginning of the industrial revolution in the 19th century in Great Britain saw the use of fossil fuels on a large scale. The extensive use of coal and oil has made a great contribution to the development of modern industries. Various energy conversion devices were then invented to enable the use of fossil fuels to drive automobiles, aeroplanes and other means of transport, to generate electricity, to heat and to cook. Nowadays, nuclear energy, wind energy, hydro-energy and solar energy are in use. However, fossil fuels still play a dominant role in the world,

and it will still account for the main part of energy sources in the foreseeable future.

Unfortunately, fossil fuels are not a renewable resource. They will eventually become depleted. Moreover, the emission of carbon dioxide and NO_x gases has been linked to the problem of global warming. These present challenges to the world and have become key factors that must be considered for a sustainable development in the 21st century. A sustainable energy supply has thus become increasingly necessary.

Hydrogen is the only universal fuel that can run everything from spaceships to automobiles as summarized in Figure 1. The main problems are how to generate hydrogen from renewable resources and how to store it in a manageable form since hydrogen has the minimum density among all the gases. At the present time, the lack of practical storage methods has hindered the more widespread use of the renewable and environmentally friendly hydrogen fuels. Various methods have been investigated for hydrogen storage such as high-pressure gas cylinders, liquid hydrogen, adsorption using carbon nano-tubes and metal hydride compounds. Research so far has proven that

the use of the hydrolysis of sodium borohydride ($NaBH_4$) is one of the most promising methods of hydrogen storage. This is because $NaBH_4$ is a stable compound and the hydrolysis reaction can be carried out in mild conditions (Kim *et al.*, 2004; Richardson *et al.*, 2005).

The main advantages of using sodium borohydride are as follows: High temperature is needed for producing H_2 by some methods, but via the hydrolysis of $NaBH_4$, H_2 can be produced in a more controllable way at a wide and moderate temperature range (from $-5\ ℃$ to $100\ ℃$). $NaBH_4$ is a non-flammable compound at normal pressure. During the hydrolysis, there are no side reactions or other volatile products. The generated hydrogen has a high purity (no carbon monoxide and sulphur) with just some water vapour. However, there are two main barriers for its commercialisation. One is how to improve its energy density. The other is how to recycle the by-product sodium metaborate ($NaBO_2$). In this paper, a detailed review is given of the production, hydrolysis and applications of sodium borohydride, as well as the routes for transformation of sodium metaborate back to sodium borohydride.
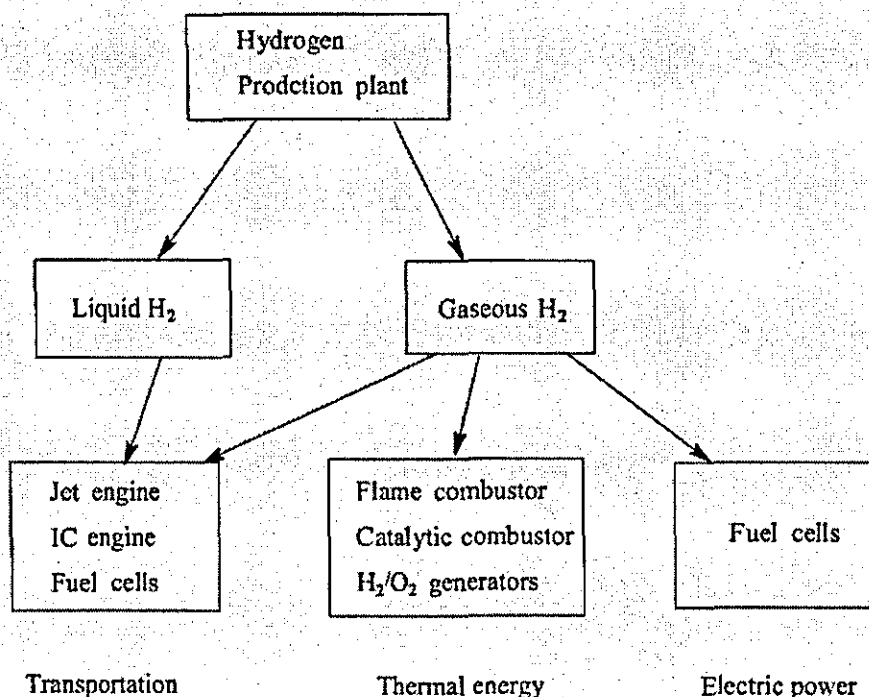

Fig. 1. The uses of hydrogen in a liquid or gas form.

2. Production of sodium borohydride

The discovery of sodium borohydride by H. J. Schlesinger, H.C. Brown, H. R. Hoeckstra, and L. R. Rapp can be traced back to 1942 (Brown, 1972). It was first synthesized as a consequence of the atomic bomb related efforts at the University of Chicago, together with many novel compounds containing boron and hydrogen. Soon after its discovery, it was found that this compound could be used as a hydrogen generation agent. After that, its chemical and physical properties were studied in detail. Extensive research of its synthesis and application was mainly conducted in 1950s. In the 1990s, the hydrolysis of NaBH$_4$ has been actively investigated due to the strong desire to look for alternative clean energies. Over 100 methods for the preparation of sodium borohy-

dride have been described, but few of these have achieved any practical significance. So far, two main technologies have been widely applied, the organic process (the Schlesiger method) and the inorganic process (Bayer method).

The Schlesiger method to manufacture NaBH$_4$ uses sodium hydride and trimethyl borate in a mineral oil medium at about 275 ℃ (Schlesinger et al., 1953). The flow diagram of the process is shown schematically in Figure 2, and the main reaction is given in Scheme 1. In this process, sodium hydride is prepared in mineral oil in a reactor and then transferred to another reactor, where trimethyl borate is added to react with the sodium hydride forming sodium borohydride. After that, a complex separation procedure is performed to recover pure sodium borohydride. The yield is over 90%.
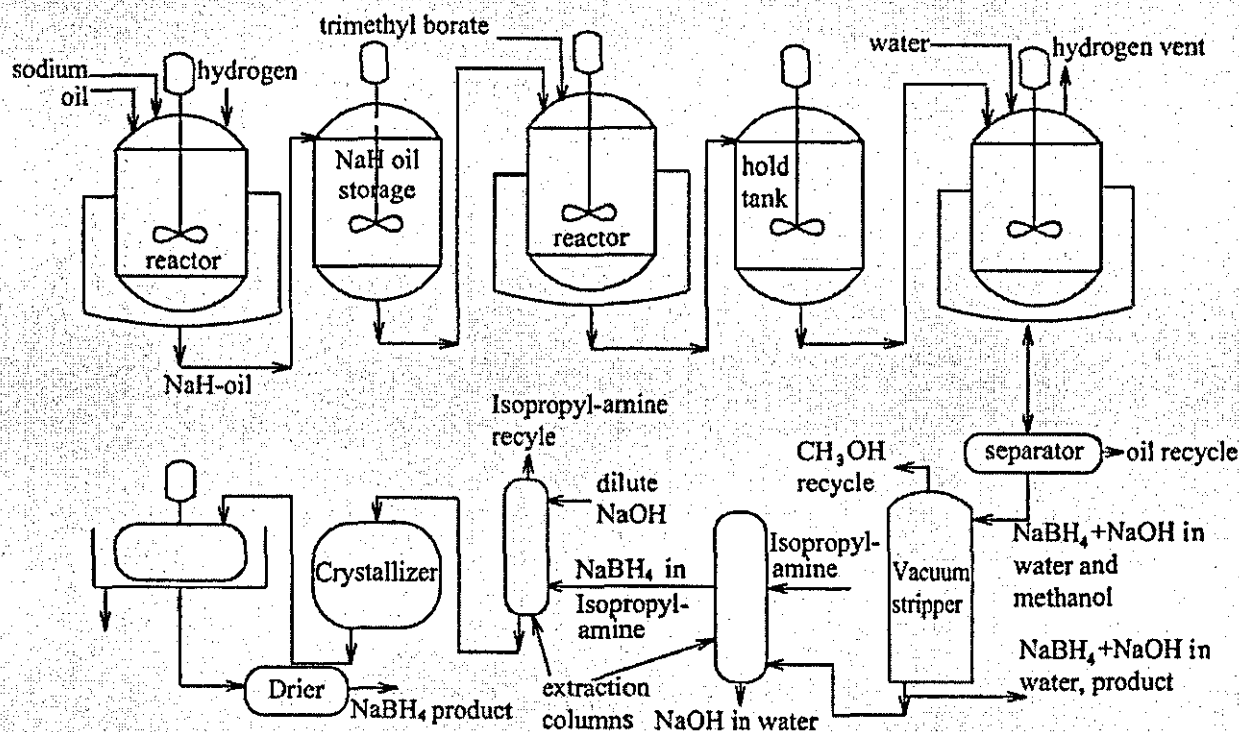

Fig. 2. The Schlesiger process for production of NaBH$_4$.

$$4NaH + (CH_3O)_3B \longrightarrow NABH_4 + 3NaOCH_3$$

Scheme 1. Organic process for preparation of sodium borohydride.

The Boyer method was first developed by the Bayer Company (Buchner and Niederprum, 1977), and is referred to as the Bayer process.

The flow diagram of the Bayer method is shown schematically in Figure 3, and the main reaction is given in Scheme 2. In this process, the borosilicate (Na$_2$B$_4$O$_7$·7SiO$_2$) is produced by the fusion of borax (Na$_2$B$_4$O$_7$) and quartz sand (SiO$_2$). The borosilicate is cooled, ground, and then reacted with sodium in an atmosphere of hydro-

gen at 300 kPa and 400 – 500 °C in a partly hetero-geneous reaction. The sodium borohydride is extract-ed from the borosilicate-silicate mixture with liquid ammonia under pressure. The yield is over 90%.
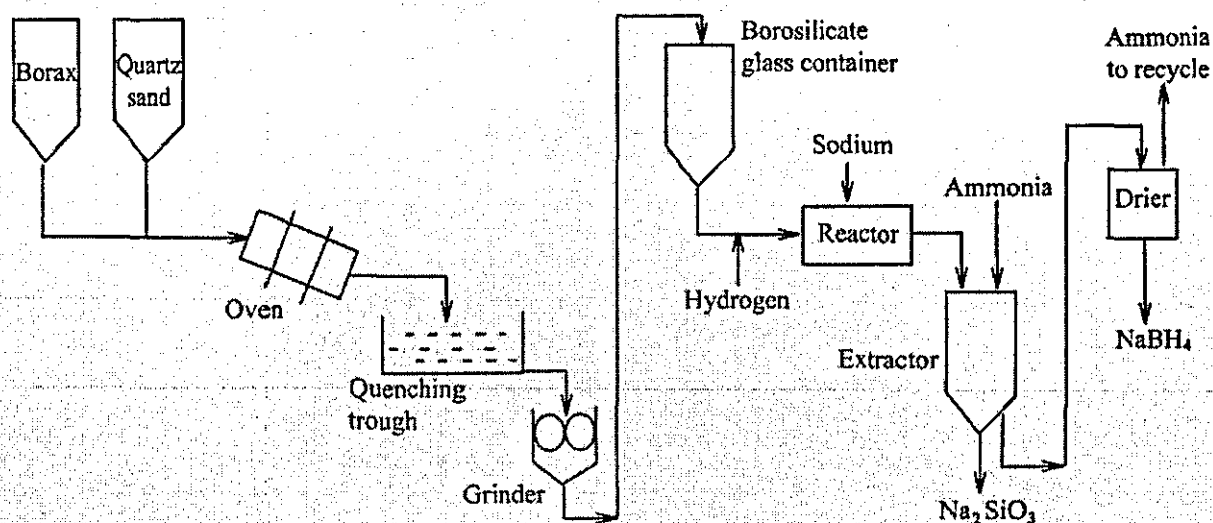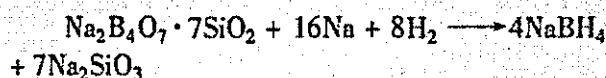

Fig. 3. The Bayer process for production of NaBH₄.

$$Na_2B_4O_7 \cdot 7SiO_2 + 16Na + 8H_2 \longrightarrow 4NaBH_4 + 7Na_2SiO_3$$

Scheme 2. The main reaction in the Bayer process.

3. Properties of sodium borohydride

In order to better understand the hydrolysis re-action to produce hydrogen from NaBH₄, its main properties are introduced in this section. The physi-cal and thermodynamic properties are listed in Tables 1 and 2 respectively, which were mainly obtained

from spectroscopic studies (Davis *et al.*, 1949).

An important physical property is its solubili-ty in water, which is related to hydrolysis reac-tion. Jensen (Jensen) has accurately measured the solubility of sodium borohydride in water at the different temperatures, and the results are re-produced in Figure 4.

The data presented in Figure 4 shows the equi-librium temperature of the two crystal forms NaBH₄ and NaBH₄·2H₂O. The curve below 36.4 °C repre-sents the solubility of the dehydrate, and above 36.4 °C, the solubility of anhydrous NaBH₄.

Table 1
Physical properties of sodium borohydride.

Molecular weight	37.84
Colour	White
Crystaline form (anhydrous)	Face centred cubic a = 6.15 Å
Melting point	505 °C (10 bar H₂) Decomposes above 400 °C in vacuum
Thermal stability	Will not ignite above 400 °C on a hot plate. Ignites from free flame in air, burning quietly
Desity (g/cm³)	1.074

Table 2
Thermodynamic properties of sodium borohydride (Davis *et al.*, 1949; Johnston and Hallett, 1953; Gunn and Green, 1955; Stockmayer *et al.*, 1955).

Sodium borohydride	
Free energy of formation	-125.82 kJ mol^{-1}
Heat of formation	-190.32 kJ mol^{-1}
Entropy	101.41 J mol^{-1}K^{-1}
Heat capacity	86.40 J mol^{-1}K^{-1}
Free energy of ionisation $NaBH_4(s) = Na^+ + BH_4^-$	-23.66 kJ mol^{-1}

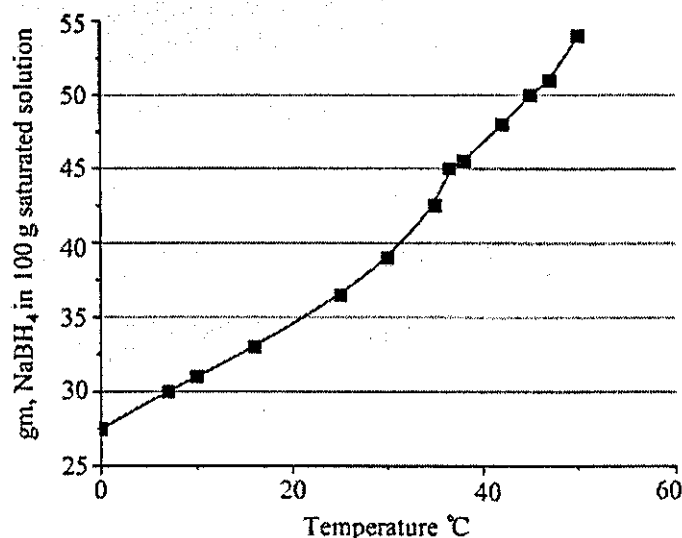| Borohydride ion BH_4^-	
Free energy of formation	-199.55 kJ mol^{-1}
Heat of formation	51.83 kJ mol^{-1}
Entropy	106.59 J mol^{-1}K^{-1}
Heat of hydrolysis $BH_4^- + H^+ + 3H_2O(liq) = H_3BO_3 + 4H_2(g)$	-371.18 kJ mol^{-1}
Half electric reaction $BH_4^- + 8OH^- = B(OH)_4^- + 4H_2O + 8e^-$	1.24 V

Fig. 4. The solubility of sodium borohydride in water.

Sodium borohydride is used extensively for the reduction of organic compounds. Its broad synthetic utility is based on its ability to reduce aldehydes and ketones selectively and efficiently in the presence of other functional groups, and to reduce other functional groups, e.g., esters, di-

and polysulfides, imines and quaternary iminiium compounds, under special conditions or with added catalysts or co-reagents.

4. Hydrolysis of NaBH₄

Sodium borohydride is a white solid, stable in dry air up to a temperature of 300 ℃. It decomposes slowly in moist air or in vacuum at 400 ℃ (Kroschwitz, 1995). The aqueous solution of sodium borohydride is also stable at normal environmental temperatures and pressures provided that the pH of the solution is high, which is usually achieved by adding NaOH to stabilize it (Davis and Swain, 1960; Kreevoy and Jacobson, 1979). However, when an acid, a metal salt or a selective catalyst is added, NaBH₄ starts to hydrolyse to release hydrogen. In the following, the mechanisms for the three types of hydrolysis are reviewed respectively.

4.1. Acid catalysis

Acid catalysis can be classified into two types: general acid catalysis and specific acid catalysis (Miller, 2004).

In a typical acid catalysed reaction A + B =

product, a reactive protonated intermediate AH^+ is formed as shown in Scheme 3, where A and B are the reaction substrates.

$$A + H^+ \underset{k_{-1}}{\overset{k_1}{\rightleftharpoons}} AH^+$$

$$AH^+ + B \xrightarrow{k_2} product$$
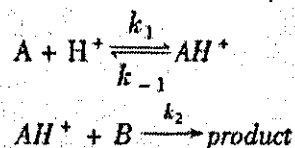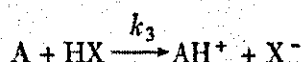
Scheme 3. *The mains steps for acid catalysis reaction.*

If step 2 is the rate-determining step and step 1 is the acid-base equilibrium, the mechanism is called specific acid catalysis. The rate depends only on the concentration of specific acid H^+, i.e. the pH value of the solution, as shown in equation (1).

$$rate = k_2[AH^+][B] = \frac{k_1 k_2}{k_{-1}}[A][B][H^+] \quad (1)$$

If step 1 is the rate-determining step, the mechanism is called general acid catalysis. The rate depends not only on pH but also on total acid concentration since any general acid can provide H^+ as shown in Scheme 4. The rate equation for this type of mechanism is shown in equation (2). A general case is shown in Table 3.

Table 3
Different rate laws for acid catalysed hydrolysis of sodium borohydride.

Specific acid catalysis	General acid catalysis
$rate = \dfrac{d[\text{Products}]}{dt}$ $= \dfrac{d[\text{Substrate}]}{dt}$ $= k_{obs}[\text{Substrate}]$ $= k_{obs} = k_0 + k_{H^+}[H^+]$ k_0 = rate constant for uncatalyzed reaction (s^{-1}) k_{H^+} = hydroxideion catalytic coefficient $(M^{-1}s^{-1})$	$rate = \dfrac{d[\text{Products}]}{dt}$ $= \dfrac{d[\text{Substrate}]}{dt}$ $= k_{obs}[\text{Substrate}]$ $k_{obs} = k_0 + k_{H^+}[H^+] = \sum k_{HA,j}[HA]_j$ k_0 = rate constant for uncatalyzed reaction (s^{-1}) k_{H^+} = hydroxideion catalytic coefficient $(M^{-1}S^{-1})$ $k_{HA,j}$ = catalytic coefficient for general acid $HA_j (M^{-1}S^{-1})$

$$A + HX \xrightarrow{k_3} AH^+ + X^-$$
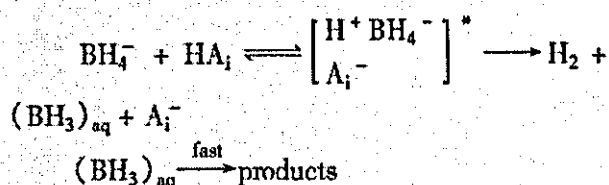
Scheme 4. General acid catalysis reaction.

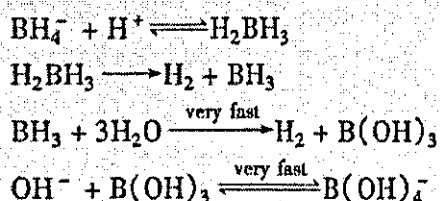$$reate = k_1[A][H^+] + k_3[A][HX] \quad (2)$$

It has been confirmed that the hydrolysis reaction of sodium borohydride is a general acid catalysis not specific acid catalysis (Abts *et al.*, 1975). Davis and Swain (Davis and Swain, 1960) studied alkali metal borohydrides hydrolysis

in dilute buffer solutions. They found that the rate expression was first order in hydrogen ion concentration in the pH range of 7.7 to 10.1, and the rate is less sensitive to hydrogen ion concentration at high pH (12 to 14). The apparent reaction order in hydrogen ion concentration decreases to about 0.4. Davis and Bromels (Davis and Swain, 1960; Davis et al., 1962) found that the rate depended upon the ionic strength and upon the anion component of the buffer solution. They suggested a mechanism which involved a rate-determining proton transfer from a general acid onto the borohyride ion (as shown in Scheme 5), in which the hydrolysis of the borohydride solution was controlled by the formation of $[H^+ BH_4^- Ai^-]^*$. The intermediate hydrolyzed immediately to an aquated borine radical $((BH_3)_{aq})$ which also hydrolyzed rapidly:

$$BH_4^- + HA_i \rightleftharpoons \begin{bmatrix} H^+ BH_4^- \\ A_i^- \end{bmatrix}^* \longrightarrow H_2 +$$

$$(BH_3)_{aq} + A_i^-$$

$$(BH_3)_{aq} \xrightarrow{fast} products$$

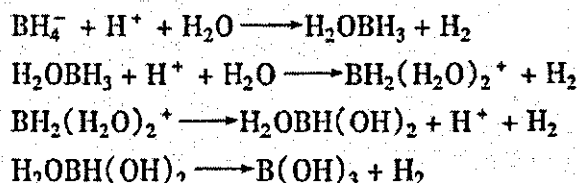Scheme 5. Proposed hydrolysis mechanism for borohydride catlysed by acid.

Kreevoy's work (Kreevoy and Hutchins, 1972; Kreevoy and Oh, 1973; Abts, Langland et al., 1975; Kreevoy and Jacobson, 1979) on the hydrolysis of BH_4^- by acid has shown that the loss of the first hydrogen determines the overall rate, and the reaction is first order to both the concentrations of BH_4^- and H^+. In acidic solution, the rate-determining step is the formation of H_2BH_3. He proposed the mechanism of this reaction as shown in Scheme 6.

$$BH_4^- + H^+ \rightleftharpoons H_2BH_3$$

$$H_2BH_3 \longrightarrow H_2 + BH_3$$

$$BH_3 + 3H_2O \xrightarrow{very\ fast} H_2 + B(OH)_3$$

$$OH^- + B(OH)_3 \xrightleftharpoons{very\ fast} B(OH)_4^-$$

Scheme 6. Proposed reaction mechanism for the hydrolysis of borohydride.

Wang and Jolly (1972), however, suggested

H_2OBH_3, $BH_2(H_2O)_2^+$, $H_2OBH(OH)_2$ as intermediates in low temperature reactions as shown in Scheme 7.

$$BH_4^- + H^+ + H_2O \longrightarrow H_2OBH_3 + H_2$$

$$H_2OBH_3 + H^+ + H_2O \longrightarrow BH_2(H_2O)_2^+ + H_2$$

$$BH_2(H_2O)_2^+ \longrightarrow H_2OBH(OH)_2 + H^+ + H_2$$

$$H_2OBH(OH)_2 \longrightarrow B(OH)_3 + H_2$$

Scheme 7. Proposed reaction mechanism for the hydrolysis of borohydride.

No matter what the intermediate is, the hydrolysis of the borohydride is confirmed to be first order in both hydrogen ion and borohydride ion. The rate equation can be expressed using equation (3).

$$\frac{dH_2}{dt} = k_H (BH_4^-)(H_3O^+) + k_{H_2O} (BH_4^-)$$

$$(H_2O) + k_{HA}(BH_4^-)(HA) \qquad (3)$$

Equation (3) can be simplified to equation (4), where (BH_4^-), (H_3O^+), (H_2O) and (HA) represent the activities of the corresponding species in the system.

$$\frac{dH_2}{dt} = (BH_4^-)[\sum k_{HA}(HA_i)] \qquad (4)$$

Schlesinger et al. (1953) have shown that the rate of hydrogen release slows down rapidly as the pH increases due to the increased presence of borate ion. Since the borate ions produced are alkaline, acids are therefore not an efficient catalyst.

4.2. Transition metal salt catalysis

Acid catalysis comprised the majority of the research on the hydrolytic reaction of $NaBH_4$. In the 1950s and 1960s, the search for more practical catalysts led to investigations of some first row transition metal chlorides (1953), which includes $MnCl_2$, $FeCl_2$, $CoCl_2$, $NiCl_2$ and $CuCl_2$. Kaufman (Kaufman, 1981; Kaufman and Sen, 1985) conducted detailed research on the effect of these salts and concluded that the transition metal salts can accelerate the hydrolysis greater than acids.

The catalysis by metal salts can be described as an additive combination of acid catalysis and metal surface catalysis, the kinetics of which can be approximated by equation (5) (Kaufman, 1981).

$$rate = k_{H^+}(BH_4^-)(H^+) + k_M \qquad (5)$$

where k_{H^+} is the rate constant for the acid catalysis and k_M is the rate constant for the metal surface catalysis.

4.3. Metal catalysis

Due to the low efficiency of acid catalysis, high efficiency catalysts have been investigated to hydrolyse sodium borohydride to hydrogen. The most efficient catalysts so far are the transition metals.

The advantages of transition metal catalysis over acid catalysis are as following (Kaufman, 1981):

· The hydrolysis rate can be controlled by the amount of catalyst used and is usually unaffected by changes in solution alkalinity.

· Minimal foaming of solutions.

· Possible recovery and reuse of catalysts.

As early as the 1950s, Schlesinger et al (1953) reported that alkaline borohydride solutions undergo hydrolysis, in the presence of various transition metal catalysts, to produce hydrogen. Based on this data, various metals such as Pt, Ru, Ni, Co and their supporting materials have been developed for hydrogen production from borohydride solutions and reported in recent years.

Brown (1962) examined several metal catalysts for the hydrolysis of sodium borohydride solutions and found that Ru and Rh liberated hydrogen rapidly. Amendola et al. (2000) used supported high surface area Ru on ion exchange resin beads to catalyse the hydrolysis. Wu et al. (2004) used carbon supported platinum as the catalyst for the hydrolysis. Richardson (2005) used Ru as the catalyst without any carrier. Krishnan et al. (2005) stated that CoO_2 can be used as an efficient carrier for Pt, Ru and Li for catalysis.

The mechanism of metal catalysis is not well understood. Some researchers proposed a zero-order reaction mechanism (Kaufman, 1981), while some others proposed a first-order reaction mechanism (Richardson et al., 2005).

4.4. Factors affecting the hydrolysis

The pH of the solution has a great effect on the hydrolysis of sodium borohydride in the absence of catalyst. The solution temperature also has a significant effect on the hydrolysis. Kreevoy and Jacobson (1979) proposed the following empirical equation to predict the rate of hydrolysis of $NaBH_4$.

$$\log(t_{1/2}) = pH - (0.034T - 1.92) \qquad (6)$$

Where $t_{1/2}$ is the time it takes for one-half of a $NaBH_4$ solution to decompose (min), pH represents the pH value of the solution and T is the temperature (K).

5. Transformation of $NaBO_2$ to $NaBH_4$

5.1. Properties of $NaBO_2$

After hydrolysis, sodium metaborate ($NaBO_2$) is produced as the by-product (Scheme 8). In this section, the properties of sodium metaborate and possible routes to transform it back to $NaBH_4$ are reviewed. $NaBO_2$ is relatively inert and non-toxic; it is a common detergent and soap additive but is toxic to ants and is an ingredient in ant poisons. An anhydrous form can be obtained when crystallizing from melts of $1:1$ of $Na_2O \cdot B_2O_3$. The octahydrate, $Na_2O \cdot B_2O_3 \cdot 8H_2O$, the tetrahydrate, $Na_2O \cdot B_2O_3 \cdot 4H_2O$, and the monohydrate, $Na_2O \cdot B_2O_3 \cdot H_2O$, occur in the system Na_2O-B_2O_3-H_2O. However, there is no evidence for the existence of a dihydrate (Kemp, 1956).

$$NaBH_4 + 2H_2O \longrightarrow NaBO_2 + 4H_2$$
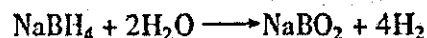
Scheme 8. The hydrolysis of sodium borohydride.

The simple ionic unit (BO_2^-) only exists in the sodium metaborate vapour in the form $M^+(O^- \!-\! B^+ \!-\! O^-)$ (Kemp, 1956). The anhydrous solid sodium metaborate is composed of sodium ion and trimeric metaborate ion, $(B_3O_6)^{3-}$, as shown in Scheme 9. However, the

solution of sodium metaborate is a binary electrolytes system, which has been proved by cryoscopic results and Raman spectrum of dissolved sodium metaborate (Kemp, 1956). The cyclic triborate ions present in the crystals of the solid salts evidently break up on dissolution. Therefore, what is referred to as a solution of sodium metaborate is in fact a solution of the binary electrolyte $NaB(OH)_4$ that is usually simplified as $NaBO_2$.
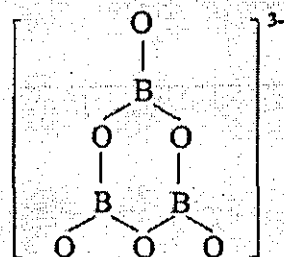
Scheme 9. The structure of the trimeric metaborate ion, $(B_3O_6)^{3-}$.

A solution of sodium metaborate is highly basic. It can be used as a component of photographic developers and replenishers due to its strong buffering function, which can control the pH with-

in close limits. It is also a component for the preparation of starch and dextrin adhesives, due to the high degree of alkalinity. Sodium metaborate can also be used as a stabilizer for textile processing. It can also be incorporated into liquid laundry detergents for pH control and enzyme stabilization.

5.2. Routes for transforming $NaBO_2$ back to $NaBH_4$

In order to use $NaBH_4$ hydrolysis in a sustainable way, the by-product must be converted back into $NaBH_4$. Little attention has been paid so far to the conversion of $NaBO_2$ to $NaBH_4$ in the literature. This section gives possible routes for the conversion.
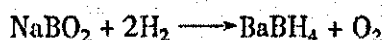
5.2.1. Coupling reactions

One possible way to convert $NaBO_2$ into $NaBH_4$ is to use the reaction expressed in Scheme 10. However, this reaction has a very high positive Gibbs energy $(\Delta_r G^\theta = 796.8 \text{ KJ.mol}^{-1})$, as shown in Table 4 for the relationship between reaction Gibbs energy, equilibrium constant for chemical reaction (K) and reaction directions. This indicates that direct reaction through this route is impossible.

Table 4
Calculation of possible coupling reaction with reaction 10. The values of the fundamental thermodynamic function were taken from Literature (Alberty, 2001).

Basic reaction	Coupling reaction	Overall reaction	$\Delta_r G^\theta (\text{kJ} \cdot \text{mol}^{-1})$
$NaBO_2 + 2H_2 = NaBH_4$ $+ O_2$	$4Na + O_2 = 2Na_2O$ $SiO_2 + Na_2O = Na_2SiO_3$	$NaBO_2 + 2SiO_2 + 4Na +$ $2H_2 = NaBH_4 + 2Na_2SiO_3$	-40.7
	$Na_2O + Si + O_2 = Na_2SiO_3$	$NaBO_2 + Na_2O + Si + 2H_2$ $= NaBH_4 + Na_2SiO_3$	-290.5
	$2Mg + O_2 = 2MgO$	$NaBO_2 + Mg + 2H_2 =$ $NaBH_4 + 2MgO$	-341.8
	$4Al + Na_2O + 3O_2 =$ $4NaAlO_2$	$3NaBO_2 + 4Al + 2NaO +$ $6H_2 = NaBH_4 + 4NaAlO_2$	-3720.8

$$NaBO_2 + 2H_2 \longrightarrow BaBH_4 + O_2$$

Scheme 10. A direct reaction to convert sodium metaborate into sodium borohydride.

It is known that some reactions with negative ΔG can drive a reaction that is not spontaneous as coupling reactions (just as the combustion of gasoline supplies enough free energy to move a car

(Silberberg, 2001)). Therefore, some reactions with very negative reaction Gibbs energy are proposed to couple with reaction (10) to make it possible to convert $NaBO_2$ back into $NaBH_4$. The potential chemical species for coupling with the $NaBO_2$ conversion reaction should not have any chemical reactions with $NaBH_4$ and the resulting $NaBH_4$ should be separated from the reaction mixture easily. Metal oxidation, such as that of sodium, silicon and aluminium, satisfy the above criteria and therefore can be used to couple with the conversion reaction. The nature of the industrial inorganic method for producing $NaBH_4$ can be classified as a coupling reaction. The calculation of the reaction Gibbs energy for the overall reaction is given in Table 4. As can be seen, all of the above coupling reactions can be used to drive reaction (10) to completion. Coupling reactions are possible routes for converting $NaBO_2$ back into $NaBH_4$.

5.2.2. Electrochemical methods

From the thermodynamic analysis, it is known that it is impossible to transfer $NaBO_2$ into $NaBH_4$ without the use of a coupling reaction. In order to make the reaction proceed quickly, tricky conditions such as high temperature and hydrogen pressure are needed to fulfil the requirements of the coupling reaction. Electrolysis may be an alternative to solve the problem. In contrast to the coupling reaction approach, this is a relatively simple technology.

There are two electrode reactions dealing with BH_4^- preparation in the Handbook of Physics and Chemistry (Dean and Lange, 1999) as shown in Scheme (11) and (12). Electrode reaction (12) may not be suitable for use in the production of borohydride because the borohydride ion is readily hydrolysed in an acidic environment.

$$H_2BO_3^- + 5H_2O + 8e \rightleftharpoons BH_4^- + 8OH^-$$
$$E° = -1.24 \text{ V}$$
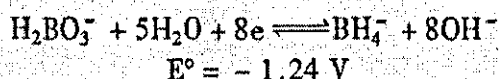
Scheme 11. Half-cell reaction of boric acid in basic conditions.

$$H_3BO_3 + 7H^+ + 8e \rightleftharpoons BH_4^- + 3H_2O$$
$$E° = -0.481 \text{ V}$$
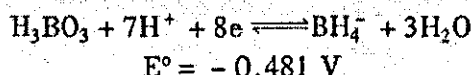
Scheme 12. Half-cell reaction of boric acid in acidic conditions.

The solution of sodium metaborate is a binary electrolytes system. However, the ions in its aqueous solution are not Na^+ and BO^{2-}. Actually, the anion in the solution is $B(OH)_4^-$ (Mellor, 1981). Hence, Scheme 11 should be written as Scheme 13, which can be designed as the cathode reaction of an electrolytic cell (Paidar *et al.*, 2002). Oxygen evolution is the main anodic reaction, as shown in Scheme 14. The overall reaction is given in Scheme 15. A schematic diagram of the cell required to produce $NaBH_4$ from a $NaBO_2$ solution is shown in Figure 5. The cell contains one anode, one cathode, one semi-permeable membrane. Under an external electric power, $B(OH)_4^-$ is reduced to BH_4^- in the cathode and OH^- is oxidized to O_2 in the anode.

$$B(OH)_4^- + 4H_2O + 8e = BH_4^- + 8OH^-$$
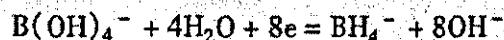
Scheme 13. The actual half cell reaction of metaborate ion in basic conditions.

$$4OH^- = O_2 + 2H_2O + 4e$$
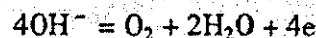
Scheme 14. Oxygen-evolution reaction on anode.

$$B(OH)_4^- = BH_4^- + 2O_2$$
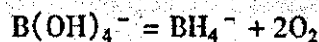
Scheme 15. Overall reaction of electrolysis of metaborate ions.

In practice, there are competing reactions on the cathode. Because the cathode reaction with the higher reduced potential reacts at the cathode first, water may be reduced into hydrogen on the cathode instead of the metaborate ion, $B(OH)_4^-$, due to its low standard electrode potential, as shown in Schemes 16. By selecting suitable cathode materials and hydrogen pressure, the electrochemical method may be possible.

$$2H_2O + 2e = H_2 + 2OH^-$$
$$E° = -0.8277 \text{ V}$$
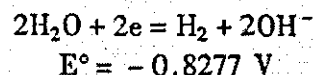
Scheme 16. Hydrolysis of water on cathode.

5.2.3. Raw materials for existing processes

Sodium metaborate may be changed into the raw materials for the existing processes. For an

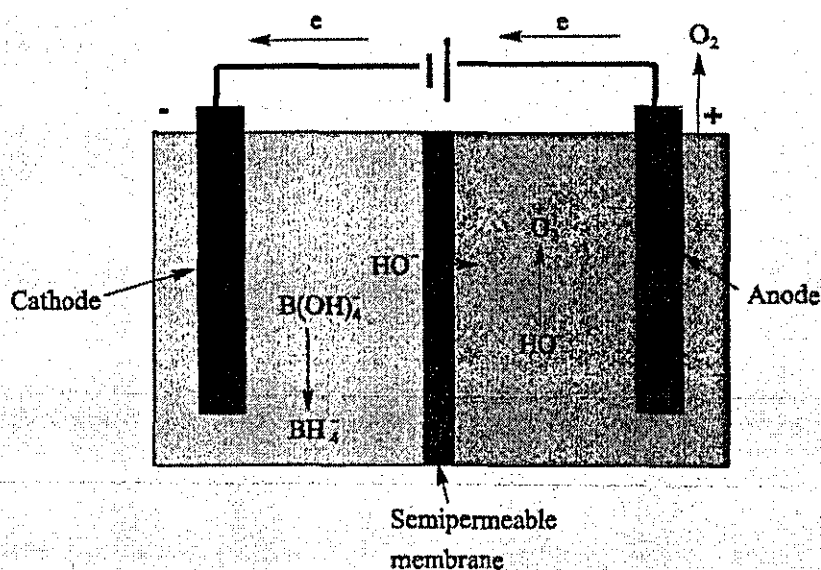Fig. 5. A schematic diagram of the proposed electrolytic cell for $NaBO_2$.

inorganic process, $NaBO_2$ can be transformed into borax through the following reactions. When contacted with boric acid, sodium metaborate can be changed into borax (Scheme 17). Sodium metaborate can absorb atmospheric carbon dioxide, forming borax and sodium carbonate (Scheme 18). For the organic process, sodium metaborate reacts with strong mineral acids to form boric acid, which can react with methanol further to give trimethyl borate. This is the raw material for the production of sodium borohydride by the Schlesiger method. The process can be expressed as shown in Schemes 19 and 20.

$$2NaBO_2 + 2B(OH)_3 \longrightarrow Na_2B_4O_7 + 3H_2O$$

Scheme 17. Transformation of sodium metaborate into borax using boric acid

$$4NaBO_2 + CO_2 \longrightarrow Na_2B_4O_7 + Na_2CO_3$$
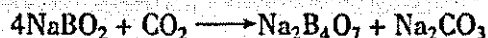
Scheme 18. Transformation of sodium metaborate into borax using CO_2.

$$NaBO_2 + H^+ + H_2O \longrightarrow Na^+ + B(OH)_3$$
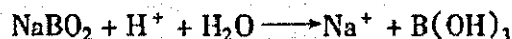
Scheme 19. Transformation of metaborate into boric acid

$$B(OH)_3 + 3MeOH \longrightarrow B(OMe)_3 + 3H_2O$$

Scheme 20. Transformation of boric acid into trimethyl borate.

6. Current status of $NaBH_4$ as a hydrogen source

Sodium borohydride has been known as a viable hydrogen generator since 1943 (Schlesinger *et al.*, 1943). At first, it was used as a convenient hydrogen source when a small amount of hydrogen was needed. It was overlooked after World War II due to its high cost. However, in recent years, it has attracted great attention as an alternative hydrogen storage method. Currently, several companies and groups such as Millennium Cell, Toyota Motor Company, and Hydrogenics are investing in this research.

Great efforts have been made to commercialise the sodium borohydride system as a hydrogen source. For example, Millennium Cell has established a portable hydrogen generator using aqueous sodium borohydride solution with Ru catalyst (Amendola *et al.*, 2000). In Oak Ridge National Laboratory of USA, a 500 W power system based on sodium borohydride hydrolysis has been constructed (Richardson *et al.*, 2005). It is optimistic the commercialization of $NaBH_4$ hydrogen product system.

7. Conclusions

• There are two commercially available methods for producing $NaBH_4$: an organic process and an inorganic process. Both processes are

commercially available.

• Three mechanisms are used for the hydrolysis of NaBH$_4$: acid catalysis, metal salt catalysis and metal catalysis. Metal catalysis is believed to be the most efficient.

• Although there is a significant amount of research and development being focused on the use of NaBH$_4$ as a hydrogen source, some important issues remain with regard to its utilisation, such as its optimal concentration and conversion of the side product NaBO$_2$.

• Three routes to transform sodium metaborate into sodium borohydride have been proposed: coupling reaction, electrochemical methods and a raw materials approach.

• From a calculation of Gibbs free energy, direct hydrogen adsorption by NaBO$_2$ is thermodynamically impossible due to the high positive Gibbs energy. Direct hydrogen adsorption by NaBO$_2$ can be conducted by coupling with other reactions with high negative Gibbs energy change such as the oxidation reaction of magnesium, sodium and silicon.

• A simple and practical transformation is the electrochemical approach. The key to this method is the choice of suitable cathode materials to prevent hydrogen evolution.

• Transformation of the by-product NaBO$_2$ into raw materials for the existing process of manufacturing NaBH$_4$ is a feasible method.

References

Abts, L.M., Langland, J.T., Kreevoy, M.M., 1975. Role of water in the hydrolysis of tetrahydroborate. Journal of American Chemical Society 97 (11), 3181-3185.

Alberty, S., 2001. Physical Chemistry. New York, John Wiley and Sons.

Amendola, S.C., Sharp-Goldman, S.L., Janjua, M.S., Spencer, N.C., Kelly, M.T., Petillo, P.J., Binder, M., 2000. A safe, portable, hydrogen gas generator using aqueous borohydride solution and Ru catalyst. International Journal of Hydrogen Energy 25, 969-975.

Brown, H.C., 1972. Boranes in organic chemistry. Cornell University Press, Ithaka.

Brown, H.C., Brown, C.A., 1962. New, highly active metal catalysts for the hydrolysis of borohydride. Journal of American Chemical Society 84, 1493.

Buchner, W., Niederprum, H., 1977. Sodium borohy-

dride and amine-boranes, Commercially important reducing agents. Pure and Applied Chemistry 49, 733-743.

Davis, R.E., Bromels, E., Kibby, C.L., 1962. Boron hydrides. III. Hydrolysis of sodium borohydride in aqueous solution. Journal of American Chemical society 84, 885-892.

Davis, R.E., Swain, C.G., 1960. General acid catalysis of the hydrolysis of sodium borohydride. Journal of American Chemical society 82, 5949-5950.

Davis, W.D., Mason, L.S., Stegeman, G., 1949. The heats of formation of sodium borohydride, lithium borohydride and lithium aluminum hydride. Journal of American Chemical Society 71(8), 2775-2781.

Dean, J.A., Lange, N.A., 1999. Lange's handbook of chemistry, New York: McGraw-Hill.

Gunn, S.R., Green, L.G., 1955. The Heat of Solution of Sodium Borohydride and the entropy of borohydride Ion. Journal of American Chemical society 77, 6197-6198.

Jensen, E.H., 1954. A study on sodium borohydride. NytNordisk forlag amold busck, copenhagen, 1954- (out of print).

Johnston, H.L., Hallett, N.C., 1953. Low temperature heat capacities of inorganic solids. XIV. Heat capacity of sodium borohydride from 15-300K. Journal of American Chemical society 75, 1467-1468.

Kaufman, C.M., 1981. Catalytic generation of hydrogen from the hydrolysis of sodium borohydride: application in a hydrogen/oxygen fuel cell, lousiana State University and Agricultural and Mechanical College, 166.

Kaufman, C.M., Sen, B., 1985. Hydrogen generation by hydrolysis of sodium tetrahydroborate: effects of acids and transition metals and their salts. Journal of the Chemical Society, Dalton Transaction, 307-313.

Kemp, P.H., 1956. The chemistry of borates, Part I. London, Borax consolidated limited.

Kim, J.H., Lee, H., Han, S.C., Lee, J.Y., 2004. Production of hydrogen from sodium borohydride in alkaline solution: development of catalyst with high performance. International Journal of Hydrogen Energy 29, 263-267.

Kreevoy, M.M., Hutchins, J.E.C., 1972. H2BH3 as an Intermediate in Tetrahydridoborate Hydrolysis. Journal of American chemical society 94, 6371 - 6376.

Kreevoy, M.M., Jacobson, R.W., 1979. The rate of decomposition of NaBH4 in basic aqueous solutions. Ventron Alembic, 15, 2-3.

Kreevoy, M.M., Oh, S.W., 1973. Relation between rate and equilibrium constants for proton-transfer reactions. Journal of American Chemical society 95(15),

4805-4810.

Krishnan, P.K., Yang, T.H., Lee, W.Y., Kim, C. S., 2005. PtRu-LiCoO2-an efficient catalyst for hydrogen generation from sodium borohydride solutions. *Journal of Power Sources* 143, 17-23.

Kroschwitz, J.I., 1995. Encyclopedia of chemical technology. New York, Wiley.

Mellor, J.W., 1981. Supplement to Mellor's comprehensive treatise on inorganic and theoretical chemistry. London, London: Longman.

Miller, B., 2004. Advanced organic chemistry. Upper Saddle River, N.J., USA, Prentice Hall.

Paidar, M., Bouzek, K., Bergmann, H., 2002. Inflence of cell construction on the electrochemical reduction of nitrate. *Chemical Engineering Journal* 85, 99-109.

Richardson, B.S., Birdwell, J.F., Pin, F.G., 2005. Sodium borohydride based hybrid power system. *Journal of Power Sources* 145, 21-29.

Schlesinger, H.I., Brown, H.C., Finholt, A.E., 1953. The preparation of sodium borohydride by the high temperature reaction of sodium hydride with borate esters. *Journal of American Chemical Society* 75, 205-209.

Schlesinger, H.I., Brown, H.C., Flinholt, A.E., Gilbreath, J.R., Hoetra, H.R., Hyde, E.K., 1953. Sodium borohydride, its hydrolysis and its use as a reducing agent and in the generation of hydrogen. *Journal of American Chemical society* 75, 215-219.

Schlesinger, H.I., Brown, H.C., Schaeffer, G.W., 1943. The borohydrides of galium. *Journal of American Chemical Society* 65, 1786.

Silberberg, M., 2001. Chemistry: the molecular nature of matter and change. St Louis, Missouri, Mosby-Year Book Inc.

Stockmayer, W.H., Rice, D.W., Stephenson, C.C., 1955. Thermodynamic properties of sodium borohydride and aqueous borohydride ion. *Journal of American Chemical society* 77, 1980-1983.

Wang, F.T., Jolly, W.L., 1972. Kinetic study of the intermediates in the hydrolysis of the hydroborate ion. *Journal of American Chemical Society* 11(8), 1933-1941.

Wu, C., Zhang, H., Yi, B., 2004. Hydrogen generation from catalytic hydrolysis of sodium borohydride for proton exchange membrane fuel cells. *Catalysis Today* 93(95), 477-483.
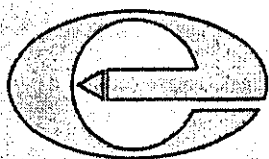
The concentration of sodium borohydride hydrolysis system used for compact hydrogen storage

Y. Shang, R. Chen* and R. Thring

Department of Aeronautical and Automotive Engineering, Loughborough University. E-mail: r.chen@lboro.ac.uk.
Corresponding author.

Abstract

Sodium borohydride ($NaBH_4$) in an aqueous solution reacts with the water and produces hydrogen under a catalytic condition. This phenomenon has been studied as a potential hydrogen storage method. The water contained in the aqueous solution has a significant impact on the hydrogen production density. In this report, using the concepts of thermodynamic dissolution equilibrium and the van Hoff's equation, a model to simulate and analyse the solubilities of $NaBH_4$ and $NaBO_2$ at varying temperature has been developed. The parameters employed in the model were obtained from existing measured data. The calculated results showed that the optimum concentration of the $NaBH_4$ solution used for the hydrolysis reaction is about half the level of its saturated solution. It increases as the solution temperature increases but only up to 378K. Further increase in temperature will results in decrease in optimised concentration.

1. Introduction

With the increasing concern about air pollution and oil depletion, hydrogen, H_2, has been intensively studied as an alternative energy source. The main problem with hydrogen application is that it is not readily transported in bulk. In order to use hydrogen widely, especially for mobile applications, a compact and safe method for storage is needed. Various methods have been developed for H_2 storage, such as high-pressure gas (Loubeyre, 2004), liquefied hydrogen (Amann, 1992; Zuettel, 2004), adsorption on materials with high specific surface area (Zhou and Zhou, 2001), reforming of natural gas, alcohols and hydrocarbons (Dudfield *et al.*, 2000), catalytic reduction of water with metals (John, 1997), and slush hydrogen (DeWitt *et al.*, 1990) etc. Each of these technologies has its inherited advantages as well as drawbacks, but the still poor stored energy density remains.

One alternative solution which has potential to store more H_2 safely for mobile applications is to utilize the catalytic reduction of water with hydrides (Dudfield *et al.*, 2000; John, 1997; Kojima *et al.*, 2004). There are many different

types of hydrides which have the potential to react with water and produce hydrogen gas. To use such materials for H_2 production for mobile applications, the energy density and the system operation safety are the major concerns. Table 1 listed the energy release during the hydrolysis reaction from a number of typical hydrides. It can be seen that most reactions between metal hydrides and water are vigorous. The large amount of heat can be released during the reaction which may cause explo-

sion. Table 2 listed the density of these potential hydrides. Apart from LiH which clearly shows the safety concern, the sodium borohydride, $NaBH_4$, has the least weight density. In comparison, it is clear that $NaBH_4$ produces the least heat energy during the hydrolysis reaction while has a low weight density. It has therefore the potential to be a successful candidate as an alternative hydrogen storage technology for mobile application in particular.

Table 1
Heat released for 1 gram hydrogen with different hydrides.

Hydrides	$NaBH_4$	LiH	$LiAlH_4$	$NaAlH_4$	CaH_2
$\Delta H^o (kJmol^{-1})$	−27.1	−54.3	−62.5	−56.2	−58.0

Table 2
Weight of reductants necessary for 1 gram of hydrogen.

Hydrides	$NaBH_4$	LiH	$LiAlH_4$	$NaAlH_4$	CaH_2
Weight(g)	4.73	4.00	12.2	14.3	10.5

The generation of hydrogen from $NaBH_4$ in aqueous solution is shown in Eq. (1). It can be seen that one mole of $NaBH_4$ in a water solution reacts with 2 moles of the water and produces 4 moles of H_2 and one mole of sodium metaborate ($NaBO_2$) as a by-product. Half of the produced H_2 is extracted from the water.

$$NaBH_4 + 2H_2O \longrightarrow 4H_2 + NaBO_2 \quad (1)$$
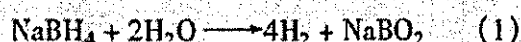
As a by-product, $NaBO_2$ has to be removed during the hydrolysis reaction to avoid clogging the catalyst which will significantly reduce the system reaction efficiency (Davis and Swain, 1960; Davis et al., 1962). A practical way to remove the $NaBO_2$ from the catalytic reaction bed is to dissolve it into the water left from the hydrolysis reaction and bring the solution into a exhaust system. Clearly, the water contained in the $NaBH_4$ hydrolysis reaction system has to not only cover the hydrolysis reaction but also to dissolve and remove the by-product. Too much water will reduce the hydrogen generation density of the system (Amendola et al., 2000; Kojima et al., 2004), while insufficient water may results in catalyst clogging and reduce the system reaction

efficiency. This necessitates the optimisation of the $NaBH_4$ concentration. In order to identify the optimised concentration, a semi-empirical simulation method based on dissolution equilibrium principles has been developed and reported in this paper.

2. Theoretical solubility model

When a solid solute is left in contact with a solvent, it dissolves until the solution is saturated, i.e. an equilibrium between undissolved and dissolved solutes is reached. This dissolution equilibrium can be expressed in a general term:

$$AB \cdot nH_2O \overset{K}{\rightleftharpoons} A^+ + B^- + nH_2O \quad (2a)$$
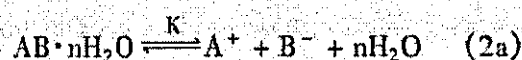
where n is number of water crystallized with the solute AB, K is the equilibrium constant.

Due to the interaction among the dissolved substances and the solvent, the performances of the dissolved substances in a real solution differ from that in the ideal-dilute one. Such differences are represented by the activities of the substances in the solution. Hence, the equilibrium constant

of the dissolution can be expressed as:

$$K = \frac{a_A{}^{\cdot\cdot} \cdot a_B{}^{\cdot\cdot} \cdot a_{H_2O}{}^{n}}{a_{AB\cdot nH_2O}} \qquad (2b)$$

where a_i is the activity, and the subscript denotes the substances.

Activity coefficient of a substance is defined as the ratio between activity and ideal-dilute concentration,

$$\gamma_i = \frac{a_i}{m_i/m_i{}^0} \qquad (3)$$

where m_i is the molarity of substance i in the solution, which is the moles of substance contained by 1000g of solvent in the solution, and $m_i{}^0$ is the molarity of the substance at standard conditions.

The activity of a solid material is unity. Since the water is the bulk phase in the solution, its activity is assumed to be a constant. Substitute Eq. (3) into (2b), the equilibrium constant can then be obtained as:

$$K = a_{H_2O}{}^n \cdot \gamma_A{}^{\cdot\cdot} \cdot \gamma_B{}^{\cdot\cdot} \cdot m_A{}^{\cdot\cdot} \cdot m_B{}^{\cdot} = K_\gamma \cdot m_A{}^{\cdot\cdot} \cdot m_B{}^{\cdot}$$

$$(4)$$

If the molarity of substance A^+ equal to that of B^- and the solute AB in the solution, $m_A{}^\cdot = m_B{}^\cdot = m_{AB}$ then the equilibrium constant Eq. (4) can be further simplified as

$$K = K_\gamma m_{AB}{}^2 \qquad (5)$$

The equilibrium constant changes with temperature. This can be expressed using the van't Hoff equation (Atkins, 1990)

$$\frac{d\ln K}{dT} = \frac{\Delta H^\circ}{RT^2} \text{ or } \frac{d\ln K}{d(1/T)} = \frac{\Delta H^\circ}{R} \qquad (6)$$

where T is temperature, ΔH° is the change of enthalpy of the dissolution process which equals to the molar heat of solution and R is the universal gas constant.

Integration of the van't Hoff equation and substitute the equilibrium constant with Eq. (6), gives
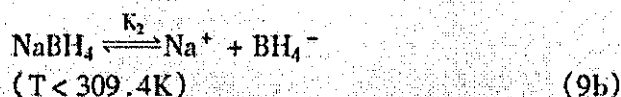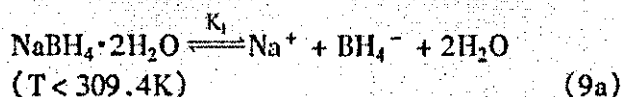
$$2\ln m_{AB} = -\frac{\Delta H^c{}_{AB}}{RT} + C \qquad (7)$$

where C is an integration constant, which includes all the activity coefficients.
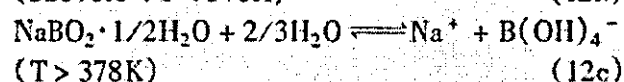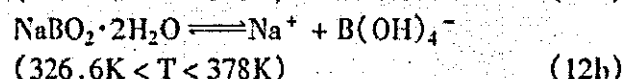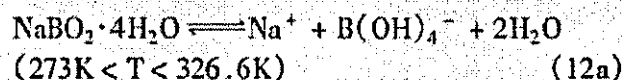
Rearrange Eq. (7) then gives the molality of the solute AB in the saturated solution,

$$m_{AB} = Ae^{-\Delta H^0{}_{AB}/2RT} \qquad (8)$$

For sodium borohydride, $NaBH_4$, two potential crystalline states, $NaBH_4 \cdot 2H_2O$ and $NaBH_4$, may exist as the undissolved solid in its saturated solution depending upon the temperature of the solution as shown in Eq. (9a,b) (Mellor, 1981). When the temperature is lower than 309.4K, the undissolved part is in the form of $NaBH_4 \cdot 2H_2O$. Above this temperature, the undissolved part is in the form of pure $NaBH_4$.

$$NaBH_4 \cdot 2H_2O \overset{K_1}{\rightleftharpoons} Na^+ + BH_4{}^- + 2H_2O$$
$$(T < 309.4K) \qquad (9a)$$

$$NaBH_4 \overset{K_2}{\rightleftharpoons} Na^+ + BH_4{}^-$$
$$(T < 309.4K) \qquad (9b)$$

For sodium metaborate, $NaBO_2$, there are three crystalline states in the saturated sodium metaborate solution $NaBO_2 \cdot 4H_2O$, $NaBO_2 \cdot 2H_2O$, and $NaBO_2 \cdot 1/2H_2O$, as shown in Eq. (12a, b, c). Again, the solubility of each state depends on the temperature of the solution (Mellor, 1980).

$$NaBO_2 \cdot 4H_2O \rightleftharpoons Na^+ + B(OH)_4{}^- + 2H_2O$$
$$(273K < T < 326.6K) \qquad (12a)$$
$$NaBO_2 \cdot 2H_2O \rightleftharpoons Na^+ + B(OH)_4{}^-$$
$$(326.6K < T < 378K) \qquad (12b)$$
$$NaBO_2 \cdot 1/2H_2O + 2/3H_2O \rightleftharpoons Na^+ + B(OH)_4{}^-$$
$$(T > 378K) \qquad (12c)$$

Using Eqs. (7) and (8), the solubility of both $NaBH_4$ and $NaBO_2$ in terms of molality can be obtained as:

$$2\ln m_{NaBH_4} = \frac{-\Delta H^0{}_{NaBH_4}}{RT} + C \qquad (13)$$

$$2\ln m_{NaBO_3} = \frac{\Delta H^r_{NaBO_2}}{RT} + C \qquad (14)$$

which gives

$$m_{NaBH_4} = A\, e^{-\Delta H^0_{NaBH_4}/2RT} \qquad (15)$$

$$m_{NaBO_2} = A'\, e^{-\Delta H^0_{NaBO_2}/2RT} \qquad (16)$$

where, $\Delta H^0_{NaBH_4}$ and $\Delta H^0_{NaBO_2}$ is the standard enthalpy change of sodium metaborate solution, which equals to the molar heat of solution. is an integral constant, which is related to the overall activity coefficient, and R is the universal gas constant.

From equations (15) and (16), it can be seen that the solubility is related to the heat of solution and the temperature at which the dissolving process takes place. When the dissolving process is endothermic, i.e. $\Delta H^0 > 0$, a higher temperature results in a larger solubility. When the dissolving process is exothermic, i.e. $\Delta H^0 < 0$, a higher temperature gives smaller solubility.

3. Semi-empirical solubility model

Equations (13) and (14) shows that there is potentially a linear relationship between $2\ln m$ and $1/T$. If such relationships can be identified, we may then be able to use these equations to analyse the solubility of both reactant and by-product of the NaBH$_4$ hydrolysis system and to develop a model to simulate and optimise the solution for the NaBH$_4$ hydrolysis system.

Figure 1 shows the measured solubility data of NaBH$_4$ at varying temperature (Mellor, 1980; 1981). It can be seen that the solubility of sodium borohydride increases as the temperature increases. Below 36. 4℃ (309. 4K), the crystalline state in the dissolution equilibrium is NaBH$_4$ · 2H$_2$O, and above this temperature the crystalline state in the dissolving equilibrium is NaBH$_4$. At 36.4℃(309.4K), two kinds of crystalline, NaBH$_4$·2H$_2$O and NaBH$_4$, coexist in the saturated solution, which is regarded as the invariant point.
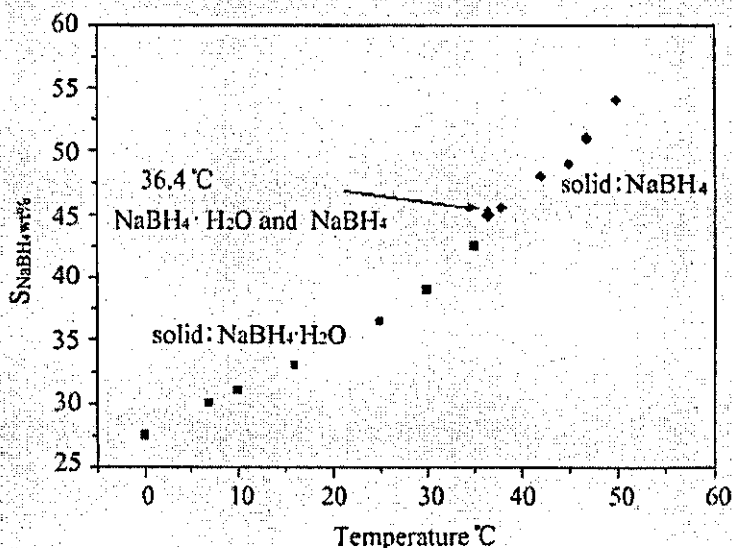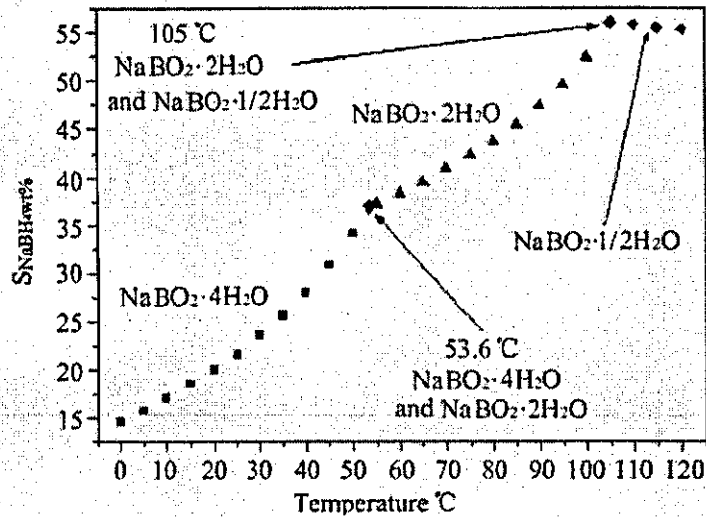

Fig. 1. Measured solubility of NaBH$_4$(Mellor, 1981).

Figure 2 shows the measured solubility of NaBO$_2$ at varying temperature (Mellor, 1980; 1981). There are two invariable points at 53.6℃ and 105℃, respectively. These correspond to the transition temperatures of the sodium metaborate between its three crystalline states, NaBO$_2$ · 4H$_2$O, NaBO$_2$ · 2H$_2$O, and NaBO$_2$ · 1/2H$_2$O.

Overall, its solubility increases as the temperature increases up to the level of 105℃. This indicates that the enthalpy change of the dissolution is positive when the crystalline state is NaBO$_2$·4H$_2$O or NaBO$_2$·2H$_2$O. If the solution temperature further increases, the solubility of sodium metaborate starts to decline.

Fig. 2. Measured solubility of $NaBO_2$ (Mellor, 1980).

The solubility data cited in Figures 1 and 2 are in percentage by mass $(S_{wt\%})$. In order to obtain the parameters in the models, this needs to be converted into molality defined as

$$m = \frac{1000 S_{wt\%}}{(100 - S_{wt\%}) M} \qquad (17)$$

where M is the molecular weight of $NaBH_4$ (equals to 37.83 g/mol) or $NaBO_2$ (equals to 65.8 g/mol).

Figures 3 and 4 shows the rearranged solubility data cited in Figures 1 and 2 by converting the mass solubility into molality in the form of $2\ln m$ vs. $1/T$ for $NaBH_4$. It can be seen that a reasonable linearity exists at each temperature range. There are some differences between the measured data and the linear fit. This is probably mainly due to the fact that the water activity in the solution has been assumed to be constant at various $NaBH_4$ concentration and temperature. Further work in the area is undertaking.
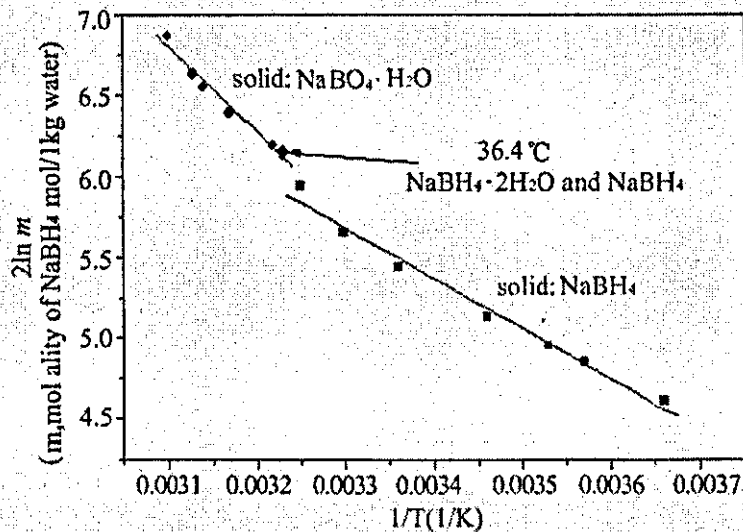
Fig. 3. Temperature effect on $NaBH_4$ solubility.
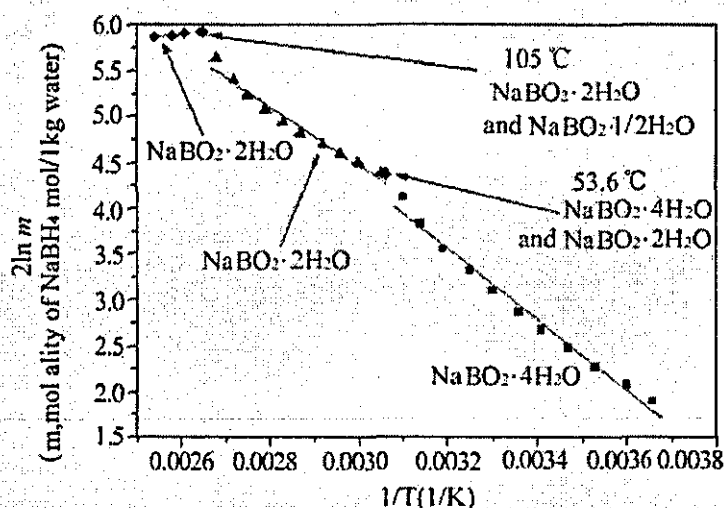
Fig. 4. Temperature effect on $NaBO_2$ solubility.

Comparing the linearity with the dissolution equilibrium theory, Eqs. (13) and (14), both ΔH and constant C can be obtained. These are listed in Table 3. The positive value of the heat of solution suggests that the dissolving process is endothermic. Increasing temperature is favourable for the dissolution. On the other hand, the negative heat value indicates that the dissolution process is exothermic and increase in temperature will decrease the solubility of the solute.

Table 3
Semi-empirical parameters ΔH and C.

Species		Parameters	
		ΔH^0 (kJ/mol)	Pre-exponential factor (Mol/kg water)
NaBH$_4$	NaBH$_4$.2H$_2$O (<309.4K)	26.0	2980
	NaBH$_4$ (≥309.4K)	43.7	10400
NaBO$_2$	NaBO$_2$.4H$_2$O (<326.6K)	31.9	2750
	NaBO$_2$.2H$_2$O (326.6 – 378K)	26.8	1180
	NaBO$_2$.1/2H$_2$O (≥378K)	−4.6	9.25

Substitute the heat and the constant into Eqs. (15) and (16), the solubility of NaBH$_4$ and NaBO$_2$ in the form of percentage by mass at various temperatures can then be obtained as:

$$S_i = \frac{100 E_i e^{-F_i/T}}{1000 + E_i e^{-F_i/T}} \qquad (18)$$

where E_i and F_i are semi-empirical parameters listed in Table 4.

Figures 5 and 6 show the comparison between calculated solubility using Eq. (18) and the measured value. It can be seen that a good agreements are obtained at all temperature ranges.

Table 4
Semi-empirical parameters E_i and F_i.

Species		Parameters	
		E_i	F_i
NaBH$_4$	NaBH$_4$·2H$_2$O (<309.4K)	1.13×10^5	1561
	NaBH$_4$ (≥309.4K)	3.93×10^6	2629
NaBO$_2$	NaBO$_2$·4H$_2$O (<326.6K)	1.81×10^5	1921
	NaBO$_2$·2H$_2$O (326.6 – 378K)	7.76×10^4	1613
	NaBO$_2$·1/2H$_2$O (≥378K)	6.09×10^2	– 277
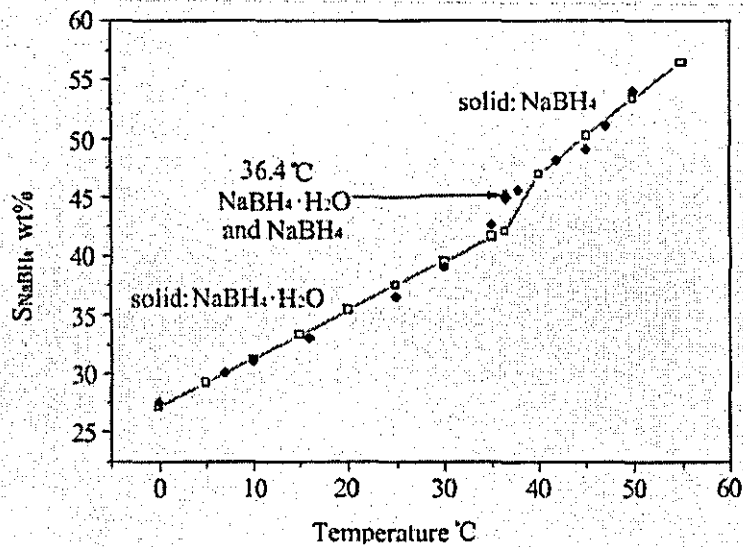
Fig. 5. Comparison of calculated and measured solubility of NaBH$_4$.
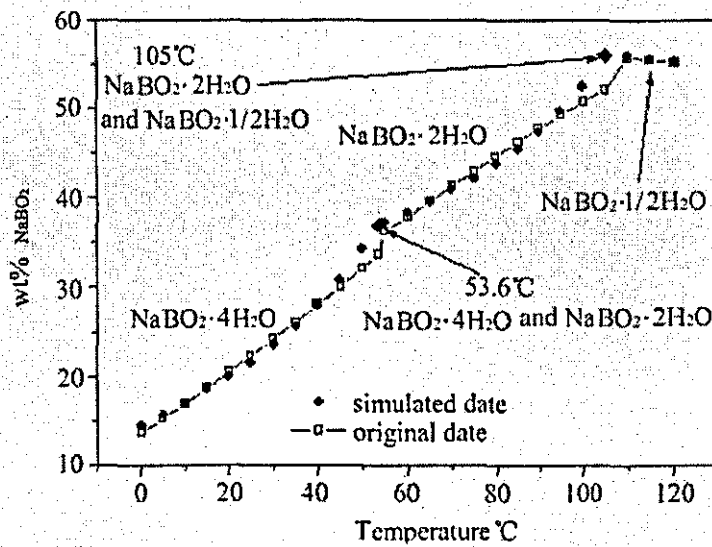
Fig. 6. Comparison of calculated and measured solubility of NaBO$_2$.

4. System optimisation

In order to obtain the maximum possible hydrogen production density, the water contained in the $NaBH_4$ hydrolysis system needs to be optimised. There are three parts of water involve in the hydrolysis reactions: water used to produce a saturated $NaBH_4$ solution, w_1, water consumed by the hydrolysis reaction, w_2, and the water needed to dissolve and remove the by-product, w_3.

Table 5 listed the minimum amount of water required by each part of the requirement of the hydrolysis system at varying temperature ranges as shown.

Table 5
Water needed for $NaBH_4$ hydrolysis system.

Temperature range (K)	Water in saturated $NaBH_4$ solution w_1 (g)	Water required for hydrolysis, w_2 (g)	Water required for dissolving $NaBO_2$, w_3 (g)	Water required by the system $(w_2 + w_3)$ (g)
273 – 309.4	102.0	36.0	180.0	216.0
309.4 – 326.6	47.0	36.0	130.0	166.0
326.6 – 378	30.0	36.0	60.0	96.0
> 378	10.0	36.0	50	86.0

It can be seen that the amount of water needed to react with NaBH4 and to solve the $NaBO_2$ is significantly larger than the amount of water contained in the saturated $NaBH_4$ solution. In other words, it is the water required to hydrolysis the $NaBH_4$ and dissolve the by-product $NaBO_2$ decides the optimised water content in the hydrolysis system. The optimised concentration of the system can thus be calculated by

$$C_{NaBH_4 (wt\%)} = \frac{100 w_{NaBH_4}}{w_2 + w_3 + w_{NaBH_4}} \quad (19)$$

where w_{NaBH_4} is the weight of $NaBH_4$.

Figure 7 shows both calculated maximum optimised $NaBH_4$ concentration in the hydrolysis system and the concentration of saturated $NaBH_4$ solution at various temperatures. Two interesting phenomena need to be addressed. First, the optimised concentration of $NaBH_4$ for the hydrolysis system is about half the level of saturated solution of $NaBH_4$. By simply looking at the concentration of the $NaBH_4$ to design the hydrolysis reaction system is clearly insufficient. Second, the optimised concentration increases as the solution temperature
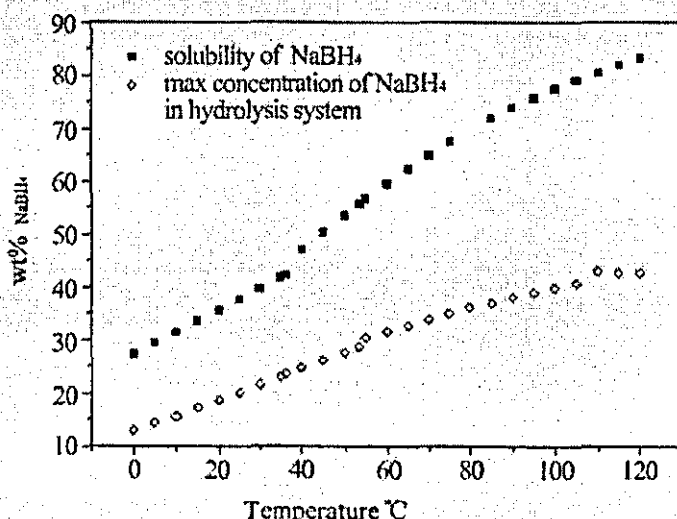

Fig. 7. Calculated $NaBH_4$ solubility and its maximum concentration in the hydrolysis system.

increases. This clearly increases the hydrogen production density. However, such benefit only exists when the solution temperature is lower than 378K. Further increase in temperature would decrease the optimised concentration, so reduces the hydrogen production density of the system. This is due to the fact that the dissolution of $NaBO_2$ at temperatures above 378K becomes exothermic and high temperature will reduce its solubility.

5. Conclusions

Based on the van Hoff's equation, a thermodynamic dissolution equilibrium model has been developed.

Using existing measured solubility data, a group of semi-empirical parameters required by the thermodynamic dissolution equilibrium model for $NaBH_4$ and $NaBO_2$ were obtained.

Using these semi-empirical parameters, the solubility of both $NaBH_4$ and NaBO2 was predicted by the thermodynamic dissolution equilibrium model agrees well with the measured data.

The calculated results showed that the optimum concentration of the $NaBH_4$ solution used for the hydrolysis reaction is about half the level of its saturated solution. It increases as the solution temperature increases but only up to 378K. Further increase in temperature will results in decrease in optimised concentration.

References

Amann, C.A., 1992. The passenger car and the greenhouse effect. *International Journal of Vehicle Design* 13(4), 305-334.

Amendola, S.C., Sharp-Goldman, S.L., Janjua, M. Saleem, Spencer, Nicole C., Kelly, Michael T., Petillo, Phillip J., Binder, Michael, 2000. A safe, portable, hydrogen gas generator using aqueous borohydride solution and Ru catalyst. *International Journal of Hydrogen Energy* 25, 969-975.

Atkins, P.W., 1990. Physical Chemistry. Oxford, Oxford University Press, pp. 216-218.

Davis, R.E., Bromels, E., Kibby, Charles L., 1962. Boron Hydrides. III. Hydrolysis of Sodium Borohydride in Aqueous Solution. *Journal of American Chemical society* 84, 885-892.

Davis, R.E., Swain, C.G., 1960. General Acid Catalysis of the Hydrolysis of Sodium Borohydride. *Journal of American Chemical society* 82, 5949-5950.

DeWitt, R.L., Hardy, T.L., Whalen, Margaret V., Richter, G. Paul, 1990. Slush hydrogen (SLH2) technology development for application to the National Aerospace Plane (NASP). *Advances in Cryogenic Engineering* 35, 1741-1754.

Dudfield, C., Chen, R., Adcock, P.L., 2000. Compact CO selective oxidation reactor for solid polymer fuel cell powered vehicle application. *Journal of Power Sources* 86(1-2), 214-222.

Dudfield, C., Chen, R., Adcock PL., 2000. Evaluation and modelling of a CO selective oxidation reactor for solid polymer fuel cell automotive applications. *Journal of Power Sources* 85(2), 237-244.

John, W., 1997. Hydrogen-powered automobile with in situ hydrogen generation. *USP* 5690902, H Power Corporation (Belleville, NJ).

Kojima, Y., Suzuki, K.-I., Fukumoto, K., Kawai, Y., Kimbara, M. Nakanishi, H., Matsumoto, S., 2004. Development of 10 kW-scale hydrogen generator using chemical hydride. *Journal of Power Sources* 125(1), 22-26.

Loubeyre, P., Celliers, P.M., Hicks, D.G., Henry, E., Dewaele, A., Pasley, J., Eggert, J., Koenig, M., Occelli, F., Lee, K.M., Jeanloz, R., Neely, D., Benuzzi-Mounaix, A., Bradley, D., Bastea, M., Moon, Steve, Collins, G.W., 2004. Coupling static and dynamic compressions: First measurements in dense hydrogen. *High Pressure Research* 24(1), 25-31.

Mellor, J.W., 1980. Supplement to Mellor's comprehensive treatise on inorganic and theoretical chemistry 5. Boron Part A. Publication: London; Longman, pp.257

Mellor, J.W., 1981. Supplement to Mellor's comprehensive treatise on inorganic and theoretical chemistry 5. Boron Part B1. Publication: London; Longman, pp. 223.

Zhou, L., Zhou, Y., 2001. Determination of compressibility factor and fugacity coefficient of hydrogen in studies of adsorptive storage. *International Journal of Hydrogen Energy* 26(6), 597-601.

Zuettel, A., 2004, Hydrogen storage methods. *Naturwissenschaften* 91(4), 157-172.